

CHAPTER ONE

INTRODUCTION

1.1. Hydrazones

Hydrazones are the organic compounds whose molecules contain the $R_1R_2C=N-NH$ -atomic linkage (Deepa and Aravindakshan, 2005; Saeed *et al.*, 2016). They are usually derived from the condensation reaction of hydrazine with carbonyl compounds such as ketones or aldehyde (Fig. 1.1). In these reactions, there is the substitution of the carbonyl oxygen with the NNH_2 functional group of the hydrazine (Stork and Benaim, 1977). Hydrazones belong to the azomethine class by possessing the $(C=N)$ bond and they are differentiated from the imines and oximes by the presence of two adjacent N-N atoms (Gup *et al.*, 2015). Research had shown that the lone pair of electron on the trigonally hybridised nitrogen atom of the azomethine group $(C=N)$ is significant for their chemical and biological properties.

The chemistry of hydrazine derivatives began in 1863 when Hofmann carried out a successful experiment to convert azobenzene to hydrazobenzene, thus synthesising the hydrazine derivative. In 1875, Emil Fischer was able to synthesise phenylhydrazine which was subsequently used by his assistant at that time (Ludwig Knorr) for reactions with acetoacetic acid esters. The result was the production of antipyrine which was used as antipyretic (used to prevent or reduce fever) during the influenza epidemic of 1889/1890 (Brune, 1997).

In the early 1950's, isonicotinhydrazide and its isopropyl derivative yielding hydrazone, were discovered to be effective drugs in the treatment of human tuberculosis (Buu-Hoi *et al.*, 1953). Tuberculocidal activities were similarly shown to be present in a wide series of non-pyridinic hydrazides and all these gave impetus to the research and development of hydrazides derivatives and their condensation reaction products with aldehyde and ketones now widely known as hydrazones. Buu-Hoi *et al.*, (1953) wrote "these condensation products were studied in view of the probability of their being of lower toxicity than the parent hydrazides, as a result of the blocking of the free NH_2 group".

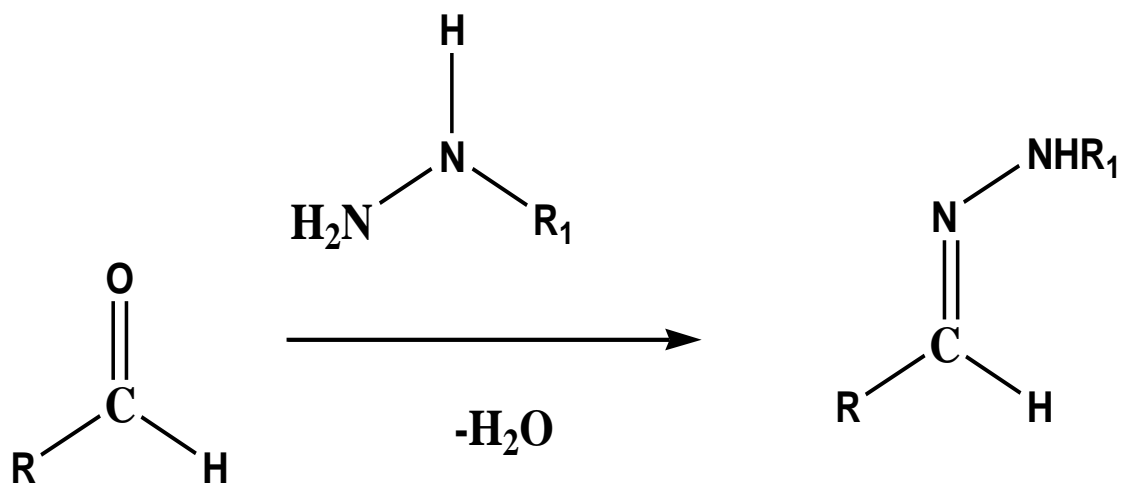
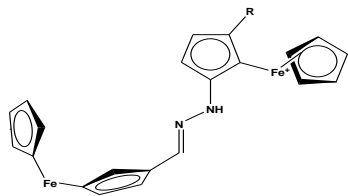


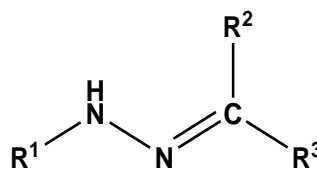
Figure 1.1. Formation of Hydrazones (R= Alkyl, Phenyl, Heterocyclic, R₁=H, Phenyl, Heterocyclic).

1.2 Types of hydrazones

There are different types of hydrazones that have been reported (Domiano *et al.*, 1975; Chen *et al.*, 2010; Patel *et al.*, 2013; and Knittl, *et al.*, 2018). They include (Fig. 1.2):



Organometallic Hydrazone

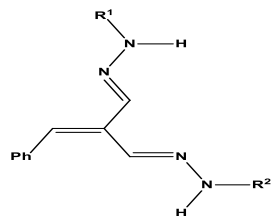


Aryl Hydrazone.

R¹= Ph, Alkyl.

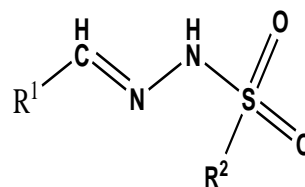
R²=H, Alkyl, phenyl, heterocyclic.

R³ = Alkyl, Ph.



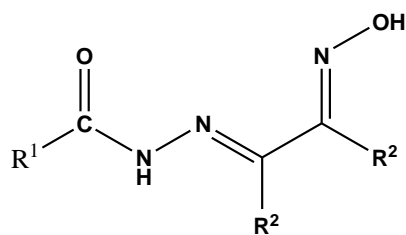
β -diketone hydrazone

R¹ = R² = Aryl, heterocyclic

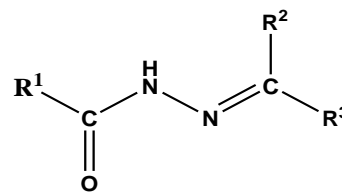


Sulphonyl Hydrazone

R¹=R²=Aryl, alkyl, substituted aryl.



Oxime hydrazone



Aroyl hydrazone

R¹ = Ph, heterocyclic

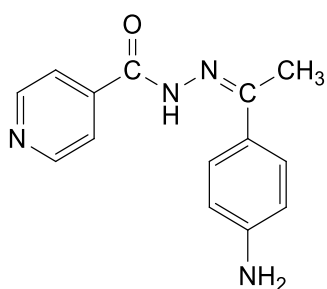
R² = H, Alkyl, R³ = Ph, heterocyclic.

Figure 1.2. Representative Hydrazones

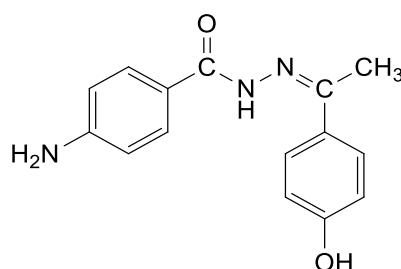
Among the various types of hydrazones, the Aroylhydrazones have received the greatest attention due to their particularly interesting properties which include: relatively easy method of preparation, more hydrolytic stability when compared to imines and ability to form crystals readily (Makcova *et al.*, 2012; Gup *et al.*, 2015).

1.2.1. Naming of hydrazones

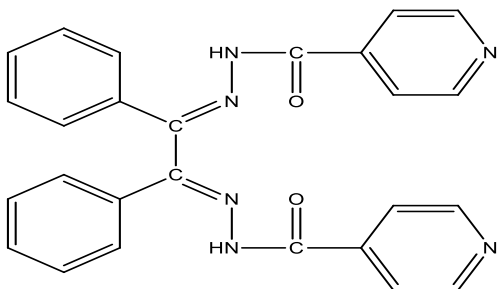
Hydrazones are named (Figure 1.3) after the carbonyl compound from which they are condensed (Ainscough, 1998; Nawar and Hosny, 1999).



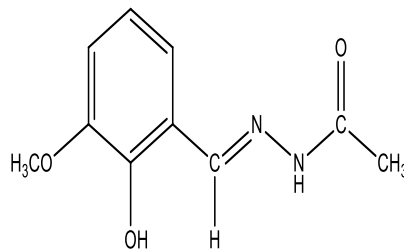
p-aminoacetophenone-isonicotinoylhydrazone



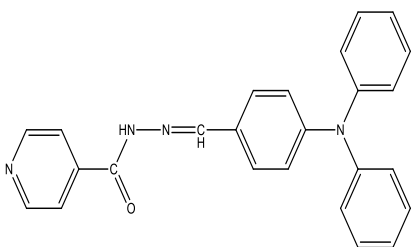
p-hydroxy-acetophenone-4-amino-benzoylhydrazone



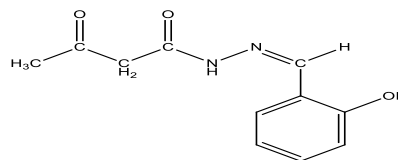
Benzil-isonicotinoylhydrazone



o-Vanillin-acetylhydrazone



Isonicotinoylhydrazone-4-diphenylamino-benzaldehyde

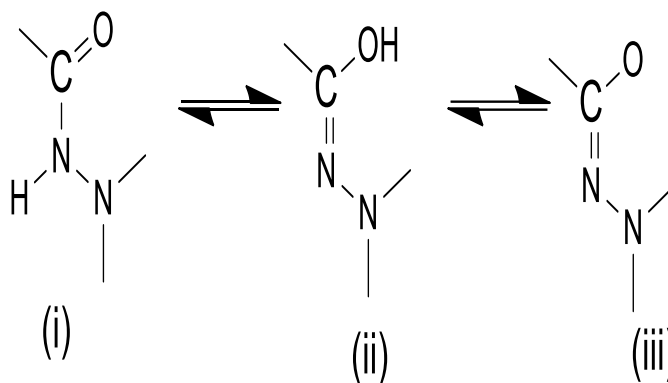


Salicylaldehyde-acetoaceticacidhydrazone

Figure 1.3. Structures and names of some hydrazones

1.2.2 Tautomerism in hydrazone

Hydrazones undergo keto-enol tautomerism in solution (Scheme 1.1) while the enol form is also in equilibrium with its deprotonated form (Jing-lin *et al.*, 2014; Mostafa, 2011).



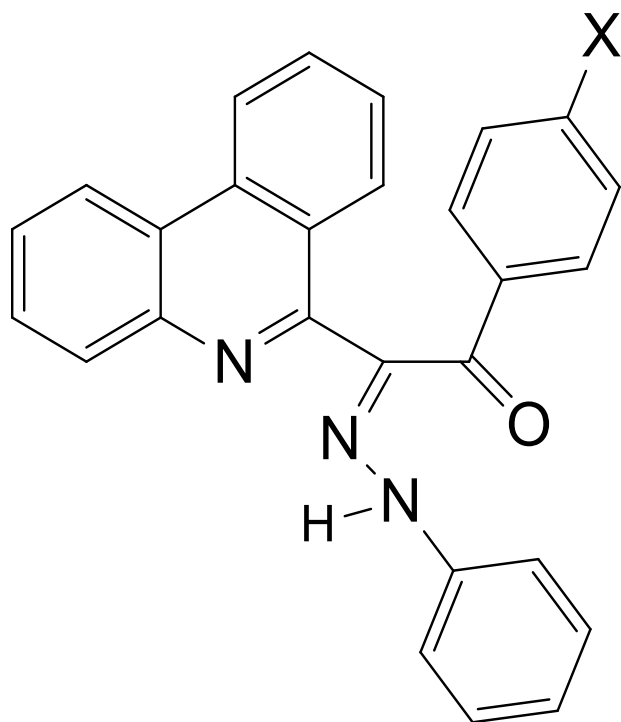
Scheme 1.1: Keto-Enol tautomerism in hydrazones

The relative abundance of these tautomers is pH-dependent. The keto form is more abundant in weakly acidic or neutral medium while the enol predominates at a higher pH (Eflhymiou *et al.*, 2009).

1.3. Preparative methods of hydrazones

The general method for the preparation of hydrazones is by refluxing an equimolar mixture of hydrazides (hydrazine derivatives) with aldehydes or ketones in ethanol for 3 - 8 hours. Glacial acetic acid (few drops) are sometimes added to catalyse these reactions (Diouf *et al.*, 2006). Recrystallisations of the products are usually done in ethanol.

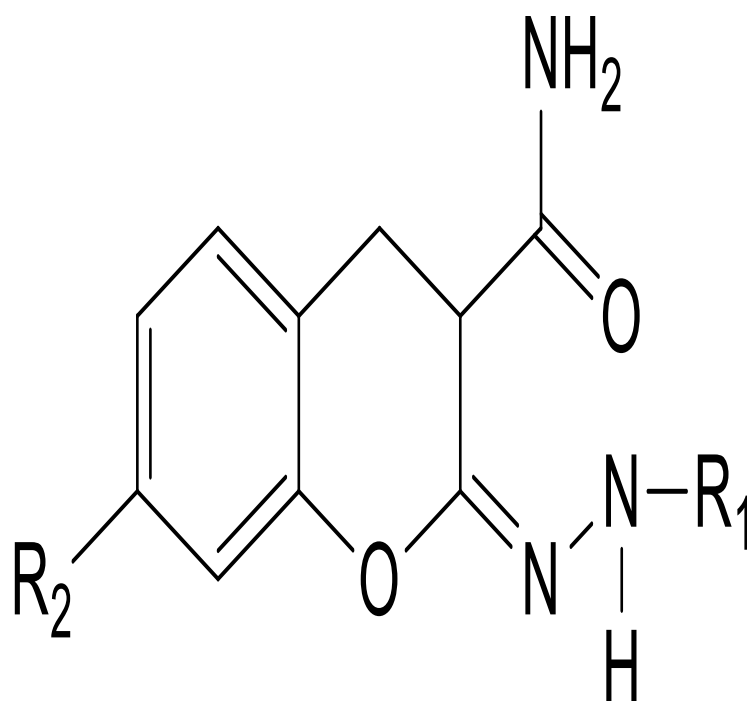
A method of coupling reaction of diazonium salts with active methylene compounds (Parmeter, 1959; Debnath *et al.*, 2015) has also been used in the synthesis of arylhydrazones. Hydrazone derived from 6-ketomethylphenanthridines was prepared by cooling the appropriate 6-ketomethylphenanthridines in an ice bath, followed by addition to benzene diazonium chloride in ethanol (Fig. 1.4). There was mild stirring of the reaction mixture, after which the precipitated solid was purified in ethanol.



X = OCH₃, Br, OH.

Figure. 1.4. Hydrazone derived from 6-ketomethylphenanthridines

In recent time, Microwave-assisted synthesis of organic compounds has been adopted (Ajani *et al.*, 2018). This method shortens the time required for synthesis which usually ranges from 2-6 hours for hydrazones to 2-5minutes. It also reduce the use of chemical solvents which may be harmful. The synthesis of 2-hydrazonecoumarins from the reaction of imine with arylhydrazines under reflux that should have lasted for 2 hours, took place in 2 minutes under microwave-assisted synthesis (Fig. 1.5)

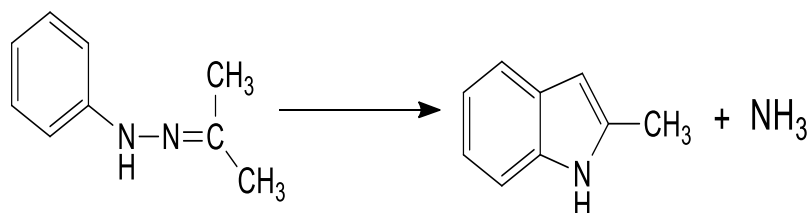


$R_1 = t\text{-Bu, Ph 4-NO}_2\text{C}_6\text{H}_4$; $R_2 = 6\text{-Cl, H}$

Figure 1.5. Microwave assisted synthesised hydrazonecoumarins

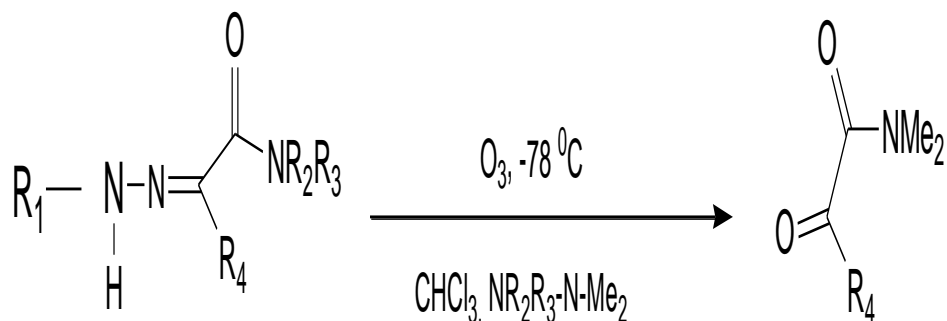
1.4 Chemical reaction of hydrazones

The two nitrogen atoms of the hydrazone group have been found to be nucleophilic with the azomethine nitrogen (C=N) more reactive (Kim, 2004). These properties have been useful in the preparation of some heterocyclic compounds. For example, in Fischer indole synthesis (Scheme 1.2), phenylhydrazones was heated in dehydrating acids or sometimes neutral medium to give indole or indole derivatives (Kim, 2004; Owolabi and Olarinoye, 2008)



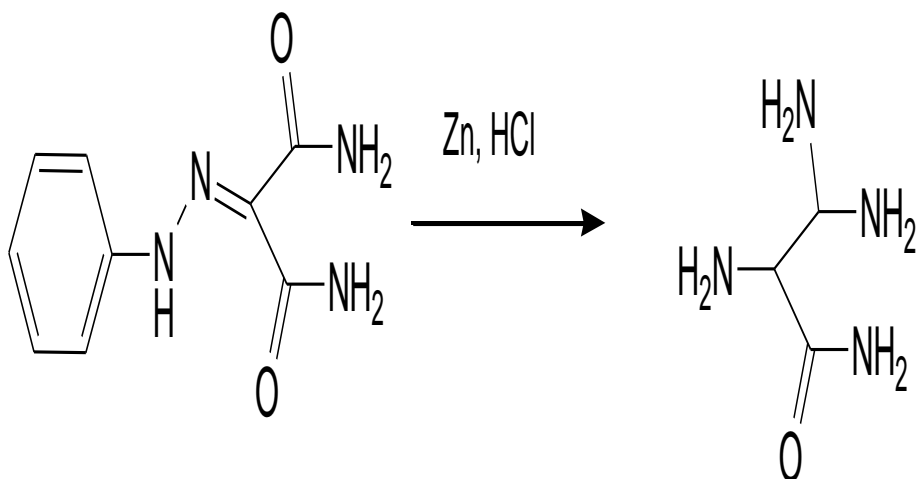
Scheme 1.2. Fischer indole synthesis

Hydrazone was found to undergo oxidative substitution reaction (Dell' erba *et al.*, 1996) in the presence of ozone gas at very low temperature, to form 1, 2-diketones. (Scheme 1.3)



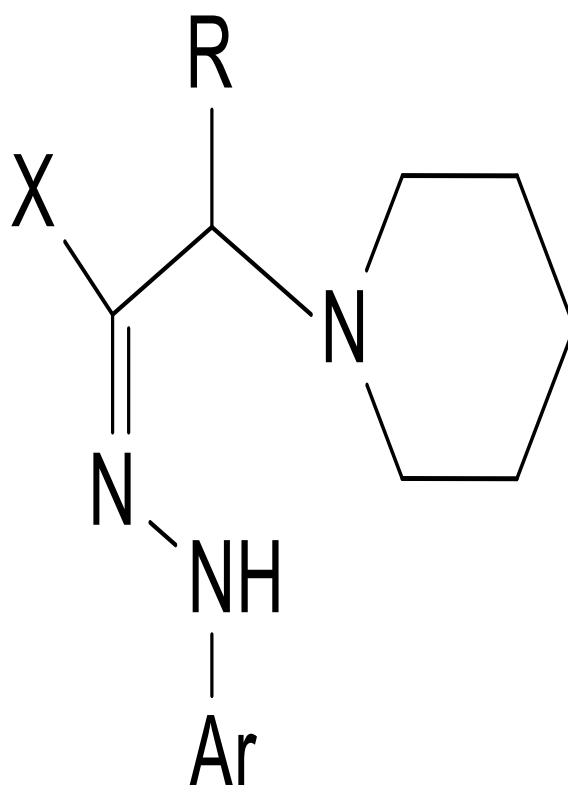
Scheme 1.3. Oxidative substitution of hydrazone

Hydrazone undergoes reduction reaction in the reaction of 2-phenylhydraacetamide with zinc metal in acid medium (Scheme 1.4). This leads to the cleaving of the hydrazone N-N bond, leading to the formation of 2, 3-diamino-3-aminopropanamide in quantitative yield (Shaw, 1950).



Scheme 1.4. Cleavage of the hydrazone N-N bond

Hydrazones were found to undergo reaction with Mannich reagents at the azomethine carbon to yield an intermediate product, which subsequently, undergoes Japp-Klingemann cleavage to give the final product (Fig.1.6) in good yields (Mustafa *et al.*, 1965).

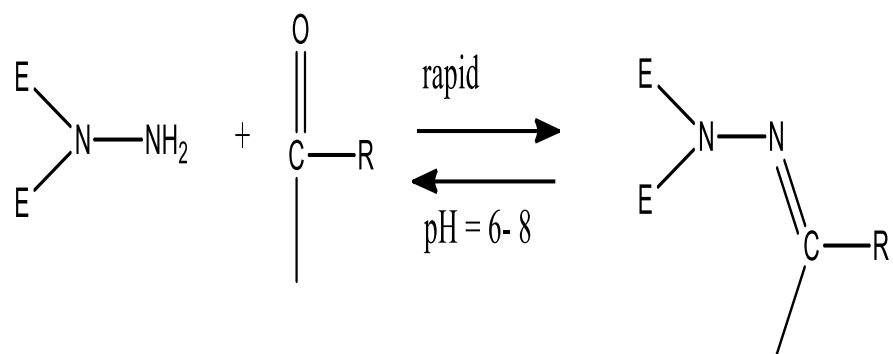


R= Ph, Alkyl

Figure 1.6. Hydrazone from Mannich reagents

1.4.1 Reversible reactions in hydrazones.

Reversible reactions have been reported to occur in some hydrazones that were formed from condensation of hydrazine derivatives (bearing electron withdrawing groups) with aromatic or aliphatic aldehyde (Scheme 1.5). They were found to hydrolyse in water at a pH that is neutral. Substituents on the ketone and hydrazide functionality were found to have affected the pH and stability towards hydrolysis (Christie *et al.*, 2010).



Scheme 1.5. Reversibility of hydrazone.

CHAPTER TWO

LITERATURE REVIEW

2.1 Metal(II) Complexes of hydrazones.

Hydrazones as an organic ligand has assumed great importance among bio-inorganic chemist because of their readiness to form complexes with metal ions, which can be studied as models for metalloenzymes in various biological processes. The coordination of hydrazone ligands are highly affected by factors such as metal ion, pH value, and counter ion (Anacona and Maria, 2015; Cao *et al.*, 2018). These ligands can bind in the keto or enol form depending on the acidity, the solvent and type of metal salts. Generally, aroylhydrazones can form coordinated compounds in keto form when in acidic solutions and enol-form in basic solutions (Ainscough *et al.*, 1998). They coordinate in the keto form on reaction with metal sulphates, nitrates, or perchlorates; in either keto- or enol-form with metal chlorides and in enol-form with metal acetates. (Seleem, 2011; Knittl, 2018). These versatility has given rise to monomeric, dimeric and polymeric forms of metal(II) complexes of hydrazones which also account for the various geometries exhibited by the first row transition metal complexes.

Hydrazones form coordination compounds using the oxygen atom of either carbonyl or the enol group and through the azomethine nitrogen atom, forming a five membered ring (Figure 2.1).

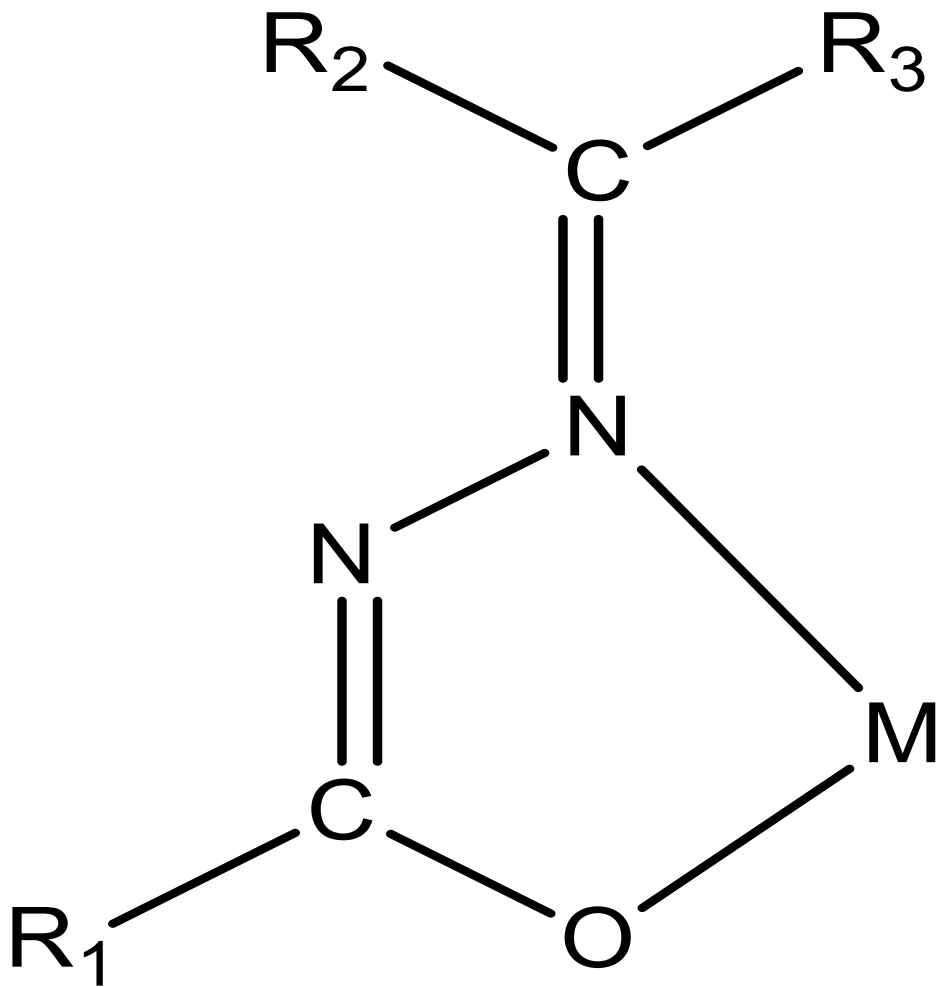
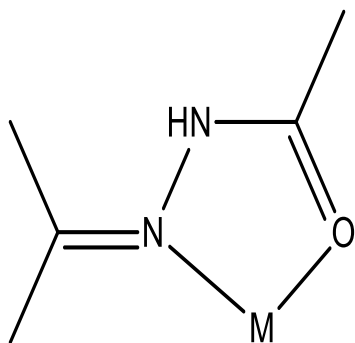
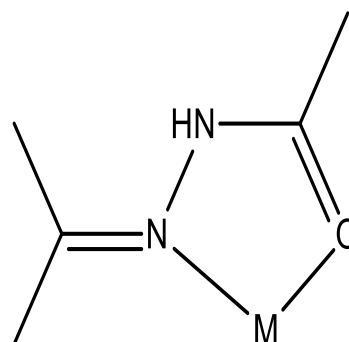


Figure.2.1. Typical bidentate coordination mode of hydrazones.

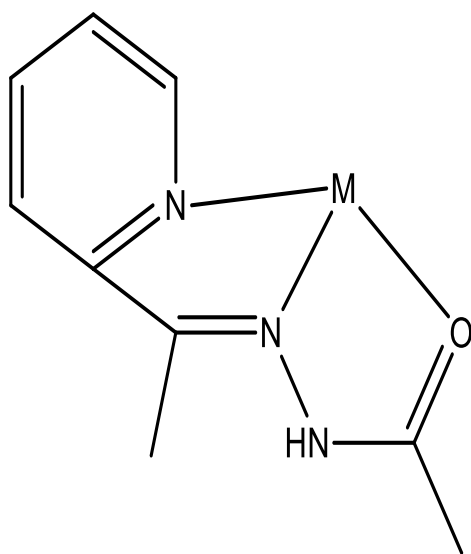
Hydrazones can behave as a bidentate, tridentate or polydentate chelating agent (Figure 2.2).



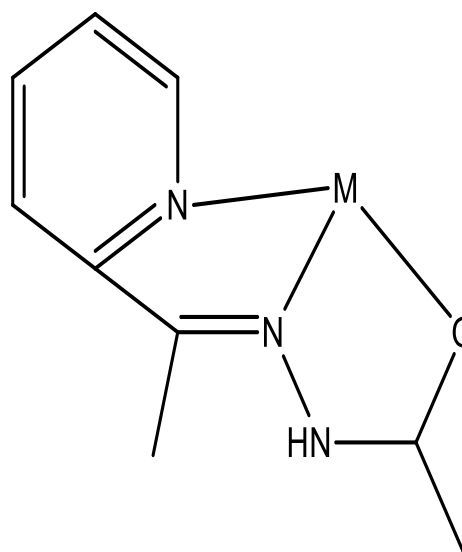
Neutral bidentate



Uninegative bidentate



Neutral tridentate



Uninegative tridentate

Figure 2.2. General modes of coordination of hydrazones.

Chelation of hydrazones with metal(II) ions was initially aimed at comparing biological activities of the metal chelates with the free ligands (Buu-Hoi, 1953).

However, Domiano *et al.*, 1975, synthesised bis(N-picolinylylidene-N' – salicyloylhydrazinato)nickel(II) and established with the aid of crystal structure, that the nickel(II) was octahedrally coordinated by two anionic ligands after they had been deprotonated. The ligands acted in tridentate mode by coordination through the azomethine nitrogen (C=N), the amide type oxygen and the pyridine nitrogen. There had recently been upsurge of interest in the study of compounds that contain hydrazide and hydrazone moieties and their complexes with transition metals (Devi and Singh, 2011; Gup, *et al.*, 2015).

Cu(II) and Ni(II) salts were reacted with the ligand: 6-amino-5-formyl-1, 3-dimethyluracil-benzoylhydrazone that is coded as (H₂BEZDO). The compounds were characterised by IR, electronic spectra, EPR spectroscopy and magnetic measurements. The results obtained from the analysis were in agreement with the proposed structure: [Ni(BEZDO)]·H₂O·NH₃; [Cu(BEZDO)]·H₂O·NH₃ and [Cu(BEZDO)(H₂O)]·H₂O. The structure of the four coordinated [Cu(BEZDO)(H₂O)]H₂O was determined by X-ray diffraction method (Fig. 2.3) and it revealed that the coordination environment around the Cu(II) atom was a square planar geometry with the dianionic ligand acting in tridentate mode. The fourth coordination site was completed with the oxygen atom from a water molecule (Hueso-Urena *et al.*, 2000).

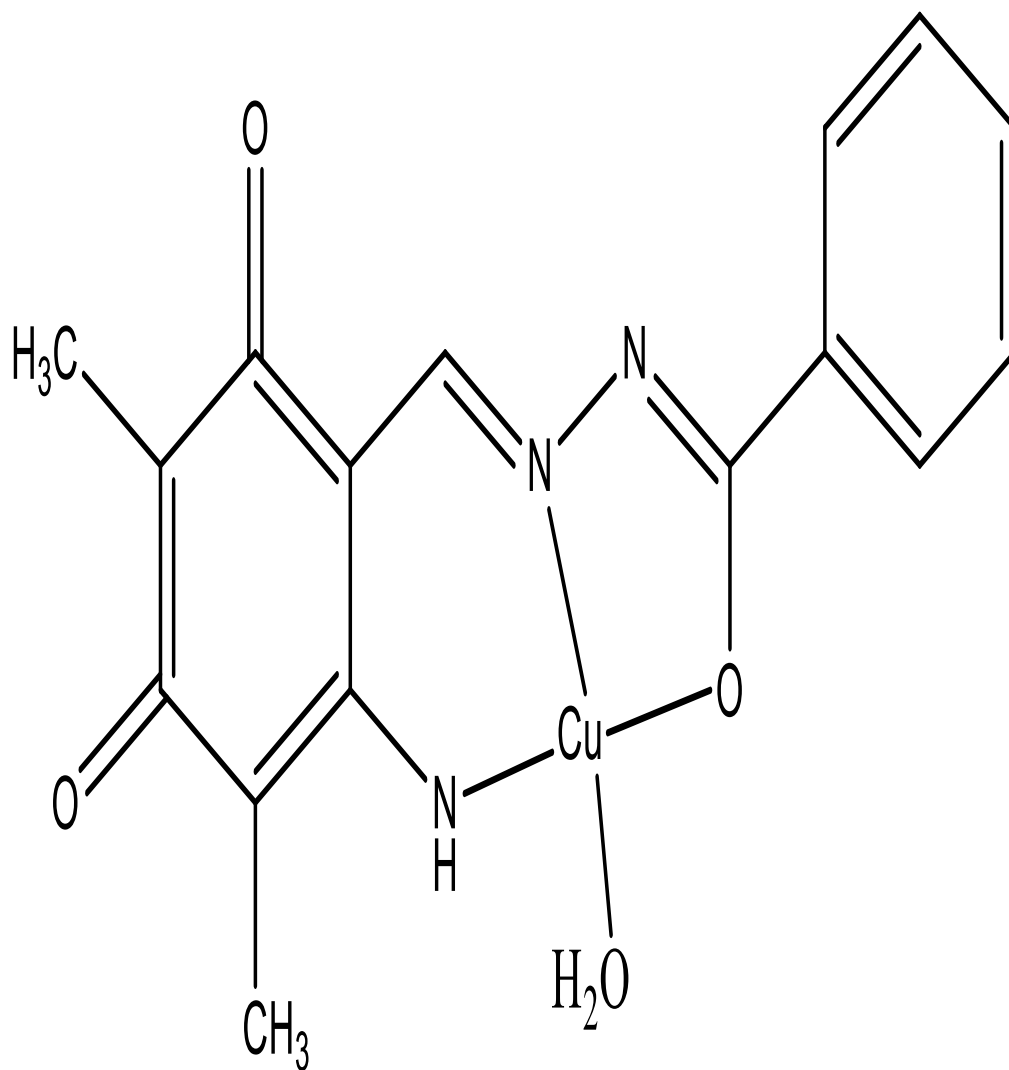


Figure 2.3. Coordination environment around [Cu(BEZDO)(H₂O)].

The theoretical studies of a polydentate ligand, *N*-(1-phenyl-3-methyl-4-propyl-pyrazolone-5)-salicylidene hydrazone (H_2L), and its Cu(II) complex $[Cu_2L_2CH_3OH] \cdot 2CH_3OH$ were investigated (Zhang *et al.*, 2010). The X-ray crystal analysis of the complex revealed that the two copper(II) centres displayed different coordination frameworks showing the versatility of hydrazone ligands. The theoretical calculation of the ligand and its deprotonated form had earlier indicated that the likely point for electrophilic attack were oxygen atoms and this agreed with the experimental data. (Fig.2.4.)

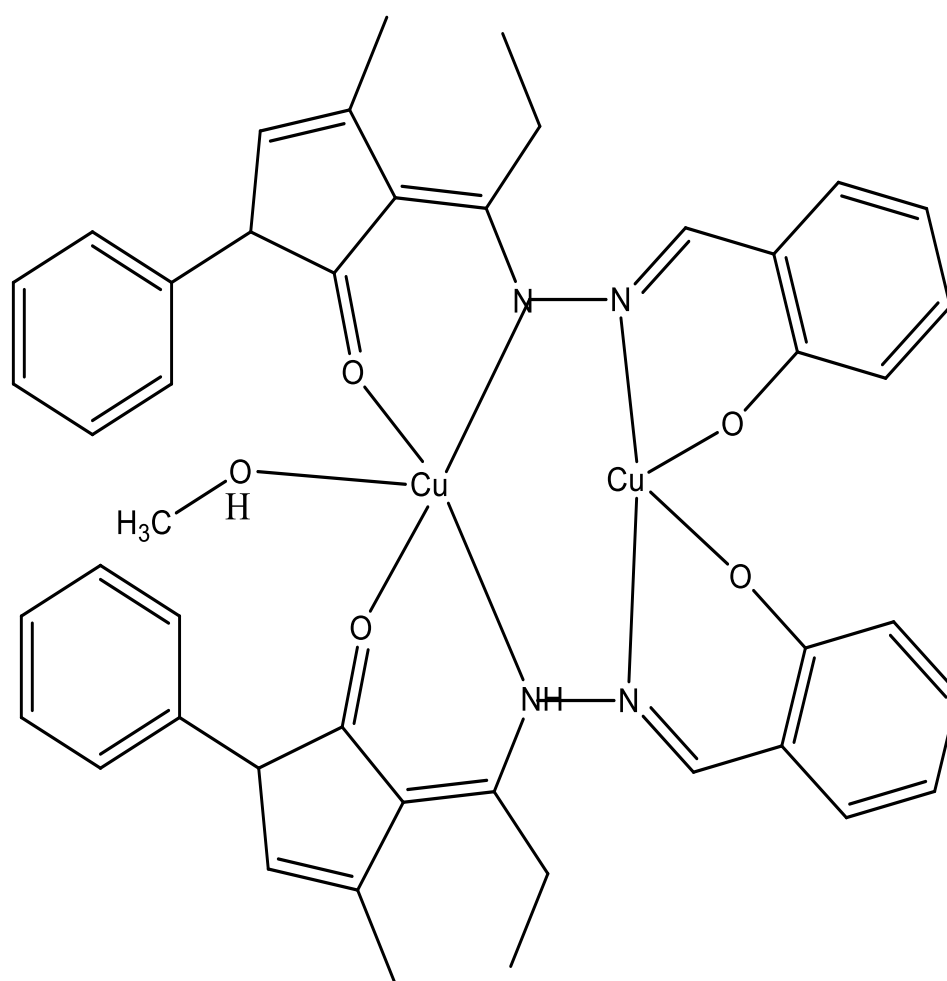


Figure 2.4. Two Cu centres having different geometries.

Jing-lin *et al.*, 2014, have reported metal(II) complexes of aroyl hydrazone namely: 1-methyl-4-nitro-1H-pyrrole-2-carbohydrazone and 1-methyl-4-nitro-2-(trichloroacetyl)pyrrole. The crystal structure of the Co(II) complex (Fig. 2.5) showed that each cobalt ion is octahedrally coordinated by O,N,O atoms of the uninegative ligand. The cobalt complex, which is dimeric in nature, has two bridging chloride ions. The sixth coordination sphere was filled by water molecule.

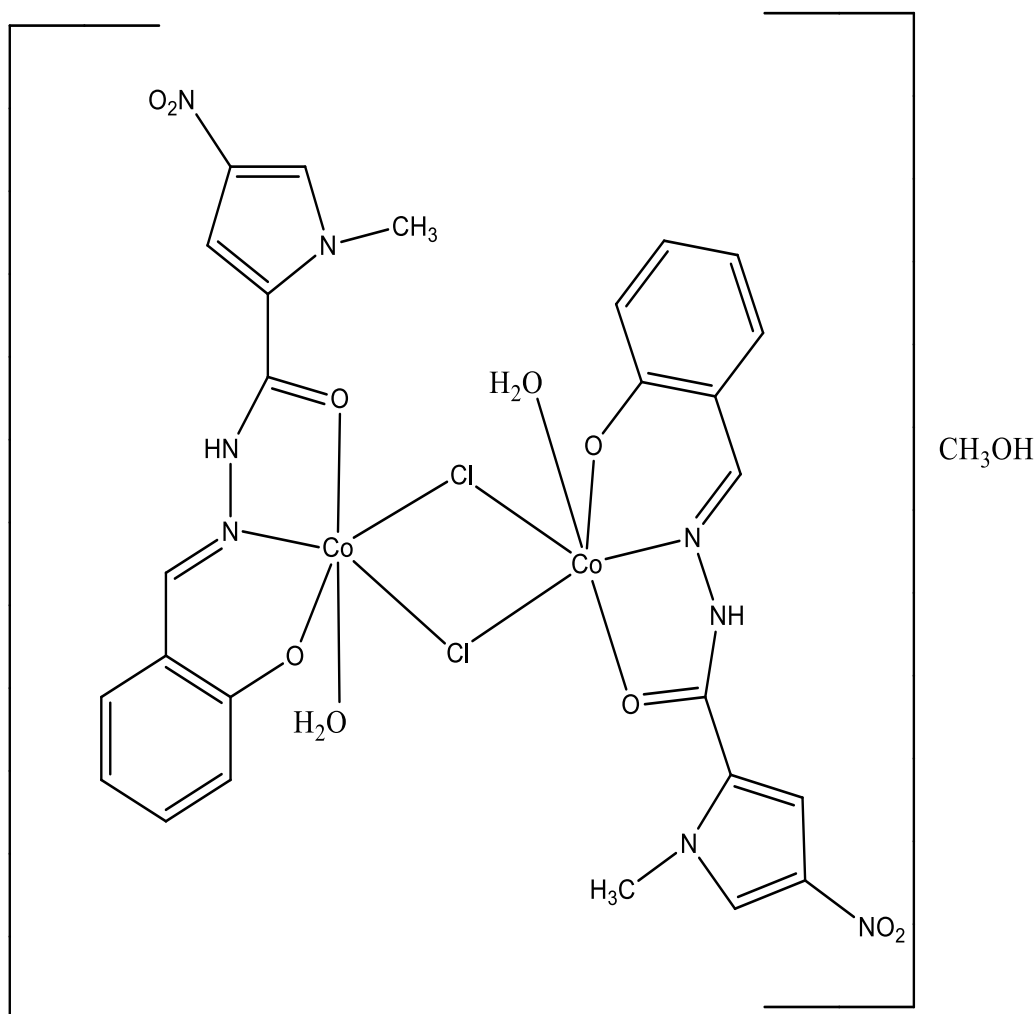


Figure 2.5. Co(II) hydrazone with bridging Chloride ligands.

Transition metal complexes of 3-isatin -2-thiophenecarbonyl hydrazone (H_2L_1), 3-isatin-2-furoic hydrazones (H_2L_2) and 3-(N-methyl)isatin (HL_3), having the formula $[M(L)_2] \cdot nX$, ($X =$ ethanol or/and water) have been synthesised. The ligands had a preferred keto form in solid state and the keto form was also the more pronounced tautomer in solution. They behaved as bidentate ligands through the N, O donor atoms in the cobalt(II) and zinc(II) complexes. The X-ray crystal structure of the pseudo tetrahedral zinc(II) complex revealed the N, O coordination mode of the mono deprotonated ligands (Rodríguez-Argüelles *et al.*, 2009).

Some new isatinic quinolyl hydrazone were reacted with Pd(II), VO(II), Fe(III), Co(II), Ni(II), and Cu(II) ions, leading to formation of various mononuclear and binuclear complexes. The bonding points were: (NO), $(NNO)^{2-}$ and $(NO)^-$. This underline its ambidentate and flexidentate characters. It was concluded that the various mode of bonding and basicity of the ligand was influenced by the type of the metal cation and the counter anion (chloro and sulphate ions) present. For instance, the Pd(II) complexes had the preferred square planar geometry (D_{4h} - symmetry). In studying the counter anion effect on the complexes formation, it was found that the isatinic hydrazone uses its lactim form in all the chloro complexes, whereas, lactam form was adopted in the sulfato complexes (Seleem, 2011).

2.2. Preparative methods of metal(II) complexes of Hydrazones.

Metal(II) complexes of hydrazones are generally prepared by the drop wise addition of ethanolic or methanolic solution of metal salts to the solution of ligand in a suitable solvent (commonly ethanol or methanol) with subsequent refluxing for a period ranging from 30 minutes to 12 hours on water bath or hot plate. Slow evaporation of the solvent for days usually lead to crystallisation of the product. The precipitate are washed with appropriate solvents and purified by recrystallisation (Domiano *et al.*, 1975; Shen and Jiang, 1995; Mostafa, 2011).

A modified method of preparation is a one-pot reaction of the hydrazide precursor, the carbonyl compound and the metal salts in a round bottom flask, using suitable solvent. This reactions are done under reflux for a period of 2-6 hours before precipitate of metal(II) complexes are formed. This procedure is called *in-situ* method of reaction (Howlader *et al.*, 2009; Gup *et al.*, 2015).

Metal(II) complexes of hydrazones are also prepared by stirring the reactants together in a beaker at room temperature. Suitable solvent such as alcohol or mixture of solvents such as methanol/acetone (1:1) can be used where the ligand is insoluble or sparingly soluble in one solvent. The reaction can proceed for 30 minutes to 72 hours before precipitate are formed (El-Sherif, 2009; Mohanan and Murakan, 2005)

2.3 Infrared spectra of metal(II) complexes of hydrazone

Four bands are diagnostic in the infrared spectra of hydrazones. These are: $\nu(\text{N-H})$, $\nu(\text{C=O})$, $\nu(\text{C=N})$ and $\nu(\text{N-N})$ frequencies (Shen and Jiang, 1995; Chen *et al.*, 2010; Knittl *et al.*, 2018). The band due to $\nu(\text{N-H})$ usually occur between 3,100 - 3,300 cm^{-1} , while the $\nu(\text{C=O})$ band is usually found between 1620 - 1710 cm^{-1} , although it has been observed as low as 1600 cm^{-1} in some hydrazones..

The azomethine $\nu(\text{C=N})$ stretching vibration and the $\nu(\text{N-N})$ bands have been observed between 1500 cm^{-1} – 1580 cm^{-1} and 1100 cm^{-1} – 910 cm^{-1} respectively. *o*-Vanillin acetylhydrazone (Diouf *et al.*, 2006) showed bands assigned to $\nu(\text{O-H})$ at 3480 cm^{-1} , $\nu(\text{C=O})$ at 1680 cm^{-1} , $\nu(\text{C=N})$ at 1580 cm^{-1} and $\nu(\text{C-O})$ at 1252 cm^{-1} . The ligand, *o*-methoxybenzaldehyde benzoylhydrazone (*o*-MBH) showed three bands located at 3130 cm^{-1} , 2986 cm^{-1} and 2900 cm^{-1} assigned to $\nu(\text{N-H})$, $\nu(\text{C-H})$ (aromatic) and $\nu(\text{C-H})$ vibrations respectively. The characteristic sharp bands at 1646 cm^{-1} , 1600 cm^{-1} , 1296 cm^{-1} and 1250 cm^{-1} were assigned to $\nu(\text{C=O})$ (amide I), $\nu(\text{C=N})$ (azomethine), $\delta(\text{C-O})$ (methoxy) and $\delta(\text{N-H})$ modes, respectively in the *o*-methoxybenzaldehyde benzoylhydrazone (Adekunle *et al.*, 2010).

In order to study the mode of bonding of ligands to metal ions in the complexes, the infrared of free ligands are usually compared with the spectra of the metal complexes (Alhadi *et al.*, 2012). In a study of complexes of Mn(II), Fe(II), Co(II), Ni(II), Cu(II) and Zn(II) with a bishydrazone (Mohanan and Murakan, 2005), the structurally significant bands: $\nu(\text{N-H})$, $\nu(\text{C=O})$, $\nu(\text{C=N})$ and $\nu(\text{N-N})$ were found to occur at 3198 cm^{-1} , 1637 cm^{-1} , 1612 cm^{-1} and 994 cm^{-1} in the ligand respectively. These bands shifted marginally in the complexes to 3216 cm^{-1} , 1642 cm^{-1} , 1587 cm^{-1} and 1012 cm^{-1} respectively. The shifts in these bands indicated interaction between the ligands and the metal ion. In addition, there were new bands in the spectra of the metal(II) complexes at 514 cm^{-1} and 466 cm^{-1} which were attributed to new metal - oxygen bond $\nu(\text{M-O})$ and metal to nitrogen bond $\nu(\text{M-N})$ respectively. The presence of these new bands provided further

evidence of metal-ligand complex formation (Knittl *et al.*, 2018). Presence of coordinated water molecules in complexes are usually revealed by broad bands between 3400 - 3500 cm^{-1} (Nakamoto, 1997; Hosny *et al.*, 2010).

The presence of anions like the nitrate, sulphate and acetate ions in metal complexes have been well studied with the aid of infrared spectra since some of the anions are infrared active (Nakamoto, 1997., Devi and Singh, 2011; Agarwal *et al.*, 2006).

In metal complexes with nitrate ions, three (N-O) stretching bands are observed between 1455 – 1385 cm^{-1} , (ν_5); 1305 - 1315 cm^{-1} , (ν_1) and 1015 - 1030 cm^{-1} , (ν_2). The separation of the two highest frequency bands ($\nu_5 - \nu_1$) have been used to differentiate between unidentate and bidentate coordination of the nitrate anion (Nakamoto, 1997; Diouf, 2006; Salem *et al.*, 2015).

The free sulphate ion has a symmetry with T_d point group. Out of the four fundamental vibrations in sulphate ion, only ν_3 and ν_4 are infrared active, and these bands occur between 1060 – 1130 cm^{-1} [$\nu(\text{SO})$] and between 600 - 700 cm^{-1} [$\nu(\text{OSO})$] vibration modes. The ν_1 stretching ($\nu(\text{SO})$) and bending $\delta(\text{OSO})$ fundamentals are not infrared active (Eflhymiou *et al.*, 2009).

Coordination of acetate anion ligand is usually revealed on the infrared spectra of metal(II) complexes by the presence of two bands. The first band ranges between 1510 - 1640 cm^{-1} and it is ascribed to the $\nu_{\text{asymmetric}}$ carboxylate ion (COO^-) and the second is the $\nu_{\text{symmetric}}$ carboxylate ion (COO^-) which range from 1370 cm^{-1} to 1450 cm^{-1} . The difference between the values of the $\nu_{\text{symmetric}}$ and $\nu_{\text{asymmetric}}$ ($\nu_{\text{asy}} - \nu_{\text{sym}}$) had been applied to differentiate between bidentate and unidentate mode of coordination for the acetate anion (Agarwal, *et al.*, 2006; Seleem, 2015). A difference of less than 200 cm^{-1} in the values of ($\nu_{\text{asy}} - \nu_{\text{sym}}$) are ascribed to bidentate mode while values greater than 200 cm^{-1} are usually ascribed to unidentate mode of coordination for the acetate ligand.

2.4 Electronic spectra of metal(II) Hydrazones

Electronic spectra of hydrazone metal complexes had been studied and absorption bands due to intraligand transitions, intramolecular charge transfer and visible region d-d transitions were observed. In the ultraviolet region, which is between 200 - 400 nm ($50,000\text{ cm}^{-1}$ - $25,000\text{ cm}^{-1}$), significant intraligand transitions in this area include $\pi - \pi^*$ and n- π^* transitions (Devi and Singh, 2011; Debnath *et al.*, 2015)

The electronic spectrum of a mononucleating hydrazone ligand, formed by condensing salicyloylhydrazine and (2-formylphenoxy) acetic acid exhibited bands between $37,878\text{ cm}^{-1}$ - $32,786\text{ cm}^{-1}$ due to $\pi - \pi^*$ transitions, and another band between $26,945\text{ cm}^{-1}$ - $27,520\text{ cm}^{-1}$ due to n- π^* transitions of the imine functional group. In the complexes, these bands were shifted to higher or lower wavenumber values indicating coordination of the ligand to metal ions (Baliga and Revankar, 2006).

The ligand, 2-carboxyphenylhydrazoacetanilide showed bands at $33,670\text{ cm}^{-1}$, $28,612\text{ cm}^{-1}$ and $25,126\text{ cm}^{-1}$ assigned to $\pi - \pi^*$, n- π^* and charge transfer (CT) transitions within the molecule (Mostafa, 2011). These bands had a blue shift in all the complexes.

An intramolecular charge transfer band in some hydrazone complexes had been observed at $23,500$ - $24,800\text{ cm}^{-1}$. In a study of synthesis, and structural elucidation of azo/hydrazone tautomeric equilibrium of 1,3-dimethyl-5-(arylo)-6-amino-uracil (Debnath *et al.*, 2015), two absorption bands in the range of $38,461\text{ cm}^{-1}$ - $37,037\text{ cm}^{-1}$ and $27,770\text{ cm}^{-1}$ - $24,096\text{ cm}^{-1}$ were seen in the spectrum. The former band was assigned to the $\pi - \pi^*$ transitions within the aromatic moiety, while the latter absorption band was attributed to an overlap of n - π^* and $\pi - \pi^*$ transition within the hydrazone/azo form of the dyes (Toro *et al.*, 2008). The strong $\pi - \pi^*$ transition generally overrides the feeble n - π^* transitions and might obscure it from being observed in the spectra.

The visible region of the electronic spectrum ($25,000$ - $10,000\text{ cm}^{-1}$) usually reveals d-d transitions within the metal complexes and suggests the geometry or the kind of environment in which the metal ion is present (Ainscough *et al.*, 1998; Housecroft and Sharp, 2008). Nickel(II) complexes usually show three transitions in octahedral environment. The absorption bands in the region $8,000$ - $13,120\text{ cm}^{-1}$ (ν_1), $14,780$ - $19,000\text{ cm}^{-1}$ (ν_2), and $25,000$ - $29,000\text{ cm}^{-1}$ (ν_3), are assigned to ${}^3A_{2g}(F) \rightarrow {}^3T_{2g}(F)$ (ν_1),

${}^3A_{2g}(F) \rightarrow {}^3T_{1g}(F)$ (ν_2), and ${}^3A_{2g}(F) \rightarrow {}^3T_{1g}(P)$ (ν_3) transitions in an octahedral geometry (Gupta *et al.*, 2007; Odunola *et al.*, 2003)

Nickel(II) complexes of benzyl bis-hydrazone macrocyclic Schiff bases showed three bands at $10,992\text{ cm}^{-1}$ (ν_1), $15,259\text{ cm}^{-1}$ (ν_2), and $21,968\text{ cm}^{-1}$ (ν_3), assigned to ${}^3A_{2g}(F) \rightarrow {}^3T_{2g}(F)$, ${}^3A_{2g}(F) \rightarrow {}^3T_{1g}(F)$, and ${}^3A_{2g}(F) \rightarrow {}^3T_{1g}(P)$ respectively, which indicated octahedral geometry for the complexes (Lakshmi *et al.*, 2011).

Electronic spectra of six-coordinate Cu(II) complexes have either D_{4h} or C_{4v} symmetry, and the 2E_g and 2T_g level of the 2D free-ion term will split into ${}^2B_{1g}$, ${}^2A_{1g}$, ${}^2B_{2g}$ and 2E_g levels. Thus, three spin allowed transitions are expected in the visible and near infrared region, but only few complexes are known in which such bands are resolved. These bands may be assigned to the following transitions, $10,928 - 12,190\text{ cm}^{-1}$ ($d_{x^2-y^2} \rightarrow d_z^2$) (ν_1); $18,860 - 21,790\text{ cm}^{-1}$ ($d_{x^2-y^2} \rightarrow d_{xy}$) (ν_2) and $26,570 - 28,160\text{ cm}^{-1}$ ($d_{x^2-y^2} \rightarrow d_{zx}$, d_{yx}) (ν_3) (Housecroft and Sharpe, 2008)

The spectral of metal(II) complexes of copper on many occasions show a single, poorly resolved broad band, assignment of which is usually determined by the position of the band (Cotton *et al.*, 2003; Diouf *et al.*, 2006). The d-d transition occurs at $13,000\text{ cm}^{-1}$ in the octahedral complexes (Lakshmi *et al.*, 2011). The band considerably exhibit blue shift due to Jahn-Teller distortion, and in extreme case, it occurs in the region $16,600 - 14,500\text{ cm}^{-1}$ in square planar complexes while in square pyramidal complexes, it is observed in the region $18,800\text{ cm}^{-1} - 15500\text{ cm}^{-1}$. The spectra of two copper(II) complexes of glyoxal salicylaldehyde-acyldihydrazones (Singh and Gupta, 2008), showed broad bands centred at $14,640\text{ cm}^{-1}$ and $14,450\text{ cm}^{-1}$ which may be assigned to superimposed transitions ${}^2B_{1g} \rightarrow {}^2B_{2g}$ and ${}^2B_{1g} \rightarrow {}^2E_g$ respectively, suggesting a distorted octahedral configuration. Conversely, Cu(II) complexes of 4-hydroxy-4-methyl-2-pentanone-1-H-benzimidazol-2-yl-hydrazone, showed a broad band in the region $18,181 - 21,978\text{ cm}^{-1}$. The position and shape of this band suggested the merging of the three electronic transitions ${}^2B_{1g} \rightarrow {}^2B_{2g}$, ${}^2B_{1g} \rightarrow {}^2A_{1g}$ and ${}^2B_{1g} \rightarrow {}^2E_g$. A square planar geometry was suggested for the complex. Two copper(II) complexes of 4-hydroxyacetophenone-4-aminobenzoylhydrazones showed only one broad absorption band at $12,760\text{ cm}^{-1}$ and $16,110\text{ cm}^{-1}$ which were assigned to the ${}^2E_g \rightarrow {}^2T_{2g}$ indicating an octahedral geometry (Singh *et al.*, 2009)

2.5 Magnetic moment of metal(II) hydrazones.

A spin-only magnetic moment of 2.83 B. M is expected for a nickel(II) ion in an octahedral field. However, an experimental magnetic moments of 2.9 – 3.4 B. M. are usually observed due to spin–orbit coupling of the $^3A_{2g}$ and $^3T_{2g}(F)$ terms (Housecroft and Sharpe, 2008). In a tetrahedral field, higher moments than spin only value (3.5 – 4.2 B. M.) are expected due to large orbital contributions. Ni(II) complex of hydrazone derived from benzofuran-2-carbohydrazide and 2-acetylthiopene showed magnetic moment of 2.95 B. M. which was slightly higher than the spin only value, indicating an octahedral environment (Halli *et al.*, 2011). Magnetic moments in the range 2.98-.3.15 B. M. were similarly reported for Ni(II) complexes of cinnamaldehyde hydrazone indicating octahedral geometry (Uma *et al.*, 2010).

Nickel(II) complexes having tetrahedral geometry usually have values in the range of 3.5 - 4.2 B. M. This is as a result of large orbital contribution, and is known to diminish markedly with increasing temperature. In the study of nickel(II) complexes of isatin-3, 2'-quinolyl-hydrazones having the general formula $[Ni(L)X]$; (where $X = Br^-$, ClO_4^- , Cl^- , NO_3^- , CH_3COO^-) and their adducts $Ni(L)X \cdot 2Y$ (where $Y =$ dioxane or pyridine; and $X = Cl^-$, Br^- , ClO_4^- , NO_3^-), it was found that the room temperature magnetic moment of the compounds were in the range of 3.78 – 3.94 B. M. Hence, it was concluded that the complexes had tetrahedral geometry in solid state (Gupta *et al.*, 2007). Similarly, Alhadi *et al.*, (2012) have reported a magnetic moment value of 3.4 B. M, for Ni(II) complexes of 5-bromo-2-hydroxybenzylidene-3,4,5-trihydroxybenzohydrazide. This result showed that the Ni(II) complex is paramagnetic and had a high spin tetrahedral configuration with a ground state of $^3T_1(F)$. Square planar Ni(II) complexes are diamagnetic since a spin singlet is the ground state. (Ozmen and Olgun, 2008).

The magnetic moments usually observed for magnetically dilute copper(II) complexes is between 1.70 – 2.20 B. M, with compounds whose geometry approaches octahedral having moments at the lower end and those approaching tetrahedral geometry at the higher end (Earnshaw and Greenwood, 1984; Patel and Woods, 1990). A magnetic moment of 1.80 B. M was reported for copper(II) complex of 2-hydroxybenzaldehyde-(4,6-dimethylquinolin-2-yl)-hydrazone, which therefore suggested a distorted octahedral structure for the complex. However, unusual values of 1.1 B. M. had been observed for dimeric copper(II)chloro-N-(-2-hydroxypropyl)salicylaldimine. (Bertrand

et al, 1970). This phenomenon is due to antiferromagnetic interaction between the copper metal centres that lowers the magnetic moment compared to the spin only value. Similarly, Osowole *et al*, 2015 had reported a magnetic moment of 0.86 B. M. for Cu(II) complexes derived from mixed-drugs of aspirin and vitamin B₃. Occurrence of strong antiferromagnetic interaction between these dimeric copper(II) complexes was reported to be responsible for the unusually low moments.

The observed values of magnetic moment for cobalt(II) complexes are generally diagnostic of the coordination geometry about the metal ion. Low-spin square-planar cobalt(II) complexes have been reported to have values ranging from 1.7 - 2.9 B. M, arising from one unpaired electron coupled with a large orbital contribution. Both tetrahedral and high-spin octahedral cobalt(II) complexes have three unpaired electrons but may be distinguished by the magnitude of the deviation of the effective magnetic moment from the spin-only value. The magnetic moment of tetrahedral cobalt(II) complexes with an orbitally non degenerate ground term is increased above the spin-only value via contribution from higher orbitally degenerate terms and is in the range 4.2 – 4.7 B. M (Nawar and Hosny, 1999). Octahedral cobalt(II) complexes however maintain a large contribution due to ⁴T_{2g} ground term and exhibit μ_{eff} in the range 4.8 – 5.6 B. M. Argawal *et al*, 2005, reported the magnetic moments of cobalt(II) complexes of N-Isonicotinamido-2',4'-dichlorobenzalaldimine in the range 4.7 – 5.1 B. M, suggesting that the complexes are paramagnetic with three unpaired electrons, and have high-spin octahedral configuration. However, deviations from expected values are frequently encountered. A magnetic moment of 3.26 B.M was reported for tetrahedral cobalt(II) complex of aminoindanyl Schiff base, which is lower than the expected value of 4.2 - 4.7 B. M. This low magnetic moment was attributed to the phenomenon of anti-ferromagnetism that was present among the cobalt metal centres. (Osowole and Balogun, 2012).

2.6. Biological properties of hydrazone compounds

Hydrazones moieties bearing azomethine -NHN=CH- proton are useful and promising for new drug development (Rollas and Kucukgel, 2007). This has therefore, inspired many researchers to synthesise compounds of hydrazones and to evaluate their biological activities with a view to discover new antimicrobial agents. The pioneering work of Buu-hoi *et al* (1953), was significant in this direction, as they were able to synthesise new hydrazones that had lower toxicity than the hydrazides precursors. This was possibly due the blockage of -NH_2 - group of the hydrazides. Iproniazide, a hydrazone compound (Fig. 2.6), just like isonicotinic acid hydrazide, is applied for the treatment of tuberculosis, and also possess antidepressant effect. Patients are said to be in a better mood during the treatment with iproniazide (Rollas and Kucukguzel, 2007).

The spread of multi drug-resistant *Plasmodium falciparum* has brought to fore the need to discover new antimalarial drugs. In line with this, aroylhydrazone chelator: 2-hydroxy-1-naphthylaldehyde-isonicotinoylhydrazone was synthesised and found to show greater antimalarial activity than desferrioxamine against chloroquine-resistant parasite (Walcourt *et al.*, 2004).

Furthermore, several hydrazones and their derivatives have been synthesised and found to exhibit good antimicrobial activities against several Bacteria and Fungi (Anacona and Maria, 2015; Ajani, *et al*, 2018). Some metal(II) complexes of unsymmetrical Cinnamaldehyde-hydrazone were studied for biological activity against bacteria (gram positive and gram negative) and fungi. The study concluded that manganese(II) complex of the hydrazone had good inhibitory activity against the tested bacteria and fungi. (Cao *et al.*, 2018)

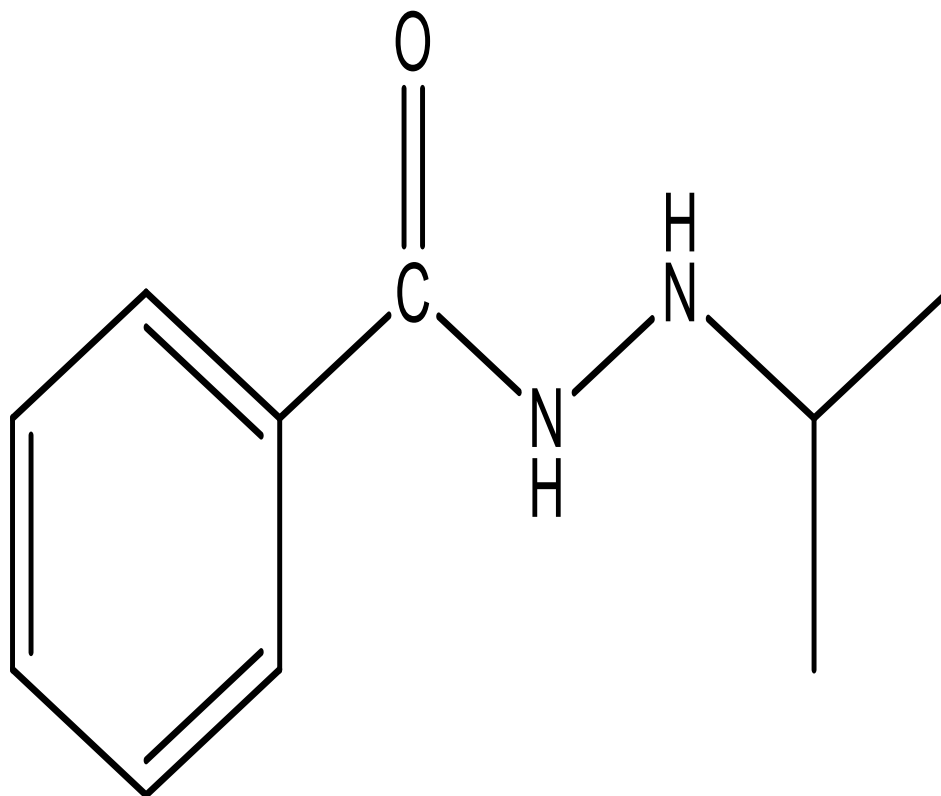


Figure 2.6. Structure of Iproniazide

Metal chelation with organic compounds has been known for decades to enhance the biological activities of hydrazones (Buu-Hoi *et al*, 1953; Anacona and Maria, 2015). A substantial number of metal(II) hydrazones had been synthesised and their biological activity studied and reported (Shen and Jiang, 1995; Rollas and Kucukgel, 2007).

Copper(II) and zinc(II) complexes of 4-hydroxyacetophenone oxaloyldihydrazone and acylhydrazone was found to show appreciable antimicrobial activity against some fungi when compared with the ligands. This may be due to the chelation of the ligand with the metal, which increases the lipid solubility of the compounds, thereby facilitating its passage through the lipid layer of the fungi membrane (Singh and Singh, 2008). Copper(II) salicylaldehyde benzoylhydrazone was found to be an effective inhibitor of DNA synthesis and cell growth. The copper(II) complex also found to be more potent than the uncoordinated ligand (Ainscough *et al.*, 1998). Six lanthanides complexes of the ligand: 3, 5-dibenzoyloxybenzoyl-2, 4-dihydroxybenzaldehyde hydrazone were

studied and discovered to have good scavenging abilities on 2, 2-diphenyl-picrylhydrazyl radicals. The metal complexes similarly had better scavenging abilities than the uncoordinated ligand (El-Sherif, 2009). The antibacterial activity of some sulfonyl hydrazones and their metal complexes were studied in-vitro and the results showed that the compounds had considerable inhibitory activity against the tested organisms. (Ozmen and Olgun, 2008).

Transition metal complexes of aryl hydrazones have been reported to be effective inhibitors of cell growth, DNA syntheses and also act as DNA-binding agents. These compounds exhibit moderate to strong DNA binding ability due to planar fragment of the hydrazone ligands which can intercalate between DNA base pairs. These structural similarities of hydrazone Schiff bases with neutral biological systems have enabled researchers to study metal complexes of hydrazones as models for metallo-enzyme active sites. In addition, the imine groups present in the hydrazone ligands are utilized in elucidating the mechanism of transformation of racemisation reactions in biological system (Shen *et al.*, 2017).

2.7. Application of hydrazone compounds.

Hydrazones compounds have been used as catalyst in various chemical and photochemical reactions. For example, ethylene oligomerisation has been found to be an effective method in the conversion of ethylene into useful fine chemicals such as, environmentally suitable fuels, plastics, lubricants, surfactants and feedstock for linear low-density polyethylene. Ethylene oligomerisation was therefore investigated using nickel(II) complexes of hydrazone namely 4, 5-diazafluorene-9-one-benzoylhydrazone; 4, 5-diazafluorene-9-one-4-nitrobenzoylhydrazone and 4, 5-diazafluorene-9-one-3-nitrobenzoylhydrazone as catalyst, with methylaluminoxane (MAO) in a solvent. These catalytic systems assisted the dimerisation of ethylene with good yield. The nickel(II) complex without nitro-substituent on its aryl ring was found to be the better catalyst (Chen *et al.*, 2003).

Some arylhydrazinatonicel(II) complexes form novel family of metal-containing liquid crystals with high thermal stability and a wide variety of liquid phases (Howlader *et al.*, 2009). This property can be utilised to develop promising molecular materials for technological application like electro-optical memory devices, solar cell and

semiconductors. Similarly, dye-sensitized solar cells (DSSCs) are looked upon as the future generation of photovoltaic cells. In view of this, aromatic hydrazone derivatives have been widely studied and applied as hole-transporting materials for electrophotographic photoreceptors and as organic nonlinear optical devices. The main advantages of these compounds are simple synthesis and their rapid charge-transporting ability (Urnikaite *et al.*, 2015). Benzoyl hydrazone derivatised coumarin ligand has been shown to be a copper(II) selective fluorescent chemosensor which can be used for bio imaging (Huang, 2011).

The discovery of new blue-ray discs (BDs) techniques, which is a new generation optical disk format and possessing the ability to offer more than 5 times the storage capacity of traditional DVDs on a single-layer disk; has generated a renewed interest in the upgrading and updating of recording materials for the new generation of blue laser (405 nm) recording media. Nickel(II) hydrazonate thin film had been experimented and used as recording layer for static optical recording and results suggested that the hydrazone complex could be promising in producing a good optical recording platform for blue-ray disc-recordable system (Chen *et al.* 2010).

2.8. Aim of the work

Aroylhydrazones and their metal(II) complexes have been of interest to researchers due to their relative ease of preparation, tendencies towards crystallinity and their potency to form stable complexes with most of the transition metal ions, in addition to their abilities to inhibit the growth of microorganisms. A search in the literature revealed that aroylhydrazone compounds derived from condensation of benzoylhydrazide (and its substituted analogues) with various ketones and aldehydes have been synthesised and reported. However, information on the ligand; benzylacetone-benzoylhydrazone and its *p*-hydroxy- and *p*-nitro- substituted analogues, which can be derived from the reaction of benzoylhydrazide, *p*-hydroxyl-benzoylhydrazide and *p*-nitro- benzoylhydrazides with benzylacetone, are not available. In addition, the copper(II), nickel(II) and cobalt(II) complexes of these ligands have not been investigated. The aim of this study was to synthesise and characterise metal(II) complexes of these ligands and evaluate their antibacterial properties.

2.9 The Specific Objectives of the Research

To synthesise and characterise the following ligands:

- Benzylacetone-benzoylhydrazone (babh)
- *p*-hydroxyl-benzylacetone benzoylhydrazone (*p*-OH-babh)
- *p*-nitro-benzylacetone benzoylhydrazone (*p*-NO₂-babh),
- Synthesise and characterise the Cu(II), Ni(II) and Co(II) complexes of these ligands using their chloride, nitrate, acetate and sulphate salts.
- Characterise the compounds using physicochemical methods: melting point determination, percentage metal analysis, microanalysis (C. H. N), magnetic susceptibility measurement, conductivity measurement, proton nuclear magnetic resonance (¹H NMR), carbon-13 nuclear magnetic resonance (¹³C NMR), infrared (IR) and electronic spectral (UV-Vis).
- Study the effect of the various counter anions on the physical, chemical and biological properties of the synthesised compounds.
- Carry out Antibacterial activity studies of the synthesised compounds against some selected microorganisms to determine their potency as antibacterial agents.

CHAPTER THREE

EXPERIMENTAL

3.1 Materials

Analar grade reagents and solvents were obtained from Sigma-Aldrich and British Drug Houses (BDH) Chemicals Limited. The reagents were used without further purification. The organic solvents were of analar grade and used without purification. The organisms used for bioassay were obtained from the Department of Pharmaceutical Microbiology, Obafemi Awolowo University, Ile-Ife.

3.1.2. Reagents and Solvents

Reagents and solvents used were copper(II) chloride dihydrate, copper(II) acetate monohydrate, copper(II) sulphate pentahydrate, copper(II) nitrate tetrahydrate, nickel(II) chloride hexahydrate, nickel(II) acetate tetrahydrate, nickel(II) sulphate hexahydrate, nickel(II) nitrate heptahydrate, cobalt(II) chloride hexahydrate, cobalt(II) acetate tetrahydrate, cobalt(II) sulphate heptahydrate, and cobalt(II) nitrate hexahydrate. Ethylbenzoate, methyl-4-nitrobenzoate, methyl-4-hydroxybenzoate, acetophenone, benzylacetone, hydrazine hydrate, triethylamine, ethylenediamine-tetraacetic acid disodium salt dihydrate (EDTA), dimethyl-sulphoxide (DMSO), dimethylformamide (DMF), chloroform, diethylether, acetone, methanol, ethanol, sulphuric acid, nitric acid, perchloric acid, hydrochloric acid, ammonia and ammonium chloride, murexide dye, and solochrome dye.

3.2 Preparation of hydrazones.

The preparation of the hydrazones followed two steps.

Step one: The preparation of the precursor benzoylhydrazides and para-hydroxyl- and para-nitro- substituted derivatives. This was done by reacting suitable alkyl esters with hydrazine hydrate solution under reflux.

Step two: the benzoylhydrazides and its substituted derivatives were reacted with the ketone; benzylacetone, via a condensation reaction to yield their respective hydrazones derivatives.

3.2.1. Preparation of Hydrazides

3.2.1.1 Benzoylhydrazide

The method of Adekunle *et al.*, (2010) was adopted. 19.40 mL (400 mmole) of hydrazine hydrate was mixed with 63 mL (400 mmole) ethylbenzoate in a 500 mL round bottom flask placed on a water bath. To the mixture, 150 mL of ethanol was added as a solvent. The flask was fitted with a reflux condenser and the mixture was refluxed for 12 hours. The resultant yellowish solution was concentrated using rotary evaporator to give a white crystalline precipitate. The precipitate formed was filtered under suction and was washed with 40% ethanol. The white crystalline compound was dried in the desiccator over CaCl₂. Yield 88%. Mpt 110 – 111 °C.

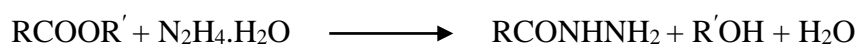
3.2.1.2 *p*-nitro-benzoylhydrazide.

10 g (55.20 mmole) of methyl-4-nitrobenzoate was weighed into a round bottom flask fitted with a reflux condenser placed on a water bath. 50 mL of ethanol was added to it and was stirred to dissolution on the hot plate magnetic stirrer. 2.67 mL (55.20 mmole) plus additional 1.33 mL of hydrazine hydrate giving a total volume of 4.00 mL of hydrazine hydrate (50% excess) was mixed with 25 mL ethanol and was added to the stirring mixture. The reaction was refluxed for 6 hours. It was then poured into a 250 mL beaker, concentrated by reducing the volume of the solvent to half initial volume and kept overnight. Brownish yellow precipitate formed overnight, it was filtered under suction, washed with distilled water and 40% ethanol, and dried over CaCl₂ in the desiccator. Yield = 76%. M.pt 218 - 220 °C.

3.2.1.3. *p*-hydroxyl-benzoylhydrazide

20 g (131.4 mmole) of methyl-4-hydroxylbenzoate was weighed into a 500 mL round bottom flask fitted with a reflux condenser and 100 ml of methanol was added to it. It was then placed on a heating mantle and heated initially for 5 mins. 12.76 mL (262.8 mmole) of hydrazine hydrate (100% excess) was mixed with 20 mL methanol and added to the reaction mixture. The mixture was refluxed for 6 hours after which it was poured into a 250 mL beaker and allowed to evaporate without heating. A white powdery precipitate formed after 24 hours of evaporation. It was filtered under suction, washed with 40% methanol and dried over CaCl₂. Yield 89%. M.pt = 268 – 270 °C

Equation for the reaction is as shown below,



3.2.2 Preparation of benzylacetone-benzoylhydrazone (bahh)

10.18 g (74.76 mmole) of benzoylhydrazide was mixed with 100 mL ethanol in a 250 mL round bottom flask fitted with a reflux condenser placed on a water bath. 11.20 mL (74.76 mmoles) of the carbonyl compound; benzylacetone, was mixed with 20 mL of ethanol and was added to the stirring mixture in the round bottom flask. The colour changed from colourless to pale yellow upon addition and the mixture was refluxed for 6 hours. It was then poured in a 250 mL beaker where the solvent was allowed to evaporate slowly and the initial volume was reduced by half. The resulting mixture was left standing for 24 hours after which a white needle-like crystalline precipitate was formed. It was filtered and washed with 40% ethanol. The precipitate was air-dried for 20 minutes and then placed in a desiccator over CaCl₂. Yield 93%. M.pt 130 – 132 °C.

3.2.3 Preparation of *p*-nitro-benzylacetone –benzoylhydrazone.

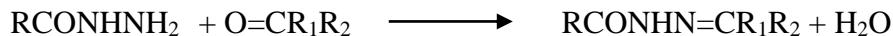
10 g (55.2 mmole) of *p*-nitro-benzoylhydrazide was poured into a 250 mL round bottom flask fitted with reflux condenser on a heating mantle. It was mixed with 150 mL ethanol and 3 mL of acetic acid added as catalyst. The resulting yellowish suspension was stirred with heating for 20 minutes. 8.27 mL (55.2 mmole) of benzylacetone mixed with 20 mL of ethanol was added to the suspension giving an instant clear yellowish solution. The reaction was done for 6 hours under reflux. The mixture was then poured into a 250 mL beaker where it was concentrated by reducing the solvent to half initial volume. It was

kept for 24 hours after which a yellow precipitate formed. The precipitate was filtered under suction and washed with 40% ethanol. It was dried over CaCl_2 in a desiccator. Yield, 80%. M.pt 137 - 138 °C

3.2.4 Preparation of benzylacetone-p-hydroxyl-benzoylhydrazone

10 g (65.70 mmole) of p-hydroxyl-benzoylhydrazide was poured into 250 mL round bottom flask fitted with a reflux condenser. It was mixed with 70/10 mL methanol/acetone mixture with 1 mL of acetic acid added as catalyst. The beaker was set on a heating mantle and heated for 5 minutes after which 9.85 mL (65.70 mmole) of benzylacetone in 20 mL methanol was added to the mixture and the reaction was refluxed for 6 hours. The mixture was thereafter poured into a 250 mL beaker and the volume of the solvent was reduced to half its initial volume by heating on the hot plate. White crystalline precipitate formed on cooling down after 3 hours. This was washed with 40% methanol under suction. It was dried in the desiccator over CaCl_2 . Yield, 91%. M.pt 147 – 149 °C.

The equation for the preparative reaction can be represented as,



Where, R= Phenyl, substituted phenyl, $\text{R}_1 = \text{CH}_3$, $\text{R}_2 = \text{benzyl}$.

3.3 Preparation of metal complexes.

3.3.1 Preparation of copper(II) benzylacetone-benzoylhydrazone (babh)

2.00 g (7.51 mmole) of babh ligand was dissolved in 20 mL ethanol in a 250 mL beaker on magnetic stirrer at room temperature. 0.75 g (3.76 mmole) of copper(II) acetate monohydrate dissolved in 20 mL of distilled water was added to the stirring mixture dropwise. There was a colour change from the colourless solution of the ligand to a greenish coloured mixture upon addition of the metal salts. The mixture was stirred for 4 hours after which a green precipitate formed. It was filtered under suction, washed with 40% ethanol and dried over CaCl_2 in the desiccator. Yield 69%. M.Pt 188 – 190 °C.

3.3.2 Preparation of nickel(II) benzylacetone-benzoylhydrazone.

1.50 g (5.64 mmole) of the hydrazone ligand was weighed into a 250 mL beaker and dissolved in 20 mL ethanol on a magnetic stirrer at room temperature. 0.67 g (2.82 mmole) of nickel(II) chloride hexahydrate was dissolved in 20 mL ethanol and added to the stirring mixture dropwise. There was a colour change from colourless to a greenish colouration upon the addition of the metal salt. Light green precipitate formed after about 10 minutes of stirring and the mixture was then stirred for two hours. The precipitate was filtered under suction, washed with 40% ethanol and dried in the desiccator over CaCl₂. Yield 66%. M.Pt. 285 – 287 °C

3.3.3 Preparation of cobalt(II) benzylacetone-benzoylhydrazone

0.94 g (3.37 mmole) of cobalt(II) acetate tetrahydrate was mixed with methanol/acetone (40/10 mL) in a 250 mL round bottom flask fitted with reflux condenser on a water bath placed on hotplate magnetic stirrer. It was heated to dissolution for 10 minutes, after which 2.00 g (6.74 mmole) of babh ligand dissolved in 20 mL methanol was added drop wise to the stirring mixture. Three drops of triethylamine were added as catalyst, and the mixture refluxed for 10 hours. A brownish pink coloured solution that resulted was poured into a beaker and kept for 72 hours for slow evaporation. Pink precipitate was formed and it was filtered under suction, washed with 40% ethanol and dried in the desiccator over CaCl₂. Yield 71%. Mpt. 185 – 187 °C

3.3.4. Preparation of copper(II) *p*-hydroxyl-benzylacetone-benzoylhydrazone

0.50 g (1.76 mmole) of the ligand was dissolved in 30 mL of 2:1 methanol/acetone mixture in a 250 mL beaker. It was stirred to dissolution on the magnetic stirrer at room temperature. 0.21 g (0.88 mmole) of Cu(II) nitrate tetrahydrate was dissolved in 10 mL of methanol in a 25 mL beaker and the solution of the metal salt was added to the stirring solution dropwise. The colour of the mixture changed from colourless to green and a green precipitate formed immediately. The mixture was thereafter stirred for one hour, after which the green precipitate was filtered under suction, washed with distilled water, and then with acetone/methanol mixture. It was dried in the desiccator over CaCl₂. Yield. 82%, Mpt. 205 - 207 °C

3.3.5. Preparation of Ni(II) *p*-hydroxyl-benzylacetone-benzoylhydrazone

0.50 g (1.76 mmole) of the ligand was dissolved in 30 ml of methanol/acetone (2:1) mixture in a 250 mL beaker on a magnetic stirrer at room temperature. 0.26 g (0.88 mmole) of nickel(II) nitrate heptahydrate in 10 mL methanol was added dropwise to the stirring mixture. There was an immediate precipitation of a green precipitate. The mixture was thereafter stirred for one hour, after which it was filtered under suction, washed with distilled water and methanol/acetone mixture and dried in a desiccator over CaCl₂. Yield 81% Mpt. > 300 °C.

3.3.6. Preparation of Co(II) *p*-hydroxyl-benzylacetone-benzoylhydrazone.

0.50 g (1.76 mmole) of the ligand was dissolved in 30 mL methanol/acetone (2:1) mixture in a 250 mL beaker on a magnetic stirrer at room temperature. 0.26 g (0.88 mmole) of cobalt(II) nitrate hexahydrate was dissolved in 10 mL methanol and was added dropwise to the stirring mixture. A pink precipitate formed instantly and the reaction mixture was thereafter stirred for two hours. The pink precipitate was filtered, washed with distilled water and then with methanol/acetone mixture. It was kept in the desiccator over CaCl₂ to dry. Yield 76%. Mpt. 278 – 280 °C.

All the metal(II) complexes of *p*-hydroxyl-benzylacetone-benzoylhydrazone were prepared by similar method. Mixture of ratio 2:1 methanol/acetone was used to dissolve the ligand completely. Although it dissolved in methanol easily when warmed. Metal(II) chloride and metal(II) nitrate were dissolved in 10 mL of methanol, while metal(II) acetates and metal(II) sulphates were dissolved in 20 mL of distilled water prior to addition to the ligand.

3.3.7 Preparation of copper(II) *p*-nitro-benzylacetone-benzoylhydrazone

2.00 g (6.42 mmole) of the ligand was dissolved in 30 mL of methanol/acetone mixture (ratio 2:1) in a 250 mL beaker placed on a magnetic stirrer at room temperature. 0.80 g (3.21 mmole) of copper(II) sulphate pentahydrate was dissolved in 20 mL of distilled water and was added dropwise to the stirring mixture. There was an immediate precipitation of a light green coloured precipitate and the mixture was then left to stir for 12 hours. The precipitate was filtered, washed with 40% methanol and kept in the desiccator to dry over CaCl₂. Yield 79%. Mpt. 212 - 214°C

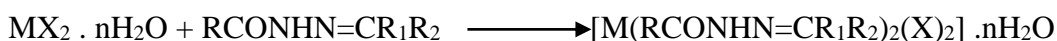
3.3.8. Preparation of nickel(II) *p*-nitro-benzylacetone-benzoylhydrazone

1.50 g (4.82 mmole) of the ligand was dissolved in 30 mL methanol/acetone mixture (2: 1) in a 250 mL beaker placed on a magnetic stirrer at room temperature. 0.63 g (2.41 mmole) of nickel(II) sulphate hexahydrate was dissolved in 20 mL distilled water and was added dropwise to the stirring mixture. There was no formation of the precipitate instantly. The mixture was then stirred at room temperature for 72 hours after which a light blue precipitate formed. It was filtered under suction, washed with 40% methanol and dried in the desiccator over CaCl₂. Yield 33%. Mpt. > 300°C.

3.3.9 Preparation of cobalt(II) *p*-nitro-benzylacetone-benzoylhydrazone

1.50 g (4.82 mmole) of the ligand in 30 mL methanol/acetone mixture (2: 1) in a 250 mL beaker on a magnetic stirrer was stirred at room temperature to dissolution. 0.68 g (2.41 mmole) of cobalt(II) sulphate heptahydrate dissolved in 20 mL distilled water was added dropwise to the stirring mixture. The reaction was stirred for 72 hours after which a peach coloured precipitate formed. This was filtered under suction and washed with 40% methanol and dried over CaCl₂ in a desiccator. Yield 79%. M.Pt. 212 – 214 °C.

The same procedure was adopted in the preparation of all the complexes of *p*-nitro-benzylacetone-benzoylhydrazone. The equation for the preparation of the metal(II) complexes is represented as follows:



Where, M = Ni(II), Cu(II) and Co(II); X = Cl, NO₃, OAc and SO₄.

3.4. Preparation and standardization of reagents.

3.4.1 Preparation of 0.005 M EDTA solution.

1.8612 g of disodium dihydrogen ethylenediamine tetraacetate was dissolved with distilled water in a 1000 mL standard flask and the solution was made up to the mark.

3.4.2 Preparation of 0.005 M zinc(II) sulphate heptahydrate solution.

1.4375 g of zinc(II) sulphate heptahydrate was dissolved in a 1000 mL standard flask with distilled water. The solution was shaken vigorously and made up to mark with distilled water.

3.4.3 Preparation of ammonia/ammonium chloride buffer solution.

17.80 g of ammonium chloride was dissolved in 142mL concentrated ammonia in a 250 mL standard flask with distilled water.

3.4.4 Preparation of murexide indicator.

25 g of sodium chloride (analar) was thoroughly mixed with 0.05 g of murexide dye to give murexide indicator.

3.4.5 Standardisation of EDTA solution.

20 mL of freshly prepared 0.005M $ZnSO_4 \cdot 7H_2O$ was transferred into a conical flask by means of pipette. 3 mL of NH_3/NH_4Cl buffer solution was added to adjust the pH to 10, followed by addition of specks of Solochrome indicator. The resulting purple solution was thereafter titrated against the EDTA solution to a blue coloured end point. (Appendix 4, Table 6.1)

3.5 Metal analysis of the complexes.

The percentage metal composition was determined by complexometric titration using EDTA. This was done by preparing solutions of known amount of the digested complexes and then, they were titrated against the standardised EDTA solution (Appendix 4). The results are shown in Table 4.1.

3.5.1 Digestion of sample.

A sample of the metal complex weighing between 0.01 - 0.03 g was accurately weighed into a sample bottle and a few drops of 1:1 nitric/perchloric acid mixtures were added to it. It was heated on the hot plate until the mixture dried. Few drops of distilled water were added to it after cooling and it was returned to the hot plate and heated again to dryness. After it cooled, about 5 mL of distilled water was added to dissolve the content and it was carefully transferred into a 100 mL standard flask and made up to mark with distilled water.

3.6 Physical measurements

3.6.1 Melting point/decomposition temperature

The melting point/decomposition temperatures of the synthesised compounds were determined using a Gallenkamp (variable heater) Melting Point apparatus at Obafemi Awolowo University, Ile-Ife and Sherwood melting point apparatus at University of Ibadan. The results are shown in Table 4.1.

3.6.2 Elemental Analysis

Microanalysis was done on Elementar Vario ELIII elemental analyser (Hanau Germany) at the State Key Laboratory of Organic Geochemistry, Guangzhou Institute of Geochemistry, Guangzhou, China.

3.6.3 Solubility

The solubility of the babh compounds was determined in seven common solvents and the results are shown in Table 4.2.

3.7. Spectral measurements

3.7.1 Infrared spectra

The infrared spectra of all the complexes and those of the ligands were recorded on Perkin Elmer FT-IR Spectrophotometer covering the region ($4000 - 400 \text{ cm}^{-1}$) at the University of Ibadan. The compounds were run as nujol. The results are shown in table 4.3.

3.7.2 Electronic spectra

The electronic spectra of the ligands and for the ultraviolet region of all the synthesised complexes were done in methanol, while the visible region for the complexes were determined in nujol as solid diffuse reflectance using quartz cuvettes on a Shimadzu UV-Vis 1800 Spectrophotometer at the Department of Chemistry, Obafemi Awolowo University, Ile-Ife, Osun state. The results are shown in **Tables 4.4**.

3.7.3. NMR Spectra

^1H (300MHz) and ^{13}C (75MHz) NMR Spectra were recorded on a Bruker DMX avance spectrophotometer (with internal standard) at the Department of Chemistry laboratory, University of Botswana, Gaborone, Botswana. Results are shown in **Table 4.5**.

3.8 Magnetic susceptibility measurement

Magnetic susceptibility of the metal complexes were measured using a Sherwood Scientific Magnetic Susceptibility Balance, MSB Mark1 at the Department of Chemistry, University of Ibadan, Ibadan, Nigeria.

3.9 Conductance Measurement

The molar conductance values for the newly synthesised metal(II) complexes were done in nitromethane solution at 10^{-3}M concentration, on Labtech Digital Conductivity Meter at the Inorganic Laboratory B25, University of Ibadan, Ibadan, Nigeria. Results are shown in **Table 4.6**.

3.10 X-ray Crystallography

The Single crystal X-ray crystallography of the ligand (babh) Data were collected at 100K on a Bruker AXS D8 Venture diffractometer equipped with a Mo micro focus source ($\lambda = 0.71073 \text{ \AA}$), multilayer optics, a Photon 100 CMOS detector and an Oxford Cryosystems nitrogen gas flow device (700 series Cryostream). The determination of the unit cell parameters, the integration of raw diffraction images and the multi scan absorption correction, frame to frame scaling, merging of reflections was conducted with the APEX 2 Program package, Bruker AXS, 2010. The structure was solved by direct methods using SIR 92 and refined on F2 by full matrix least-squares procedures within the independent atom model (IAM) by using SHELXL-97. All non-H atoms were refined anisotropically. It was done at Institute Jean Barriol, Universite' de Lorraine, BP 70239, Boulevard des Aiguillettes 54506, Vandoeuvre-le'Nancy, Cedex, France.

3.11 Screening of Compounds for Antimicrobial Activity

3.11.1 Test Organisms

The antimicrobial study of the synthesised compounds was done at the Pharmaceutical Microbiology Laboratory of the Department of Pharmaceutics, Faculty of Pharmacy, Obafemi Awolowo University, Ile-Ife, Nigeria.

The strains of microorganisms used include reference strains of Gram-positive and Gram-negative bacteria. The Gram-negative bacteria used were *Escherichia coli* ATCC 25922, *Shigella flexineri* (clinical strain), *Pseudomonas aeruginosa* ATCC 10145 and *Klebsiella pneumoniae* ATCC 13048 while the Gram-positive strains include *Staphylococcus aureus* NCTC 6571 and *Bacillus cereus* ATCC 11778. The strains were from stocks of culture collection maintained in the Department.

3.11.2. Qualitative Assessment of Antimicrobial Activity (Agar Diffusion Technique).

Bacteria were maintained on nutrient agar slants at 4°C. The compounds were dissolved in 20% DMSO to a concentration of 40mg/mL. Molten Mueller Hinton Agar (Oxoid) of 20 mL each was poured into sterile disposable petri-dishes and allowed to set. The surface of the Agar was swabbed with a 24 hour Broth culture of the bacteria strain diluted to 10⁶ cfu/ml using a sterile cotton swabs. Using a flamed and cooled 6 mm cork-borer, wells were made in the agar plates and the plugs were discarded aseptically. The plates were incubated for 1 hour, after which they were retrieved and 0.2 mL of 40 mg/mL concentration of the compounds were placed in each well using a sterile calibrated dropper. The plates were left on the bench for one hour to allow for diffusion of the compounds into the Agar. The plates were then incubated for 24 hours at 37 °C. Streptomycin, 250 µg/mL was used as positive control while 20% DMSO was the negative control. The zone diameter of inhibition was measured with a transparent ruler in millimetre (mm). The results are presented in Table 4.7.

3.11.3 Quantitative Assessment of Antimicrobial Activity (Agar Dilution technique)

The minimum inhibitory concentration (MIC) was determined for those compounds that showed zones of growth inhibition against test organisms from the sensitivity test at 40 mg/mL. Aliquot dilutions of 40, 20, 10, 5, 2, 1 mg/mL were prepared using the selected

compounds. They were subjected to screening using the agar dilution method. Streptomycin: 62.5, 125 and 250 $\mu\text{g}/\text{mL}$ were used as positive control. The lowest value of the dilution that exerted inhibition was taken as the minimum inhibition concentration (MIC).

CHAPTER FOUR

RESULTS

4.1 Physical properties and analytical data

The physical and analytical properties of the synthesized compounds and data observed are presented in Table 4.1. Information from the table includes empirical formulae and formula weights of the compounds, their colours, melting point/decomposition temperatures, percentage yields, percentage C, H, N and magnetic moment values. Tables 4.2 shows the solubility of the compounds in seven common polar and non-polar solvents. Table 4.6 shows the molar conductance value for those complexes soluble in nitromethane.

Table 4.1. Physical properties and analytical data for babh compounds

Compound (Colour)	formula (Formula weight (g))	Mp/dec Temp (°C)	Yield (%)	Elemental analysis. % found (% calculated)				
				Carbon	Hydrogen	Nitrogen	metal	$\mu_{\text{eff}}(\text{BM})$
babh White	C ₁₇ H ₁₈ N ₂ O (266.34)	130-132	92	76.67 (76.66)	7.34 (6.81)	10.66 (10.51)	--	--
<i>p</i> -OH-babh (White)	C ₁₇ H ₁₈ N ₂ O ₂ (282.33)	147-149	89	72.33 (72.31)	8.01 (6.43)	9.41 (9.92)	---	---
<i>p</i> -NO ₂ -babh (Yellow)	C ₁₇ H ₁₇ N ₃ O ₃ (311.34)	218-220	96	65.24 (65.58)	6.81 (5.50)	13.92 (13.50)	--	---
Cu ₂ (babh) ₂ Cl ₂ Brown	C ₃₄ H ₃₆ N ₄ O ₂ Cl ₂ Cu ₂ (730.76)	>300	41	55.96 (55.88)	5.98 (4.96)	9.27 (7.66)	8.56 (8.69)	2.90
Cu(babh)(NO ₃) ₂ .5H ₂ O Blue	C ₁₇ H ₂₈ N ₄ O ₁₂ Cu (543.96)	139-140	54	36.68 (37.54)	3.78 (5.14)	10.66 (10.51)	10.93 (11.68)	2.09
Cu(babh) ₃ (OAc) ₂ Green	C ₅₅ H ₆₀ N ₆ O ₇ Cu (980.64)	188-190	69	68.42 (67.34)	9.35 (6.17)	9.95 (8.57)	6.31 (6.48)	2.43
Cu(babh) ₂ SO ₄ .H ₂ O Brown	C ₃₄ H ₃₈ N ₄ O ₇ SCu (710.23)	>300	31	57.26 (57.49)	6.51 (5.35)	11.25 (7.89)	8.72 (8.94)	2.24

Table 4.1. Physical properties and analytical data for babh compounds (Cont'd)

Compound (Colour)	formula (Formula weight (g))	Mp/dec Temp (°C)	Yield (%)	Elemental analysis. % found (% calculated)				
				Carbon	Hydrogen	Nitrogen	metal	μ_{eff} (BM)
Cu(<i>p</i> -OH-babh) ₂ Cl ₂ (Green)	C ₃₄ H ₃₆ N ₄ O ₄ Cl ₂ Cu (700.29)	191-193	77	58.18 (58.31)	6.11 (5.18)	7.88 (8.00)	9.43 (9.07)	1.92
Cu(<i>p</i> -OH-babh) ₂ (NO ₃) ₂ (Green)	C ₃₄ H ₃₆ N ₆ O ₁₀ Cu (752.22)	205-207	82	54.80 (54.29)	5.60 (4.79)	11.20 (11.17)	8.39 (8.44)	1.88
Cu(<i>p</i> -OH-babh) ₂ (OAc) ₂ (Brown)	C ₃₈ H ₄₂ N ₄ O ₈ Cu (746.30)	197-199	63	65.02 (61.65)	6.65 (5.67)	8.98 (7.50)	8.46 (8.51)	1.98
Cu(<i>p</i> -OH-babh)SO ₄ .3H ₂ O (Green)	C ₁₇ H ₂₄ O ₉ N ₂ SCu (495)	234-236	38	40.87 (41.17)	5.47 (4.88)	9.60 (5.65)	12.69 (12.81)	2.18
Cu(<i>p</i> -NO ₂ -babh)Cl ₂ .2H ₂ O (Green)	C ₁₇ H ₂₁ N ₃ O ₅ Cl ₂ Cu (481.91)	226-228	31	33.88 (42.37)	3.51 (4.39)	11.23 (8.72)	11.50 (13.18)	2.35
Cu(<i>p</i> -NO ₂ -babh)(NO ₃) (Light green)	C ₁₇ H ₁₇ N ₄ O ₆ (436.88)	< 300	62	48.05 (46.74)	4.51 (3.92)	16.53 (12.88)	12.86 (14.54)	1.71
Cu(<i>p</i> -NO ₂ -babh) ₃ (OAc) ₂ (Green)	C ₅₅ H ₅₇ N ₉ O ₁₃ (1115.63)	210-212	73	60.16 (59.21)	7.12 (5.15)	13.34 (11.30)	6.02 (5.70)	2.27

Table 4.1. Physical properties and analytical data for babh compounds (Cont'd)

Compound (Colour)	formula (Formula weight (g)	Mp/dec Temp (°C)	Yield (%)	Elemental analysis. % found (% calculated)				
				Carbon	Hydrogen	Nitrogen	metal	μ_{eff} (BM)
Cu(<i>p</i> -NO ₂ babh)SO ₄ .2C ₂ H ₅ OH (Green)	C ₂₁ H ₂₉ N ₃ O ₉ SCu (563.02)	212-214	79	45.53 (44.80)	4.67 (5.19)	13.40 (7.46)	10.70 (11.29)	1.89
Ni(babh) ₂ Cl ₂ Light green	C ₃₄ H ₃₆ N ₄ O ₂ Cl ₂ Ni (662.36)	285-287	66	63.21 (61.65)	10.08 (5.43)	9.50 (8.46)	8.65 (8.86)	3.11
Ni(babh)(NO ₃) ₂ .2H ₂ O Blue	C ₁₇ H ₂₂ N ₄ O ₉ Ni (426.38)	253-255	61	41.28 (42.09)	4.80 (4.36)	18.68 (11.55)	10.89 (12.09)	3.1
Ni(babh) ₂ (OAc) ₂ Brown	C ₃₈ H ₄₂ N ₄ O ₆ (709.45)	150-152	46	66.13 (64.33)	6.54 (5.96)	10.40 (7.90)	8.39 (8.27)	3.87
Ni(babh)SO ₄ .5H ₂ O Blue	C ₁₇ H ₂₈ N ₂ O ₁₀ SNi (511.10)	>300	18	40.00 (39.94)	4.37 (5.52)	13.16 (5.48)	10.56 (11.48)	2.90
Ni(<i>p</i> -OH-babh) ₂ Cl ₂ (Light green)	C ₃₄ H ₃₆ N ₄ O ₄ (694.36)	>300	60	58.81 (58.81)	5.52 (5.22)	8.03 (8.35)	8.40 (8.45)	2.80
Ni(<i>p</i> -OH-babh) ₂ (NO ₃) ₂ (Light blue)	C ₃₄ H ₃₆ N ₄ O ₄ Ni (747.36)	>300	81	54.61 (54.56)	5.60 (4.85)	11.37 (11.24)	7.82 (7.86)	3.26

Table 4.1. Physical properties and analytical data for babh compounds (Cont'd)

Compound (Colour)	formula (Formula weight (g))	Mp/dec Temp (°C)	Yield (%)	Elemental analysis. % found (% calculated)				
				Carbon	Hydrogen	Nitrogen	metal	μ_{eff} (BM)
Ni(<i>p</i> -OH-babh) ₂ (OAc) ₂ (Grey)	C ₃₈ H ₄₂ N ₄ O ₈ (741.45)	202-204	75	61.09 (61.55)	5.69 (5.70)	8.00 (7.55)	7.88 (7.91)	3.22
Ni(<i>p</i> -OH-babh)SO ₄ .3H ₂ O (Blue)	C ₁₇ H ₂₄ N ₂ O ₉ SNi (491.06)	>300	53	41.49 (41.58)	5.12 (4.92)	9.01 (5.70)	11.90 (11.95)	3.50
Ni(<i>p</i> -NO ₂ -babh)Cl ₂ .4H ₂ O (Green)	C ₁₇ H ₂₅ N ₃ O ₇ Cl ₂ Ni (513.08)	< 300	30	40.01 (39.80)	4.33 (4.91)	15.30 (8.18)	11.37 (11.43)	3.06
Ni(<i>p</i> -NO ₂ -babh) ₂ (NO ₃) ₂ (Blue)	C ₃₄ H ₃₄ N ₈ O ₁₂ Ni (805.36)	182-183	56	50.03 (50.71)	7.21 (4.26)	14.80 (13.91)	7.33 (7.29)	3.22
Ni(<i>p</i> -NO ₂ -babh) ₂ (OAc) ₂ (Yellow)	C ₃₈ H ₄₀ N ₆ O ₁₀ Ni (799.44)	207-209	69	57.61 (57.09)	5.79 (5.04)	13.11 (10.51)	7.41 (7.34)	3.28
Ni(<i>p</i> -NO ₂ -babh)SO ₄ .2H ₂ O (Light blue)	C ₁₇ H ₂₁ N ₃ O ₉ SNi (502.05)	>300	33	28.73 (40.66)	4.16 (4.21)	14.38 (8.37)	10.94 (11.25)	2.99

Table 4.1. Physical properties and analytical data for babh compounds (Cont'd)

Compound (Colour)	formula (Formula weight (g))	Mp/dec Temp (°C)	Yield (%)	Elemental analysis. % found (% calculated)				
				Carbon	Hydrogen	Nitrogen	metal	μ_{eff} (BM)
Co(babh) ₂ Cl ₂ Pink	C ₃₄ H ₃₆ N ₄ O ₂ Cl ₂ Co (662.61)	241-243	64	62.78 (61.62)	9.66 (5.47)	9.44 (8.46)	8.70 (8.89)	5.04
Co(babh) ₂ (NO ₃) ₂ Pink	C ₃₄ H ₃₆ N ₆ O ₈ Co (715.615)	214-216	76	57.64 (57.06)	9.00 (5.07)	12.62 (11.74)	7.98 (8.23)	4.84
Co(babh) ₂ (OAc) ₂ Pink	C ₃₈ H ₄₂ N ₄ O ₆ Co (709.61)	185-187	71	66.55 (64.31)	6.75 (5.96)	9.46 (7.90)	8.21 (8.30)	4.74
Co(babh)SO ₄ .4H ₂ O Pink	C ₁₇ H ₂₆ N ₂ O ₉ SCo (493.32)	>300	58	40.39 (41.39)	5.81 (5.31)	13.68 (5.67)	10.91 (11.94)	4.46
Co(<i>p</i> -OH-babh) ₂ Cl ₂ (Pink)	C ₃₄ H ₃₆ O ₄ N ₄ Cl ₂ Co (694.60)	297-299	51	59.02 (58.79)	5.89 (5.22)	8.15 (8.06)	8.38 (8.47)	4.99
Co(<i>p</i> -OH-babh) ₂ (NO ₃) ₂ C ₃₄ H ₃₆ N ₆ O ₁₀ Co (Light pink)	C ₃₄ H ₃₆ N ₆ O ₁₀ Co (747.61)	278-280	76	55.69 (54.62)	6.55 (4.85)	11.61 (11.24)	7.79 (7.88)	4.76
Co(<i>p</i> -OH-babh) ₂ (OAc) ₂ (Brown)	C ₃₈ H ₄₂ N ₄ O ₈ Co (741.69)	206-208	51	62.44 (61.54)	6.54 (5.71)	8.32 (7.55)	7.57 (8.01)	4.80

Table 4.1. Physical properties and analytical data for babh compounds (Cont'd)

Compound (Colour)	formula (Formula weight (g))	Mp/dec Temp (°C)	Yield (%)	Elemental analysis. % found (% calculated)				
				Carbon	Hydrogen	Nitrogen	metal	μ_{eff} (BM)
Co(<i>p</i> -OH-babh)SO ₄ .2H ₂ O (Light pink)	C ₁₇ H ₂₂ N ₂ O ₈ SCo (473.29)	168-170	45	43.25 (43.14)	5.01 (4.69)	6.45 (5.91)	12.12 (12.45)	2.64
Co(<i>p</i> -NO ₂ babh) ₂ Cl ₂ (Light pink)	C ₃₄ H ₃₄ N ₆ O ₆ Co (752.62)	249-251	40	55.53 (54.26)	6.92 (4.55)	11.93 (11.16)	8.02 (7.83)	4.85
Co(<i>p</i> -NO ₂ -babh) ₂ (Light pink)	C ₃₄ H ₃₄ N ₆ O ₆ Co (681.61)	101-103	43	60.92 (59.69)	6.21 (5.02)	13.94 (12.32)	8.60 (8.65)	2.45
Co(<i>p</i> -NO ₂ -babh) ₂ (OAc) ₂ .3H ₂ O (Pink)	C ₃₈ H ₄₈ N ₆ O ₁₄ Co (752.62)	178-180	44	52.74 (52.36)	(5.39) (5.66)	13.77 (9.84)	7.60 (6.90)	5.39
Co(<i>p</i> -NO ₂ -babh)SO ₄ (Pink)	C ₁₇ H ₁₇ N ₃ O ₃ SCo (466.26)	250-252	60	44.62 (43.79)	4.20 (3.67)	11.02 (9.01)	12.83 (12.64)	2.46

Table 4.2. Solubility data of the compounds.

Compound	H ₂ O	MeOH	EtOH	Acetone	CHCl ₃	DMSO	DMF	MeNO ₂
babh	SH	S	S	S	S	S	S	S
<i>p</i> -OH-babh	I	S	SH	S	S	S	S	S
<i>p</i> -NO ₂ -babh	I	S	S	S	S	S	S	S
Cu ₂ (babh) ₂ Cl ₂	I	I	I	I	SS	SH	SS	I
Cu(babh)(NO ₃) ₂ .5H ₂ O	I	S	I	I	I	S	S	SS
Cu(babh) ₃ (OAc) ₂	I	I	I	I	S	S	S	S
Cu(babh) ₂ SO ₄ .H ₂ O	I	I	I	I	SS	S	S	SS
Cu(<i>p</i> -OH-babh) ₂ Cl ₂	I	SH	SH	SS	SS	S	S	SS

Table 4.2. Solubility data of the compounds (Cont'd)

Compound	H ₂ O	MeOH	EtOH	Acetone	CHCl ₃	DMSO	DMF	MeNO ₂
Cu(<i>p</i> -OH-babh) ₂ (NO ₃) ₂	I	SS	SS	SS	SS	S	S	S
Cu(<i>p</i> -OH-babh) ₂ (OAc) ₂	I	S	S	S	S	S	S	SS
Cu(<i>p</i> -OH-babh)SO ₄ .3H ₂ O	I	I	I	I	I	S	S	I
Cu(<i>p</i> -NO ₂ -babh)Cl ₂ .2H ₂ O	I	I	I	I	SS	SS	S	I
Cu(<i>p</i> -NO ₂ -babh)(NO ₃)	I	SS	SS	S	SS	S	S	SS
Cu((<i>p</i> -NO ₂ -babh) ₃ (OAc) ₂	I	SS	SS	S	S	S	S	S
Cu(<i>p</i> -NO ₂ -babh)SO ₄ .2C ₂ H ₅ OH	I	SS	SS	S	S	S	SS	S
Ni(babh) ₂ Cl ₂	I	S	SH	SH	S	S	S	SS

Table 4.2. Solubility data of the compounds (Cont'd)

Compound	H ₂ O	MeOH	EtOH	Acetone	CHCl ₃	DMSO	DMF	MeNO ₂
Ni(babh)(NO ₃) ₂ ·2H ₂ O	I	S	SH	S	SS	S	S	I
Ni(babh) ₂ (OAc) ₂	I	S	SH	S	S	S	S	S
Ni(babh)SO ₄ ·5H ₂ O	SH	S	SH	I	S	S	SH	I
Ni(<i>p</i> -OH-babh) ₂ Cl ₂	I	S	SS	SS	SS	S	S	SS
Ni(<i>p</i> -OH-babh) ₂ (NO ₃) ₂	I	SS	SS	SS	SS	SH	S	SS
Ni(<i>p</i> -OH-babh) ₂ (OAc) ₂	I	S	S	S	S	S	S	SH
Ni(<i>p</i> -OH-babh)SO ₄ ·3H ₂ O	I	I	I	I	I	SS	SS	I
Ni(<i>p</i> -NO ₂ -babh)Cl ₂ ·4H ₂ O	SH	SH	SH	SS	SS	S	SH	SS
Ni(<i>p</i> -NO ₂ -babh) ₂ (NO ₃) ₂	I	SS	S	SS	I	S	S	I

Table 4.2. Solubility data of the compounds (Cont'd)

Compound	H ₂ O	MeOH	EtOH	Acetone	CHCl ₃	DMSO	DMF	MeNO ₂
Ni(<i>p</i> -NO ₂ -babh) ₂ (OAc) ₂	I	SH	SH	S	S	S	S	S
Ni(<i>p</i> -NO ₂ -babh)SO ₄ .2H ₂ O	I	SS	SS	SS	SS	S	SH	SS
Co(babh) ₂ Cl ₂	I	S	S	SS	SS	S	S	SH
Co(babh) ₂ (NO ₃) ₂	I	S	S	I	SS	S	S	SS
Co(babh) ₂ (OAc) ₂	I	I	I	SS	SH	SH	S	I
Co(babh)SO ₄ .4H ₂ O	S	I	I	I	SS	S	SS	SS
Co(<i>p</i> -OH-babh) ₂ Cl ₂	I	S	S	SS	SS	S	S	SS
Co(<i>p</i> -OH-babh) ₂ (NO ₃) ₂	I	SS	SS	SS	SS	SH	S	SS

Table 4.2. Solubility data of the compounds (Cont'd)

Compound	H ₂ O	MeOH	EtOH	Acetone	CHCl ₃	DMSO	DMF	MeNO ₂
Co(<i>p</i> -OH-babh) ₂ (OAc) ₂	I	S	SS	S	S	S	S	SS
Co(<i>p</i> -OH-babh)SO ₄ .2H ₂ O	I	S	S	S	S	S	S	S
Co(<i>p</i> -NO ₂ -babh) ₂ Cl ₂	I	SS	SS	SS	SS	S	S	I
Co(<i>p</i> -NO ₂ -babh) ₂	I	S	S	S	S	S	S	S
Co(<i>p</i> -NO ₂ -babh) ₂ (OAc) ₂ .3H ₂ O	I	S	S	S	S	S	S	S
Co(<i>p</i> -NO ₂ -babh)SO ₄	S	S	SS	S	SS	S	S	I

S = Soluble, SH = Soluble in hot solvent, SS = Sparingly soluble, I = Insoluble.

4.2 Spectral characteristics

The relevant vibrational frequencies in the infrared spectra of the synthesized compounds and their assignments are summarised in table 4.3. Furthermore, the electronic transition bands observed in the UV-Visible spectra done in methanol solution and as solid reflectance in nujol, are listed in Table 4.4. The ^1H NMR and ^{13}C NMR data of the babh ligands are listed in Table 4.5

Table 4.3. Diagnostic Infrared vibrational frequencies for babh compounds

Compounds	$\nu(\text{O-H})$	$\nu(\text{N-H})$	$\nu(\text{C=O})$	$\nu(\text{C=N})$	$\nu(\text{N-N})$	M-O	M-N	Counter ion vibrations
babh	--	3156	1652	1537	1030	---	---	----
$\text{Cu}_2(\text{babh})_2\text{Cl}_2$	---	----	----	1524	1029	608	471	---
$\text{Cu}(\text{babh})(\text{NO}_3)_2 \cdot 5\text{H}_2\text{O}$	3400b	3122w	1644s	1554m	1025w	509w	451w	$\nu_4(1491), \nu_1(1315), \nu_2(1025)$
$\text{Cu}(\text{babh})_3(\text{OAc})_2$	-----	3055	1611w	1544m	1025w	571w	493w	$\nu_1(1590), \nu_2(1333)$
$\text{Cu}(\text{babh})_2\text{SO}_4 \cdot \text{H}_2\text{O}$		3145vw	1601m	1522s	1000m	470	396	$\nu_3(1074), \nu_4(608)$
$\text{Ni}(\text{babh})_2\text{Cl}_2$	----	3130w	1628m	1527s	1027w	531w	438	
$\text{Ni}(\text{babh})(\text{NO}_3)_2 \cdot 2\text{H}_2\text{O}$	3419w	3174b	1653s	1553m	1023	544m	460m	$\nu_4(1491), \nu_1(1315), \nu_2(1049)$

Table 4.3. Diagnostic Infrared vibrational frequencies for babh compounds (Cont'd)

Compounds	$\nu(\text{O-H})$	$\nu(\text{N-H})$	$\nu(\text{C=O})$	$\nu(\text{C=N})$	$\nu(\text{N-N})$	M-O	M-N	Counter ion vibrations
$\text{Ni}(\text{babh})_2(\text{OAc})_2$	----	3176w	1714w	1525m	1068w	530w	373w	ν_1 (1588), ν_2 (1274)
$\text{Ni}(\text{babh})\text{SO}_4 \cdot 5\text{H}_2\text{O}$	3627w	3156w	1657m	1569m	968w	613w	543w	ν_3 (1093), ν_4 (694)
$\text{Co}(\text{babh})_2\text{Cl}_2$	---	3300w	1624m	1536m	1073w	500m	378w	----
$\text{Co}(\text{babh})_2(\text{NO}_3)_2$	----	3179m	1621s	1555m	1033m	524m	462w	ν_4 (1490), ν_1 (1300), ν_2 (1033)
$\text{Co}(\text{babh})_2(\text{OAc})_2$	----	3169w	1624m	1527s	1028w	536m	469	ν_1 (1603), ν_2 (1495)
$\text{Co}(\text{babh})\text{SO}_4 \cdot 4\text{H}_2\text{O}$	3400w	3157b	1650m	1567m	971w	610w	538w	ν_3 (1092), ν_4 (695)

Table 4.3. Diagnostic Infrared vibrational frequencies for babh compounds (Cont'd)

Compounds	$\nu(\text{O-H})$	$\nu(\text{N-H})$	$\nu(\text{C=O})$	$\nu(\text{C=N})$	$\nu(\text{N-N})$	M-O	M-N	Counter ion vibrations
<i>p</i> -OH-babh	3295	3132w	1652m	1607	1060	----	---	---
$\text{Cu}(p\text{-OH-babh})_2\text{Cl}_2$	3296w	3054m	1677w	1558s	927w	619w	439w	---
$\text{Cu}(p\text{-OH-babh})_2(\text{NO}_3)_2$	3296w	3122b	1601m	1554s	926m	634w	434w	$\nu_4, (1508), \nu_1, (1343), \nu_3, (1034)$
$\text{Cu}(p\text{-OH-babh})_2(\text{OAc})_2$	3296w	3085b	1609s	1531s	934m	661m	414w	$\nu_1, (1515) \nu_2, (1340)$
$\text{Cu}(p\text{-OH-babh})\text{SO}_4 \cdot 3\text{H}_2\text{O}$	3222b	3132w	1647w	1555m	958m	624w	526w	$\nu_3, (1088), \nu_4, (610)$
$\text{Ni}(p\text{-OH-babh})_2\text{Cl}_2$	3310	3161	1610	1538	1030	631	438	
$\text{Ni}(p\text{-OH-babh})_2(\text{NO}_3)_2$	3216b	3067w	1613s	1551s	1020m	634w	427w	$\nu_4 (1509), \nu_1, (1329), \nu_3, (1020)$

Table 4.3. Diagnostic Infrared vibrational frequencies for babh compounds (Cont'd)

Compounds	$\nu(\text{O-H})$	$\nu(\text{N-H})$	$\nu(\text{C=O})$	$\nu(\text{C=N})$	$\nu(\text{N-N})$	M-O	M-N	Counter ion vibrations
$\text{Ni}(p\text{-OH-babh})_2(\text{OAc})_2$	3296w	3174w	1601m	1554w	1031w	644w	383w	$\nu_{1,(1497)}$ $\nu_2(1333)$
$\text{Ni}(p\text{-OH-babh})\text{SO}_4 \cdot 3\text{H}_2\text{O}$	3296	3211	1647s	1508s	981w	636w	593w	$\nu_3(1073), \nu_4(593)$
$\text{Co}(p\text{-OH-babh})_2\text{Cl}_2$	3300w	3165b	1609s	1538s	1031w	631w	506w	---
$\text{Co}(p\text{-OH-babh})_2(\text{NO}_3)_2$	3296w	3212b	1611s	1549s	1012s	632w	510w	$\nu_4(1509), \nu_1(1327), \nu_2(1012)$
$\text{Co}(p\text{-OH-babh})_2(\text{OAc})_2$	3296w	3174w	1600m	1497w	1031w	640w	427w	$\nu_1(1593), \nu_2(1330)$
$\text{Co}(p\text{-OH-babh})\text{SO}_4 \cdot 2\text{H}_2\text{O}$	3295b	3100w	1651m	1590m	1059w	617w	434w	$\nu_3(1105), \nu_4(617)$

Table 4.3. Diagnostic Infrared vibrational frequencies for babh compounds (Cont'd)

Compounds	$\nu(\text{O-H})$	$\nu(\text{N-H})$	$\nu(\text{C=O})$	$\nu(\text{C=N})$	$\nu(\text{N-N})$	M-O	M-N	Counter ion vibrations
<i>p</i> -NO ₂ -babh	---	3225m	1667s	1602m	1060w	---	----	ν_4 (1455), ν_1 (1348)
Cu(<i>p</i> -NO ₂ -babh)Cl ₂ .2H ₂ O	3448m	3326m	1616w	1561m	1009w	614w	539w	----
Cu(<i>p</i> -NO ₂ -babh)(NO ₃)	---	----	1617w	1515s	1009m	673w	593m	ν_4 (1403), ν_1 (1334), ν_3 (1004)
Cu(<i>p</i> -NO ₂ -babh) ₃ (OAc) ₂	---	3179w	1615m	1517s	1012w	611m	576m	ν_1 (1595), ν_2 (1341)
Cu(<i>p</i> -NO ₂ -babh)SO ₄ .2C ₂ H ₅ OH	---	3170w	1658w	1557m	1010m	664w	577w	ν_3 (1156), ν_4 (620)
Ni(<i>p</i> -NO ₂ -babh)Cl ₂ .4H ₂ O	---	3438w	1633m	1523m	1012w	611w	561w	
Ni(<i>p</i> -NO ₂ -babh) ₂ (NO ₃) ₂	----	3194w	1627m	1556m	1015w	560w	497w	ν_4 (1420), ν_1 (1313) ν_2 (10150)

Table 4.3. Diagnostic Infrared vibrational frequencies for babh compounds (Cont'd)

Compounds	v(O-H)	v(N-H)	v(C=O)	v(C=N)	v(N-N)	M-O	M-N	Counter ion vibrations
Ni(<i>p</i> -NO ₂ -babh) ₂ (OAc) ₂	-----	3200w	1600w	1538m	1010w	699w	551w	v ₂ (1339), v ₁ (1595)
Ni(<i>p</i> -NO ₂ -babh)SO ₄ .2H ₂ O	3395w	3238b	1665s	1540m	1013w	566w	462w	v ₃ (1079), v ₄ (618)
Co(<i>p</i> -NO ₂ -babh) ₂ Cl ₂	---	3112	1622m	1544m	1012w	539w	495w	----
Co(<i>p</i> -NO ₂ -babh) ₂	-----	3186w	1658m	1519m	1011w	510w	373	v ₄ (1519), v ₁ (1335), v ₂ (1011)
Co(<i>p</i> -NO ₂ -babh) ₂ (OAc) ₂ .3H ₂ O	3576	3090w	1643w	1533s	1011w	572w	550w	v ₁ (1596), v ₂ (1342)
Co(<i>p</i> -NO ₂ -babh)SO ₄	3347b	3236w	1657s	1521w	983w	561w	464w	v ₃ (1083), v ₄ (615)

Table 4.4. The electronic spectral data for babh compounds.

Compound	Intraligand transition (cm ⁻¹)	Charge transfer(cm ⁻¹)	Ligand field transition (cm ⁻¹)
Babh	48,780, 43,956 sh, 38,460	-----	-----
Cu ₂ (babh) ₂ Cl ₂	49261, 44,444		19,607, 15385, 11,111
Cu(babh)(NO ₃) ₂ .5H ₂ O	48780, 42550, 36764sh		14492
Cu(babh) ₃ (OAc) ₂	48309, 42553, 35714		16,393
Cu(babh) ₂ SO ₄ .H ₂ O	44,444, 33,333		19607
<i>p</i> -OHbabh	48309, 37195	-----	-----
Cu(<i>p</i> -OHbabh) ₂ Cl ₂	46296, 38462		16,666, 14,285sh
Cu(<i>p</i> -OHbabh) ₂ (NO ₃) ₂	49261, 35971	24390	16,666
Cu(<i>p</i> -OHbabh) ₂ (OAc) ₂	46948, 35714		16393
Cu(<i>p</i> -OHbabh)SO ₄ .3H ₂ O	48780, 37175		16666

Table 4.4. The electronic spectral data for babh compounds.

Compound	Intraligand transition (cm ⁻¹)	Charge transfer(cm ⁻¹)	Ligand field transition (cm ⁻¹)
<i>p</i> -NO ₂ -babh	48544, 37313	-----	-----
Cu(<i>p</i> -NO ₂ babh)Cl ₂ .2H ₂ O	49751, 39063		15385
Cu(<i>p</i> -NO ₂ babh)(NO ₃)	49751, 46083sh, 37735		16666
Cu(<i>p</i> -NO ₂ babh) ₃ (OAc) ₂	48780, 38461, 32362	24390	15384
Cu(<i>p</i> -NO ₂ babh)SO ₄ .2C ₂ H ₅ OH	48076, 38461	24390	16666
Babh	48,780, 43,956 sh, 38,460	-----	-----
Ni(babh) ₂ Cl ₂	49309, 39062		14705, 10309
Ni(babh)(NO ₃) ₂ .2H ₂ O	48505, 44053, 36900		16660, 13157, 10416
Ni(babh) ₂ (OAc) ₂	49505, 38461, 28571		16666
Ni(babh)SO ₄ .5H ₂ O	49079, 43859		16393, 11,111

Table 4.4. The electronic spectral data for babh compounds. (Cont'd)

Compound	Intraligand transition (cm ⁻¹)	Charge transfer (cm ⁻¹)	Ligand field transition (cm ⁻¹)
<i>p</i> -OH-babh	48309, 37195	----	----
Ni(<i>p</i> -OH-babh) ₂ Cl ₂	49505, 36231		14705, 10989
Ni(<i>p</i> -OH-babh) ₂ (NO ₃) ₂	48780, 36231	24390	17241, 10752
Ni(<i>p</i> -OH-babh) ₂ (OAc) ₂	48780, 35842		16666, 10869
Ni(<i>p</i> -OH-babh)SO ₄ .3H ₂ O	48780, 38461		18181, 15385
<i>p</i> -NO ₂ -babh	48544, 37313	-----	-----
Ni(<i>p</i> -NO ₂ -babh)Cl ₂ .4H ₂ O	49751, 46511, 38314		16666, 14925
Ni(<i>p</i> -NO ₂ -babh) ₂ (NO ₃) ₂	48543, 38314		21739, 16949
Ni(<i>p</i> -NO ₂ -babh) ₂ (OAc) ₂	----	24390	16949, 14492
Ni(<i>p</i> -NO ₂ -babh)SO ₄ .2H ₂ O	49261, 43668, 36900		20833, 17543, 11363

Table 4.4. The electronic spectral data for babh compounds. (Cont'd)

Compound	Intraligand transition (cm ⁻¹)	Charge transfer (cm ⁻¹)	Ligand field transition (cm ⁻¹)
babh	48780, 43956 sh, 38,460		
Co(babh) ₂ Cl ₂	48948 43478sh, 37174		20746, 19011
Co(babh) ₂ (NO ₃) ₂	46948, 38314		21097, 19305
Co(babh) ₂ (OAc) ₂	47393, 43478, 37174		20964, 18761, 14205
Co(babh)SO ₄ .4H ₂ O	49504, 44444, 37174		20000, 10,000
<i>p</i> -OH-babh	48309, 37195	----	----
Co(<i>p</i> -OH-babh) ₂ Cl ₂	49504, 36764		21186, 16949
Co(<i>p</i> -OH-babh) ₂ (NO ₃) ₂	49504, 36900		21974, 17361
Co(<i>p</i> -OH-babh) ₂ (OAc) ₂	46728, 36630		18050
Co(<i>p</i> -OH-babh)SO ₄ .2H ₂ O	48780, 37174		-----

Table 4.4. The electronic spectral data for babh compounds (cont'd)

Compound	Intraligand transition (cm ⁻¹)	Charge transfer (cm ⁻¹)	Ligand field transition (cm ⁻¹)
<i>p</i> -NO ₂ -babh	48544, 37313	-----	-----
Co(<i>p</i> -NO ₂ -babh) ₂ Cl ₂	49504, 38314		20920, 16129
Co(<i>p</i> -NO ₂ -babh) ₂	48780, 38167		18867
Co(<i>p</i> -NO ₂ -babh) ₂ (OAc) ₂ .3H ₂ O	49261, 38610, 29239		17857, 13333
Co(<i>p</i> -NO ₂ -babh)SO ₄	45454, 39840, 28089		21231, 19417, 15384

Table 4.5a. The ¹H NMR data of the ligands.

Compounds	δ (ppm)	signal	no of protons	Attribution
babh	1.90	singlet	(3, H)	CH ₃
	2.60	triplet	(2, H)	CH ₂
	2.80	triplet	(2, H)	CH ₂
	7.10 -7.80	multiplet	(10, H)	Aromatic protons
	10.40	singlet	(1, H)	N-H
<i>p</i> -OH-babh	1.90	singlet	(3, H)	CH ₃
	2.50	triplet	(2, H)	CH ₂
	2.80	triplet	(2, H)	CH ₂
	6.70 – 7.70	multiplet	(9, H)	Aromatic protons
	9.90	singlet	(1, H)	N-H
	10.10	singlet	(1, H)	O-H
<i>p</i> -NO ₂ -babh	3.80	singlet	(3, H)	CH ₃
	3.00	triplet	(2, H)	CH ₂
	3.10	triplet	(2, H)	CH ₂
	7.60 -8.80	multiplet	(9, H)	Aromatic protons
	11.20	singlet	(1, H)	N-H

Table 4.5b. ^{13}C NMR data of the ligands.

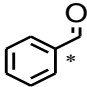
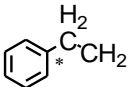
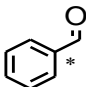
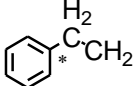
Compounds	δ (ppm)	Attribution
Babh	16.80	CH_3
	30.70	CH_2
	31.90	CH_2
	126.80 – 134.10	Aromatic carbon
	141.30	
	140.90	
	161.70	$\text{C}=\text{N}$
	163.30	$\text{C}=\text{O}$
<i>p</i> -OH-babh	16.60	CH_3
	30.60	CH_2
	31.60	CH_2
	114.60 – 129.70	Aromatic carbon
	141.30	overlap of  and 
		160.10
	163.90	$\text{C}=\text{O}$

Table 4.5c. ¹³C NMR data of the ligands. (Con'd)

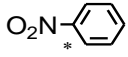
Compounds	δ (ppm)	Attribution
<i>p</i> -NO ₂ -babh	31.80	CH ₃
	17.10	CH ₂
	17.10	CH ₂
	123.30 – 139.90	Aromatic carbon
	148.90	
	163.30	C=N
	163.90	C=O

Table 4.6. Conductance measurement data of the complexes ($\text{ohm}^{-1}\text{cm}^2\text{mol}^{-1}$).

Compound	molar conductance
$\text{Cu}(\text{babh})_3(\text{OAc})_2$	42.30
$\text{Cu}(\textit{p}\text{-NO}_2\text{-babh})_3(\text{OAc})_2$	23.00
$\text{Ni}(\text{babh})_2(\text{OAc})_2$	68.10
$\text{Ni}(\textit{p}\text{-NO}_2\text{-babh})_2(\text{OAc})_2$	38.70
$\text{Co}(\textit{p}\text{-NO}_2\text{babh})_2(\text{OAc})_2 \cdot 3\text{H}_2\text{O}$	18.50

Table 4.7. Antimicrobial activity data for babh compounds at 40mg/ml

Compound	Growth inhibition zone in millimetres (mm)					
	(Gram Positive)		(Gram Negative)			
	<i>Bacillus cereus</i>	<i>Staphylococcus aureus</i>	<i>Pseudomonas aeruginosa</i>	<i>Escherichia coli</i>	<i>Klebsiella pneumoniae</i>	<i>Shigella flexneri</i>
babh	-	-	-	-	-	-
<i>p</i> -OH-babh	-	-	-	-	-	-
<i>p</i> -NO ₂ -babh	-	-	-	-	-	-
Cu(babh)(NO ₃) ₂ ·5H ₂ O	30	16	-	26	20	30
Cu(babh) ₃ (OAc) ₂	12	14	-	14	-	-

Table 4.7. Antimicrobial activity data for babh compounds at 40mg/ml

Compound	Growth inhibition zone in millimetres (mm)					
	(Gram Positive)		(Gram Negative)			
	<i>Bacillus cereus</i>	<i>Staphylococcus aureus</i>	<i>Pseudomonas aeruginosa</i>	<i>Escherichia coli</i>	<i>Klebsiella pneumoniae</i>	<i>Shigella flexneri</i>
Cu(<i>p</i> -NO ₂ -babh) ₃ (OAc) ₂	-	-	-	-	-	-
Cu(<i>p</i> -NO ₂ -babh)SO ₄ .2C ₂ H ₅ OH	-	-	-	-	-	-
Ni(babh) ₂ Cl ₂	15	28	20	-	-	12
Ni(babh)(NO ₃) ₂ .2H ₂ O	-	-	-	20	-	12
Ni(babh) ₂ (OAc) ₂	-	-	-	-	-	-

Table 4.7. Antimicrobial activity data for babh compounds at 40mg/ml

Compound	Growth inhibition zone in millimetres (mm)					
	(Gram Positive)			(Gram Negative)		
	<i>Bacillus cereus</i>	<i>Staphylococcus aureus</i>	<i>Pseudomonas aeruginosa</i>	<i>Escherichia coli</i>	<i>Klebsiella pneumoniae</i>	<i>Shigella flexneri</i>
Ni(<i>p</i> -OH-babh) ₂ Cl ₂	11	-	-	12	-	-
Ni(<i>p</i> -OH-babh) ₂ (NO ₃) ₂	-	-	-	-	-	-
Ni(<i>p</i> -NO ₂ -babh)Cl ₂ .4H ₂ O	17	22	14	21	22	-
Ni(<i>p</i> -NO ₂ -babh) ₂ (NO ₃) ₂	-	-	-	18	-	16
Ni(<i>p</i> -NO ₂ -babh) ₂ (OAc) ₂	-	-	-	-	-	-

Table 4.7. Antimicrobial activity data for babh compounds at 40mg/ml

Compound	Growth inhibition zone in millimetres (mm)					
	(Gram Positive)		(Gram Negative)			
	<i>Bacillus cereus</i>	<i>Staphylococcus aureus</i>	<i>Pseudomonas aeruginosa</i>	<i>Escherichia coli</i>	<i>Klebsiella pneumoniae</i>	<i>Shigella flexneri</i>
Ni(<i>p</i> -NO ₂ -babh)SO ₄ .2H ₂ O	22	14	-	-	-	-
Co(babh) ₂ Cl ₂	-	-	-	-	-	-
Co(babh) ₂ (NO ₃) ₂	15	12	-	16	-	15
Co(babh)SO ₄ .4H ₂ O	18	16	16	20	20	15
Co(<i>p</i> -OH-babh) ₂ Cl ₂	-	-	-	-	-	15
Co(<i>p</i> -OH-babh) ₂ (NO ₃) ₂	-	-	-	-	-	-

Table 4.7. Antimicrobial activity data for babh compounds at 40mg/ml`

Compound	Growth inhibition zone in millimetres (mm)					
	(Gram Positive)		(Gram Negative)			
	<i>Bacillus cereus</i>	<i>Staphylococcus aureus</i>	<i>Pseudomonas aeruginosa</i>	<i>Escherichia coli</i>	<i>Klebsiella pneumoniae</i>	<i>Shigella flexneri</i>
Co(<i>p</i> -OH-babh) ₂ (OAc) ₂	-	-	-	-	-	-
Co(<i>p</i> -OH-babh)SO ₄ .2H ₂ O	-	-	-	-	-	-
Co(<i>p</i> -NO ₂ -babh) ₂ Cl ₂	-	-	14	-	-	16
Co(<i>p</i> -NO ₂ -babh) ₂	-	-	-	15	-	13
Co(<i>p</i> -NO ₂ -babh) ₂ (OAc) ₂ .3H ₂ O	-	-	-	-	-	-
Co(<i>p</i> -NO ₂ -babh)SO ₄	16	25	20	21	30	25

Table 4.8: MIC screening for Antimicrobial Studies

Compound	Concentration (mg/mL)	Zone inhibition (mm)	of Organisms
Ni(babh) ₂ Cl ₂	20	14	<i>Shigella flexneri</i>
	10	12	<i>Escherichia coli</i>
	10	11	<i>Bacillus cereus</i>
Ni(babh)(NO ₃) ₂ .2H ₂ O	5	11	<i>Bacillus cereus</i>
Ni(<i>p</i> -NO ₂ babh)Cl ₂ .4H ₂ O	10	18	<i>Bacillus cereus</i>
	5	10	<i>Bacillus cereus</i>
	10	15	<i>Staphylococcus aureus</i>
	5	10	<i>Staphylococcus aureus</i>
Ni(<i>p</i> -NO ₂ babh)SO ₄ .2H ₂ O	10	12	<i>Staphylococcus aureus</i>
Co(<i>p</i> -NO ₂ babh) ₂	20	11	<i>Shigella flexneri</i>
	10	14	<i>Bacillus cereus</i>
	10	12	<i>Staphylococcus aureus</i>
Co(<i>p</i> -NO ₂ babh)SO ₄	20	15	<i>Klebsiella pneumoniae</i>
Streptomycin	0.125	20	<i>Escherichia coli</i>
	0.125	26	<i>Escherichia coli</i>
	0.125	30	<i>Klebsiella pneumoniae</i>
	0.125	30	<i>Staphylococcus aureus</i>
	0.125	32	<i>Escherichia coli</i>
	0.500	32	<i>Bacillus cereus</i>
	0.500	20	<i>Pseudomonas aeruginosa</i>

CHAPTER FIVE

DISCUSSION

5.1. General comments

The hydrazone ligands, copper(II), nickel(II) and cobalt(II) complexes have been prepared according to methods described in literature (Deepa and Aravindakshan, 2005; Howlader *et al.*, 2009; Adekunle *et al.*, 2010) and were characterised in order to propose their geometry and stoichiometries. The results are presented in **Tables 4.1 – 4.8** in chapter four and **Figures 6.7 – 6.67** in appendices.

5.2 Physico-chemical characterisation

Physical and chemical properties of the compounds are presented in **Tables 4.1 and 4.2**; these include colour, melting point/decomposition temperature, percentage yields and elemental compositions. The solubility of the compounds is shown in **Table 4.2**.

5.2.1 Colour

babh and *p*-OH-babh ligands are white, while *p*-NO₂-babh is yellow in colour. The copper(II) complexes showed colours which are green, blue and brown. Nickel(II) complexes showed colours ranging from green, blue, and brown to yellow, while cobalt(II) complexes are generally pink except Co(*p*-OH-babh)₂(OAc)₂ that is brown in colour (Table 4.1).

5.2.2 Melting point/decomposition temperature

The melting point of the hydrazone ligands ranges from 132 - 220°C. Copper(II) complexes exhibited melting points ranging from 140 – 236°C, with three of the complexes having melting point greater than 300°C. The nickel(II) complexes showed greater thermal stability with melting point between 152°C - 287°C. Six of the nickel(II) complexes had melting point greater than 300°C, without decomposing. The cobalt(II) complexes had melting points ranging from 103°C to 299°C, with only one having melting point above 300°C. It was observed that all the chloro and sulphato complexes had melting point above 200°C except Cu(*p*-OH-babh)₂Cl₂ that melted at 191°C and

Co(*p*-OH-babh)SO₄·2H₂O that melted at 170°C indicating high thermal stability for the chloro and sulphato complexes. In general, the trend in the melting point of the complexes based on the counter anions present was: SO₄ ~ Cl⁻ > NO₃⁻ > OAc⁻.

5.2.3 Percentage yield

The ligands were obtained in reasonable yield with a percentage of 89 - 96%, while the metal complexes had yield in the range 18 - 81%.

5.2.4 % Metal analysis

The metal analysis results had a good agreement between the expected and observed values. The results generally revealed a 1:3, 1:2 and 1:1 (M: L) ratio for the complexes. Some of them were found to be hydrated with various moles of water molecule.

5.2.5 Elemental analysis.

The results of the microanalysis agreed fairly with the proposed stoichiometry. The results conformed to the observation that the anions are present in the complexes. Furthermore, it also suggested that some of the compounds are hydrated.

5.3 Solubility

The synthesised compounds; the ligands and the complexes were all insoluble in water showing their covalent and non-electrolytic nature. The metal(II) complexes were fairly soluble in methanol and DMSO. There was generally, varying degree of solubility in the seven solvents used (Table 4.2).

5.4 Spectroscopic characterisation

The bond vibrational frequencies and electronic transition bands within the ligands and the metal(II) complexes were studied using the infrared and UV-Visible spectroscopic techniques respectively.

5.4.1. ^1H -NMR and ^{13}C NMR spectra

The ^1H -NMR spectra of the ligands are shown in Figures 6.61 – 6.66 and assignments of the signals are written in Table 4.6. The spectra revealed the diversity of benzylacetone-benzoylhydrazone (babh), its para-hydroxyl and para-nitro substituted analogues (Figures 6.61, 6.63, 6.65).

The ligands generally showed four sets of peaks, the first one observed as singlet at 10.40 ppm (1H, s) in babh, at 9.90 ppm (1H, s) in *p*-OH-babh and 11.20 ppm (1H, s) in *p*-NO₂-babh which was assigned to the hydrazono (N-H) proton and is also diagnostic of hydrazones (Rodrigues-Arguelles *et al.*, 2009; Christie *et al.* 2010; Gup, 2015; Saeed, 2016). The upfield signal in *p*-OH-babh was the result of electron donating effect of the hydroxy group which acted to shield the proton, whereas, the movement further downfield in *p*-NO₂-babh resulted from the electron withdrawing effect of the nitro group which left the hydrazono proton more deshielded (Chitrapriya *et al.*, 2008) In addition to the (N-H) signals in this region, *p*-OH-babh showed a signal at 10.10 ppm (1H, s) due to O-H. These hydrogen resonances appeared at a high δ values because of their attachment to highly electronegative atoms, which are oxygen and nitrogen. The position of these peaks in the downfield region indicated the possibility of extensive network of hydrogen bonding. (Al-Shaalán, 2011).

The second set of peaks appeared as a multiplet at 7.10 -7.80 ppm (10 H, multiplet) in babh; 6.70 – 7.70 ppm (9 H, multiplet) in *p*-OH-babh and 7.60 -8.80 ppm (9 H, multiplet) in *p*-NO₂-babh corresponding to the aromatic protons (Rodríguez-Argüelles *et al.*, 2009). The third set of peaks were the two adjacent methylene groups, each appearing as triplet in the 2.50–2.60 ppm range in babh; 2.60 – 2.80 ppm in *p*-OH-babh and 3.00 - 3.10 ppm in *p*-NO₂-babh. The methyl groups which were the fourth set, appeared as a singlet at 1.90 ppm (1 H, s) in babh, at 1.90 ppm (1 H, s) in *p*-OH-babh and significant shift to 3.80 ppm (1 H,s) in *p*-NO₂-babh. It was observed from the ^1H -NMR spectrum of the ligands that the keto form predominates in solution over the enol form which was also evident in the compositions of the metal(II) complexes.

The ^{13}C -NMR spectrum of the ligand babh (Figures 6.62) had peaks at 16.80 ppm assigned to the methyl carbon (CH₃), while the two peaks resonating at very close range of 30.70 and 31.90 ppm were due to the carbon of the two adjacent methylene groups

(CH₂). The aromatic carbon appeared at the region between 126.80 to 134.10 ppm while the signal at 161.70 ppm was due to the carbon of the azomethine (C=N), and 163.30 ppm due to the carbon of the carbonyl group (C=O).

In the para-hydroxyl substituted analogue (Fig. 6.64), the methyl carbon appeared at 16.60 ppm, and the methylene carbons at 30.60 and 31.60 ppm respectively. The aromatic carbons showed up at between 114.60 to 129.70 ppm, while the azomethine carbon and the carbonyl carbon resonated at 160.10 and 163.90 ppm respectively. It was found that the electron donating effect of the hydroxyl group acted to shield these carbons thereby resonating at a slightly lower δ values compared to the unsubstituted ligand.

The para-nitro substituted derivative (Fig. 6.66), had significant shifts downfield to higher δ values as a result of the electron withdrawing substituents that left the carbon atoms more deshielded. The methyl group appeared at 31.80 ppm, while the aromatic carbons resonated between 123.30 to 139.90 ppm. The azomethine carbon was observed at 163.30 ppm while the carbonyl carbon was at observed 163.90 ppm. Conclusively, the spectra data of the ligands suggested their formation and showed their diversity.

5.4.2 Infrared spectra

The infrared spectra of the synthesized hydrazone ligands, copper(II), nickel(II) and cobalt(II) complexes are shown in Table 4.3. The diagnostic and relevant vibrational frequencies obtained from the spectra (figures 6.7 – 6.25, Appendix 1) of the compounds were assigned to fundamental vibrational modes in line with literature reports on similar compounds (Deepa and Aravindakshan, 2005; Agarwal *et al.*, 2006). The infrared spectra of the ligands were compared to the spectra of the metal complexes to observe the shifts in bands which could provide an evidence of coordination to the metal ion (Agarwal *et al.*, 2006; Patel *et al.*, 2013; Cao *et al.*, 2018)

Generally, four bands have been of significance and used in the interpretation of infrared spectra of compounds of hydrazones (Baliga and Revankar, 2006; Howlader *et al.*, 2009; Mostafa, 2011). These bands are due to $\nu(\text{C=O})$, $\nu(\text{N-H})$, $\nu(\text{C=N})$ and $\nu(\text{N-N})$ vibrational frequencies. The bands usually undergo bathochromic or hypsochromic shifts on complexation of the ligands to the metal ions, which provide an evidence for coordination (Gup *et al.*, 2015). In addition, bands due to metal - oxygen and metal -

nitrogen bonds which hitherto were absent in the spectra of the ligands are usually observed in the spectrum of the complex. This provides additional evidence for coordination. Additional vibrations due to anions are also observed when they are coordinated (Nakamoto, 1997. Devi and Singh, 2011; Salem *et al*, 2015)

Therefore, in these new hydrazone ligands, the $\nu(\text{N-H})$ vibrational frequencies were observed in benzylacetone benzoylhydrazone (babh) at 3165 cm^{-1} (Figure 6.7). In *p*-OH-babh (Figure 6.14), the band shifted to a lower wavenumber at 3132 cm^{-1} . This is a bathochromic movement of the $\nu(\text{N-H})$ band and it was due to the positive inductive effect (+I) of the hydroxyl substituent on the system. El-Sherif, (2009) had made similar observation in the spectrum of a hydrazone ligand namely; 1-(phenyl-hydrazono)-propan-2-one, where the presence of an alkyl group (electron donating substituent) on para position, led to the lowering of the $\nu(\text{N-H})$ band by a magnitude of $3 - 5 \text{ cm}^{-1}$. In the infrared spectrum of *p*-NO₂-babh (figure 6.20) the $\nu(\text{N-H})$ stretching vibration appeared at a higher wavenumber of 3225 cm^{-1} . This is hypsochromic shift due to the combination of -I inductive effect and mesomeric effect of the para-nitro substituent in the ligand (Omoregie and Woods, 2011; Chitrapriya *et al*, 2008).

In the copper(II) complexes, the $\nu(\text{N-H})$ band generally had a bathochromic shift to lower wave numbers as a result of the complexation of the Cu(II) ion to the ligands. The magnitude of the lowering of this band is between ($10 - 100 \text{ cm}^{-1}$) and is highest in copper(II) complexes of *p*-OH-babh, resulting from the +I inductive effect of the substituents. Presence of counter anions similarly had influence on the lowering of the $\nu(\text{N-H})$ band with the trend in order of acetato > chloro > sulphato > nitrate complexes. However, the $\nu(\text{N-H})$ band had a hypsochromic shift to 3326 cm^{-1} in the spectrum of $\text{Cu}(p\text{-NO}_2\text{-babh})\text{Cl}_2 \cdot \text{H}_2\text{O}$ but no shift was observed in $\text{Cu}(p\text{-OH-babh})\text{SO}_4 \cdot 3\text{H}_2\text{O}$. The presence of the $\nu(\text{N-H})$ band in the spectra of copper(II) complexes indicated that the ligands coordinated in keto form in all the complexes except in $\text{Cu}_2(\text{babh})_2\text{Cl}_2$ and $\text{Cu}(p\text{-NO}_2\text{-babh})(\text{NO}_3)$ where there was the disappearance of the $\nu(\text{N-H})$ vibrational frequencies, due to enolisation of the hydrazono proton and subsequent coordination as a uninegative ligand. The appearance of a new band around 1600 cm^{-1} due to new (C=N-N=C) in these two complexes supported the findings (Gup *et al.*, 2015).

In the Ni(II) complexes, there was significant hypsochromic shifts in the vibrational frequencies of the $\nu(\text{N-H})$ in the range $18 - 113 \text{ cm}^{-1}$. These increase in frequency is of

the order $\text{Ni}(p\text{-NO}_2\text{babh})\text{Cl}_2 \cdot 4\text{H}_2\text{O} > \text{Ni}(p\text{-OHbabh})\text{SO}_4 \cdot 3\text{H}_2\text{O} > \text{Ni}(p\text{-OHbabh})_2(\text{OAc})_2 > \text{Ni}(p\text{-OHbabh})_2\text{Cl}_2 > \text{Ni}(\text{babh})_2\text{Cl}_2 > \text{Ni}(\text{babh})(\text{NO}_3)_2 \cdot 2\text{H}_2\text{O}$, and is the result of the $-I$ inductive effect of the anions on the complexes. The presence of a nitro substituent in the chloro complex; that is $\text{Ni}(p\text{-NO}_2\text{babh})\text{Cl}_2 \cdot 4\text{H}_2\text{O}$, led to a higher hypsochromic shift than others due to the combined $-I$ inductive effect of the electron withdrawing anions, whereas it was lower in the chloro and nitrate complexes of the unsubstituted babh ligand. All other Ni(II) complexes had bathochromic shift to lower wave numbers except $\text{Ni}(\text{babh})\text{SO}_4 \cdot 5\text{H}_2\text{O}$ where the band remained in the same position. The results of the IR revealed that the ligands bonded in keto form (Salem et al., 2015).

In the Co(II) complexes of all the ligands, the $\nu(\text{N-H})$ band had significant hypsochromic shift ranging from $4\text{ cm}^{-1} - 150\text{ cm}^{-1}$ in all the complexes except in $\text{Co}(p\text{-OHbabh})\text{SO}_4 \cdot 2\text{H}_2\text{O}$, $\text{Co}(p\text{-NO}_2\text{babh})_2\text{Cl}_2$, $\text{Co}(p\text{-NO}_2\text{babh})$ and $\text{Co}(p\text{-NO}_2\text{babh})_2(\text{OAc})_2$ which had bathochromic shift to lower frequency. The increase in frequency followed the order: $\text{Co}(p\text{-OHbabh})_2(\text{OAc})_2 > \text{Co}(\text{babh})_2\text{Cl}_2 > \text{Co}(p\text{-OHbabh})_2(\text{NO}_3)_2 > \text{Co}(p\text{-NO}_2\text{babh})_2\text{SO}_4 > \text{Co}(p\text{-OHbabh})_2\text{Cl}_2 > \text{Co}(\text{babh})_2(\text{NO}_3)_2 > \text{Co}(\text{babh})_2(\text{OAc})_2 > \text{Co}(\text{babh})\text{SO}_4 \cdot 4\text{H}_2\text{O}$.

The carbonyl band $\nu(\text{C=O})$ was observed in babh ligand at 1652 cm^{-1} . It was found at 1651 cm^{-1} in the $p\text{-OH-babh}$ ligand having a medium intensity. In $p\text{-NO}_2\text{-babh}$, the carbonyl band was shifted to higher wavenumber at 1667 cm^{-1} , and this hypsochromic shift was due to the mesomeric effect of the nitro substituents on the system which increases the C=O bond order. On complexation of the ligands with the Cu(II) ions, there was a bathochromic shift of the magnitude of $5\text{-}50\text{ cm}^{-1}$ in the C=O bands in all the copper(II) complexes except in $\text{Cu}(p\text{-OH-babh})_2\text{Cl}_2$ that had hypsochromic shift, and $\text{Cu}_2(\text{babh})_2\text{Cl}_2$ in which the ligand coordinated in enol form which led to the loss of the $\nu(\text{C=O})$ band and emergence of a new band at around 1240 cm^{-1} assigned to $\nu(\text{C-O})$ (Chitrapriya et al, 2008; Seleem, 2011). Nickel complexes similarly had bathochromic shifts to lower wavenumber for the carbonyl bands in all the compounds except $\text{Ni}(\text{babh})_2(\text{OAc})_2$ and $\text{Ni}(\text{babh})\text{SO}_4 \cdot 5\text{H}_2\text{O}$ that had a shift to higher wavenumber. All the cobalt(II) complexes likewise experienced bathochromic shifts to lower wavenumbers for the carbonyl bands. It could therefore be concluded that the ligands coordinated in keto form through the carbonyl oxygen, while the disappearance of the carbonyl band due to deprotonation in some complexes suggested that the hydrazones acted as a

uninegative ligands coordinating to the metal ion through the deprotonated carbonyl oxygen (Al-Shaalan, 2011).

The azomethine band $\nu(\text{C}=\text{N})$, which is usually the other point of coordination in hydrazone occurs in the range $1537 - 1607 \text{ cm}^{-1}$ in the ligands. This band experienced blue or red shifts of the magnitude of $5 - 60 \text{ cm}^{-1}$ in the complexes. This indicated coordination of the azomethine $\nu(\text{C}=\text{N})$ bond to the metal ion through the nitrogen atom. The shifts of bands observed in the spectra of the complexes are due to the decrease in the electron density on the nitrogen atom having been bonded to the central metal ion. (Gup *et al.*, 2015)

In the infrared spectra of the synthesised hydrazone ligands, the bands in the $1030 - 1060 \text{ cm}^{-1}$ are assigned to $\nu(\text{N}-\text{N})$ vibrations (Hueso-Urena *et al.*, 2000). Upon coordination of the ligands to the metal(II) ions, the $\nu(\text{N}-\text{N})$ bands shifted to lower wavenumbers in the spectra of the metal complexes as a result of the bonding of the ligands to the metal ions (Alhadi *et al.*, 2012). Hence, the ligands generally acted as bidentate ligands.

Absorption bands due to metal-ligand vibrations appeared in the spectra of the metal complexes. The bands of weak to medium intensity in the range $500 - 666 \text{ cm}^{-1}$ and $373 - 500 \text{ cm}^{-1}$ have been assigned to the $\nu(\text{M}-\text{O})$ and $\nu(\text{M}-\text{N})$ modes respectively. These were previously not observed in the spectra of the ligands, and it further confirmed the coordination of the ligands to the metal ions (Nakamoto, 1997; Woods *et al.*, 2009b).

The coordination of nitrate, acetate and sulphate anion ligands have been well studied in the infrared spectra of metal complexes (Chitrapriya *et al.*, 2008; Seleem, 2011). In the sulphato complexes, a broad band around $1074 - 1090 \text{ cm}^{-1}$ is diagnostic of the coordination of the SO_4^{2-} to the metal ion. Coordination of anion in bidentate fashion is known to decrease the tetrahedral symmetry of the group which may therefore split this band (Devi and Singh, 2011; Seleem, 2011). Hence, in the sulphato complexes, the band at 1080 cm^{-1} splitted into two, this indicated the coordination of the sulphate anion to the metal ion in a bidentate fashion (Eflhymiou, 2009). Similarly, the acetate anion is characterised by bands at 1578 cm^{-1} and 1411 cm^{-1} , which are commonly assigned to the asymmetric $\nu_{\text{as}}(\text{COO})$ and the symmetric $\nu_{\text{sym}}(\text{COO})$ stretching vibrations of the carboxylate group (Patel *et al.*, 2013). In the synthesised acetato complexes, the frequency of $\nu_{\text{asy}}(\text{COO})$ appeared in the range $1417 - 1602 \text{ cm}^{-1}$, while those

characteristic of $\nu_{\text{sym}}(\text{COO})$, ranged from 1274 - 1495 cm^{-1} . The difference in $\Delta\nu$ ($\nu_{\text{asy}} - \nu_{\text{sym}}$) has been employed as indicators of coordination modes of the acetate group (Seleem, 2015). A difference smaller than 200 cm^{-1} can indicate a bidentate coordination mode while a difference larger than 200 cm^{-1} can indicate monodentate coordination (Shebl *et al.*, 2014). In the synthesised acetato complexes, a difference of more than 200 cm^{-1} was found indicating a monodentate coordination for the acetate group except in $\text{Cu}(\text{babh})_3(\text{OAc})_2$, $\text{Cu}((p\text{-NO}_2\text{-babh})_3(\text{OAc})_2$ and $\text{Ni}(\text{babh})_2(\text{OAc})_2$ where it was probable that the acetate anion were present outside the coordination sphere. In the nitrate complexes, the presence of the nitrate anion are characterised by the two bands usually observed in the range 1445 - 1500 cm^{-1} due to symmetric stretching mode (ν_4) and 1350 – 1400 cm^{-1} due to asymmetric stretching mode (ν_1). The presence of these bands has been used by authors to suggest that the nitrate anion is covalently bonded and present inside the coordination sphere (Patel *et al.*, 2013)). The difference in the two bands $\Delta\nu = (\nu_{\text{asy}} - \nu_{\text{sym}})$ have been used to indicate the mode of bonding. A difference of less than 200 cm^{-1} suggest monodentate binding for the nitrate ion while a value greater than 200 cm^{-1} indicate bidentate binding (Shebl *et al.*, 2014). Therefore, in the synthesised nitrate complexes, a difference of less than 200 cm^{-1} was observed and this indicated the nitrate anions are binding in a monodentate fashion.

5.4.3. Electronic spectra

The electronic spectra in methanol solution and as solid reflectance spectra for the synthesised hydrazone ligands and their metal(II) complexes are presented in figures 6.26 – 6.61, Appendix 2. Assignments of the bands in the spectra (Table 4.4) have been made based on previous assignments in similar compounds (Ainscough *et al.*, 1998; Hosny *et al.*, 2010; Cao *et al.*, 2018).

In the ultraviolet spectra of the synthesised ligands, two electronic transitions were prominent. These are the intraligand $\pi \rightarrow \pi^*$ transition within the aromatic system in the range 48,780 – 48,309 cm^{-1} (Singh *et al.*, 2009) and the bands in the range 38,460 – 37,195 cm^{-1} which are probably due to the overlap of the intraligand $\pi \rightarrow \pi^*$ and $n \rightarrow \pi^*$ transitions (Toro, 2008), within the C=N-NH-CO moiety (Halli *et al.*, 2011; Alhadi *et al.*, 2012). The intraligand $\pi \rightarrow \pi^*$ transition occurred in babh at 48780 cm^{-1} and had a marginal bathochromic shift to 48309 cm^{-1} in *p*-OH-babh and to 48544 cm^{-1} in *p*-NO₂-babh. The second prominent transition occurred from the overlap of the $n \rightarrow \pi^*$ and π

→ π^* electronic transitions in the free, uncoordinated hydrazone ligands that occurred at 38460 cm^{-1} experienced bathochromic shift to lower wavenumber in *p*-OH-babh to 37195 cm^{-1} and to 37313 cm^{-1} in *p*-NO₂-babh. The red shifts was as a result of the +I inductive effect of the hydroxyl substituent and –I inductive effect of the nitro substituent on the system (Owolabi and Olarinoye, 2008).

In the ultraviolet electronic spectra of the copper(II) complexes, there were bathochromic shift of the intraligand band $\pi \rightarrow \pi^*$, and it decreased in the order $\text{Cu}(\text{babh})_3(\text{OAc})_2 > \text{Cu}(\text{p-OH-babh})_2(\text{OAc})_2 > \text{Cu}(\text{p-OH-babh})_2\text{Cl}_2 > \text{Cu}(\text{p-NO}_2\text{-babh})\text{SO}_4 \cdot 2\text{C}_2\text{H}_5\text{OH} > \text{Cu}(\text{babh})_2\text{SO}_4 \cdot \text{H}_2\text{O}$. The decrease in energy is due to the expansion of the d electron clouds as a result of the d orbitals overlap with ligand atom orbitals (Cotton *et al.*, 2003). All other copper(II) complexes had a hypsochromic shift of the order $\text{Cu}(\text{p-NO}_2\text{-babh})\text{Cl}_2 \cdot 2\text{H}_2\text{O} > \text{Cu}(\text{p-NO}_2\text{-babh})(\text{NO}_3) > \text{Cu}(\text{p-NO}_2\text{-babh})_3(\text{OAc})_2 > \text{Cu}_2(\text{babh})_2\text{Cl}_2 > \text{Cu}(\text{p-OH-babh})\text{SO}_4 \cdot 3\text{H}_2\text{O}$. The shifts in the complexes were an indication of interaction between the metal(II) ions and the ligands (Baliga, 2006; Anacona and Maria, 2015).

The solid state spectra of the copper(II) complexes display asymmetric band in the region $14,492 - 19,607\text{ cm}^{-1}$. This is consistent with the ${}^2\text{E}_g \rightarrow {}^2\text{T}_{2g}$ transition in an octahedral environment (Cotton *et al.*, 2003; Alhadi, *et al.*, 2012). The broadening of the observed band may be due to Jahn-Teller effect arising from the unequal occupation of the e_g pair of orbital (d_z^2 , $d_{x^2-y^2}$) (Huang *et al.*, 2011). However, the visible spectra of the dimeric $\text{Cu}_2(\text{babh})_2\text{Cl}_2$ showed three transitions at $19,607\text{ cm}^{-1}$, $15,385\text{ cm}^{-1}$, and $11,111\text{ cm}^{-1}$ which may be assigned to the three well resolved electronic transitions: ${}^2\text{B}_{1g} \rightarrow {}^2\text{B}_{2g}$, ${}^2\text{B}_{1g} \rightarrow {}^2\text{A}_{1g}$ and ${}^2\text{B}_{1g} \rightarrow {}^2\text{E}_g$. The location of these bands further suggested square planar environment for the Cu(II) ion (Earnshaw and Greenwood, 1984).

In the ligand field spectra of the nickel(II) complexes, three d-d bands are expected for a nickel(II) ion in an octahedral environment corresponding to the transition, ${}^3\text{A}_{2g} \rightarrow {}^3\text{T}_{2g}$ in the range $7,000 - 13,135\text{ cm}^{-1}$, (ν_1); ${}^3\text{A}_{2g} \rightarrow {}^3\text{T}_{1g}$ in the range $11,889 - 21,000\text{ cm}^{-1}$, (ν_2), and ${}^3\text{A}_{2g} \rightarrow {}^3\text{T}_{1g}(\text{P})$ in the range $18,000 - 27,000\text{ cm}^{-1}$, (ν_3) (Woods, *et al.*, 2009a; Cotton *et al.*, 2003). However, the first transition (ν_1), that is, ${}^3\text{A}_{2g} \rightarrow {}^3\text{T}_{2g}$ is very close to the near infrared region and usually out of range of most instrument used for UV-Vis measurement, therefore may or may not be seen (Salem *et al.*, 2015). Similarly, ${}^3\text{A}_{2g} \rightarrow {}^3\text{T}_{1g}(\text{P})$ (ν_3) transition could overlap with the tail of the ligand absorption band.

Therefore, in the nickel(II) complexes, Ni(babh)(NO₃)₂.2H₂O and Ni(*p*-NO₂-babh)SO₄.2H₂O showed three clear bands ranging from 10,416 to 11,363 cm⁻¹. (ν_1), 13,157 to 17,543 cm⁻¹ (ν_2) and 16,660 to 20,833 cm⁻¹ due to (ν_3) transition in octahedral environment. All other nickel(II) complexes had two transitions in the range 14705 – 21,733 cm⁻¹ due to ${}^3A_{2g} \rightarrow {}^3T_{1g}$, (ν_3) and at 16,949 – 10,309 cm⁻¹ assigned to the ${}^3A_{2g} \rightarrow {}^3T_{1g}$ (ν_2) in an octahedral environment (Earnshaw and Greenwood, 1984; Odunola *et al.*, 2003). The exception was Ni(babh)₂(OAc)₂ that had one band at 16666 cm⁻¹, which was assigned to ${}^3T_1 \rightarrow {}^3A_2$ in a tetrahedral environment (Gupta *et al.*, 2007).

Three spin-allowed transitions are expected for octahedral Co(II) with the transition having a ground state term ${}^4T_{1g}$. These are due to: ${}^4T_{1g} \rightarrow {}^4T_{2g}$ (ν_1) at around 8,000 - 11,000 cm⁻¹; ${}^4T_{1g} \rightarrow {}^4A_{2g}$ (ν_2) 10,000 – 16,000 cm⁻¹; and ${}^4T_{1g} \rightarrow {}^4T_{1g}$ (P) (ν_3) around 19,000 -21,000 cm⁻¹. However, the spectra of octahedral Co(II) often does not show three distinct peaks that correspond to the three predicted excited states. Instead, the spectra has a broad band. The lowest energy transition is ${}^4T_{1g} \rightarrow {}^4T_{2g}$, occurred in the near infrared and is not usually observed in the visible spectrum. The main band is the energy transition ${}^4T_{1g}$ (F) \rightarrow ${}^4T_{1g}$ (P), and the slightly higher energy transition (the shoulder) is predicted to be ${}^4T_{1g} \rightarrow {}^4A_{2g}$. The small energy difference leads to the overlap of the two bands, and this explains the broad band that is commonly observed in the visible spectrum of octahedral Co(II) complexes (Jorgensen, 1954). Therefore, the electronic spectrum of the synthesised Co(II) complexes showed two d-d transitions in the range 18,761–13,331 cm⁻¹ and 21,974 cm⁻¹ – 20,704 cm⁻¹ due to the ${}^4T_{1g}$ (F) \rightarrow ${}^4A_{2g}$ and ${}^4T_{1g}$ (F) \rightarrow ${}^4T_{1g}$ (P) transitions respectively. This indicates an octahedral configuration around Co(II) ions (Sousa-Pedrares *et al.*, 2008). The ${}^4T_{1g}$ (F) \rightarrow ${}^4T_{2g}$ (F) transition would be observed in near infrared region and is usually outside the range of spectrophotometer (Al-Shaalan, 2011). However, the electronic spectra of the complexes Co(*p*-NO₂-babh)SO₄, and Co(*p*-NO₂-babh)₂ exhibited broad bands at 18,867 - 19,417 cm⁻¹ which are characteristic of square planar cobalt(II) complexes.

5.5 Magnetic Moment measurement

The room temperature effective magnetic moments were calculated using the relation ($\mu_{\text{eff}} = 2.83 (\chi'_{\text{m}} T)^{1/2}$ B. M. where χ'_{m} is the molar susceptibility corrected using Pascal's constants for diamagnetism of all atoms in the compounds (Housecroft and Sharpe, 2008; Odola and Woods, 2011). The room temperature magnetic moment for copper(II) complexes species with $S = 1/2$ usually observed for magnetically dilute copper(II) complexes is in the range 1.70 – 2.20 B. M (Patel and Woods, 1990; Earnshaw and Greenwood, 1984). A moment in the range 1.71 – 2.43 B. M. was observed in the copper(II) complexes which agrees with the values expected for monomeric, and magnetically dilute octahedral copper(II) complexes (Dutta and Syamal, 1993; Salem, 2015). There is however, the possibility of strong ferromagnetic interaction between the complexes that displayed higher than expected values. Furthermore, it was observed that dimeric complex $\text{Cu}_2(\text{babh})_2\text{Cl}_2$ had a moment of 2.90 B. M. This high value compared with the expected spin only value of 1.70 B.M for copper(II) is as a result of strong ferromagnetic coupling interaction between the two copper centres. This fact suggested that the chloro atoms are in a bridging mode between the dimeric Cu(II) complexes (Lakshmi, *et al.*, 2011).

The experimentally determined magnetic moments for the newly synthesised Ni(II) complexes were in the range 2.80 – 3.50 B. M. These values are within the range of 2.8 – 3.5 B. M, which have been reported for octahedral nickel(II) complexes in literature, and are typical for a $3d^8$ nickel(II) ion with two unpaired electrons in an octahedral environment (Woods *et al.*, 2009b; Gupta *et al.*, 2007, Alhadi *et al.*, 2012). However, $\text{Ni}(\text{babh})_2(\text{OAc})_2$ had a moment of 3.87 B. M. This value fall within those reported for tetrahedral nickel(II), and it supported the tetrahedral geometry proposed for this complex (Omoregie and Woods, 2011).

The magnetic properties for high spin octahedral Co(II) complexes are governed by the orbitally degenerate $^4T_{1g}$ ground term. This provides an orbital contribution to the magnetic moment so that room temperature moments are experimentally found to be in the range 4.7 – 5.6 B. M for octahedral Co(II) ion (Anacona and Maria, 2015).

Observed magnetic moment value for the synthesised Co(II) hydrazone complexes at room temperature was 4.74 - 5.39 B. M. These values were consistent with values reported for complexes with a high-spin octahedral environment around Co(II) in the range 4.7–5.6 B. M. Tetrahedral and high-spin octahedral Co(II) complexes possess

three unpaired electrons but may be distinguished by the magnitude of the deviation of magnetic moment from the spin-only value. To this end, the moment found for $\text{Co}(\text{babh})\text{SO}_4 \cdot 4\text{H}_2\text{O}$ was 4.46 B. M, suggesting a tetrahedral geometry for this complex, while complexes: $\text{Co}(p\text{-OH-babh})\text{SO}_4 \cdot 2\text{H}_2\text{O}$; $\text{Co}(p\text{-NO}_2\text{-babh})_2$ and $\text{Co}(p\text{-NO}_2\text{-babh})\text{SO}_4$ had a moment of 2.64, 2.45 and 2.46 B.M respectively suggesting a square planar geometry around the Co(II) (Duttal and Syamal, 1993).

5.6 Molar Conductance

Nitromethane usually gives better result for conductance measurement than other solvent due to low viscosity (Geary *et al.*, 1971). A value of 60 - 115 $\text{ohm}^{-1} \text{cm}^2 \text{mol}^{-1}$ is expected for a 1:1 electrolyte in nitromethane ((Osowole and Balogun, 2012). The molar conductance values for the synthesised metal(II) complexes that were soluble in nitromethane solution at 10^{-3} M dilution are in the range 18.5 - 42.3 $\text{ohm}^{-1} \text{cm}^2 \text{mol}^{-1}$. These values are consistent with non-electrolytic nature of the complexes in this solvent, the only exception being $\text{Ni}(\text{babh})_2(\text{OAc})_2$ which gave molar conductance value of 68.1 $\text{ohm}^{-1} \text{cm}^2 \text{mol}^{-1}$ indicating a 1:1 electrolyte. This supported the tetrahedral structure proposed for this complex and it suggested that the anion is outside the coordination sphere.

5.7 Antimicrobial activity

The compounds were screened for possible antibacterial activities at a concentration of 40 mg/mL, after which the minimum inhibitory concentrations (MIC) of the compounds with significant activity against identified organisms were done and are summarized in Tables 4.8 and 4.9. The zones of inhibition in millimetres were obtained. Compounds that inhibited microbial growth at these concentrations are generally accepted as having potential for development as an antimicrobial agent (EUCAST, 2000). The positive control used was disc of streptomycin which is an antimicrobial agent with wide spectrum of activities against bacteria.

For a compound to demonstrate antibacterial effects, it has to be taken up by the microbial cells and this can be possible when there is an appropriate balance of lipophilic and hydrophilic properties. Compounds that are too polar may not be able to act against microbes because they would not be taken up by the cells to the level at which they would be toxic to the organisms (Ang *et al.*, 2018). The synthesised ligands were

generally in-active against all the microorganisms at a concentration of 40 mg/mL used for the screening test and were not subsequently subjected to minimum inhibitory concentrations studies.

In the copper(II) complexes, $\text{Cu}(\text{babh})(\text{NO}_3)_2 \cdot 5\text{H}_2\text{O}$ was sensitive to all the tested Gram-positive and Gram-negative organisms except *P. aeruginosa* while $\text{Cu}(\text{babh})_3(\text{OAc})_2$ inhibited the Gram – positive bacteria and *Escherichia coli* which is a gram negative bacteria.

The nickel(II) complexes showed better inhibitory activities than the copper complexes. $\text{Ni}(\text{babh})_2\text{Cl}_2$ had inhibition zones of 15 mm and 28 mm against the two Gram-positive bacteria viz *B. cereus* and *S. aureus* respectively, whereas it also had inhibitory effect on two Gram-negative organisms which are *P. aeruginosa* and *S. flexneri* having a zone of inhibition of 20 mm and 12 mm respectively. $\text{Ni}(\text{p-NO}_2\text{-babh})\text{Cl}_2 \cdot 4\text{H}_2\text{O}$ similarly was active against a broad spectrum of Gram-positive and Gram-negative organisms. It had a zone of inhibition of 17 mm against *B. cereus* and 22 mm against *S. aureus* while it also exhibited activities against all the Gram-negative organisms except *S. flexneri*. $\text{Ni}(\text{babh})(\text{NO}_3)_2 \cdot 2\text{H}_2\text{O}$ and $\text{Ni}(\text{p-NO}_2\text{-babh})_2(\text{NO}_3)_2$ inhibited the growth of *E. coli* and *S. flexneri* which are Gram-negative bacteria but were not able to inhibit any of the Gram-positive test organisms. Similarly, $\text{Ni}(\text{p-NO}_2\text{-babh})\text{SO}_4 \cdot 2\text{H}_2\text{O}$ inhibited two Gram-positive organisms which were *B. cereus* and *S. aureus* but were not active against Gram-negative organisms at the concentration of 40 mg/ml used. The minimum inhibitory concentration for the nickel(II) complexes was 5 mg/mL.

In the cobalt(II) complexes, $\text{Co}(\text{babh})\text{SO}_4 \cdot 4\text{H}_2\text{O}$ and $\text{Co}(\text{p-NO}_2\text{-babh})\text{SO}_4$ had the most inhibitory effect on the test microorganisms at the concentration of 40 mg/mL, with the zones of inhibition ranging from 15 mm to 30 mm. $\text{Co}(\text{babh})_2(\text{NO}_3)_2$ on the other hand was active against *B. cereus* and *S. aureus* (Gram-positive), and *E. coli* and *S. flexneri* which are Gram-negative bacteria with zones of inhibition ranging from 12 to 16 mm. $\text{Co}(\text{p-NO}_2\text{-babh})_2\text{Cl}_2$ and $\text{Co}(\text{p-NO}_2\text{-babh})_2$ were active against Gram-negative bacteria alone which were *S. flexneri*, *E. coli* and *P. aeruginosa*. Minimum inhibitory concentration for the active cobalt(II) complexes was between 20 -10 mg/mL. However, none of the synthesised compounds had inhibitory activity comparable to streptomycin which served as the positive control.

The in-vitro antibacterial activities of the synthesized compounds revealed that the complexes had higher activities compared to that of the ligand. This behavior could be

explained based on the assumption that chelation tends to make the ligand act as a more powerful and potent antibacterial agent (Sangcharoen and Wilaipun, 2017). It had been suggested that chelation of ligands with metal atoms reduces the polarity of the metal due to the sharing of its positive charge with the donor ligand, leading to the delocalisation of π -electron over the whole chelate ring. Such a chelation could enhance the lipophilic character of the central metal atom. Subsequently, this favors the permeation of the complexes through the lipid layers of the cell membrane and thus, bears the possibility to block the metal binding site in the enzyme of a microorganism (Ang *et al.*, 2018). The activity of the complexes against various bacterial also depends either on the cells, the impermeability of the microbes or the contrasts of ribosomes in microbial cells. (Knittl, *et al.*, 2018).

CHAPTER SIX

6.1 CONCLUSIONS AND RECOMMENDATIONS

New hydrazone ligand, benzylacetone benzoylhydrazone; its para-hydroxyl and para-nitro analogues, and their copper(II), nickel(II), and cobalt(II) complexes bearing various anions have been synthesised and characterised by physical and chemical methods. Copper(II) complexes had colours ranging from green, to blue and brown, while nickel(II) complexes showed colours ranging from green, blue, brown and yellow. The cobalt(II) complexes had pink colours except $\text{Co}(p\text{-OH-babh})_2(\text{OAc})_2$ that was brown. The compounds were generally insoluble in water suggesting their covalent and non-electrolytic nature. The complexes had high melting point or decomposition temperatures which revealed a high thermal stability for the compounds.

The proton NMR of the ligands showed the diagnostic hydrazone (N-H) signals at 10.40 ppm (1H, s) in babh, at 9.90 ppm (1H, s) in *p*-OH-babh showing that the proton was more shielded in the *p*-hydroxyl derivative. The N-H proton was more deshielded in *p*-NO₂-babh resonating at 11.20 ppm (1H, s). The presence of the proton of the N-H bond is an indication of the formation of the organic compounds. The NMR studies furthermore indicated that the ligand existed in keto form in solid state and also the keto form predominates in solution. In the carbon-13 NMR, the signals at 161.70, 160.10 and 163.30 ppm in babh, *p*-OH-babh and *p*-NO₂-babh respectively are due to the azomethine C=N which is a point of bonding with the metal(II) ion. These indicate the condensation of the hydrazide and the carbonyl compound. The carbonyl carbon (C=O) which is the other point of bonding with the metal(II) ion appear at 163.30, 163.90 and 163.90 ppm in babh, *p*-OH-babh and *p*-NO₂-babh respectively.

The study of the infrared of the ligands alongside the metal(II) complexes revealed that the ligands coordinated mainly to the metal(II) ions as bidentate ligands in keto form, except in $\text{Cu}_2(\text{babh})_2\text{Cl}_2$, $\text{Cu}(p\text{-NO}_2\text{-babh})(\text{NO}_3)$ and $\text{Co}(p\text{-NO}_2\text{-babh})_2$ where the ligands coordinated in enolised form, thereby behaving as a uninegative bidentate ligand. The site of coordination being the carbonyl oxygen (C=O) and the azomethine nitrogen (C=N). In addition, there were significant infrared vibrations that confirmed

the presence of coordinated anions in the complexes. The stoichiometry of the complexes are 1:1 and 1:2 of metal: hydrazone ligands except in $\text{Cu}(\text{babh})_3(\text{OAc})_2$ and $\text{Cu}(\textit{p}\text{-NO}_2\text{-babh})_3(\text{OAc})_2$ that had a 1:3 metal : ligand ratio.

The molar conductance of the metal complexes in nitromethane were observed below $60.00 \text{ ohm}^{-1} \text{ cm}^2 \text{ mol}^{-1}$ showing that they are non-electrolytes, except $\text{Ni}(\text{babh})_2(\text{OAc})_2$ which gave a molar conductance value of $68.1 \text{ ohm}^{-1} \text{ cm}^2 \text{ mol}^{-1}$ indicating a 1:1 electrolyte.

On the basis of electronic spectra data and magnetic moment measurement, the Cu(II) complexes had a probable six coordinate octahedral geometry except $\text{Cu}_2(\text{babh})_2\text{Cl}_2$ and $\text{Cu}(\textit{p}\text{-NO}_2\text{-babh})(\text{NO}_3)$ that had a probable four coordinate square planar geometry. The Ni(II) complexes similarly had octahedral geometry except $\text{Ni}(\text{babh})_2(\text{OAc})_2$ which had a probable tetrahedral geometry.

Cobalt(II) complexes had octahedral geometry except $\text{Co}(\textit{p}\text{-OH-babh})\text{SO}_4 \cdot 2\text{H}_2\text{O}$, $\text{Co}(\textit{p}\text{-NO}_2\text{-babh})_2$ and $\text{Co}(\textit{p}\text{-NO}_2\text{-babh})\text{SO}_4$ that had a probable square planar geometry.

Generally, the synthesised compounds had varying degree of activities against tested organisms. The synthesised metal(II) complexes showed better antimicrobial activities against the test organisms than the ligands which were inactive.

On the basis of the results from the microanalysis, infrared and UV-Visible spectroscopic data and magnetic moments, the structures in Figures 6.1 -6.6 are proposed for the synthesised complexes.

6.2

Proposed structures

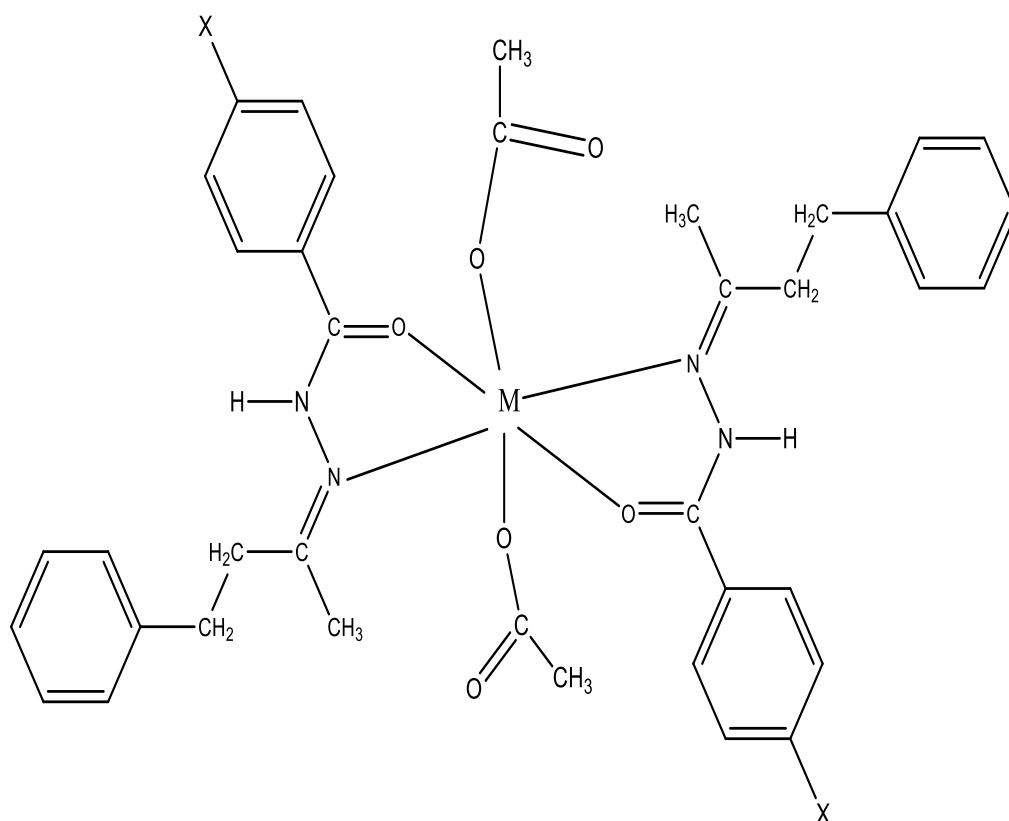


Figure 6.1. $M(L)_2(OAc)_2$ ($L = babh$, $X = OH$ and NO_2 ; $M = Cu, Ni, Co$)

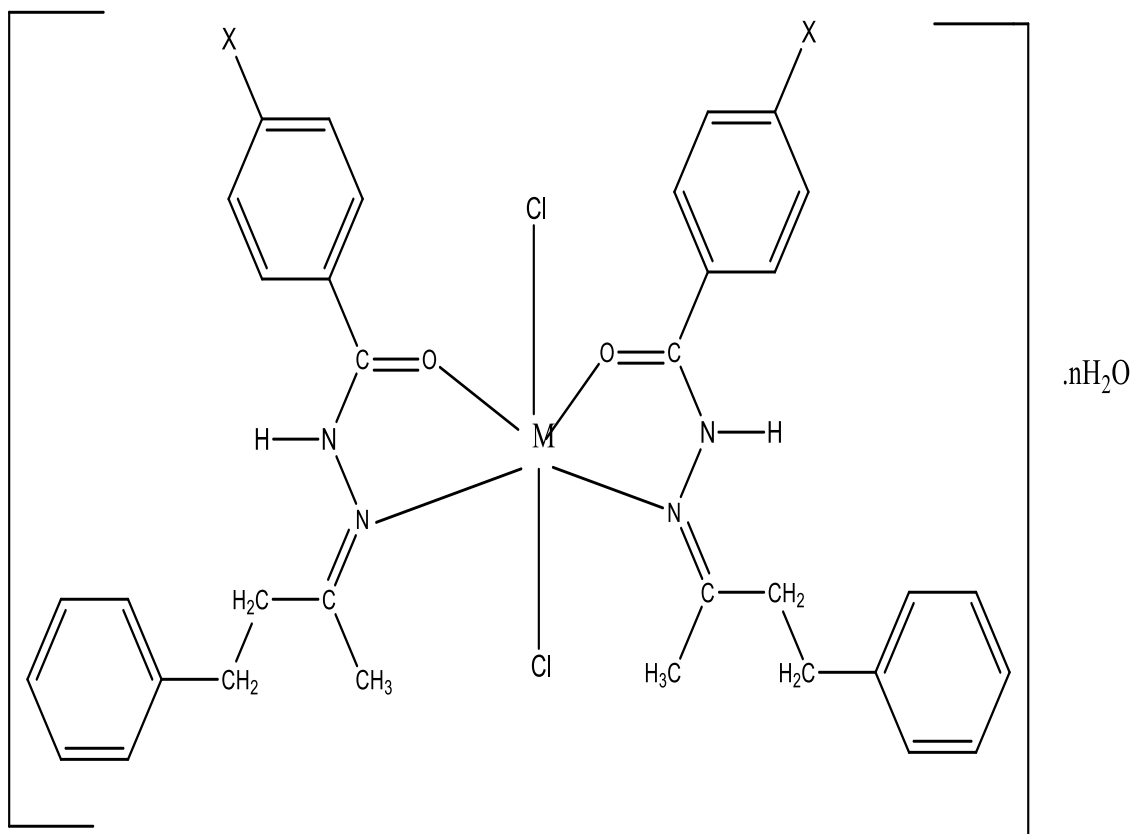


Figure 6.2. Proposed structure for $M(L)_2Cl_2 \cdot nH_2O$ ($M = Cu, Ni, Co$; $L = babh$, $X = OH$ and NO_2)

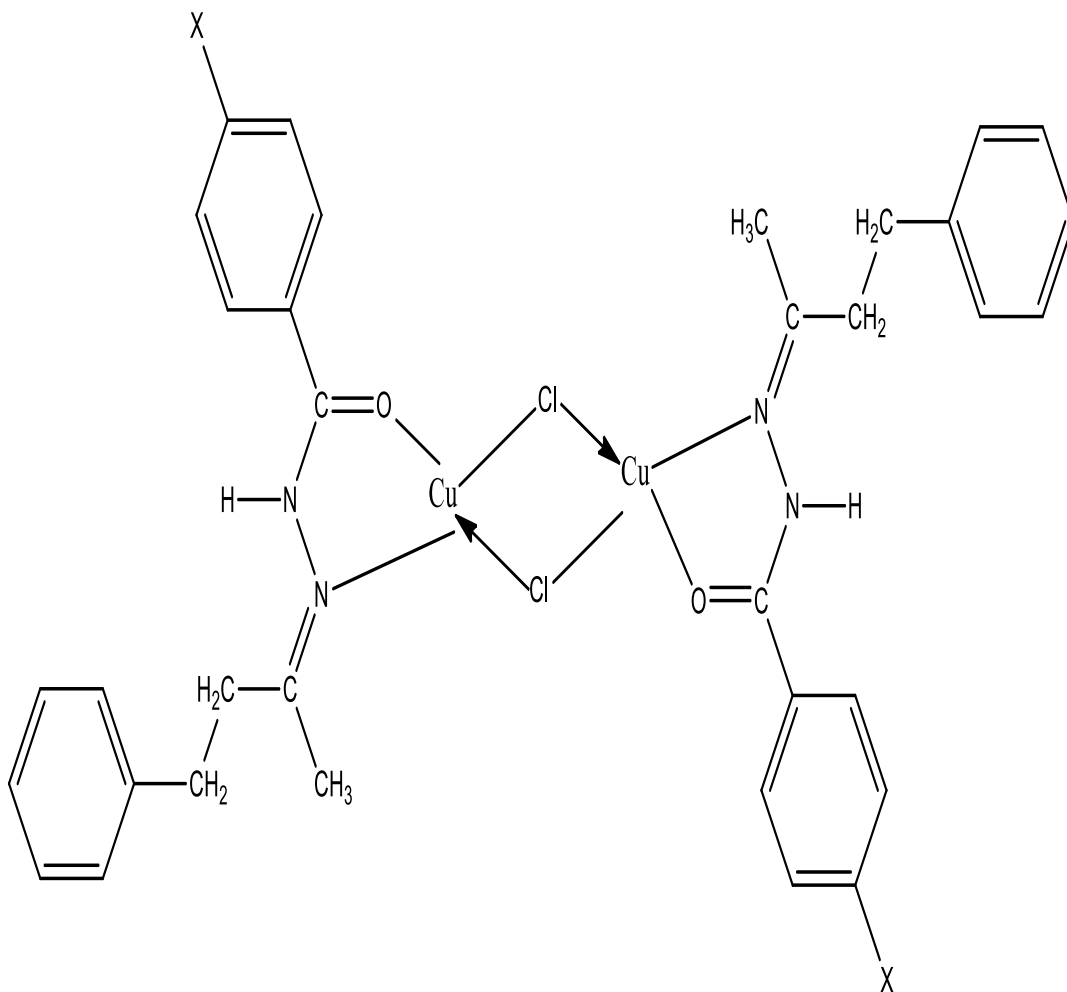


Figure 6.3. Structure for $\text{Cu}_2(\text{babh})_2\text{Cl}_2$

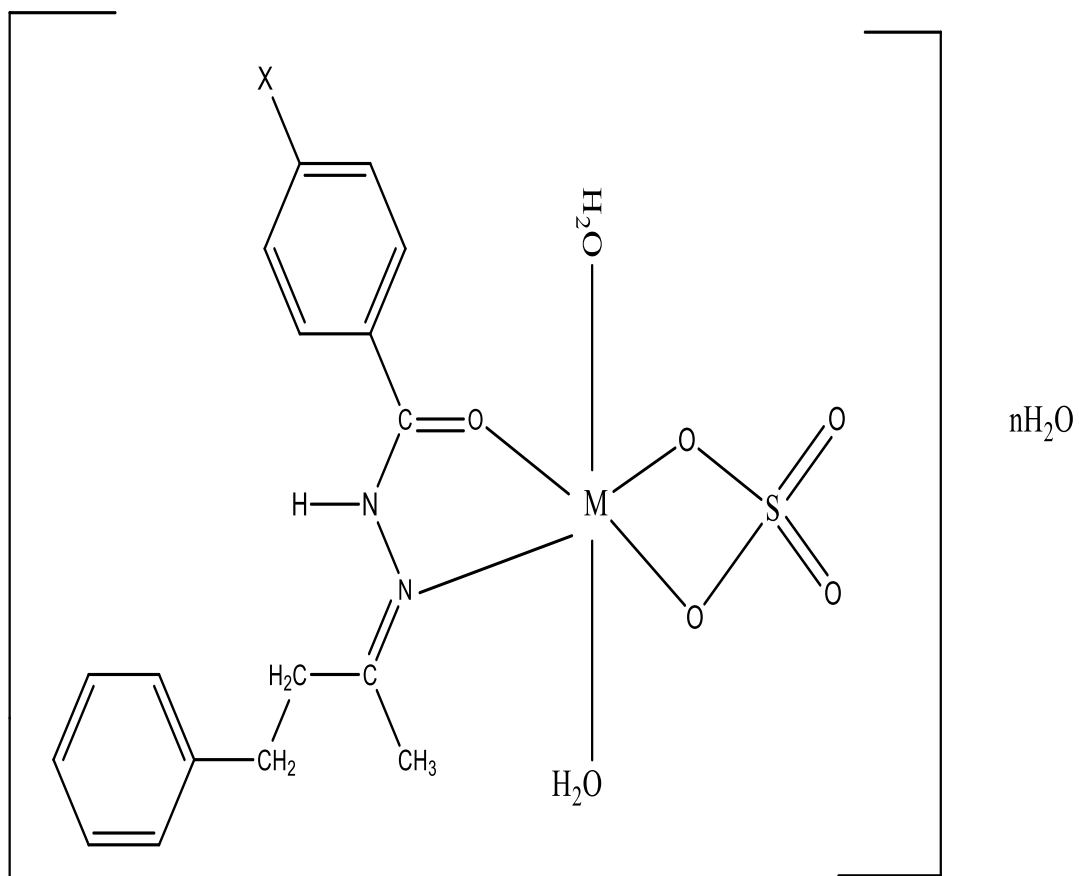


Figure 6.4. Proposed structure for (MLSO₄.nH₂O) (M= Ni, Co, L= *p*-OH-babh, *p*-NO₂babh)

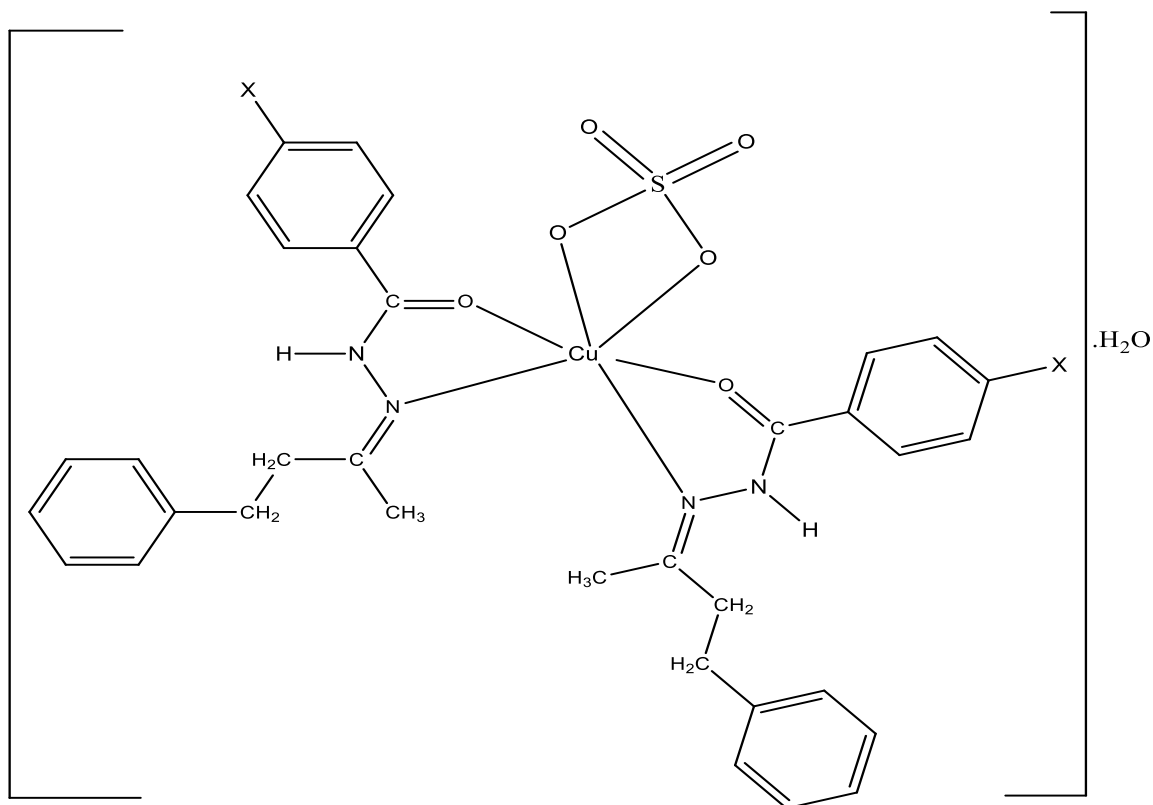


Figure 6.5. Proposed structure for $\text{Cu}(\text{L})_2\text{SO}_4 \cdot \text{H}_2\text{O}$ ($\text{M} = \text{Cu}, \text{Ni}, \text{Co}$; $\text{L} = \text{babh}, p\text{-OH-babh}$ and $p\text{-NO}_2\text{-babh}$; $\text{X} = \text{H}, \text{OH}, \text{NO}_2$)

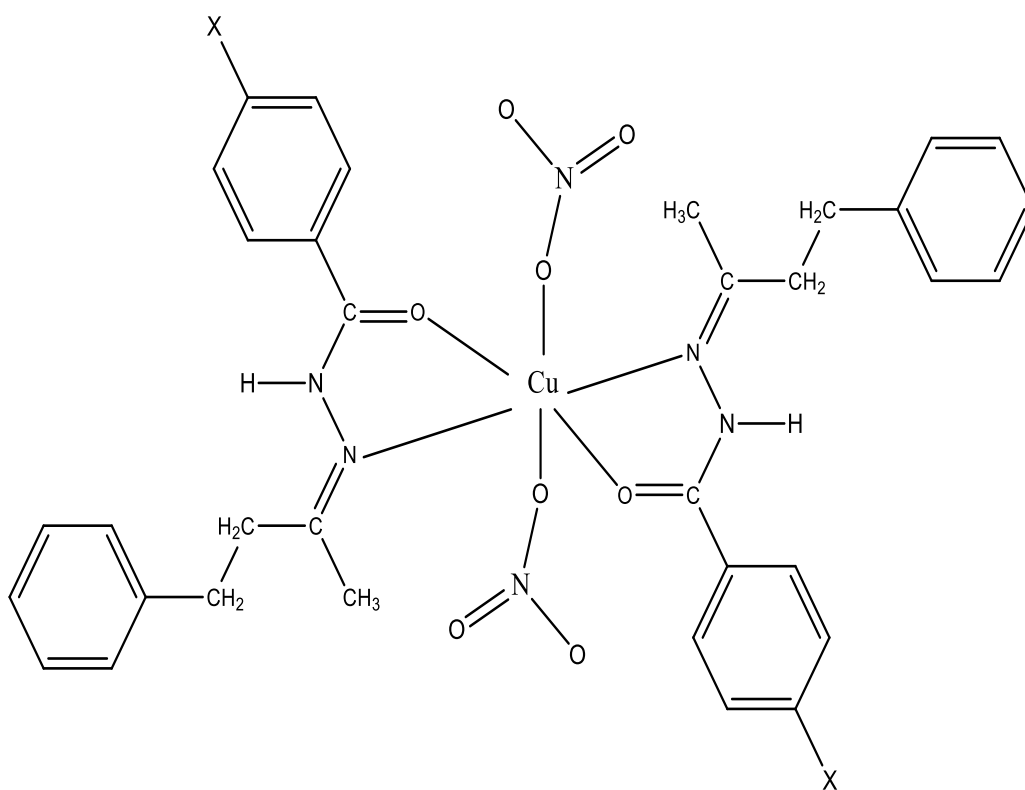


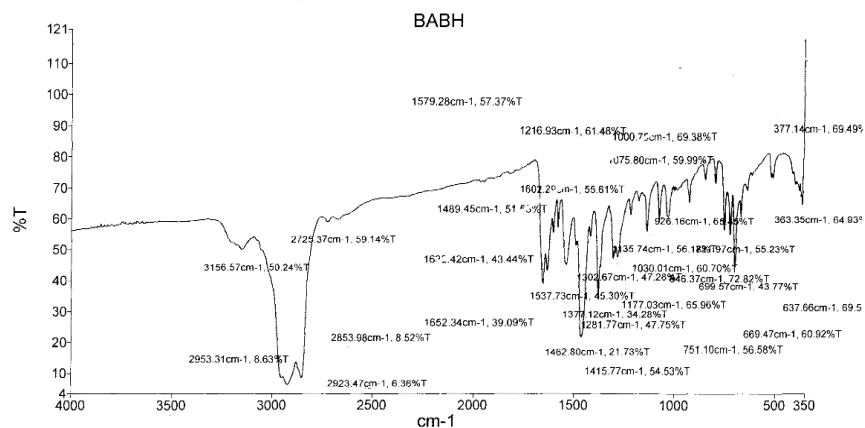
Figure 6.6. $M(L)_2(NO_3)_2 \cdot nH_2O$ ($L = \text{babh}, p\text{-OH-babh}$ and $p\text{-NO}_2\text{-babh}$; $X = \text{H}, \text{OH}, \text{NO}_2$; $M = \text{Cu}, \text{Ni}, \text{Co}$)

6.3 Suggestion for further work

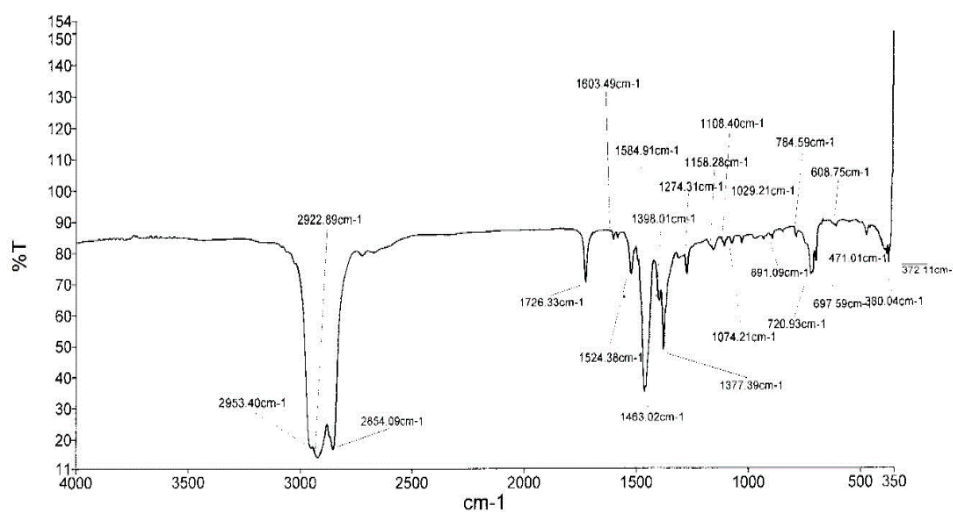
It is recommended that further studies be carried out in the following area of the work:

- i. X-ray crystallographic study on single crystals of the metal(II) complexes to confirm the geometry
- ii. Studies of thermal behaviour and thermal decomposition processes of the compounds to understand their thermal stability.
- iii. Quantitative antimicrobial and in vivo toxicological studies to know their potentials for drugs.
- iv. Tendency of the complexes to form stable adducts compounds with 2, 2'-bipyridine and 1, 10-phenanthroline.

Appendix 1: IR spectra for babh ligands and their metal(II) complexes.

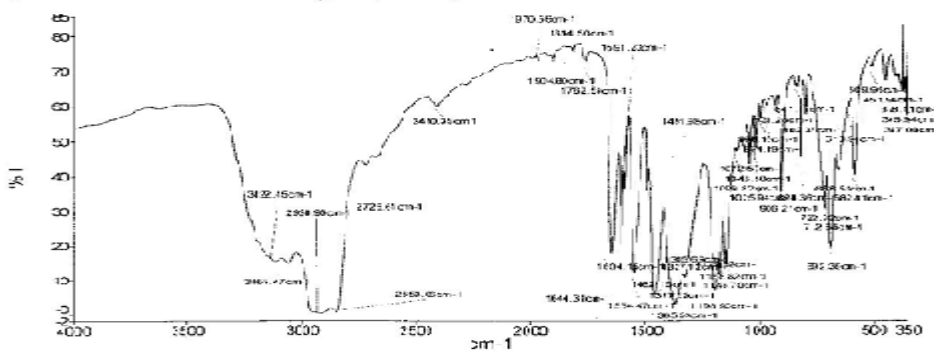


babh ligand



— CuCl2babh CuCl2babh 061 By Administrator Date Friday, May 09 2014

Cu₂(babh)₂Cl₂



— CuCl2babh CuCl2babh 060 By Administrator Date Friday, May 09 2014

Cu(babh)(NO₃)₂·5H₂O

Figure 6.7: IR spectra of babh, Cu₂(babh)₂Cl₂ and Cu(babh)(NO₃)₂·5H₂O

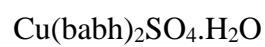
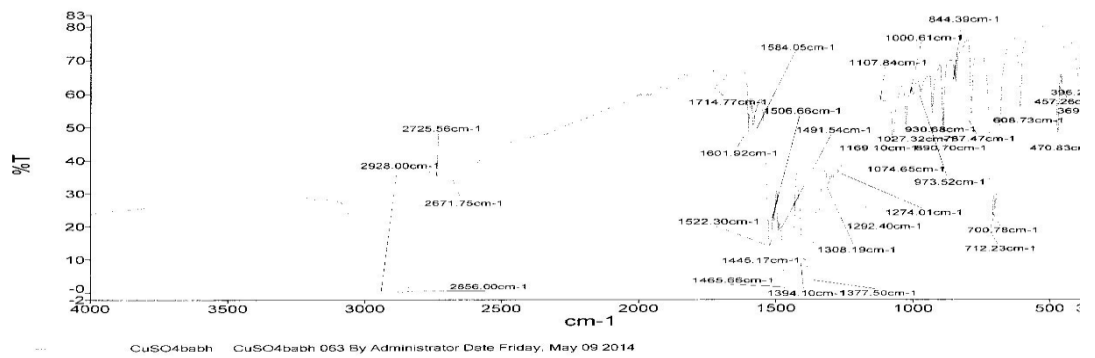
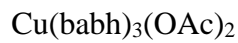
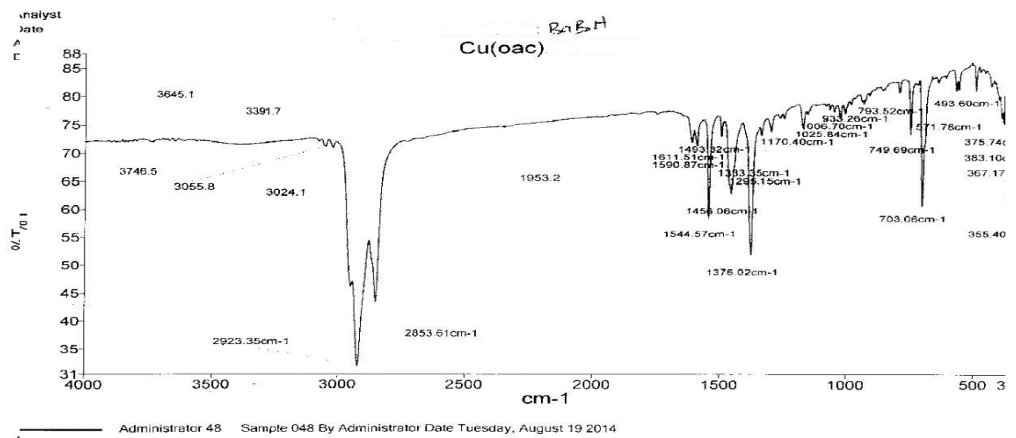
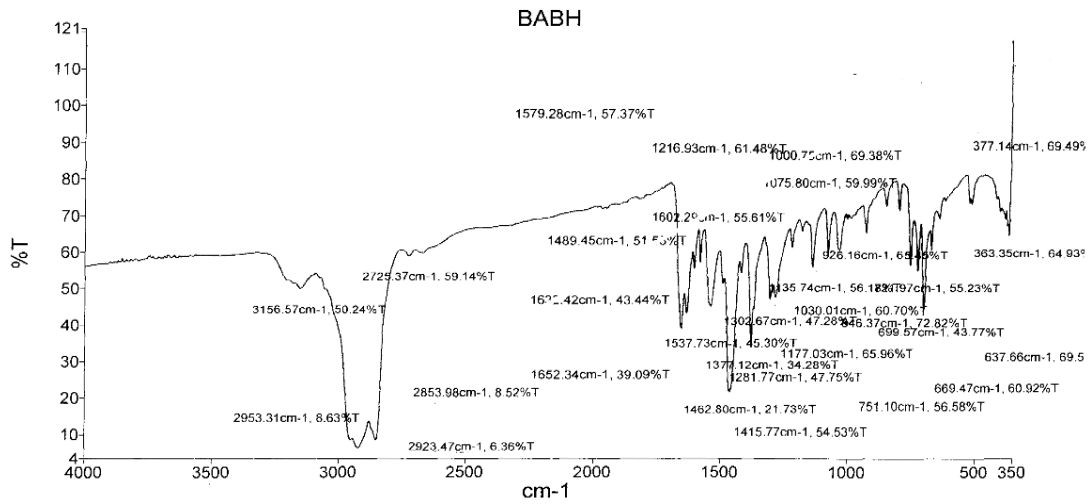
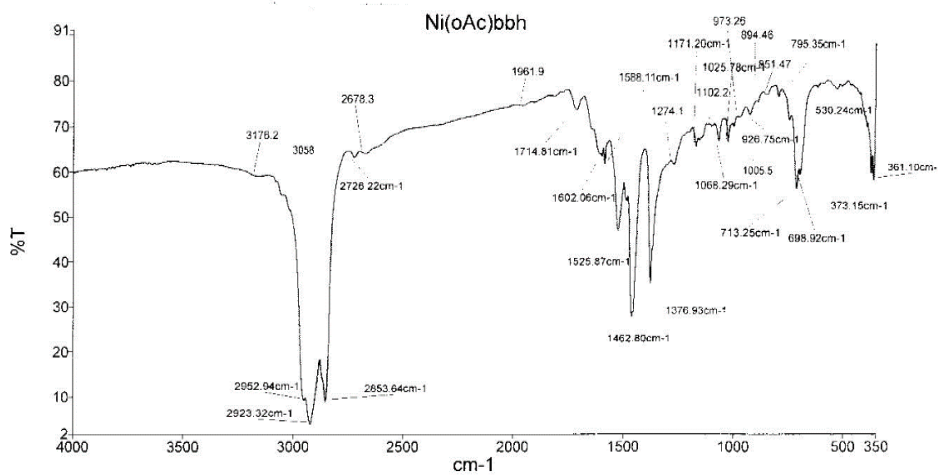
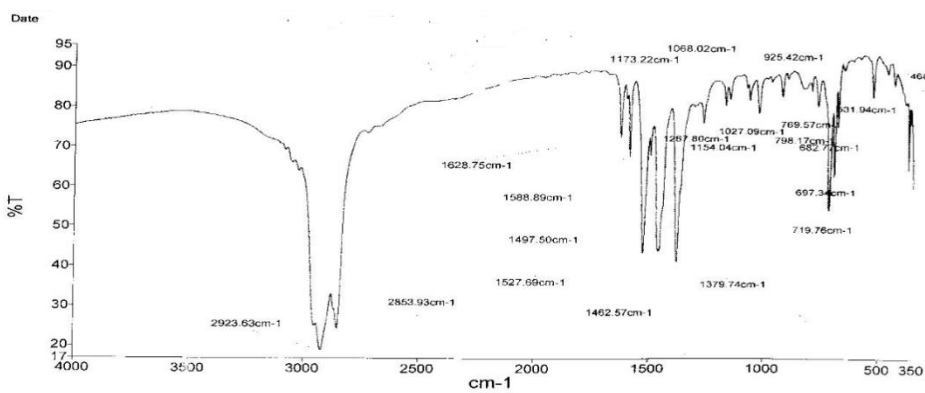
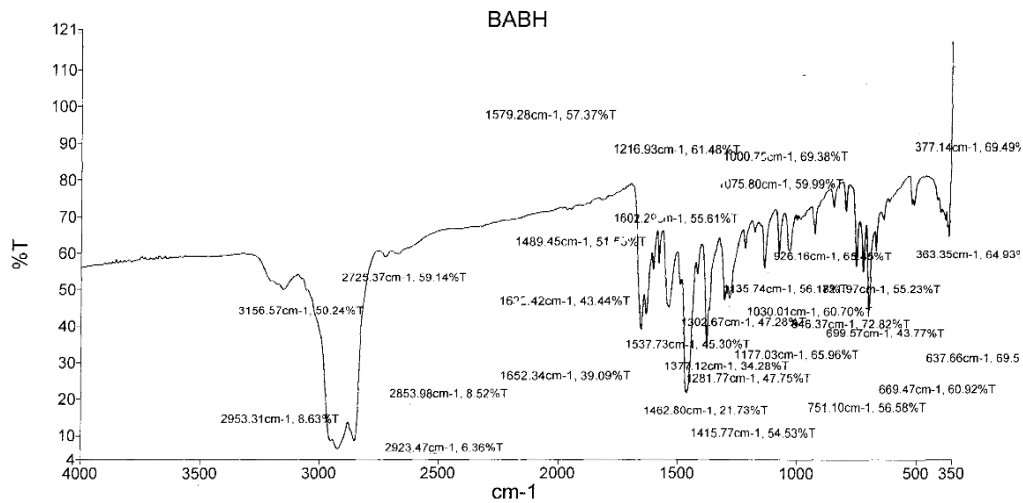


Figure 6.8. IR spectra of babh, Cu(babh)₃(OAc)₂ and Cu(babh)₂SO₄.H₂O



Administrator 69 Sample 069 By Administrator Date Monday, June 02 2014

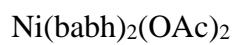
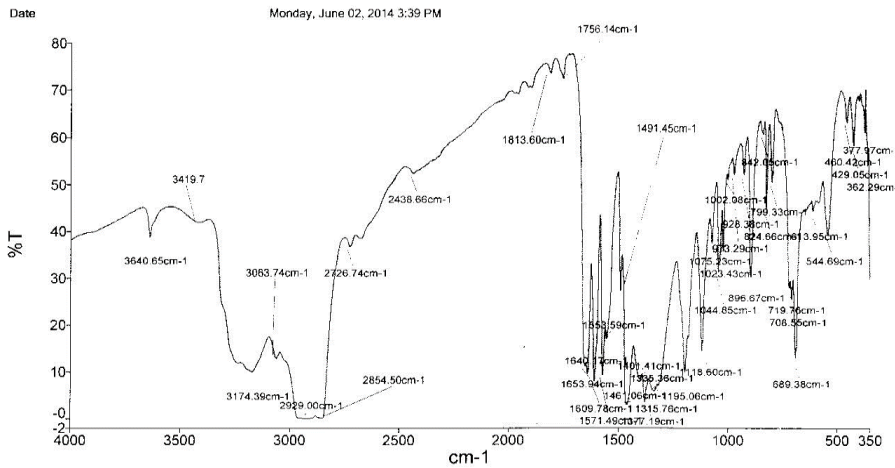
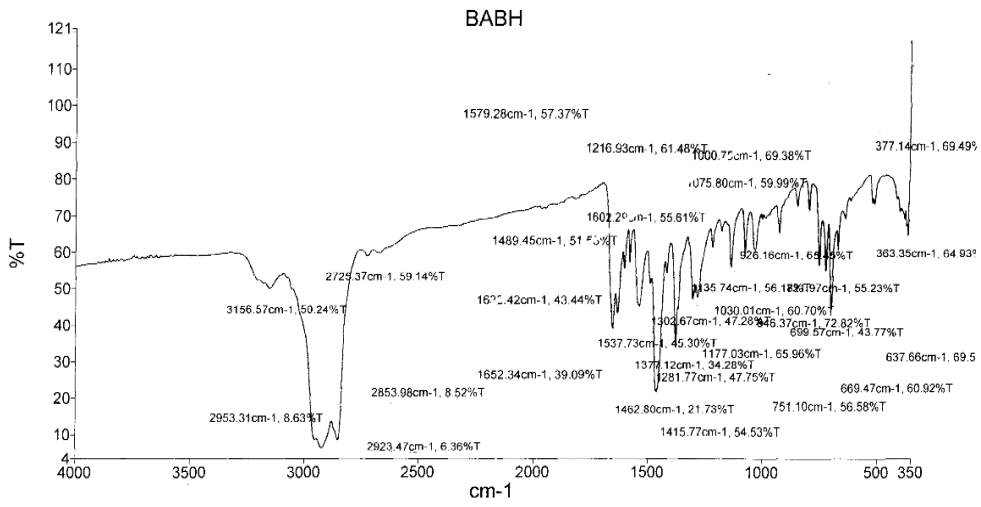
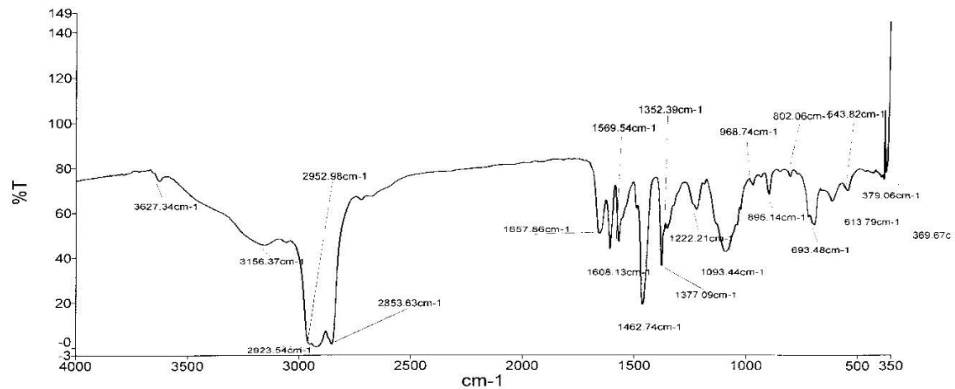
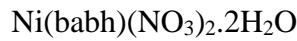


Figure 6.9. IR spectra of babh, Ni(babh)₂Cl₂ and Ni(babh)₂(OAc)₂



NiNO3babh NiNO3babh 064 By Administrator Date Friday, May 09 2014



NiSO4babh NiSO4babh 066 By Administrator Date Friday, May 09 2014

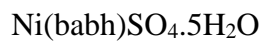


Figure 6.10: IR spectra of babh, Ni(babh)(NO₃)₂·2H₂O and Ni(babh)(NO₃)₂·2H₂O.

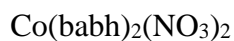
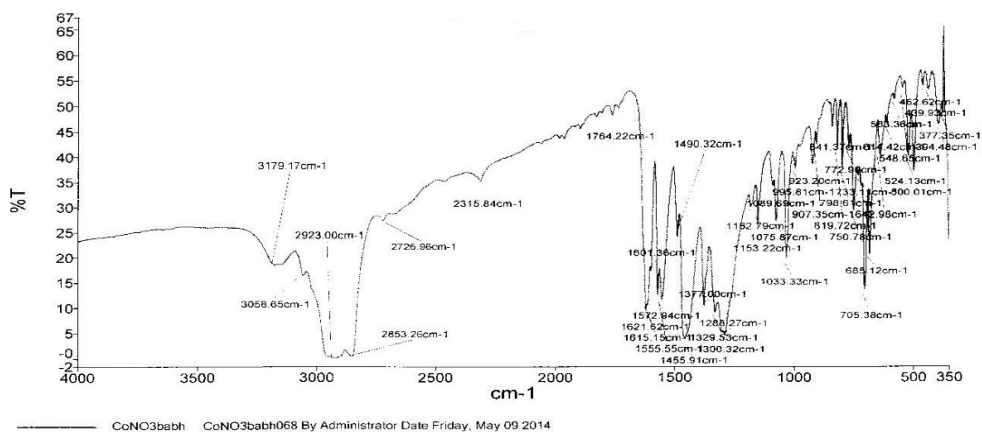
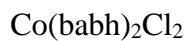
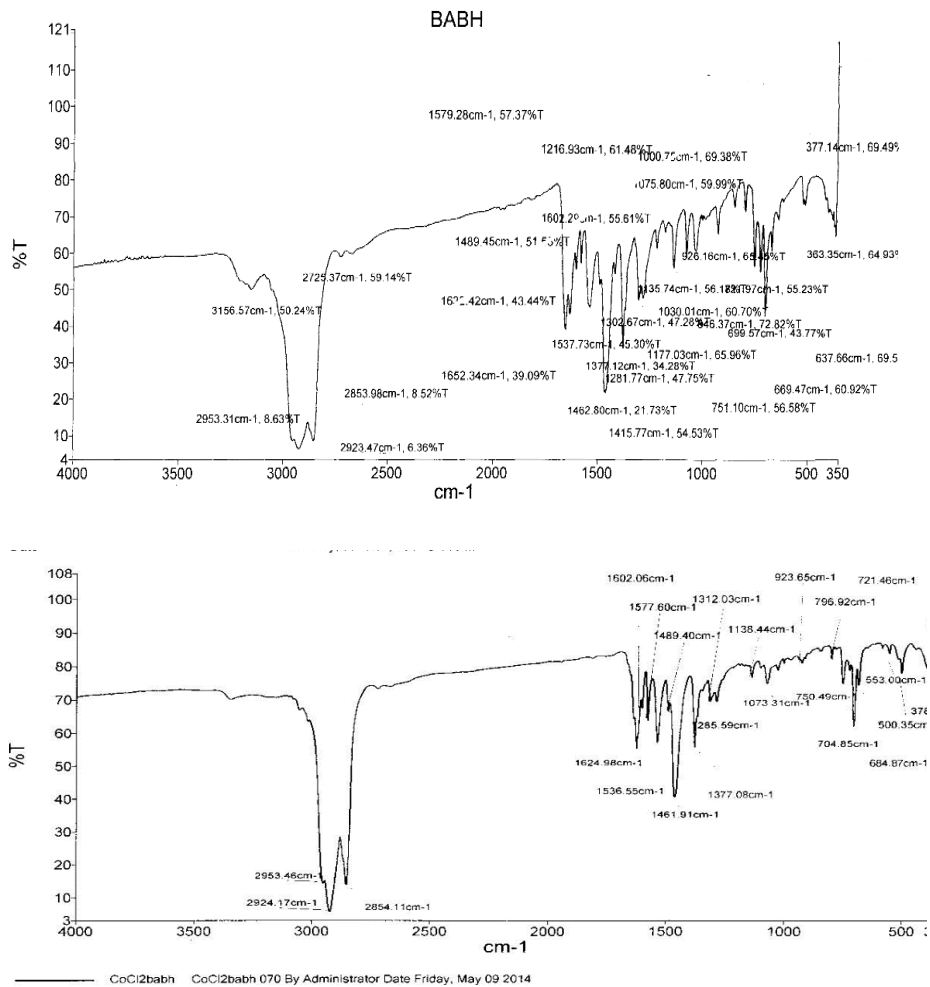
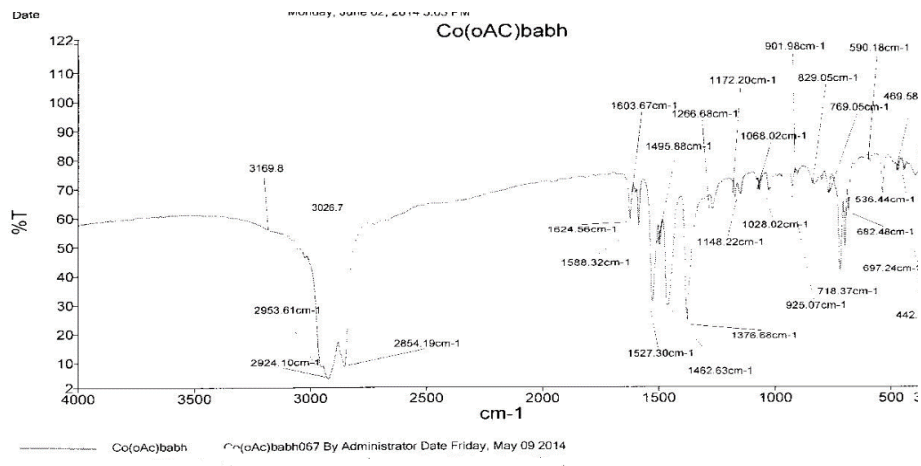
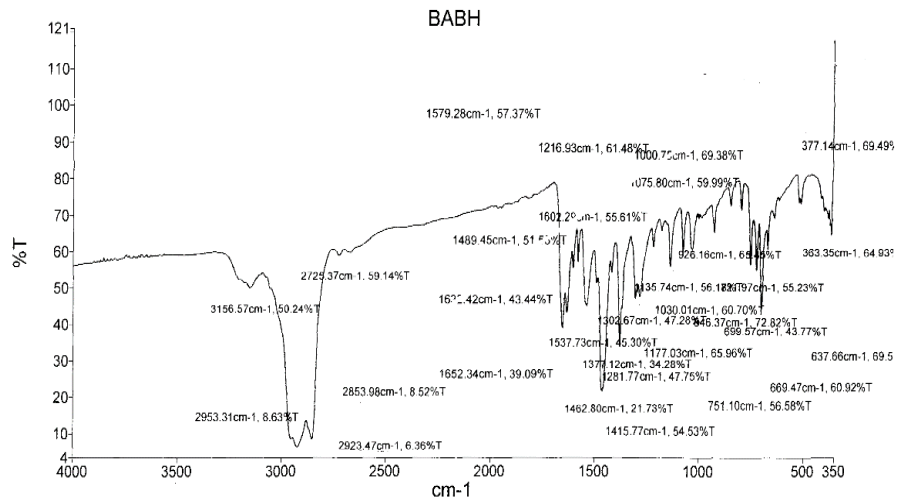
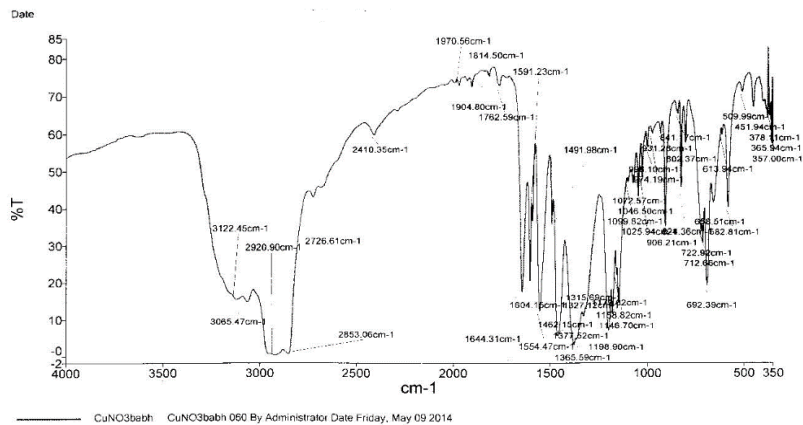


Figure 6.11: IR spectra of babh, Co(babh)₂Cl₂, and Co(babh)₂(NO₃)₂

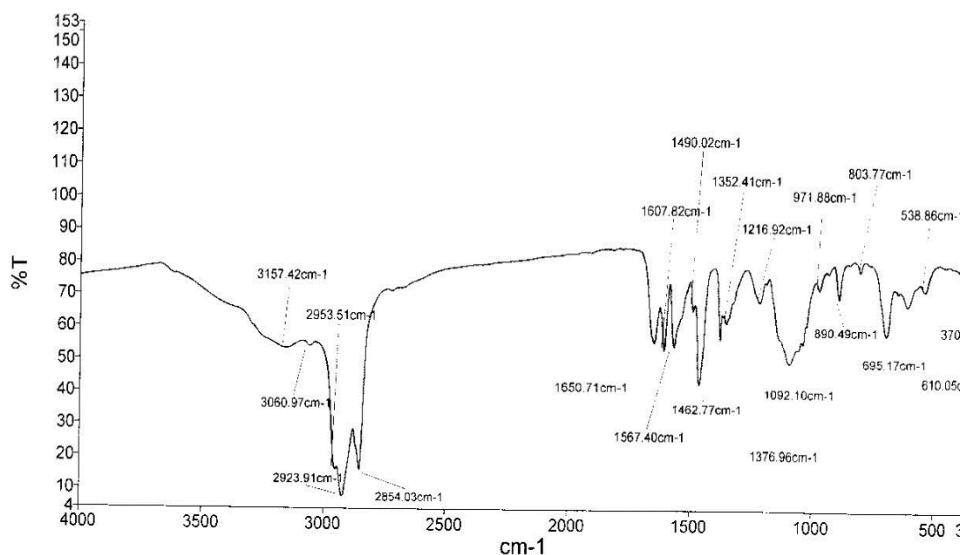
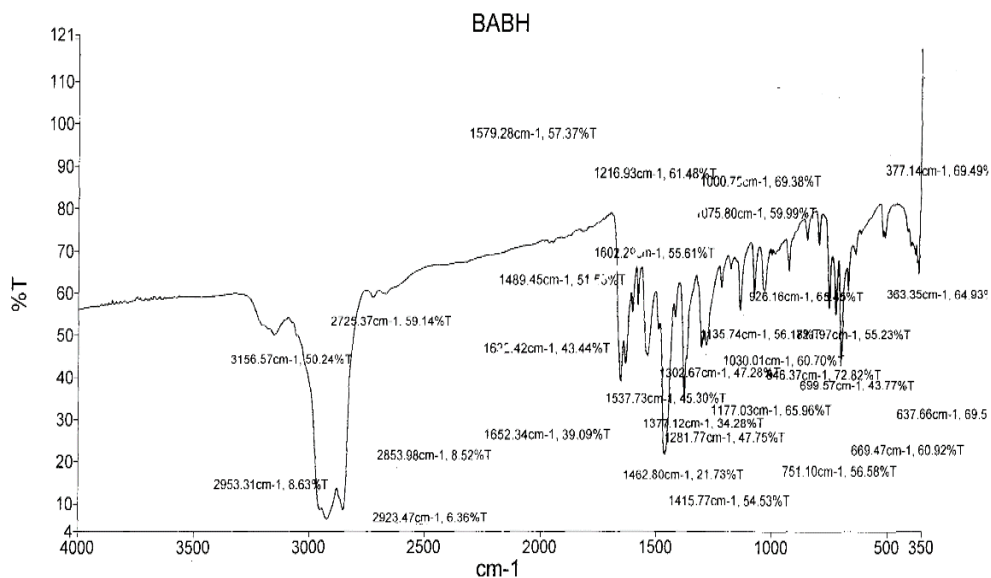


Co(babh)₂(OAc)₂



Co(babh)₂(NO₃)₂

Figure 6.12. IR spectra of babh, Co(babh)₂(OAc)₂ and Co(babh)₂(NO₃)₂



CoSO4babh CoSO4babh069 By Administrator Date Friday, May 09 2014

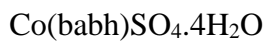
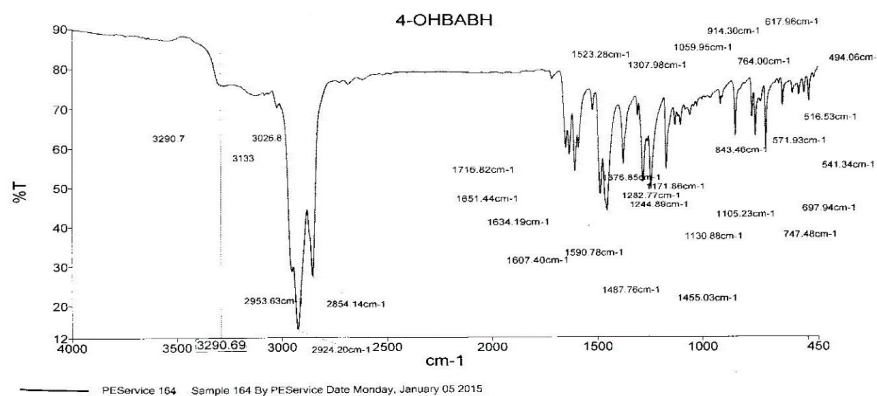
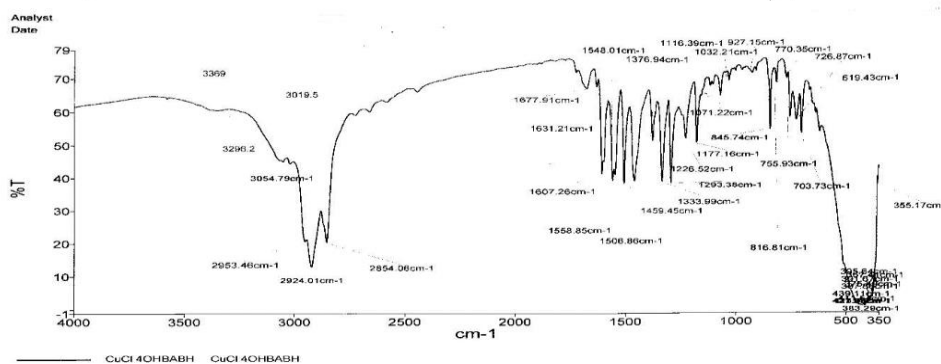


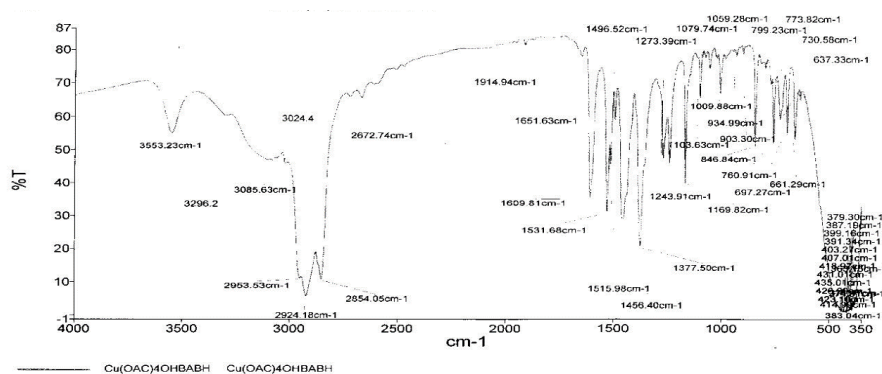
Figure 6.13. IR spectra of babh and Co(babh)SO4.4H2O



p-OH-babh ligand



$\text{Cu}(p\text{-OH-babh})_2\text{Cl}_2$



$\text{Cu}(p\text{-OH-babh})_2(\text{OAc})_2$

Figure 6.14: IR spectra of *p*-OH-babh, $\text{Cu}(p\text{-OH-babh})_2\text{Cl}_2$ and $\text{Cu}(p\text{-OH-babh})_2(\text{OAc})_2$

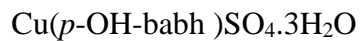
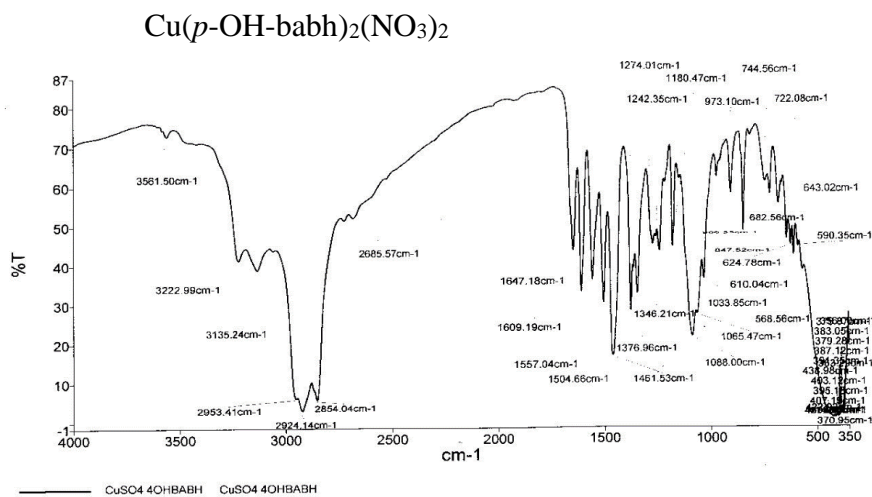
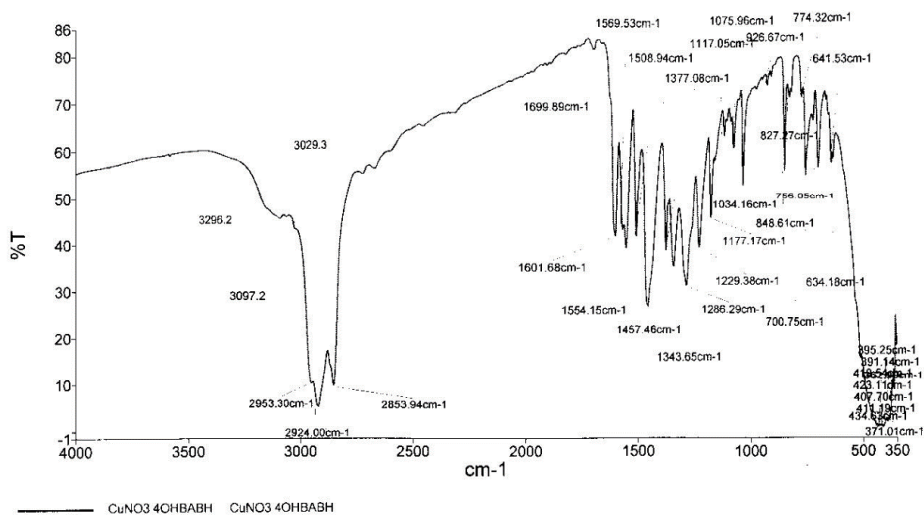
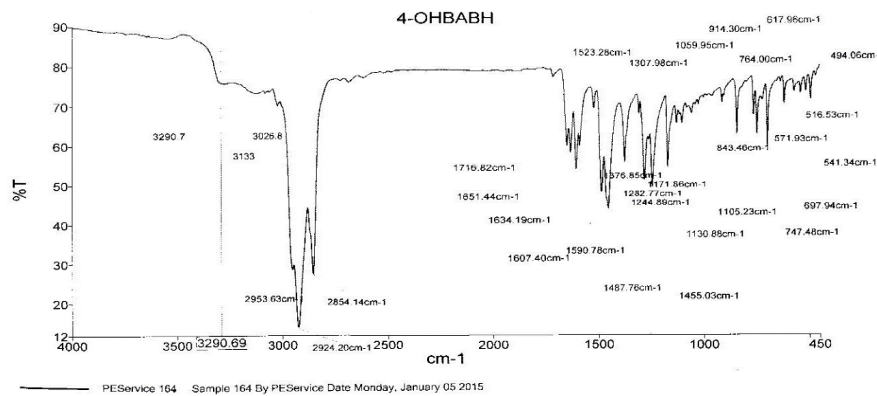


Figure 6.15: IR spectra of *p*-OH-babh, Cu(*p*-OH-babh)₂(NO₃)₂ and Cu(*p*-OH-babh)SO₄·3H₂O

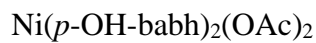
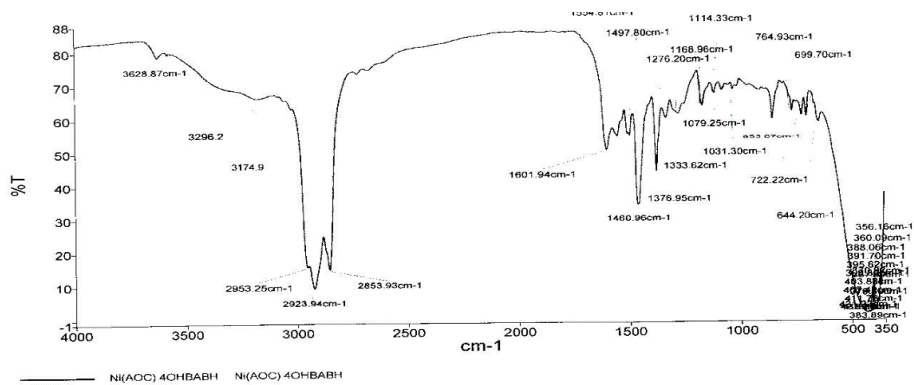
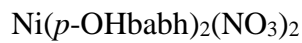
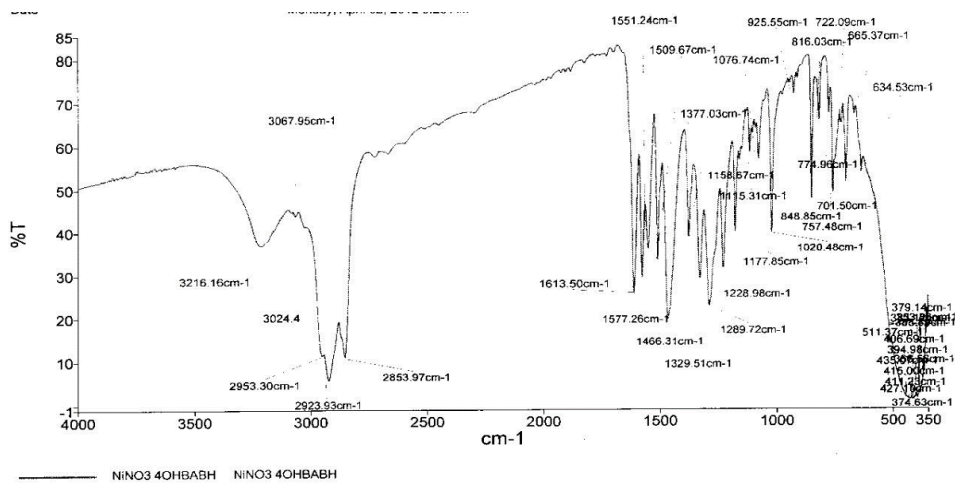
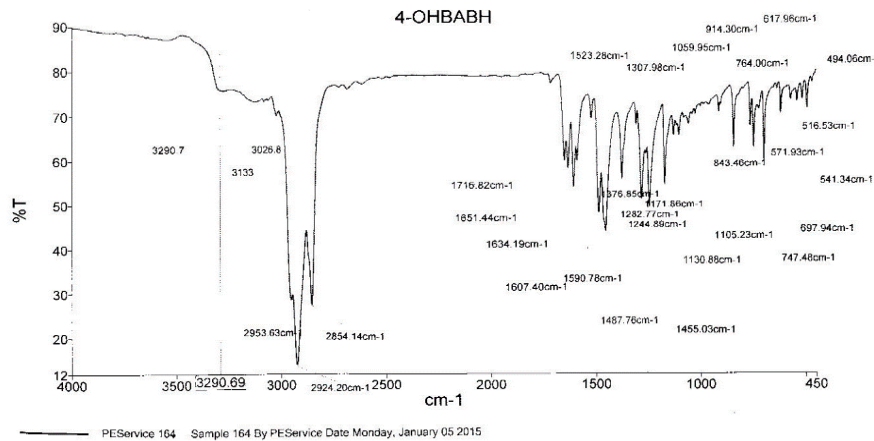
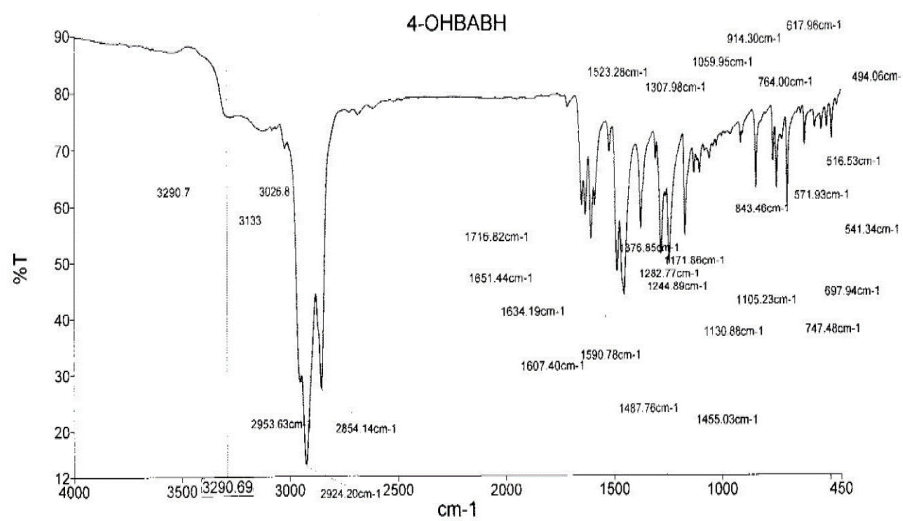
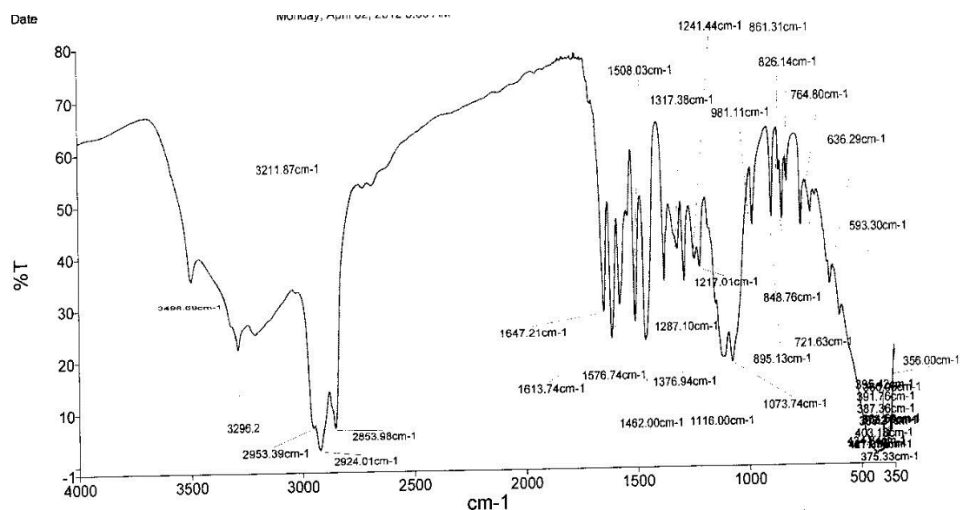


Figure 6.16: IR spectra of *p*-OH-babh, Ni(*p*-OHbabh)₂(NO₃)₂ and Ni(*p*-OH-babh)₂(OAc)₂



PEService 164 Sample 164 By PEsService Date Monday, January 05 2015



NISO44OHBABH NISO44OHBABH

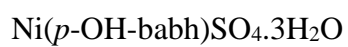


Figure 6.17: IR spectra of $p\text{-OH-babh}$ and $\text{Ni}(p\text{-OH-babh})\text{SO}_4 \cdot 3\text{H}_2\text{O}$

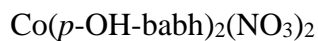
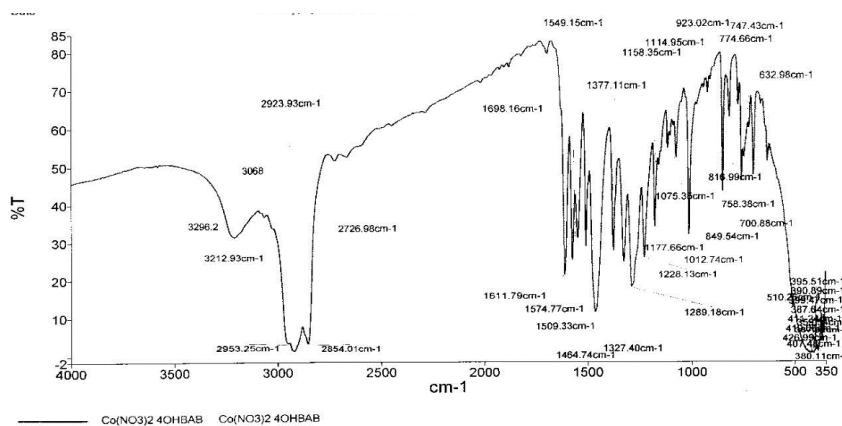
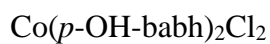
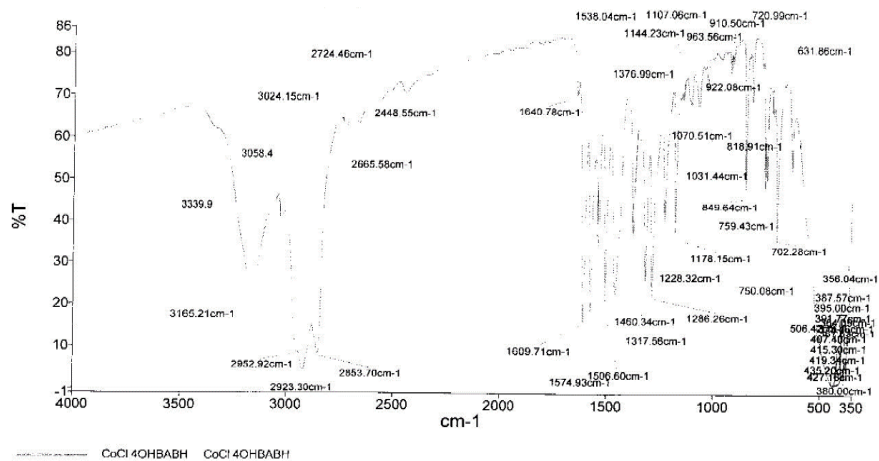
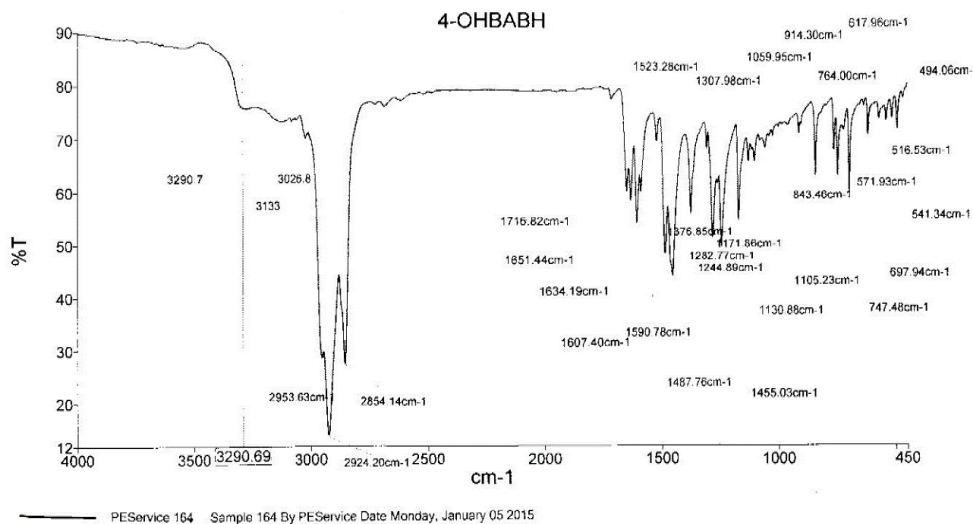
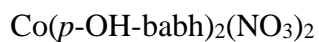
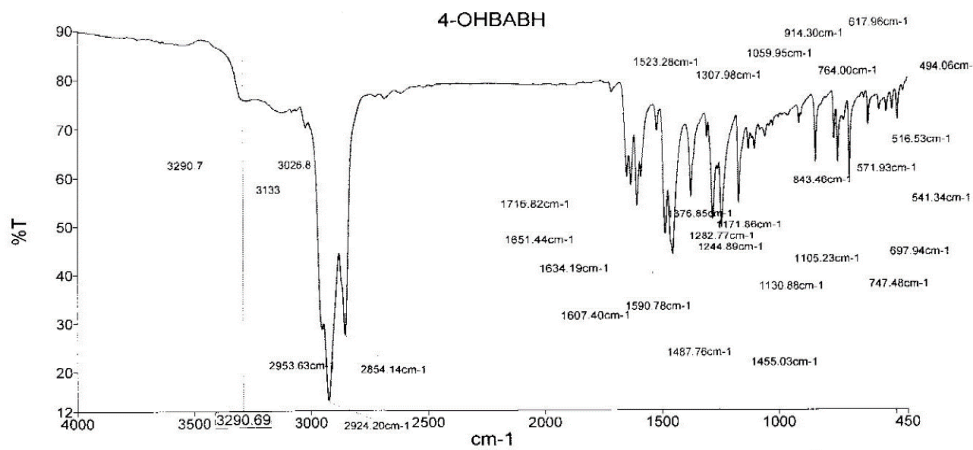
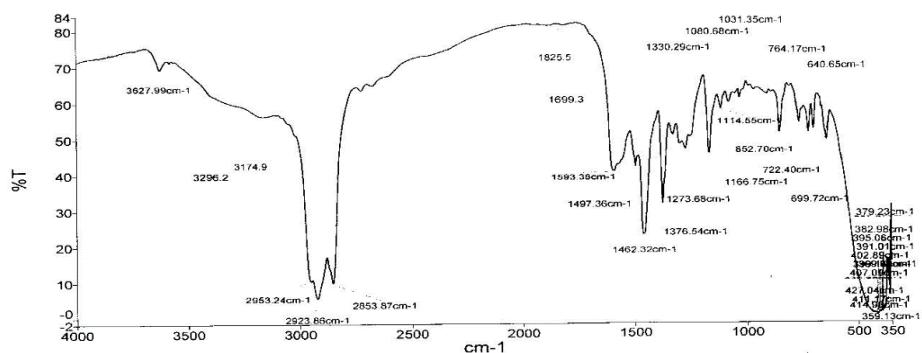


Figure 6.18: IR spectra of *p*-OH-babh, Co(*p*-OH-babh)₂Cl₂ and



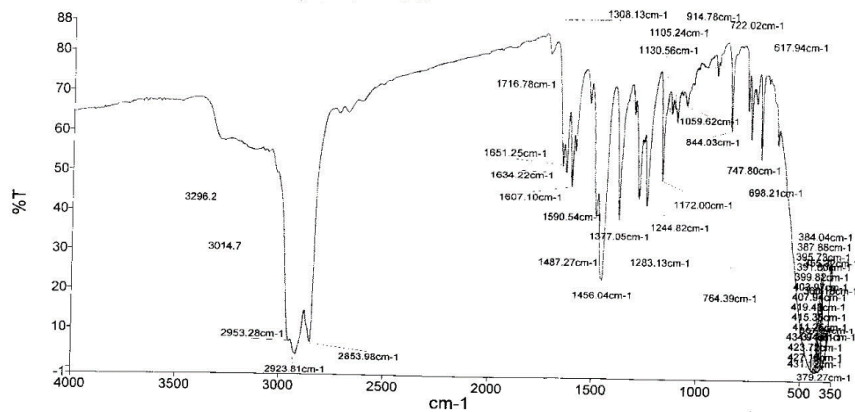


PEService 164 Sample 164 By PEsService Date Monday, January 05 2015



Co(OAc)2·4OHBABH Co(OAc)2·4OHBAB

Co(*p*-OHbabh)₂(OAc)₂



CoSO4·4OHBABH CoSO4·4OHBABH

Co(*p*-OH-babh)SO₄·2H₂O

Figure 6.19: IR spectra of *p*-OH-babh, Co(*p*-OH-babh)₂(OAc)₂ and

Co(*p*-OH-babh)SO₄·2H₂O

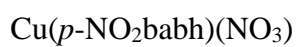
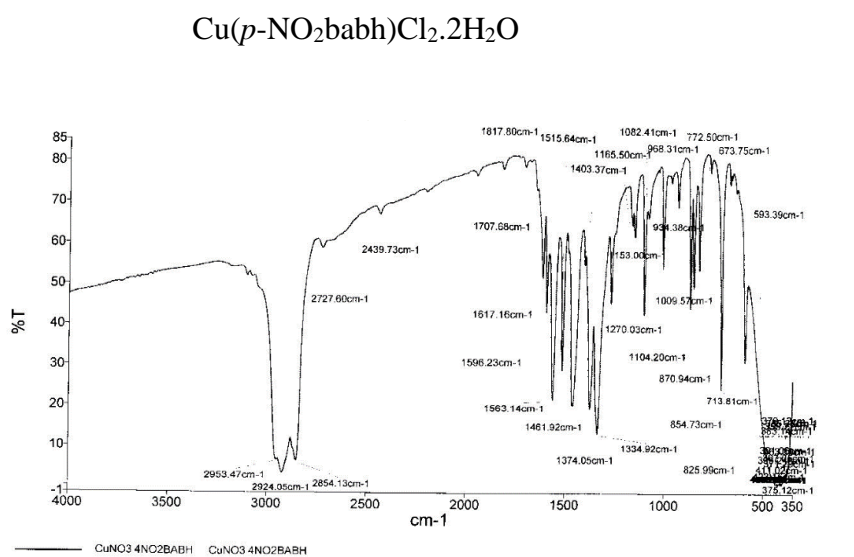
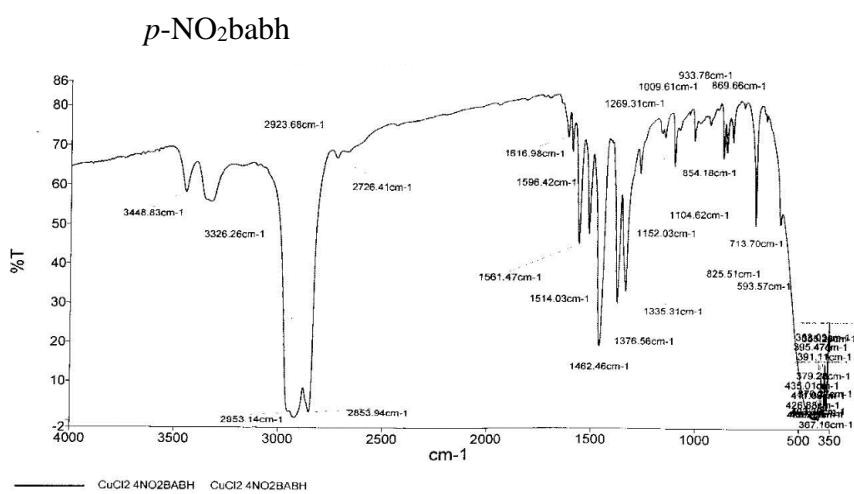
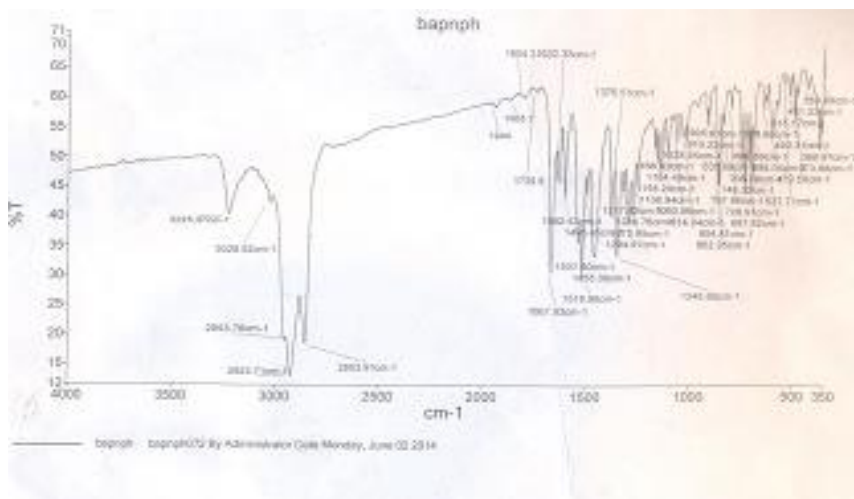


Figure 6.20: IR spectra of *p*-NO₂babh, Cu(*p*-NO₂babh)Cl₂·2H₂O and Cu(*p*-NO₂babh)(NO₃)

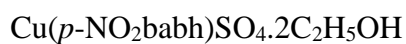
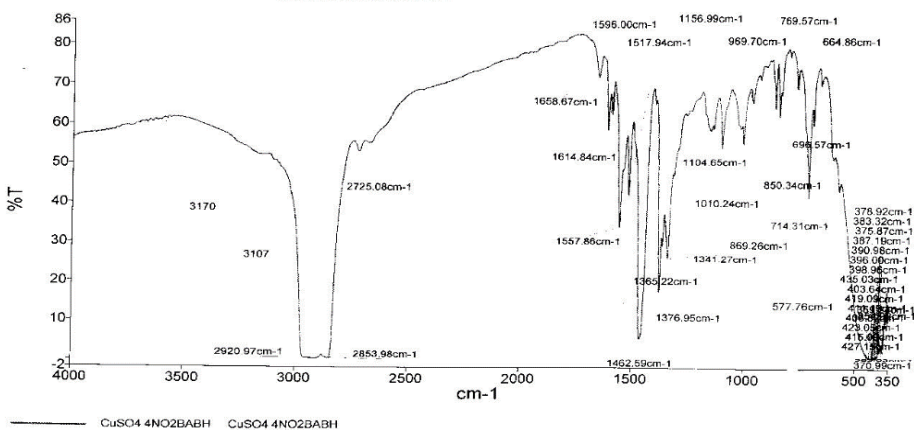
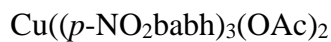
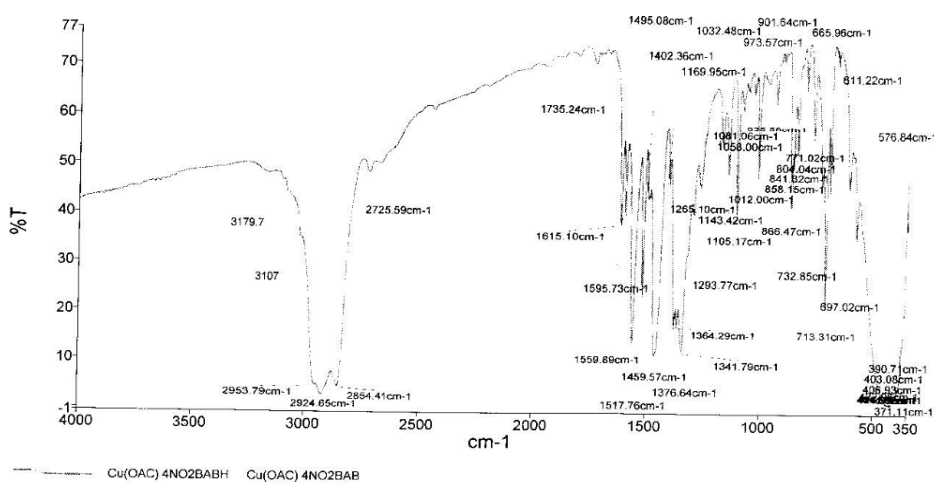
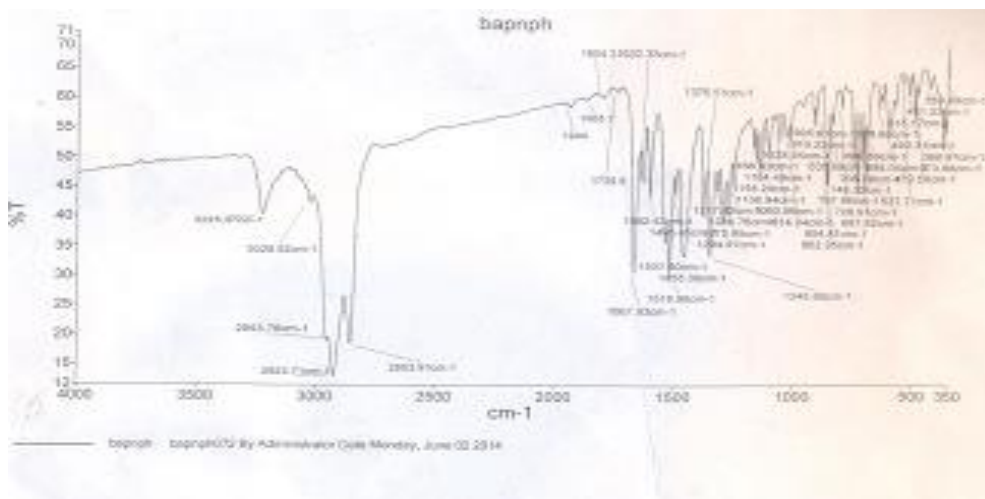


Figure 6.21: IR spectra of *p*-NO₂-babh, Cu(*p*-NO₂babh)₃(OAc)₂ and Cu(*p*-NO₂babh)SO₄·2C₂H₅OH

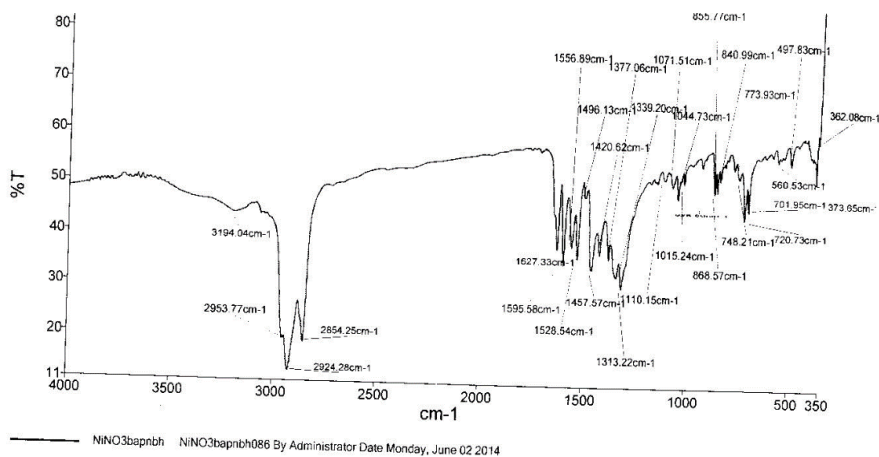
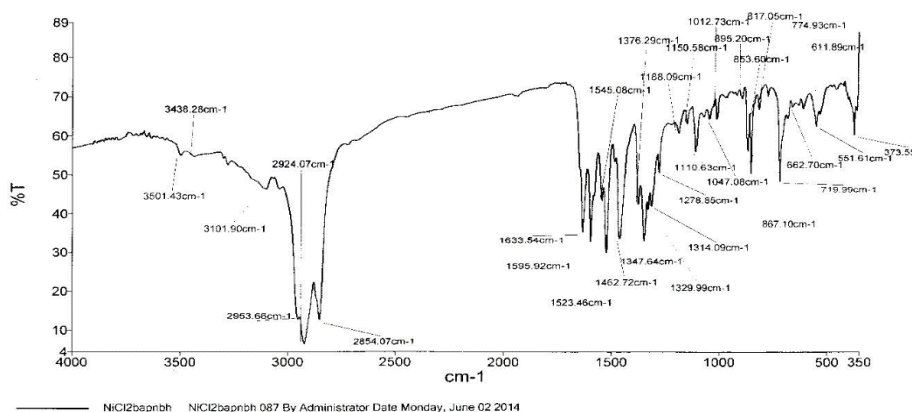
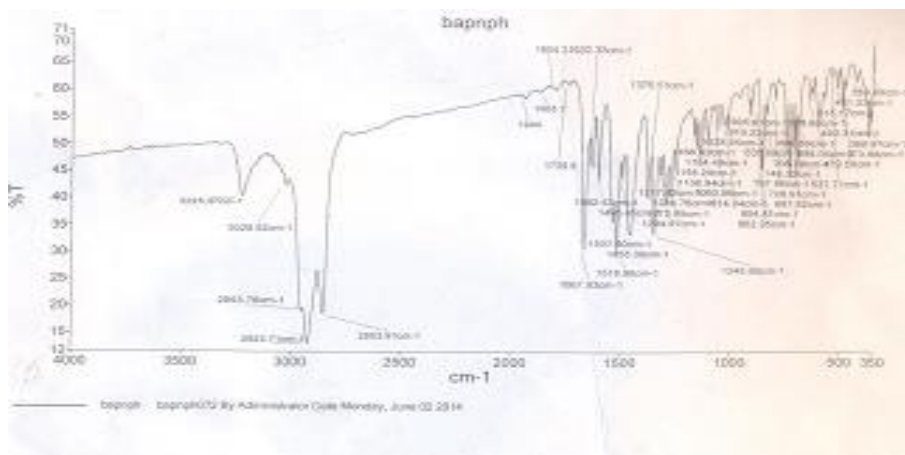


Figure 6.22: IR spectra of *p*-NO₂babh, Ni(*p*-NO₂babh)Cl₂·4H₂O and Ni(*p*-NO₂-babh)₂(NO₃)₂

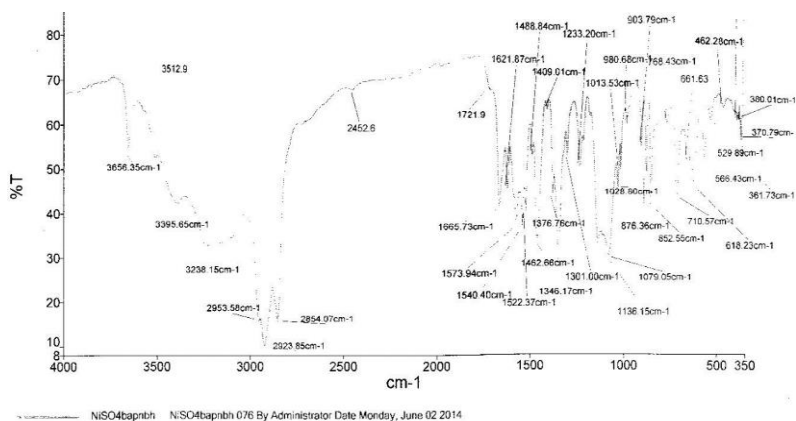
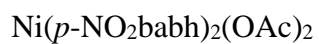
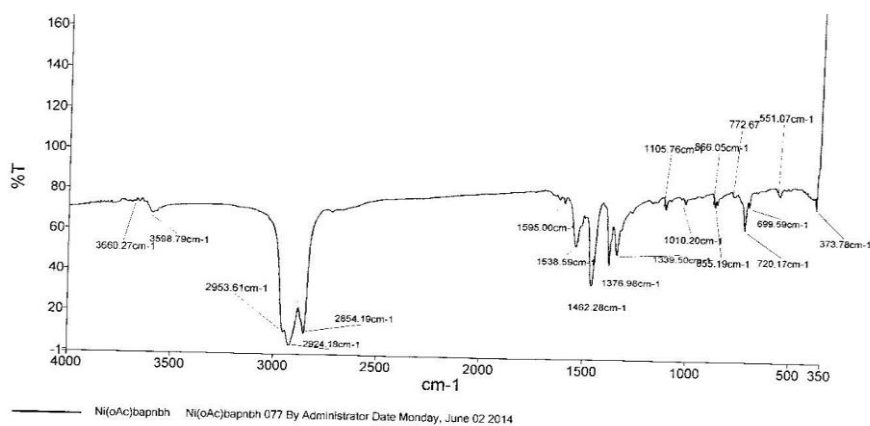
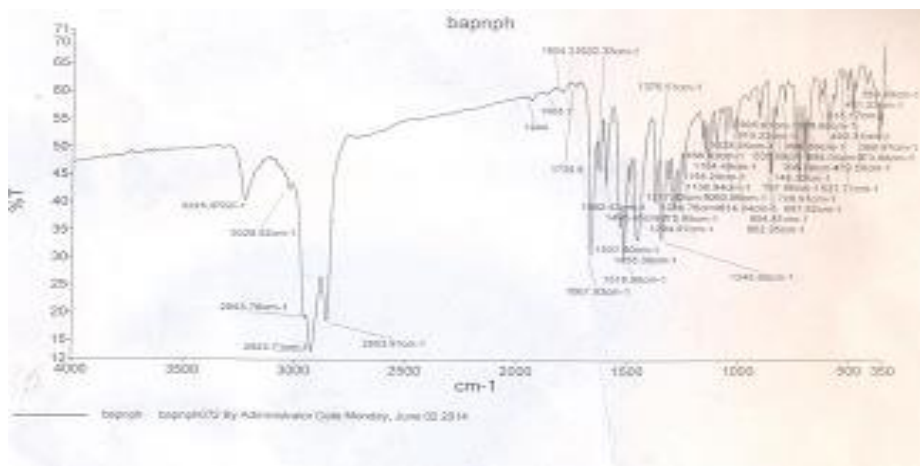
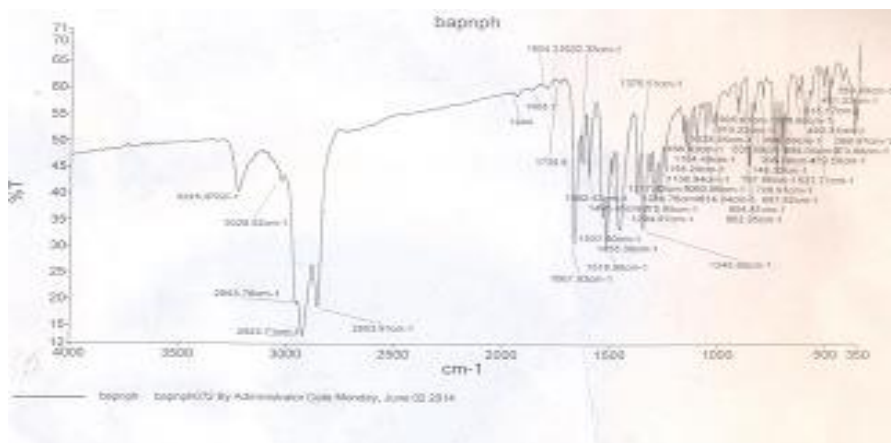
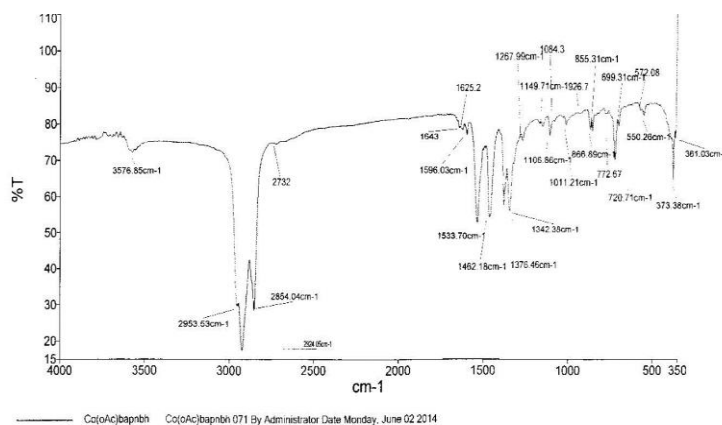


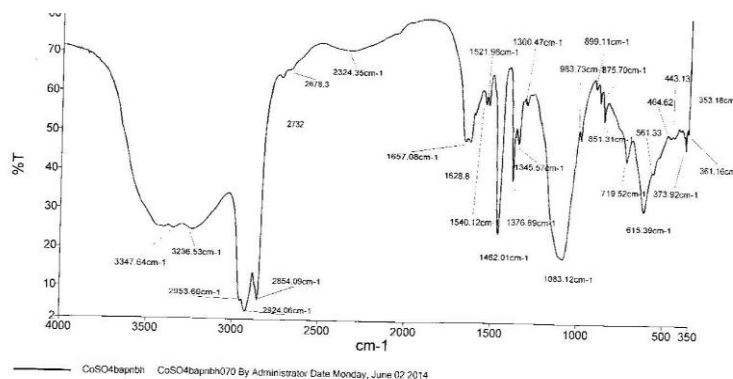
Figure 6.23: IR of *p*-NO₂-babh, Ni(*p*-NO₂babh)₂(OAc)₂ and Ni(*p*-NO₂babh)SO₄·2H₂O.



p-NO₂-babh



Co(*p*-NO₂babh)₂(OAc)₂·3H₂O



Co(*p*-NO₂babh)SO₄

Figure 6.24: IR spectra of *p*-NO₂babh, Co(*p*-NO₂babh)₂(OAc)₂·3H₂O and Co(*p*-NO₂babh)SO₄

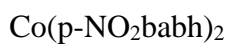
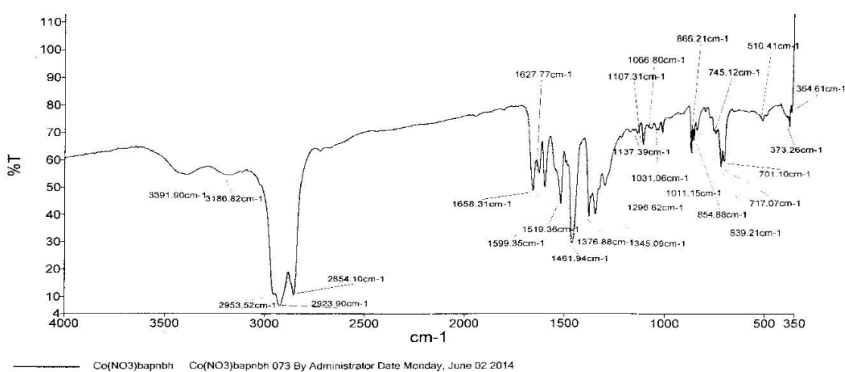
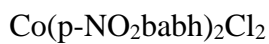
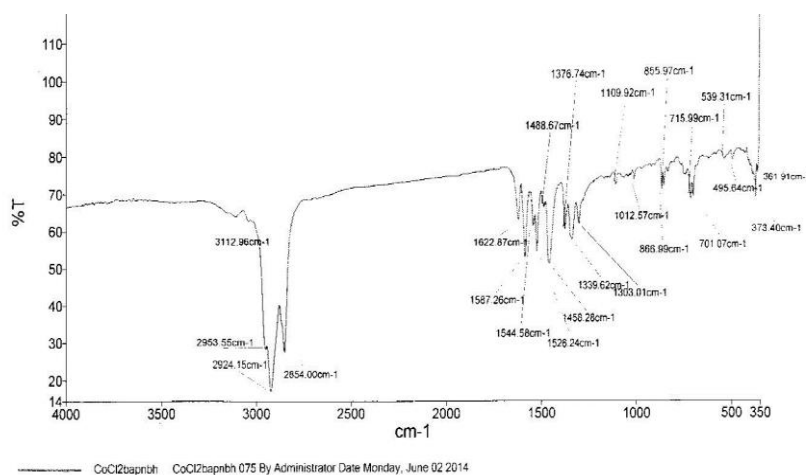
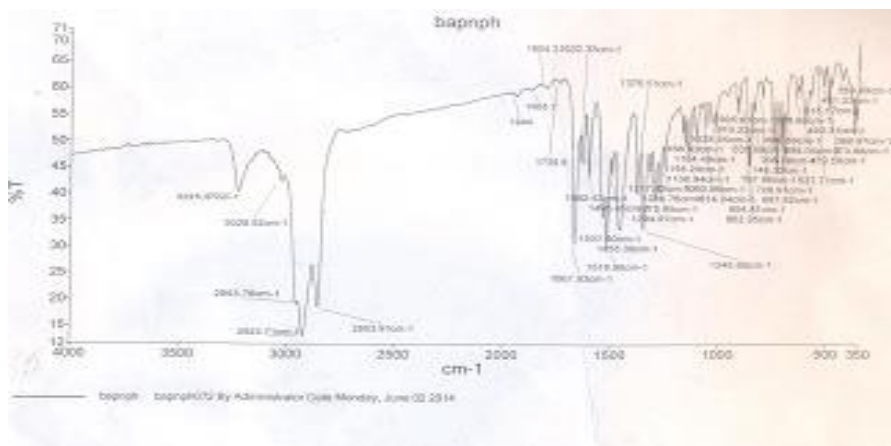
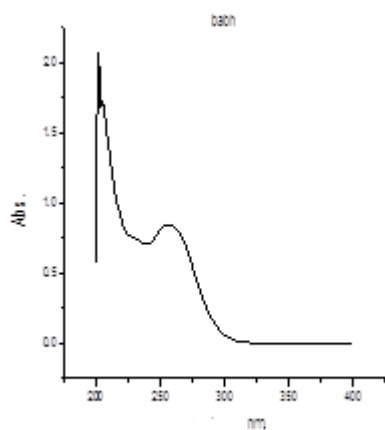
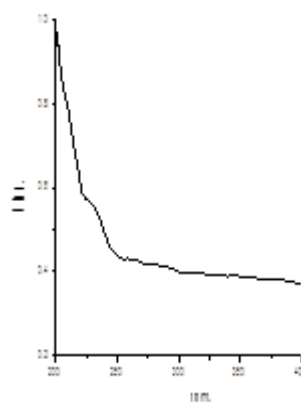


Figure 6.25: IR spectra of *p*-NO₂babh, Co(*p*-NO₂babh)₂Cl₂ and Co(*p*-NO₂babh)₂

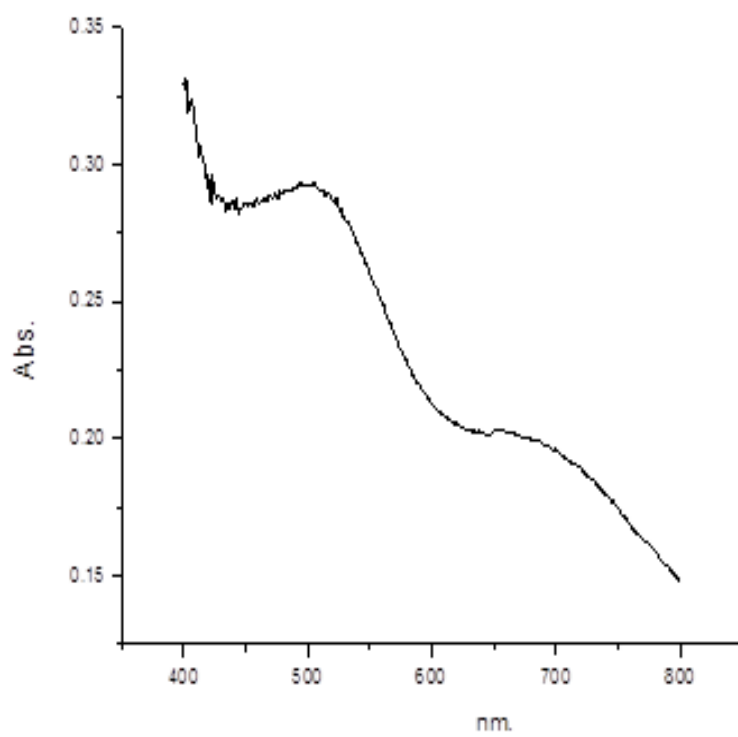
Appendix 2: UV-Visible spectra of the synthesised ligands and their metal(II) complexes.



UV of babh ligand

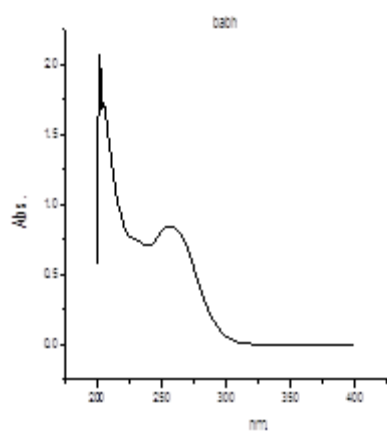


UV of $\text{Cu}_2(\text{babh})_2\text{Cl}_2$

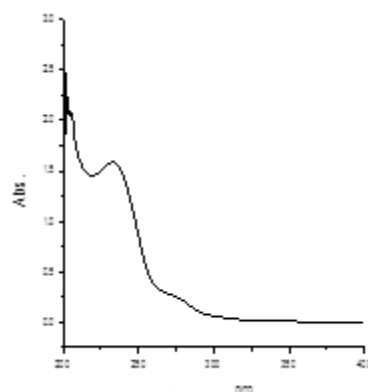


Vis of $\text{Cu}_2(\text{babh})_2\text{Cl}_2$

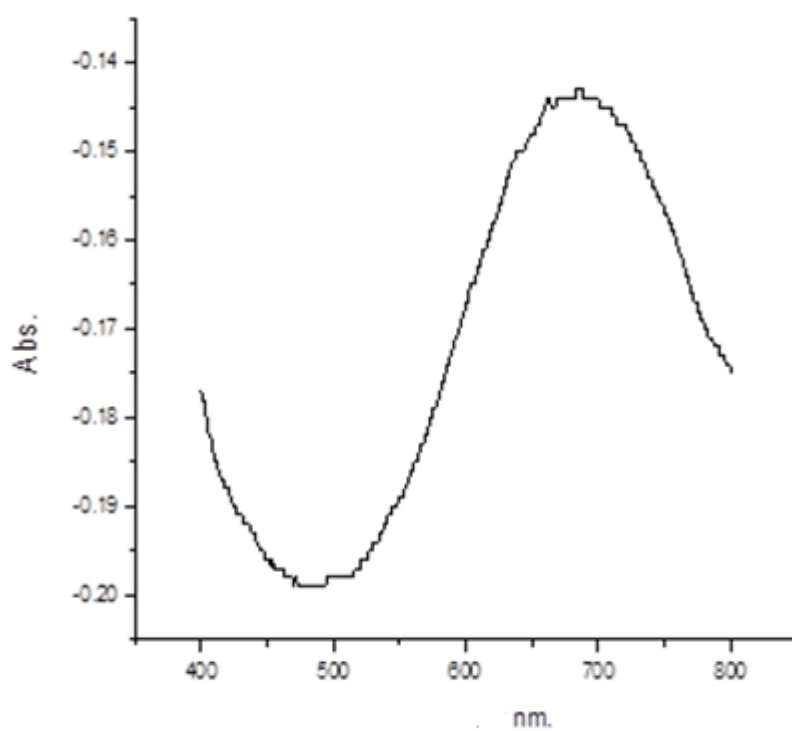
Figure 6.26. UV-Vis spectra of babh and $\text{Cu}_2(\text{babh})_2\text{Cl}_2$



UV of babh

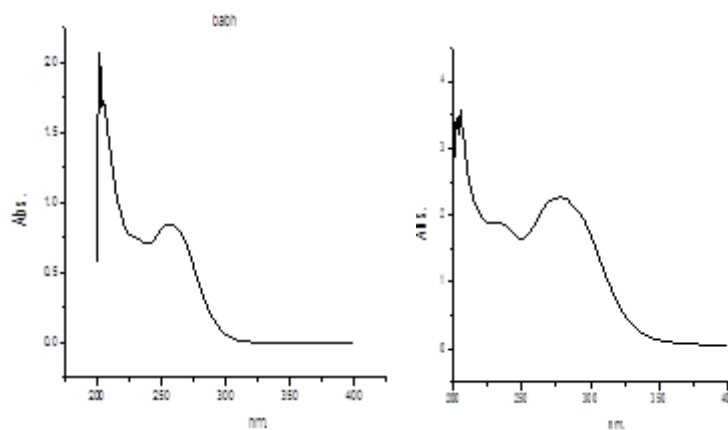


UV of $\text{Cu}(\text{babh})(\text{NO}_3)_2 \cdot 5\text{H}_2\text{O}$



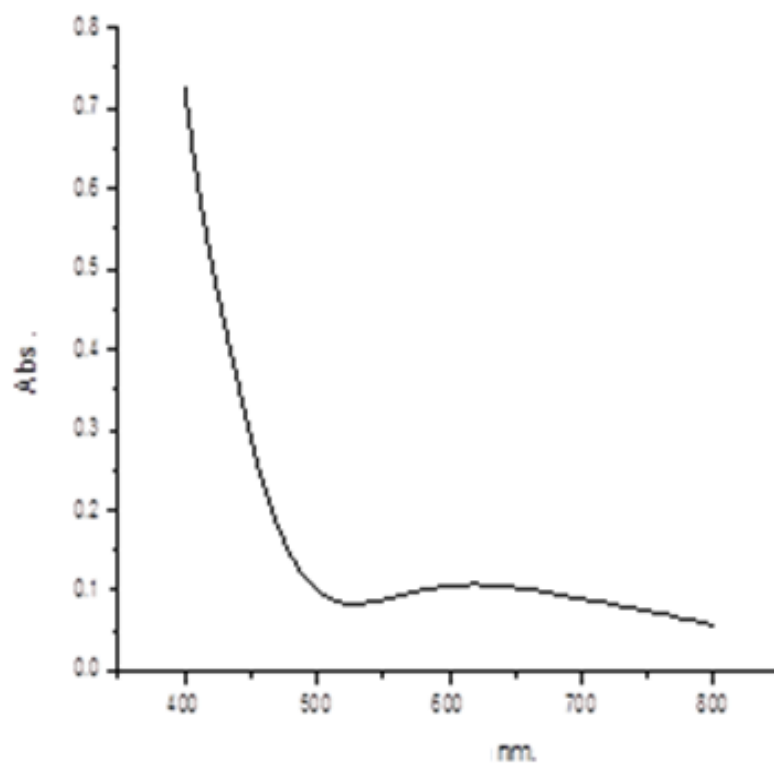
Vis of $\text{Cu}(\text{babh})(\text{NO}_3)_2 \cdot 5\text{H}_2\text{O}$

Figure 6.27: UV-Vis spectra of babh and $\text{Cu}(\text{babh})(\text{NO}_3)_2 \cdot 5\text{H}_2\text{O}$



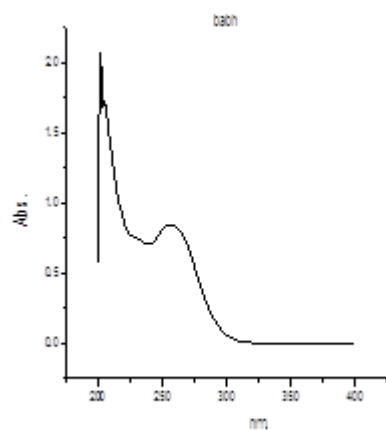
UV of babh

UV of $\text{Cu}(\text{babh})_3(\text{OAc})_2$

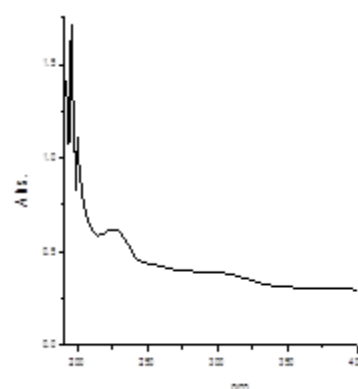


Vis of $\text{Cu}(\text{babh})_3(\text{OAc})_2$

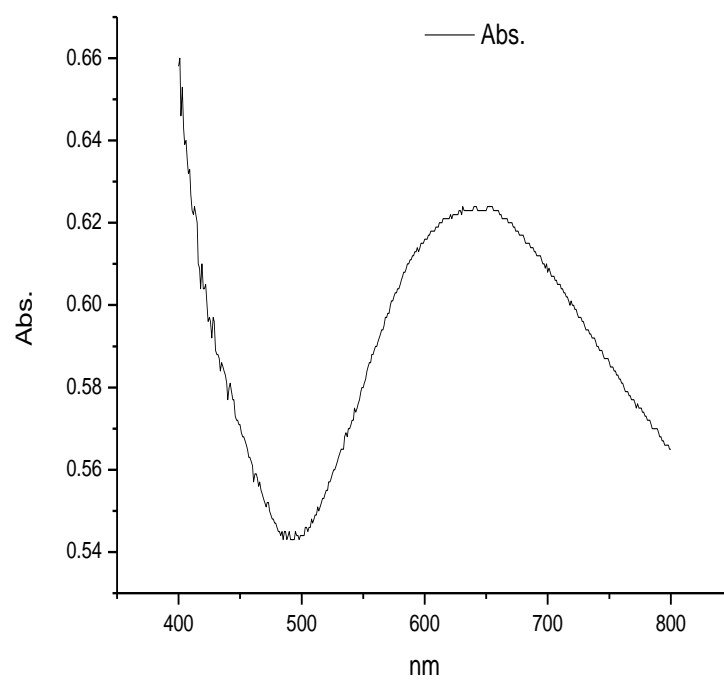
Figure 6.28: UV-Vis spectra of babh and $\text{Cu}(\text{babh})_3(\text{OAc})_2$



UV of babh

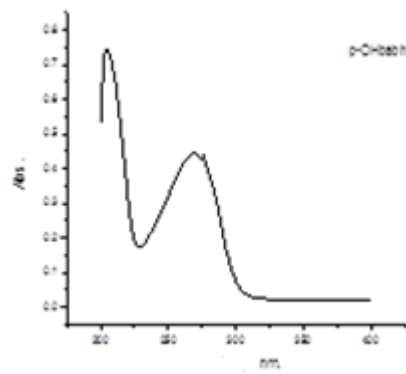


UV of $\text{Cu}(\text{babh})_2\text{SO}_4\cdot\text{H}_2\text{O}$

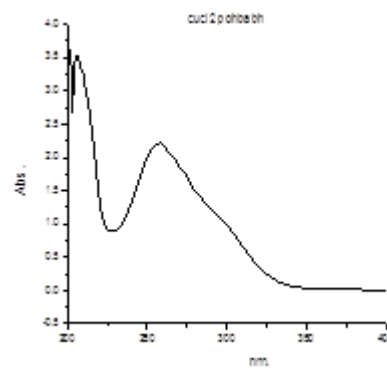


Vis of $\text{Cu}(\text{babh})_2\text{SO}_4\cdot\text{H}_2\text{O}$

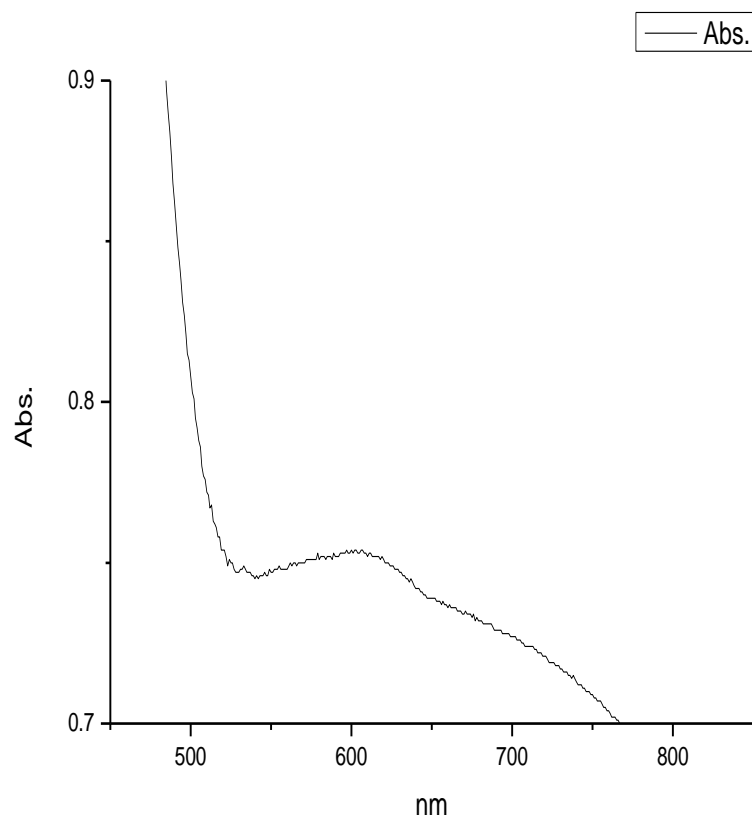
Figure 6.29: UV-Vis spectra of babh and $\text{Cu}(\text{babh})_2\text{SO}_4\cdot\text{H}_2\text{O}$



Uv of *p*-OH-babh

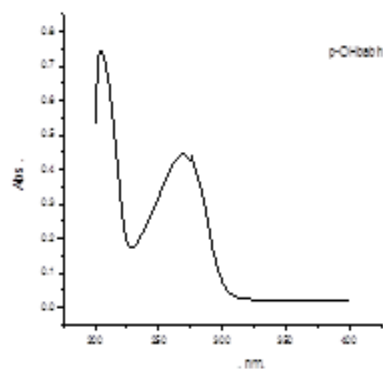


uv of $\text{Cu}(p\text{-OH-babh})_2\text{Cl}_2$

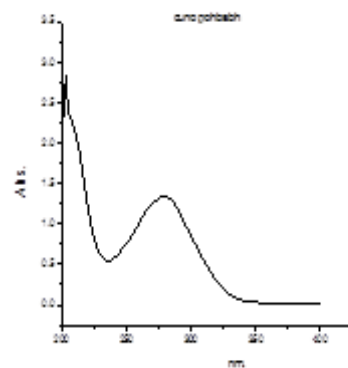


Vis of $\text{Cu}(p\text{-OH-babh})_2\text{Cl}_2$

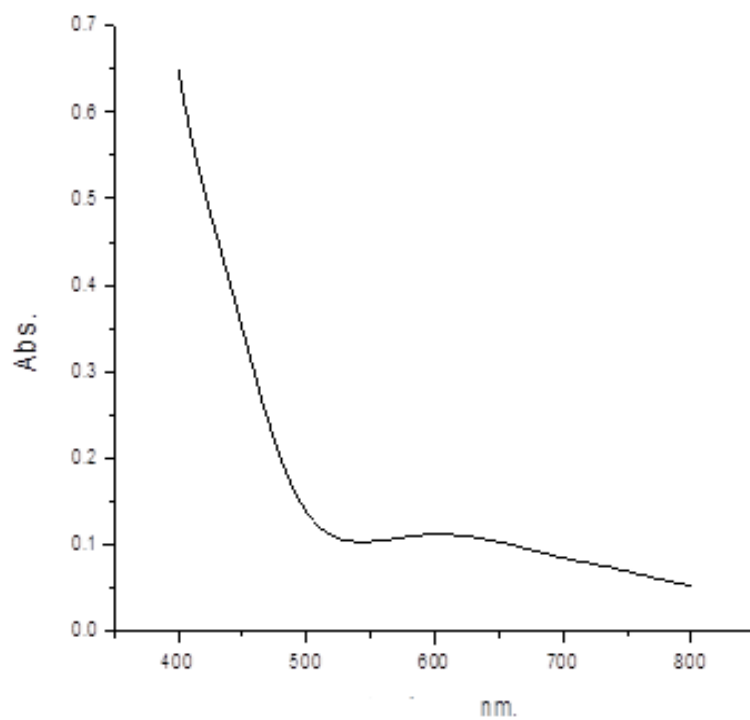
Figure 6.30: UV-Vis spectra of *p*-OH-babh and $\text{Cu}(p\text{-OH-babh})_2\text{Cl}_2$



UV of *p*-OHbabh

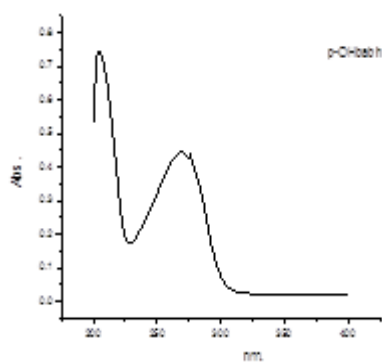


UV of Cu(*p*-OHbabh)₂(NO₃)₂

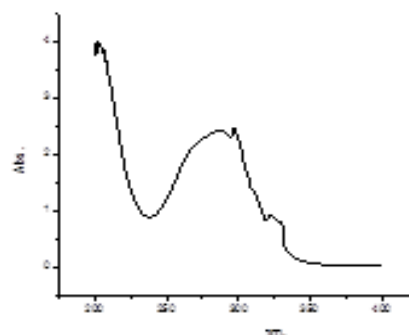


Vis of Cu(*p*-OH-babh)₂(NO₃)₂

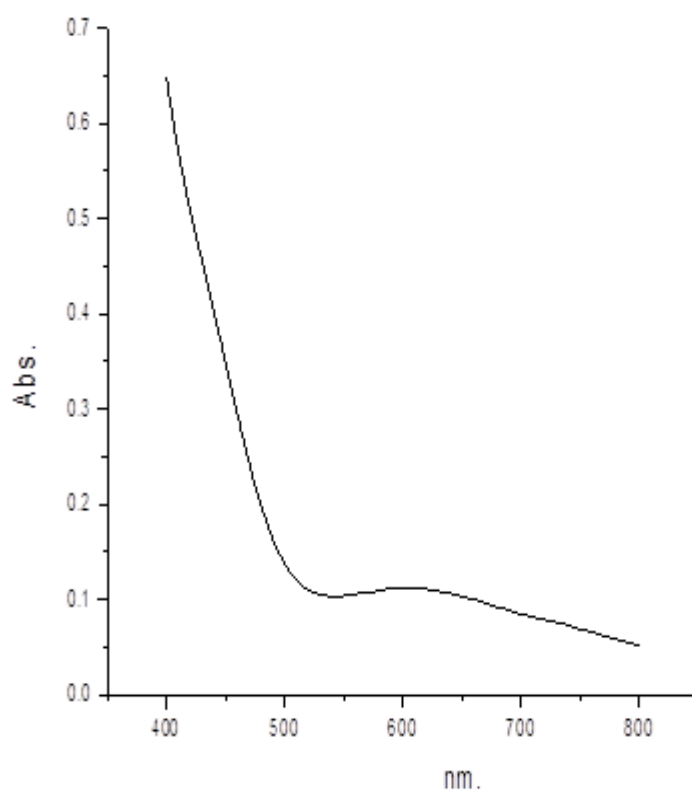
Figure 6.31: UV-Vis spectra of *p*-OH-babh and Cu(*p*-OH-babh)₂(NO₃)₂



UV of *p*-OH-babh

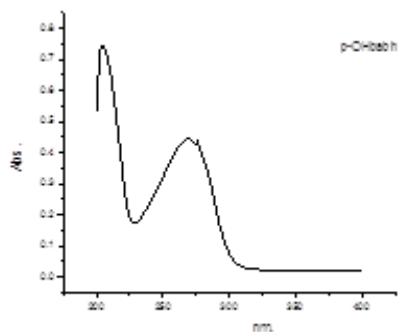


UV of $\text{Cu}(p\text{-OH-babh})_2(\text{OAc})_2$

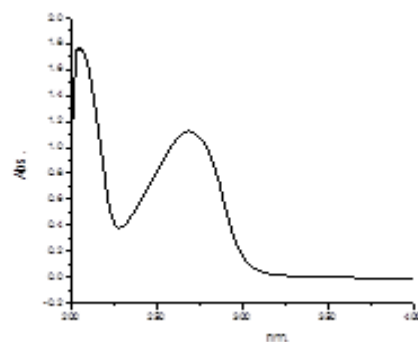


Vis of $\text{Cu}(p\text{-OH-babh})_2(\text{OAc})_2$

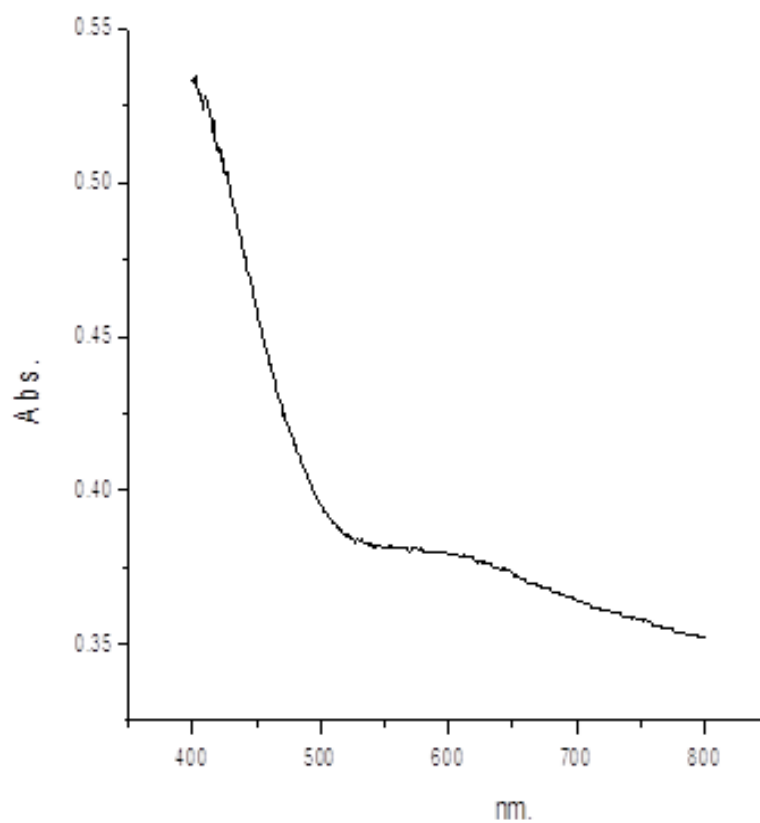
Figure 6.32: UV-Vis spectra of *p*-OH-babh and $\text{Cu}(p\text{-OH-babh})_2(\text{OAc})_2$



UV of *p*-OH-babh

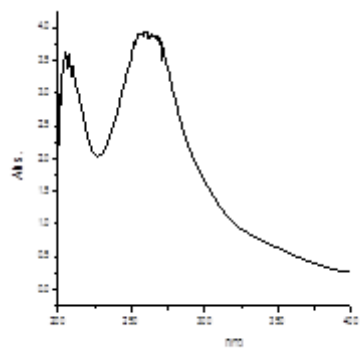


UV of $\text{Cu}(p\text{-OH-babh})\text{SO}_4 \cdot 3\text{H}_2\text{O}$

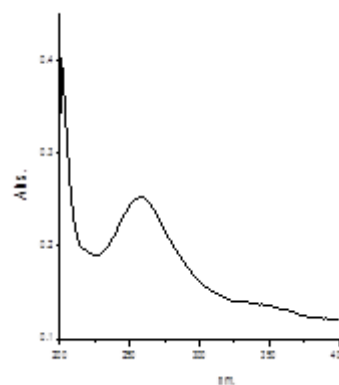


Vis of $\text{Cu}(p\text{-OH-babh})\text{SO}_4 \cdot 3\text{H}_2\text{O}$

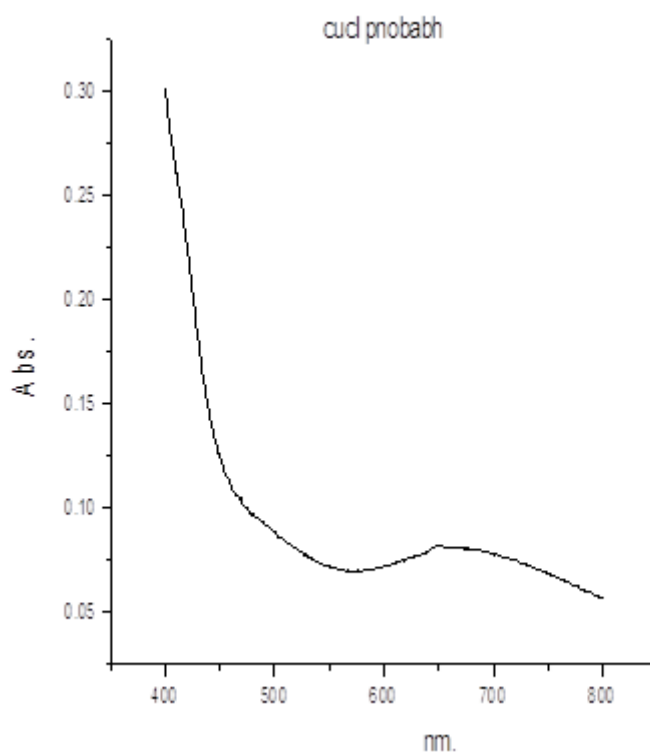
Figure 6.33: UV-Vis spectra of *p*-OH-babh and $\text{Cu}(p\text{-OH-babh})\text{SO}_4 \cdot 3\text{H}_2\text{O}$



p-NO₂babh

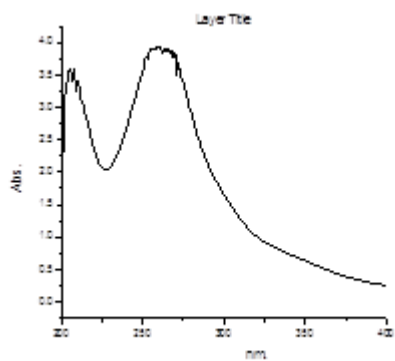


UV of Cu(*p*-NO₂-babh)Cl₂.2H₂O

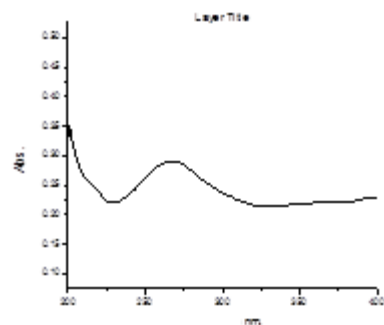


Vis of Cu(*p*-NO₂-babh)Cl₂.2H₂O

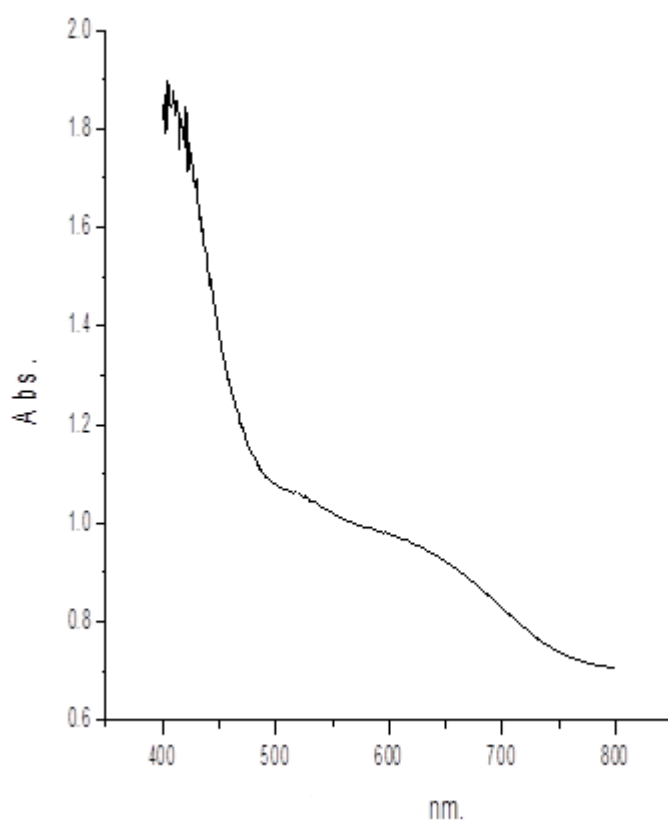
Figure 6.34: UV-Vis spectra of *p*-NO₂-babh and Cu(*p*-NO₂-babh)Cl₂.2H₂O



p-NO₂-babh

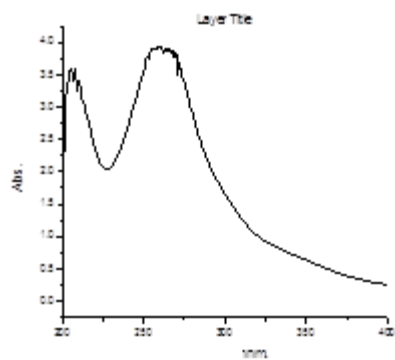


UV of Cu(*p*-NO₂-babh)(NO₃)

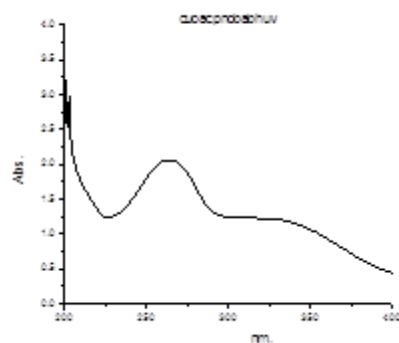


Vis of Cu(*p*-NO₂-babh)(NO₃)

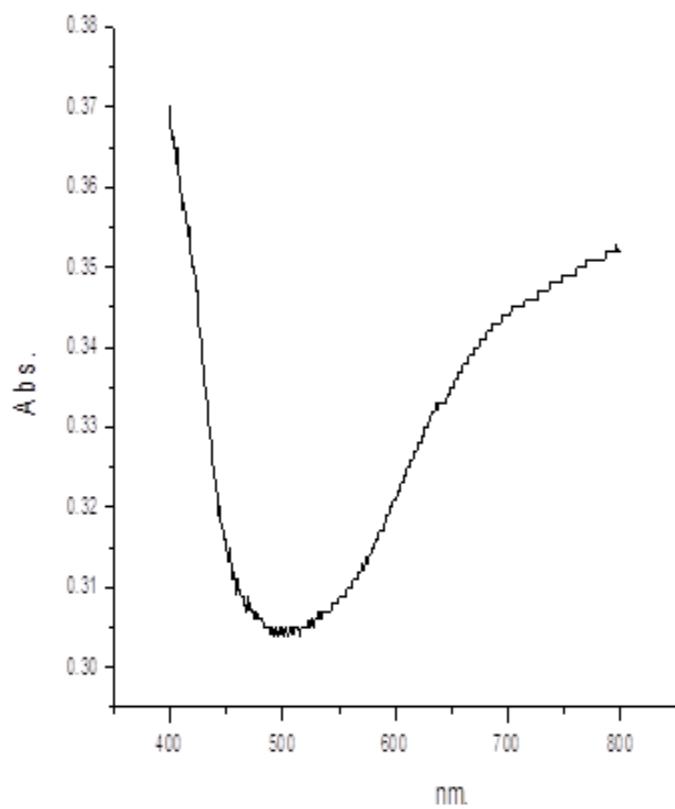
Figure 6.35: UV-Vis spectra of *p*-NO₂-babh and Cu(*p*-NO₂-babh)(NO₃)



p-NO₂babh

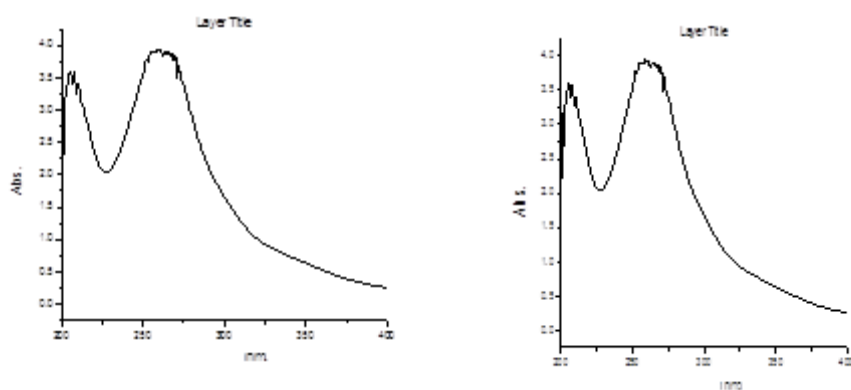


UV of Cu((*p*-NO₂-babh)₃(OAc)₂



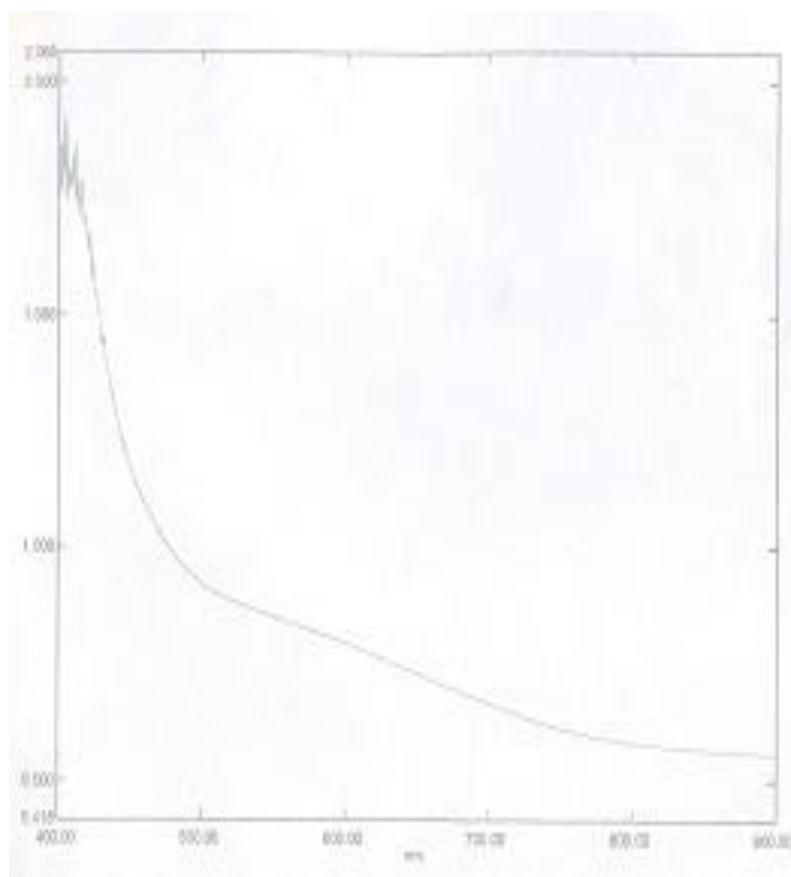
Vis of Cu((*p*-NO₂-babh)₃(OAc)₂

Figure 6.36: UV-Vis spectra of *p*-NO₂-babh and Cu((*p*-NO₂-babh)₃(OAc)₂



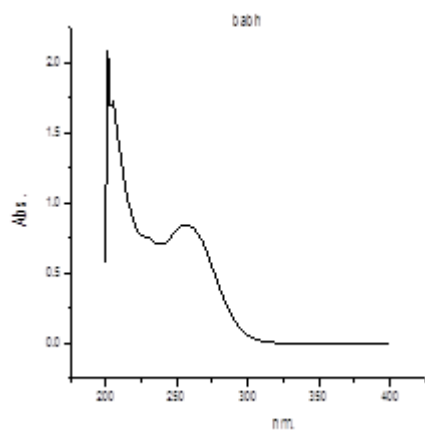
p-NO₂-babh

UV of Cu(*p*-NO₂-babh)SO₄·2C₂H₅OH

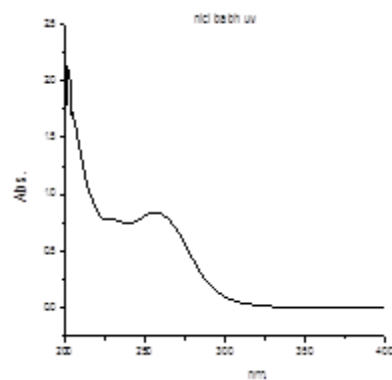


Vis of Cu(*p*-NO₂-babh)SO₄·2C₂H₅OH

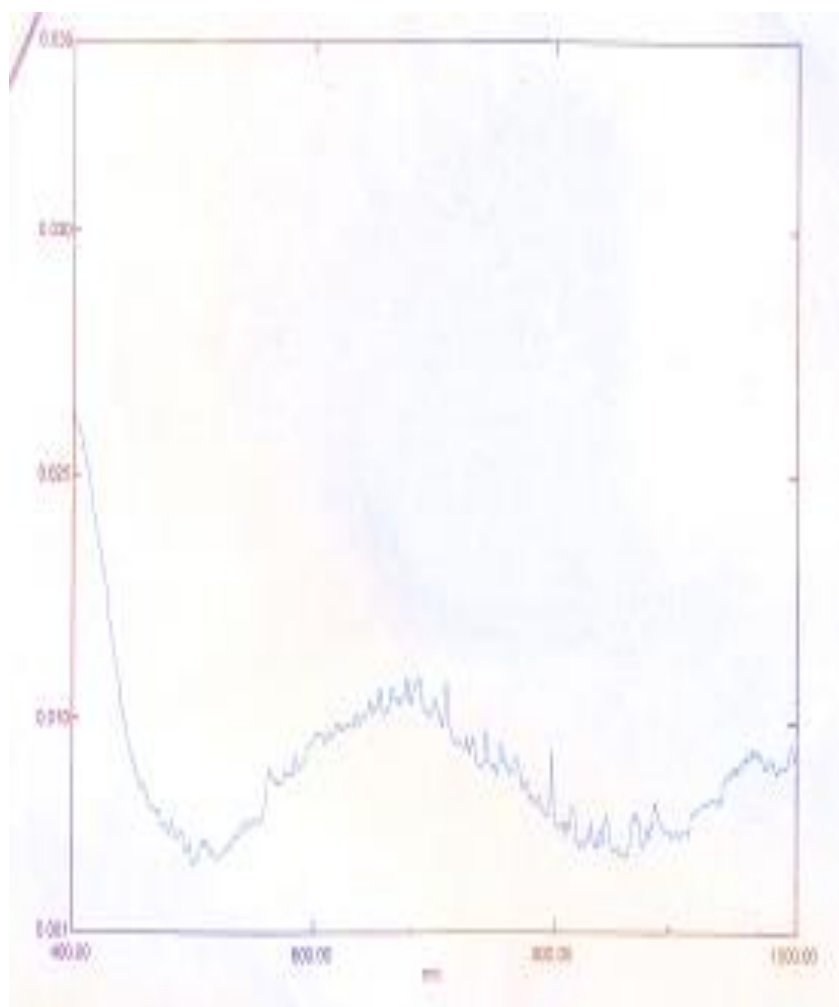
Figure 6.37: UV-Vis spectra of *p*-NO₂-babh and Cu(*p*-NO₂-babh)SO₄·2C₂H₅OH



UV of babh

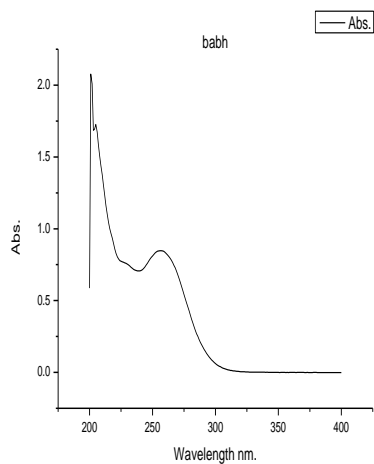


UV of Ni(babh)₂Cl₂

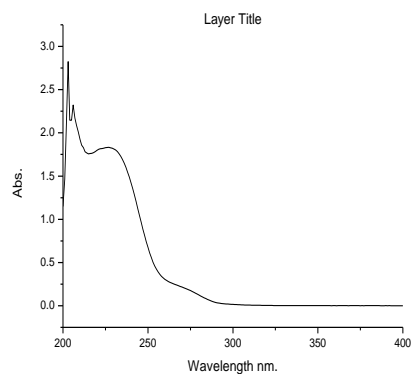


Vis of Ni(babh)₂Cl₂

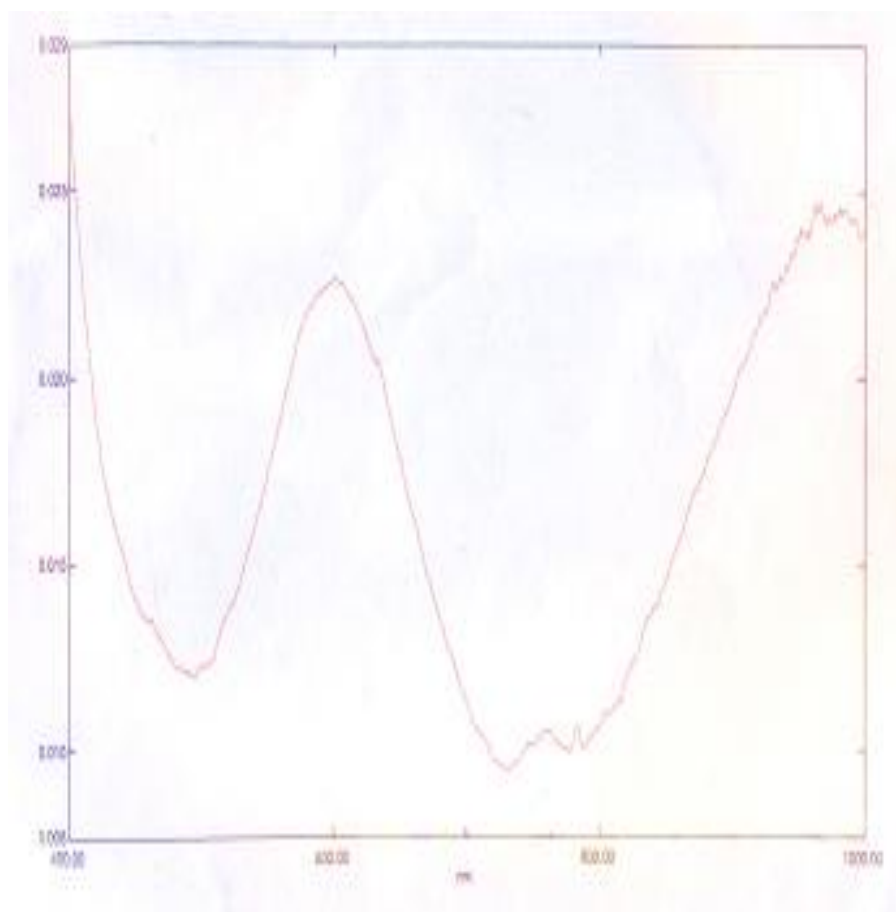
Figure 6.38: UV-Vis spectra of babh and Ni(babh)₂Cl₂



UV of babh

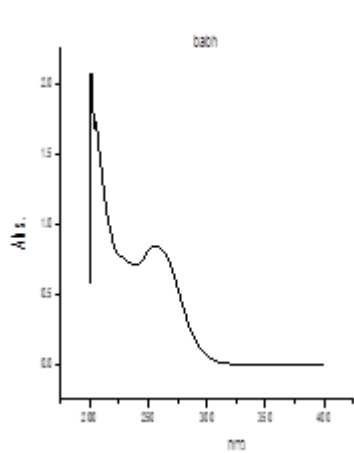


UV of Ni(babh)(NO₃)₂.2H₂O

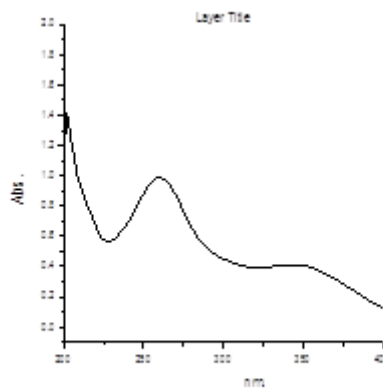


Vis of Ni(babh)(NO₃)₂.2H₂O

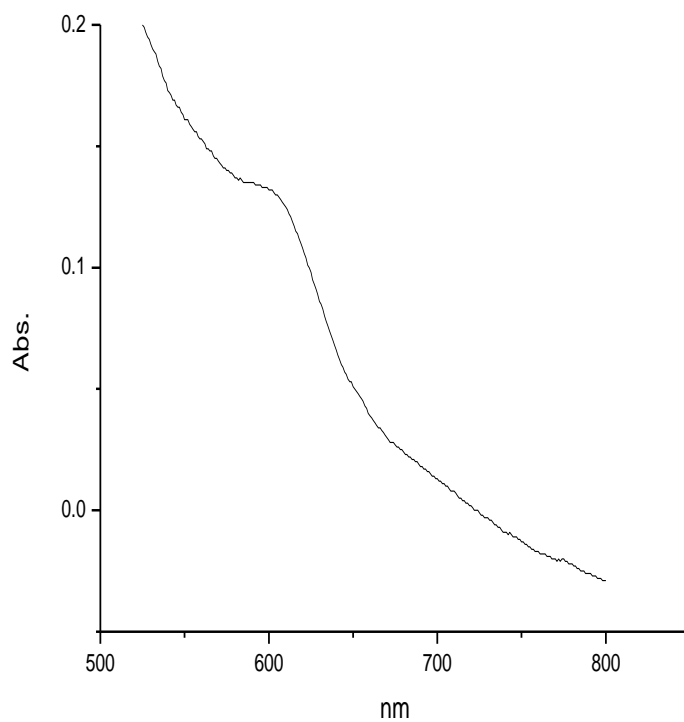
Figure 6.39: UV-Vis spectra of babh and Ni(babh)(NO₃)₂.2H₂O



UV of babh

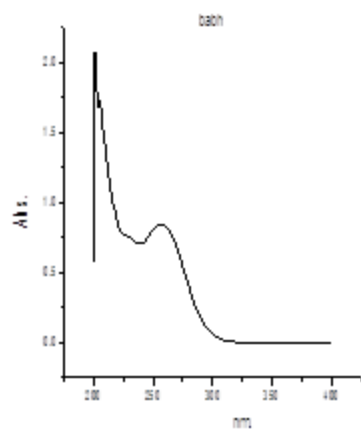


UV of Ni(babh)₂(OAc)₂

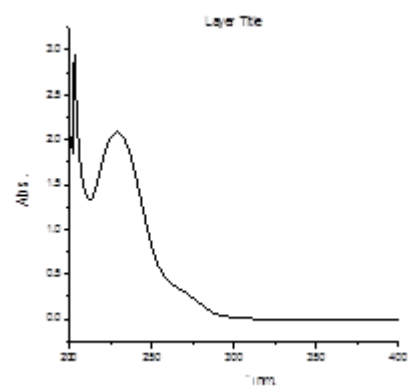


Vis of Ni(babh)₂(OAc)₂

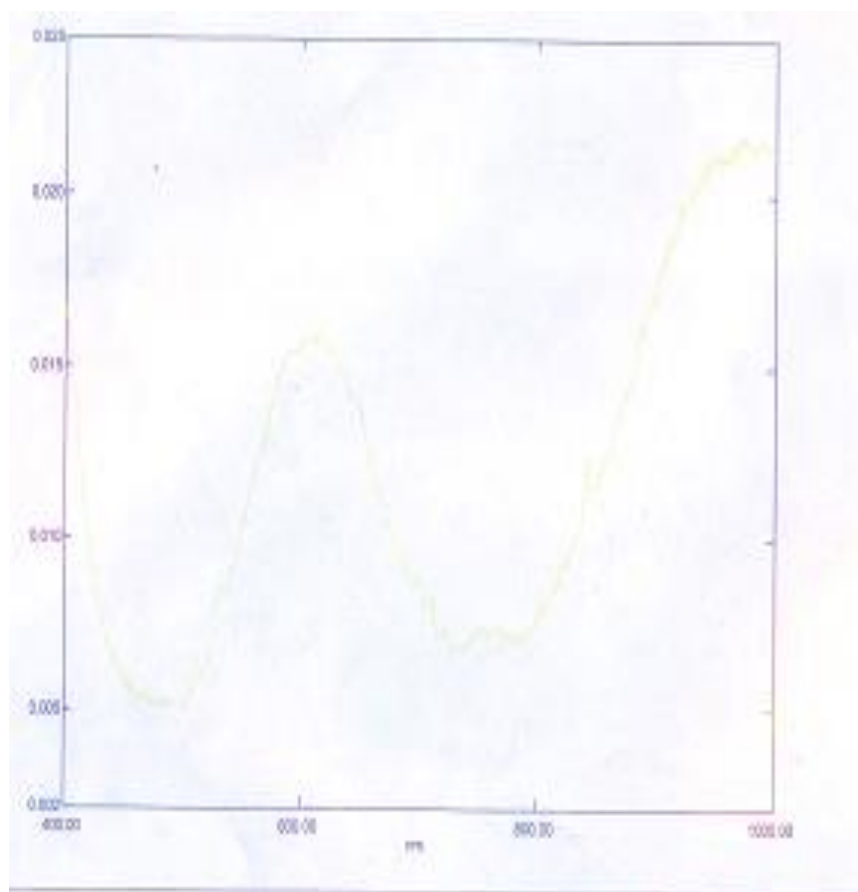
Figure 6.40: UV-Vis spectra of babh and Ni(babh)₂(OAc)₂



UV of babh

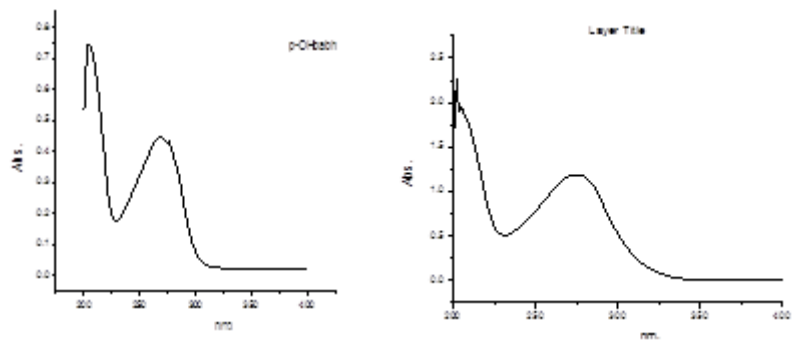


UV of Ni(babh)SO₄.5H₂O



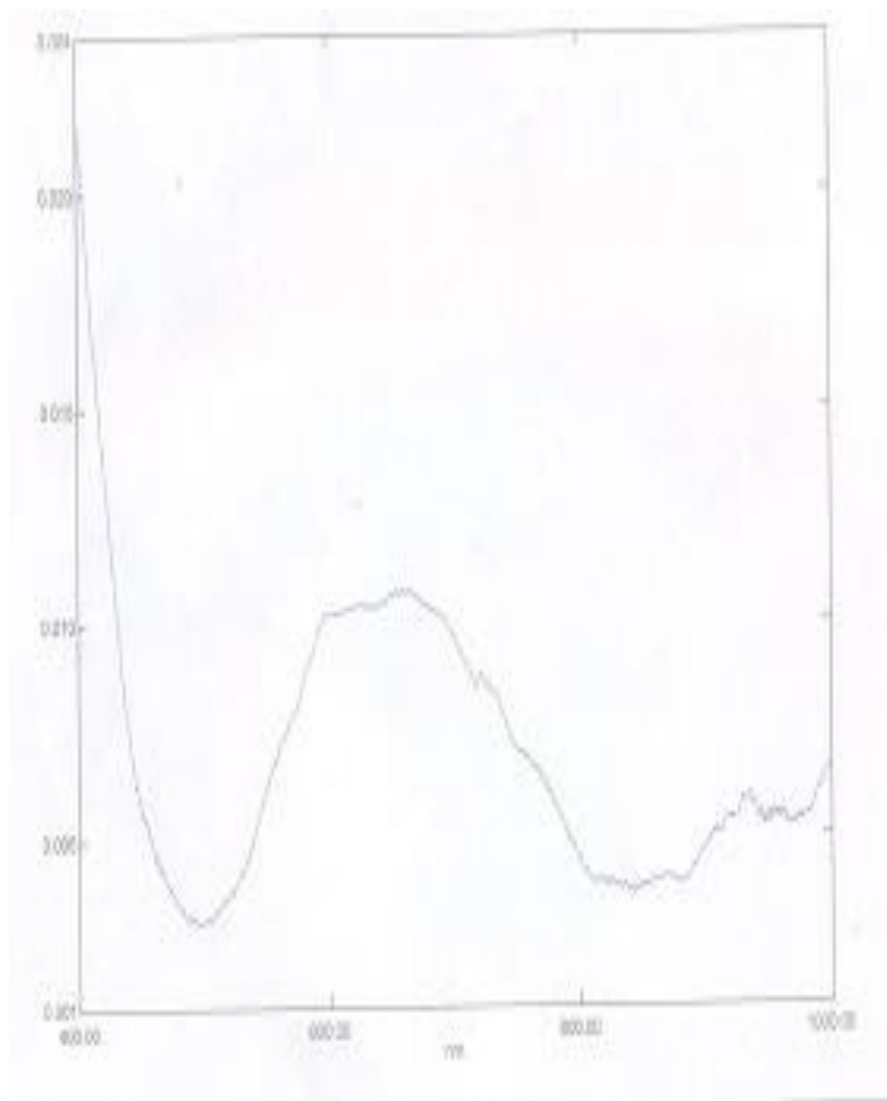
Vis of Ni(babh)SO₄.5H₂O

Figure 6.41: UV-Vis spectra of babh and Ni(babh)SO₄.5H₂O



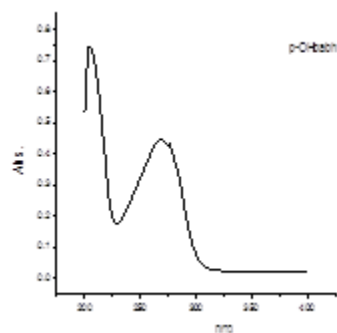
p-OH-babh

UV of Ni(*p*-OH-babh)₂Cl₂

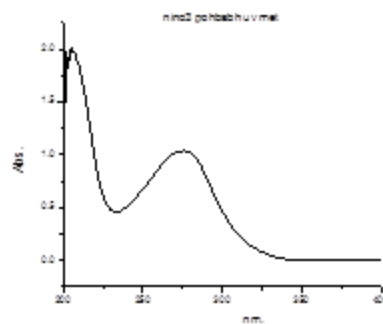


Vis of Ni(*p*-OH-babh)₂Cl₂

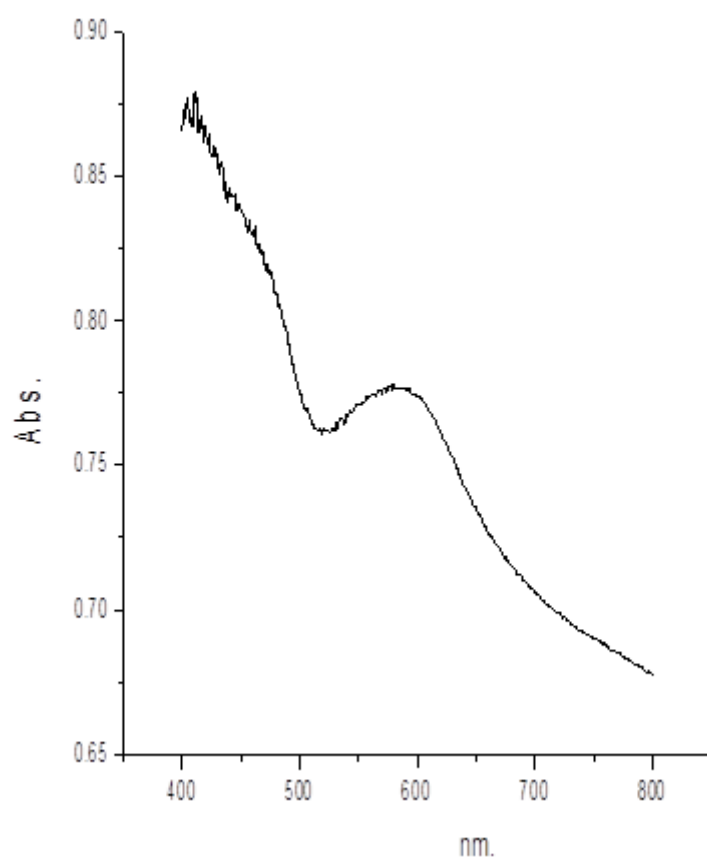
Figure 6.42: UV-Vis spectra of *p*-OH-babh and Ni(*p*-OH-babh)₂Cl₂



p-OH-babh

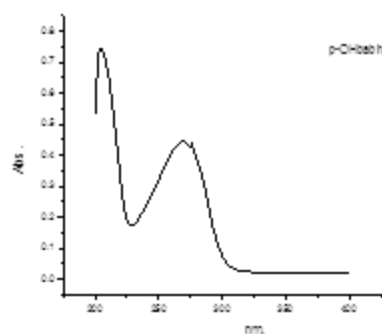


UV of Ni(*p*-OH-babh)₂(NO₃)₂

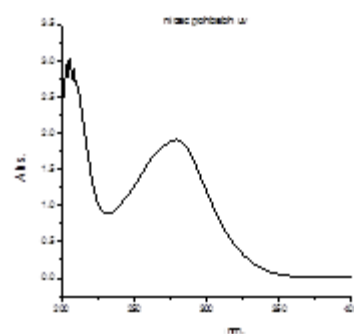


UV-Vis of Ni(*p*-OH-babh)₂(NO₃)₂

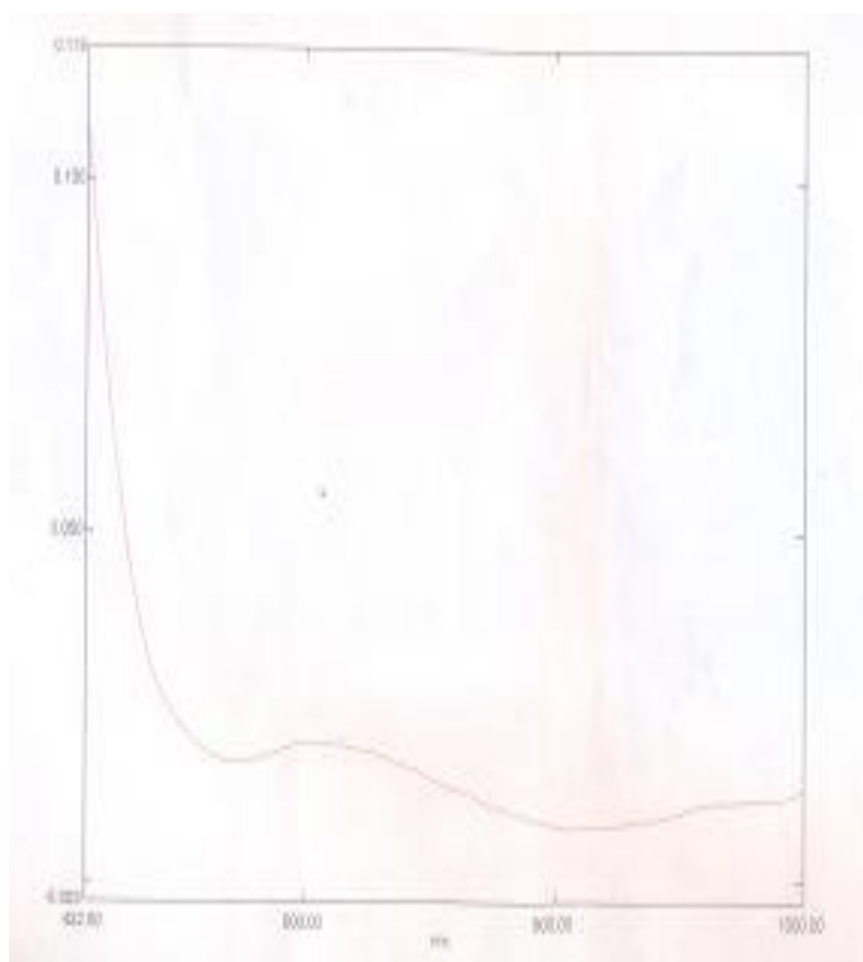
Figure 6.43: UV-Vis spectra of *p*-OH-babh and Ni(*p*-OH-babh)₂(NO₃)₂



p-OH-babh

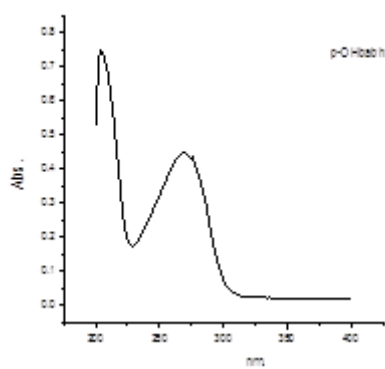


UV of Ni(*p*-OH-babh)₂(OAc)₂

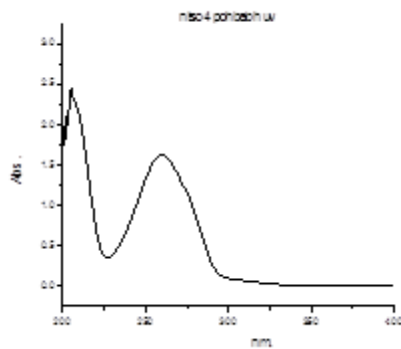


Vis of Ni(*p*-OH-babh)₂(OAc)₂

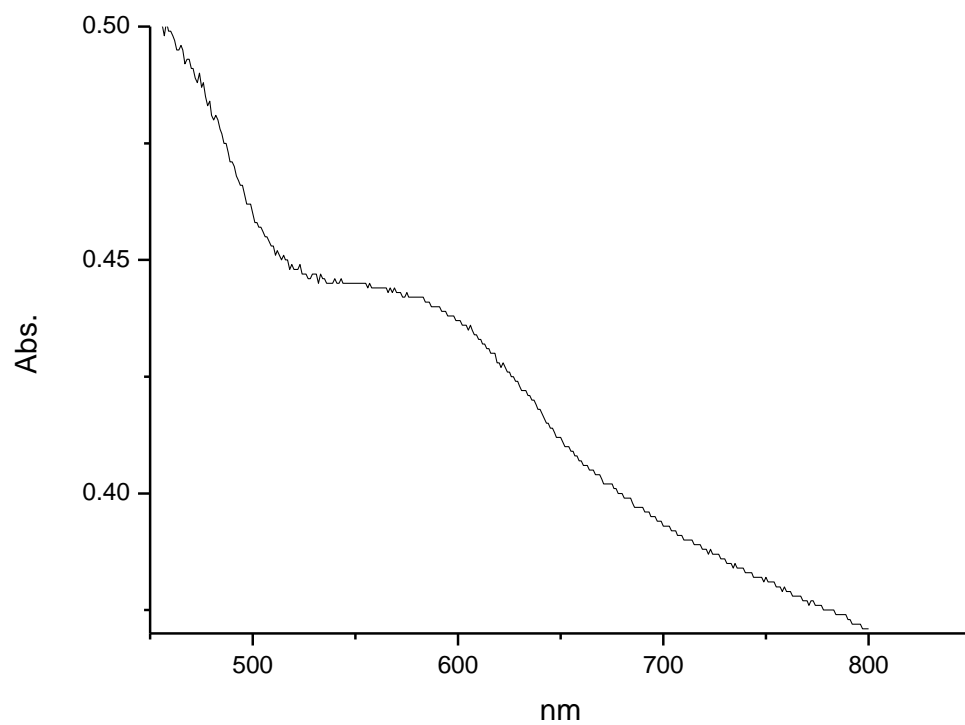
Figure 6.44: UV-Vis spectra of *p*-OH-babh and Ni(*p*-OH-babh)₂(OAc)₂



p-OH-babh

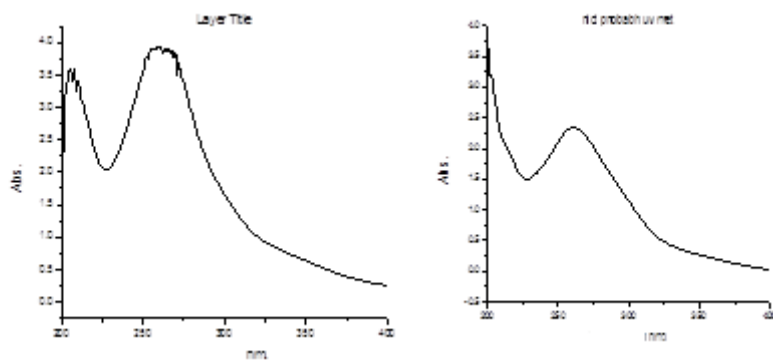


UV of Ni (*p*-OH-babh)SO₄·3H₂O



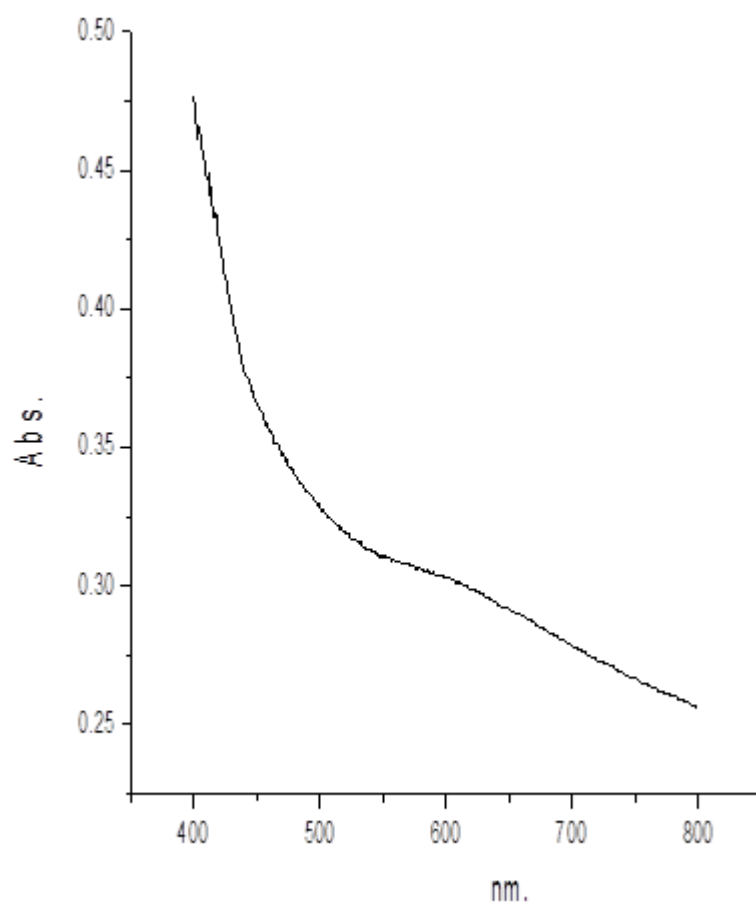
Vis of Ni(*p*-OH-babh)SO₄·3H₂O

Figure 6.45: UV-Vis spectra of *p*-OH-babh and Ni(*p*-OH-babh)SO₄·3H₂O



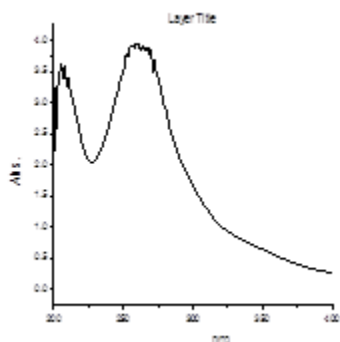
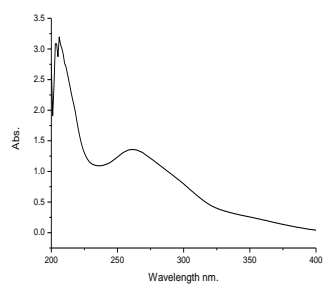
p-NO₂-babh

UV of Ni(*p*-NO₂-babh)Cl₂·4H₂O



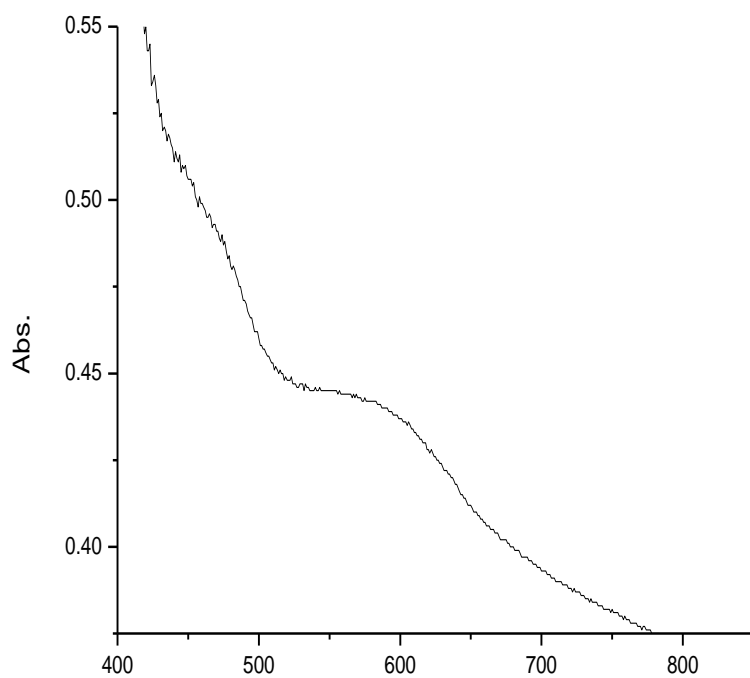
Vis of Ni(*p*-NO₂-babh)Cl₂·4H₂O

Figure 6.46: UV-Vis spectra of *p*-NO₂-babh and Ni(*p*-NO₂-babh)Cl₂·4H₂O



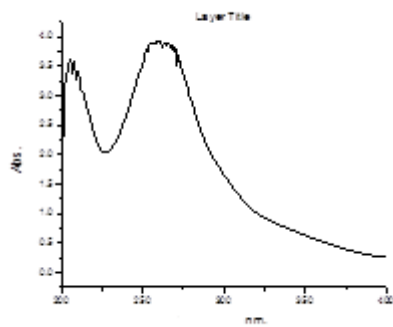
UV-Vis of $\text{Ni}(p\text{-NO}_2\text{-babh})_2(\text{NO}_3)_2$

$p\text{-NO}_2\text{-babh}$

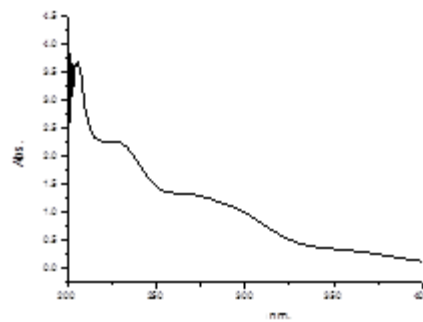


Vis of $\text{Ni}(p\text{-NO}_2\text{-babh})_2(\text{NO}_3)_2$

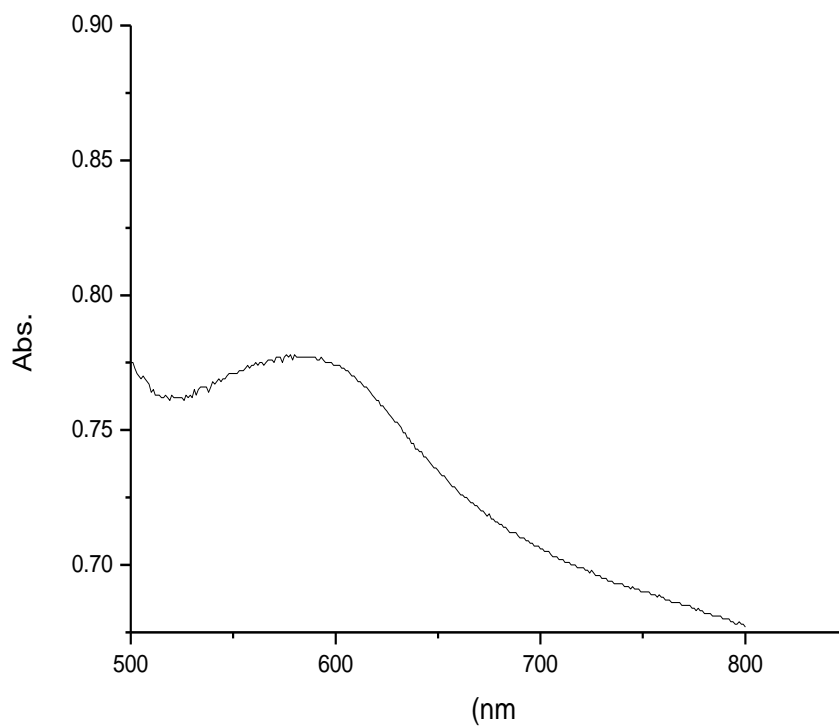
Figure 6.47: UV-Vis spectra of $p\text{-NO}_2\text{-babh}$ and $\text{Ni}(p\text{-NO}_2\text{-babh})_2(\text{NO}_3)_2$



p-NO₂-babh

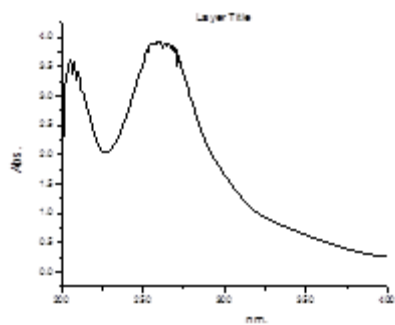


UV of Ni(*p*-NO₂-babh)₂(OAc)₂

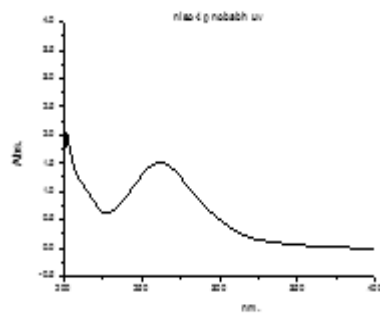


Vis of Ni(*p*-NO₂-babh)₂(OAc)₂

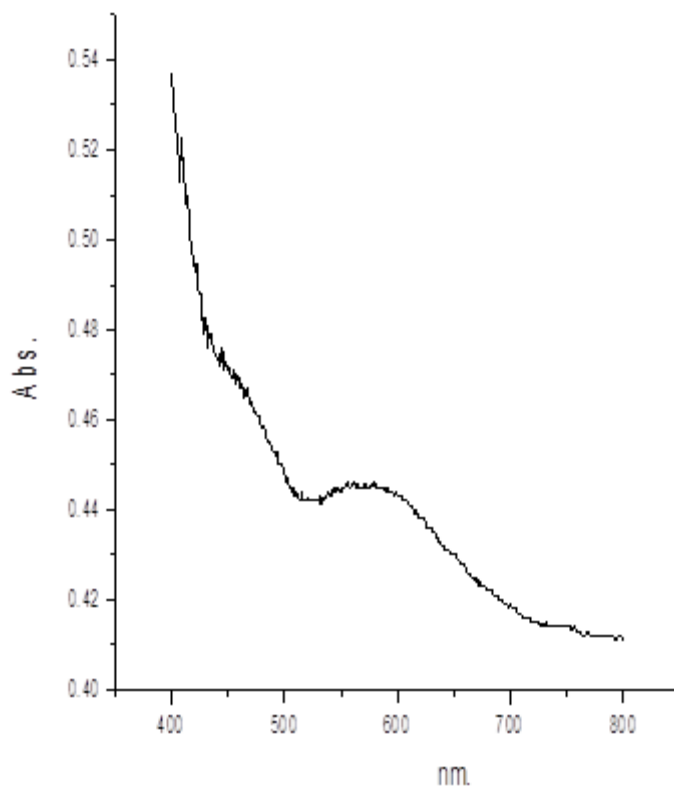
Figure 6.48: UV-Vis spectra of *p*-NO₂-babh and Ni(*p*-NO₂-babh)₂(OAc)₂



p-OH-babh

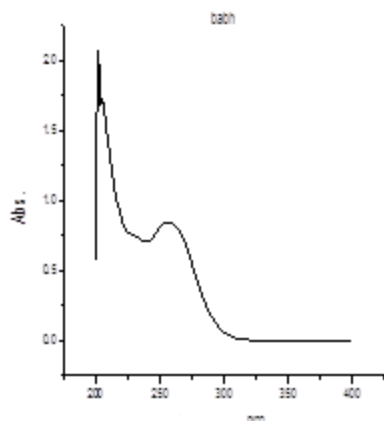


UV of $\text{Ni}(p\text{-NO}_2\text{-babh})\text{SO}_4 \cdot 2\text{H}_2\text{O}$

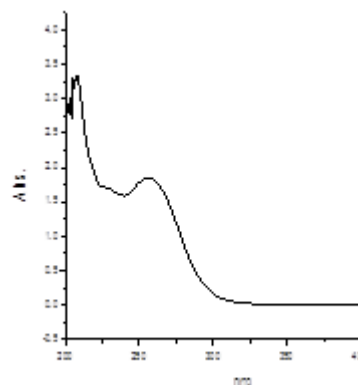


Vis of $\text{Ni}(p\text{-NO}_2\text{-babh})\text{SO}_4 \cdot 2\text{H}_2\text{O}$

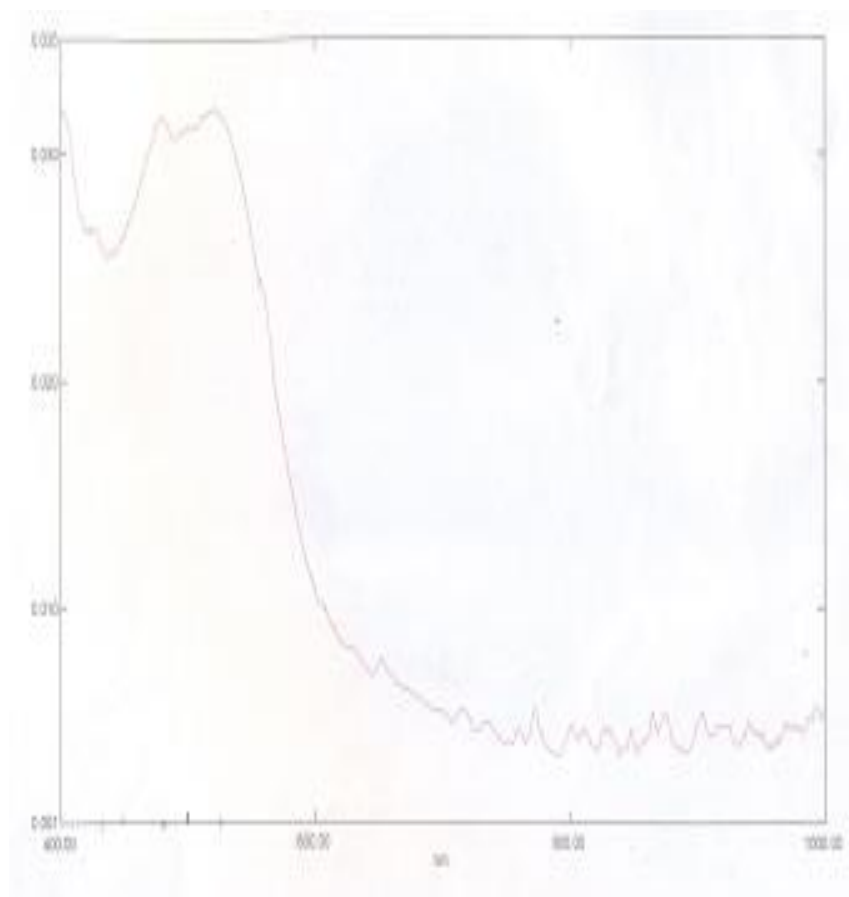
Figure 6.49: UV-Vis spectra of *p*-NO₂-babh and $\text{Ni}(p\text{-NO}_2\text{-babh})\text{SO}_4 \cdot 2\text{H}_2\text{O}$



UV of babh

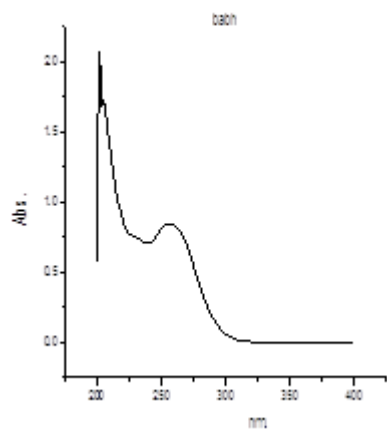


UV of $\text{Co}(\text{babh})_2\text{Cl}_2$

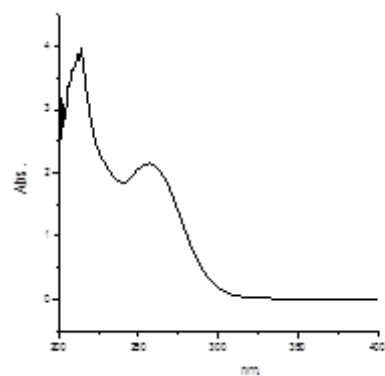


Vis of $\text{Co}(\text{babh})_2\text{Cl}_2$

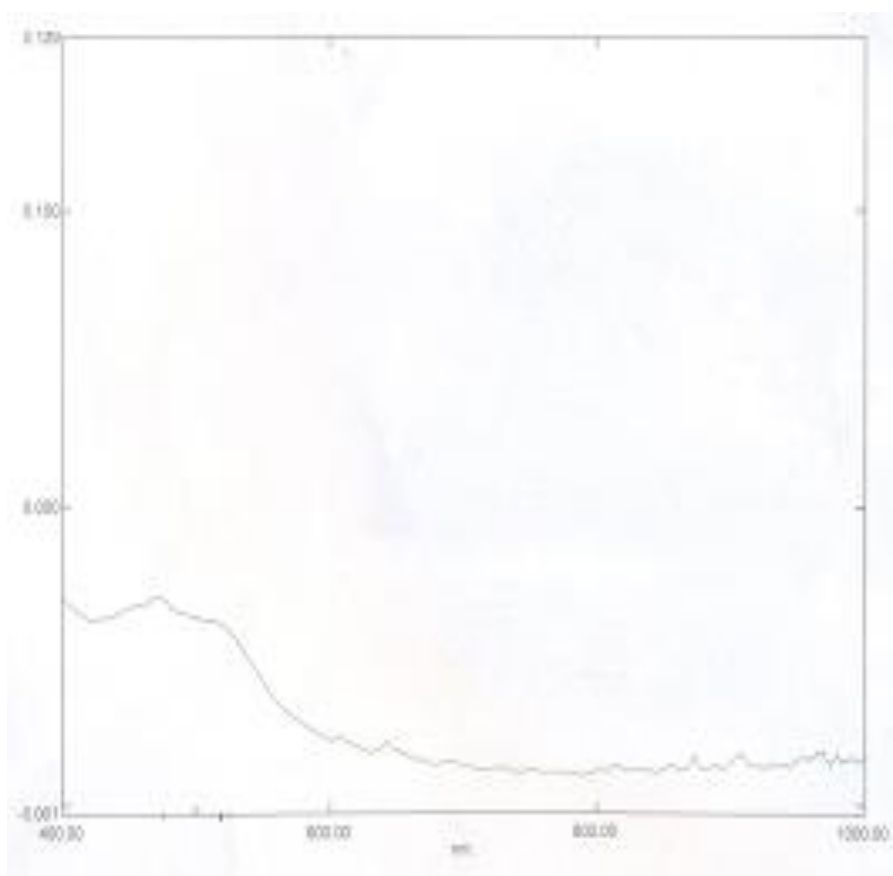
Figure 6.50: UV-Vis spectra of babh and $\text{Co}(\text{babh})_2\text{Cl}_2$



UV of babh

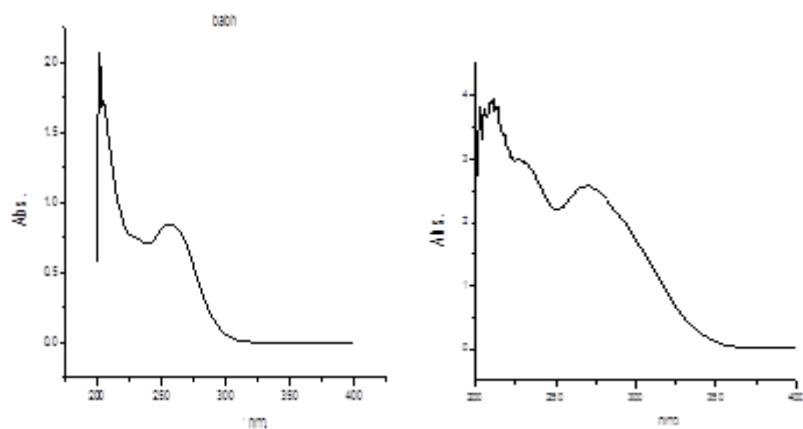


UV of $\text{Co}(\text{babh})_2(\text{NO}_3)_2$



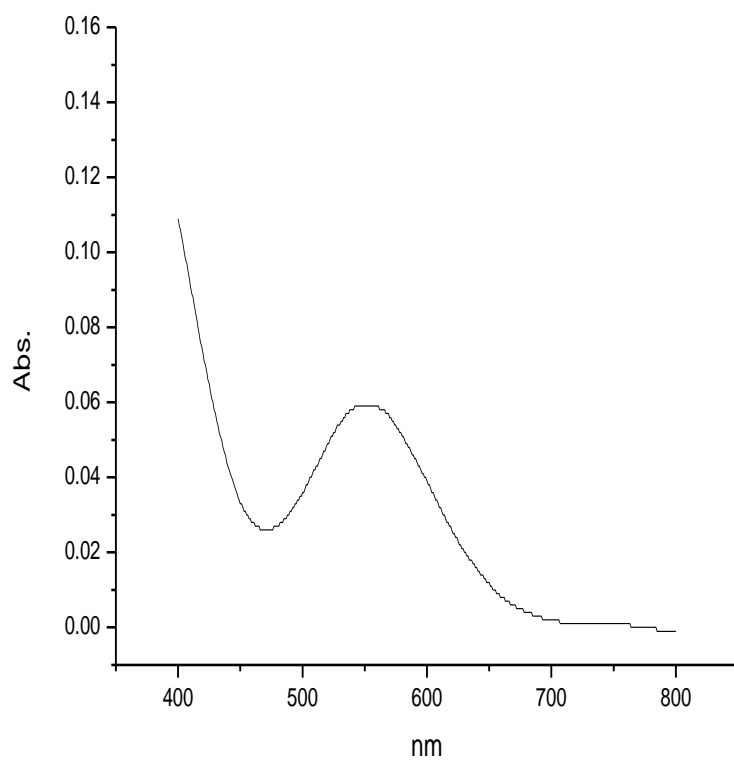
Vis $\text{Co}(\text{babh})_2(\text{NO}_3)_2$

Figure 6.51: UV-Vis spectra of babh and $\text{Co}(\text{babh})_2(\text{NO}_3)_2$



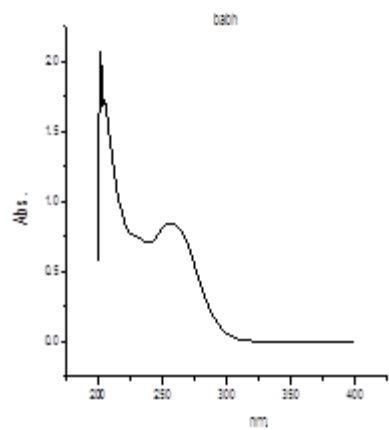
UV of babh

UV of $\text{Co}(\text{babh})_2(\text{OAc})_2$

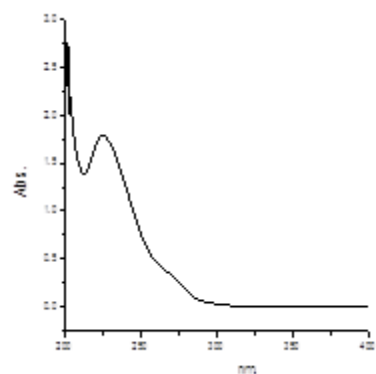


UV of $\text{Co}(\text{babh})_2(\text{OAc})_2$

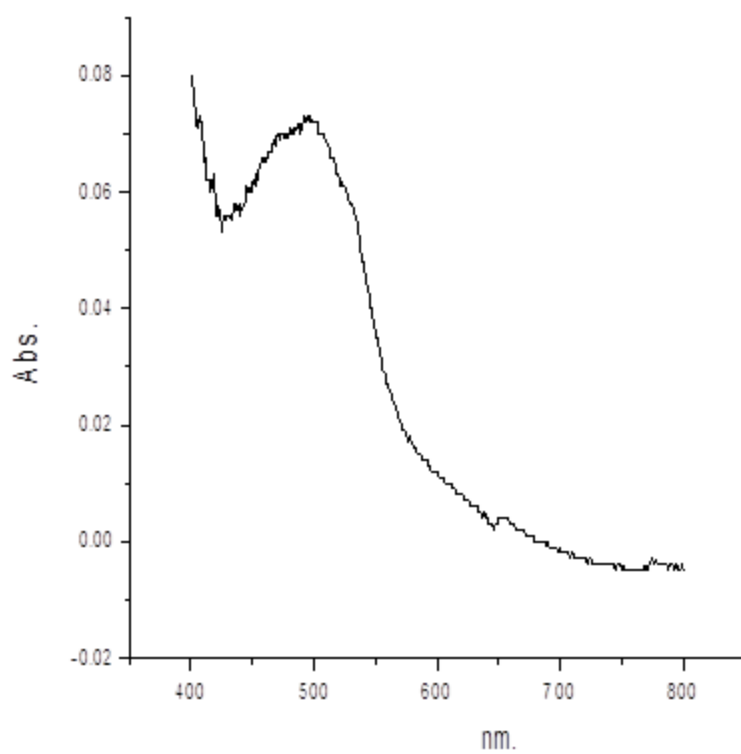
Figure 6.52: UV-Vis spectra of babh and $\text{Co}(\text{babh})_2(\text{OAc})_2$



UV of babh

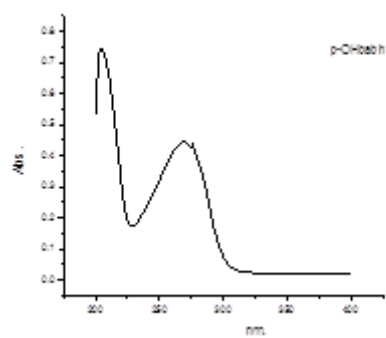


UV of $\text{Co}(\text{babh})\text{SO}_4 \cdot 4\text{H}_2\text{O}$

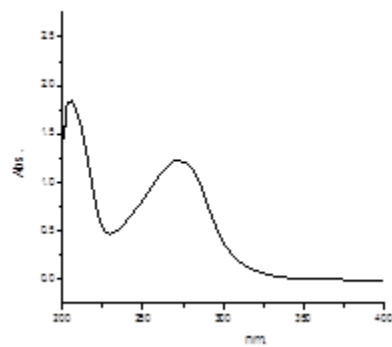


Vis $\text{Co}(\text{babh})\text{SO}_4 \cdot 4\text{H}_2\text{O}$

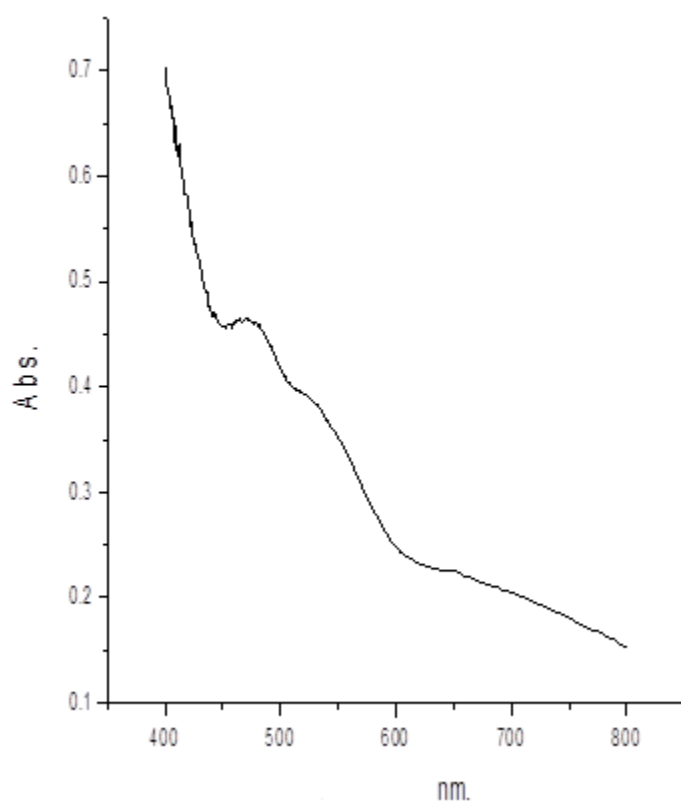
Figure 6.53: UV-Vis spectra of babh and $\text{Co}(\text{babh})\text{SO}_4 \cdot 4\text{H}_2\text{O}$



UV of *p*-OH-babh

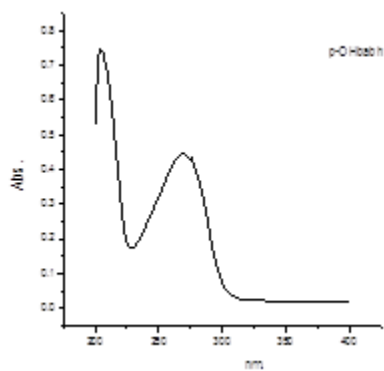


UV of Co(*p*-OH-babh)₂Cl₂

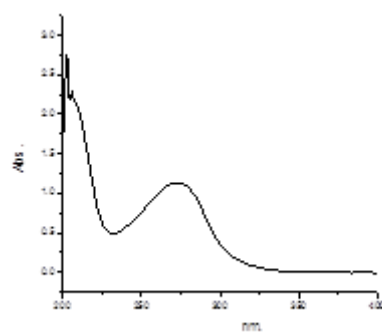


Vis of Co(*p*-OH-babh)₂Cl₂

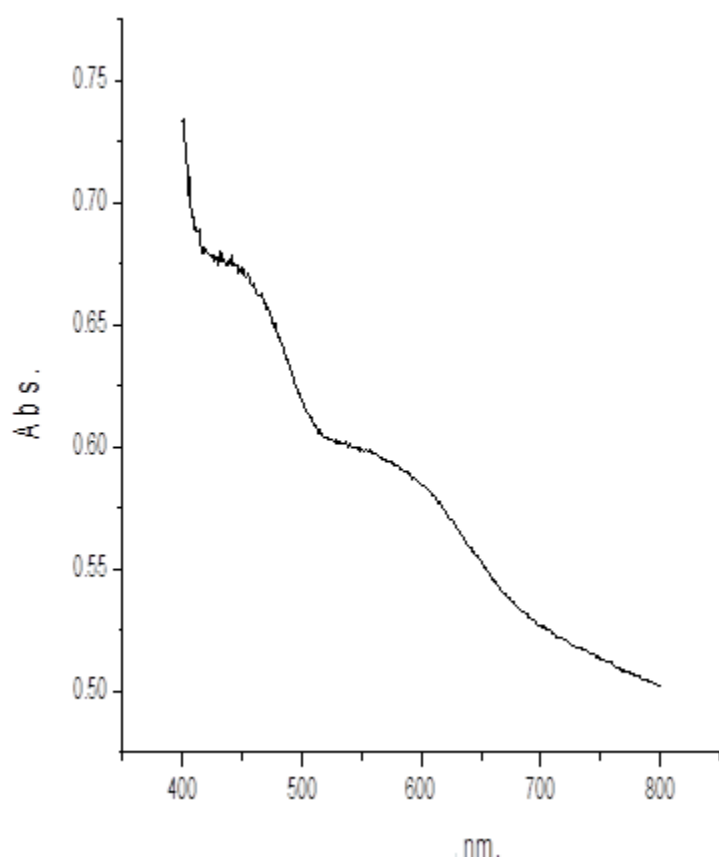
Figure 6.54: UV-Vis spectra of *p*-OH-babh and Co(*p*-OH-babh)₂Cl₂



UV of *p*-OH-babh

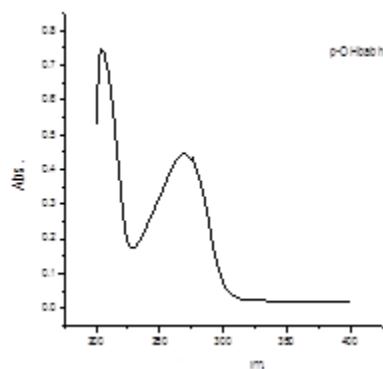


UV of $\text{Co}(p\text{-OH-babh})_2(\text{NO}_3)_2$

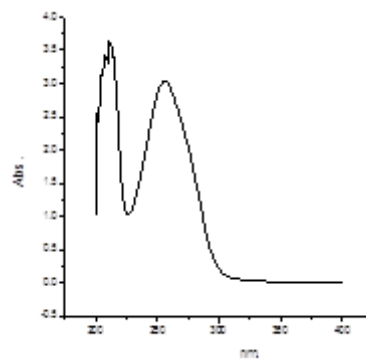


Vis of $\text{Co}(p\text{-OH-babh})_2(\text{NO}_3)_2$

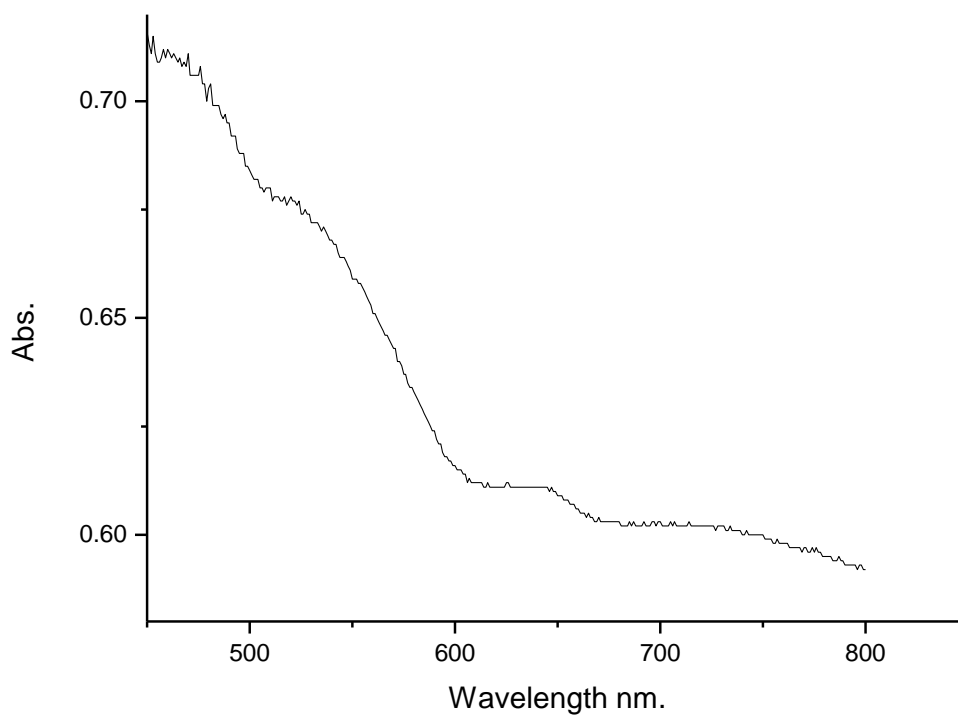
Figure 6.55: UV-Vis spectra of *p*-OH-babh and $\text{Co}(p\text{-OH-babh})_2(\text{NO}_3)_2$



UV of *p*-OH-babh

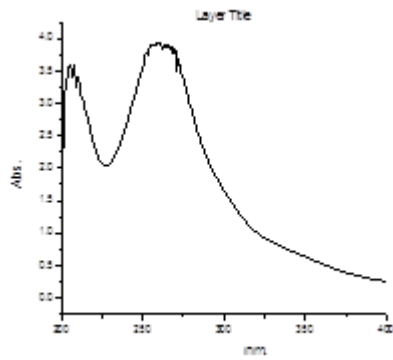


UV of $\text{Co}(p\text{-OH-babh})_2(\text{OAc})_2$

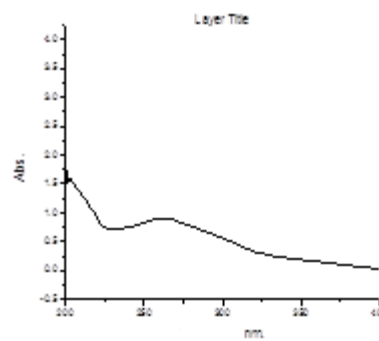


Vis of $\text{Co}(p\text{-OH-babh})_2(\text{OAc})_2$

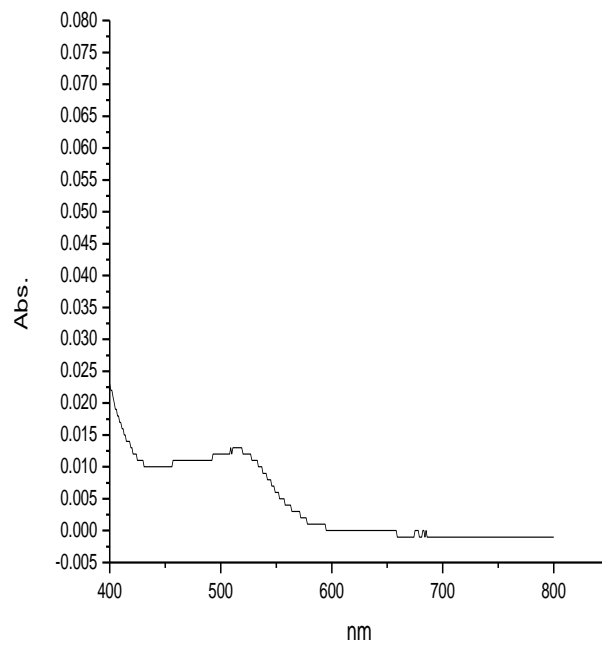
Figure 6.56: UV-Vis spectra of *p*-OH-babh and $\text{Co}(p\text{-OH-babh})_2(\text{OAc})_2$



p-NO₂-babh

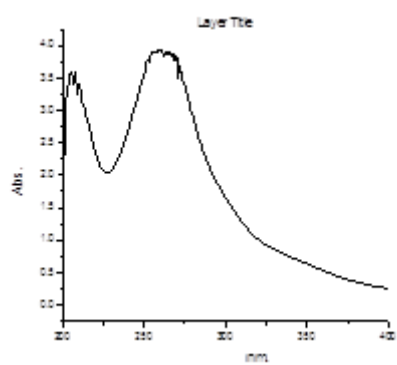


UV of Co(*p*-NO₂-babh)₂Cl₂

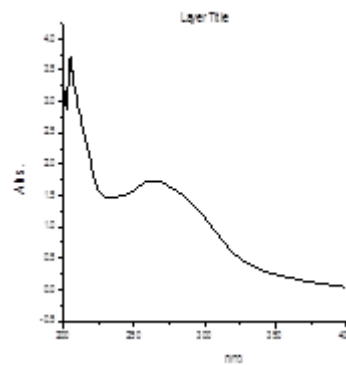


Vis of Co(*p*-NO₂-babh)₂Cl₂

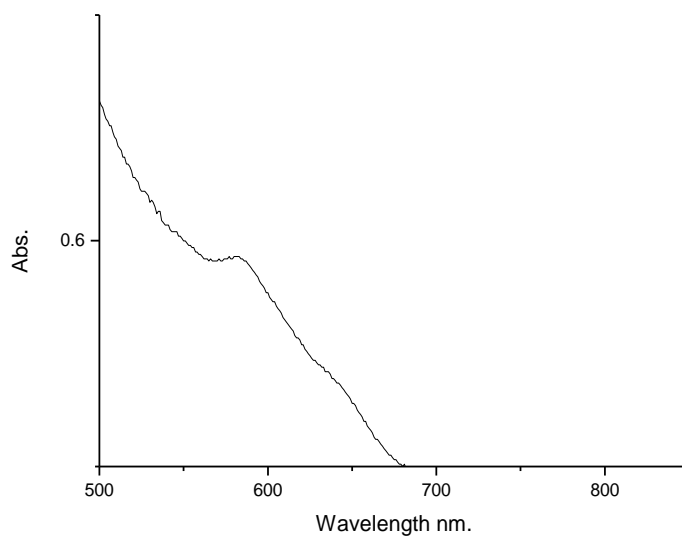
Figure 6.57: UV-Vis spectra of *p*-NO₂-babh and Co(*p*-NO₂-babh)₂Cl₂



p-NO₂-babh

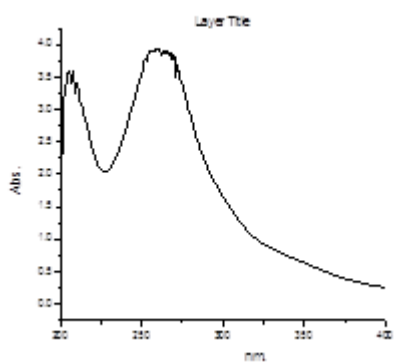


UV of Co(*p*-NO₂-babh)₂

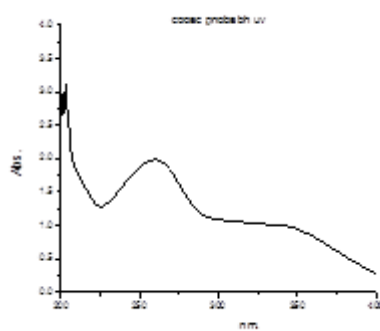


Vis of Co(*p*-NO₂-babh)₂

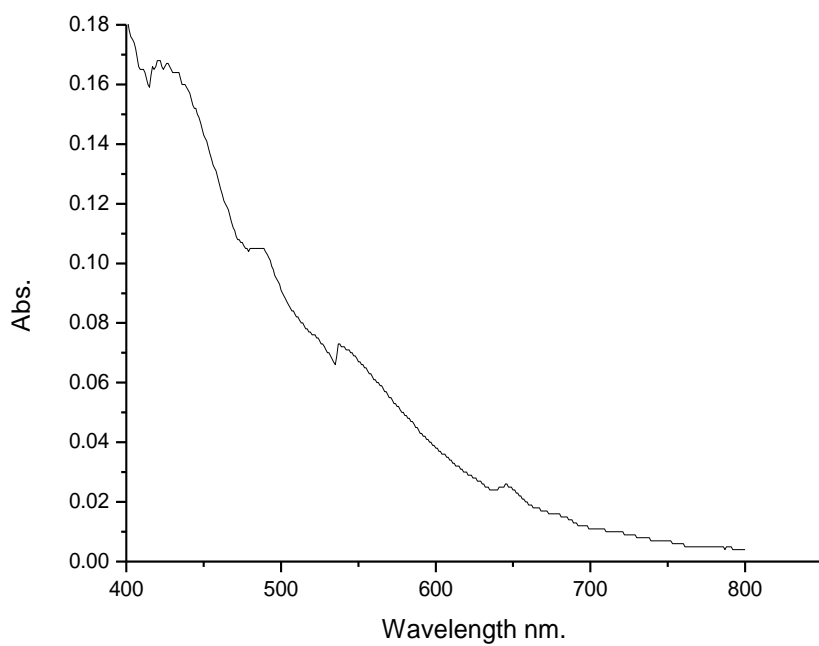
Figure 6.58: UV-Vis spectra of *p*-NO₂-babh and Co(*p*-NO₂-babh)₂



p-NO₂-babh

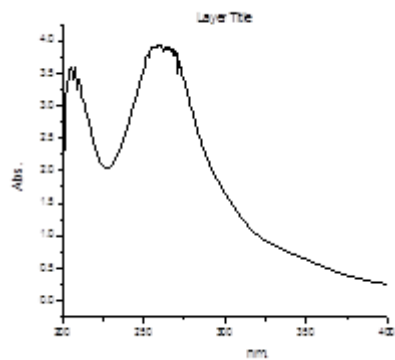


UV of Co(*p*-NO₂-babh)₂(OAc)₂·3H₂O

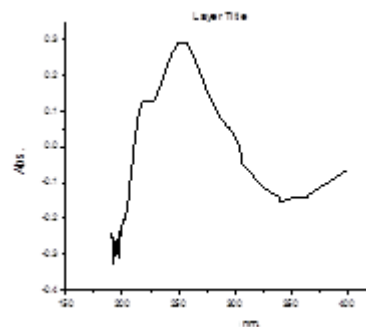


Vis of Co(*p*-NO₂-babh)₂(OAc)₂·3H₂O

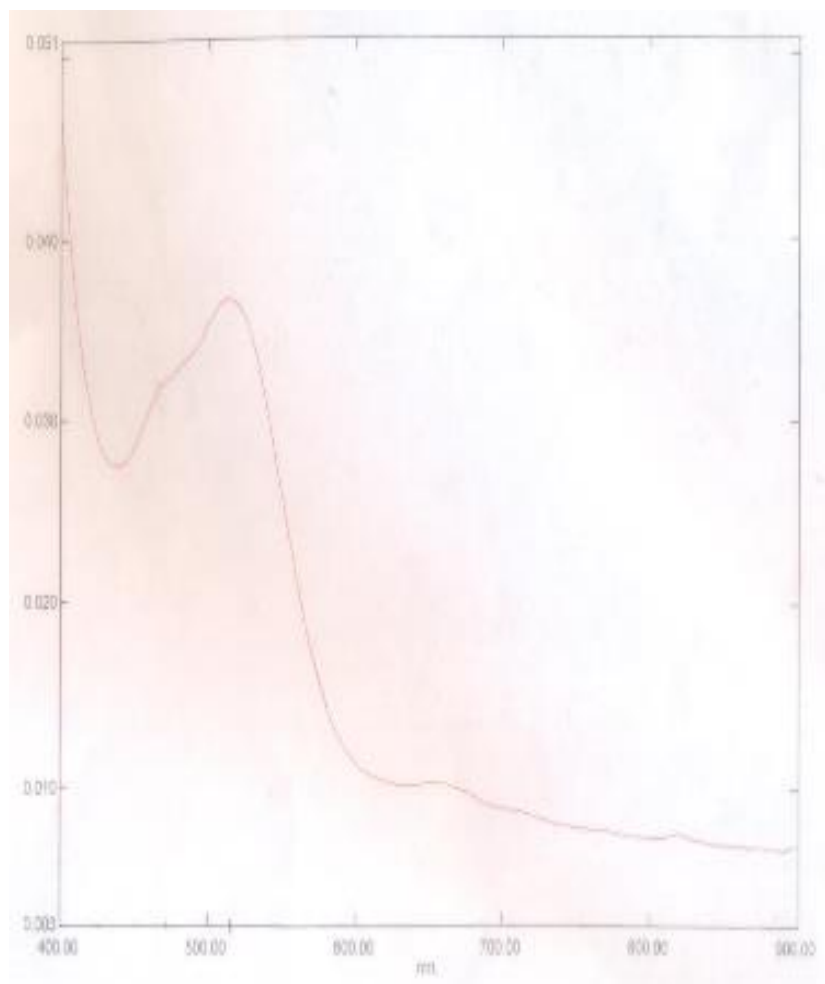
Figure 6.59: UV-Vis spectra of *p*-NO₂-babh and Co(*p*-NO₂-babh)₂(OAc)₂·3H₂O



p-NO₂-babh



UV of Co(*p*-NO₂-babh)SO₄



Vis of Co(*p*-NO₂-babh)SO₄

Figure 6.60: UV-Vis spectra of *p*-NO₂-babh and Co(*p*-NO₂-babh)SO₄

Appendix 3: ^1H NMR and ^{13}C NMR spectra of the ligands.

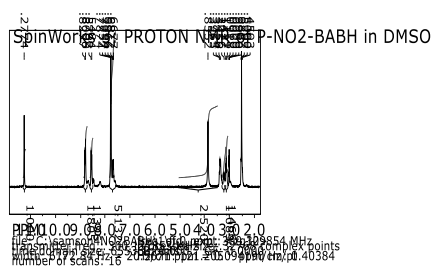


Figure 6.65. ^1H NMR of para-nitro-benzylacetone benzoylhydrazone (*p*-NO₂-babh)

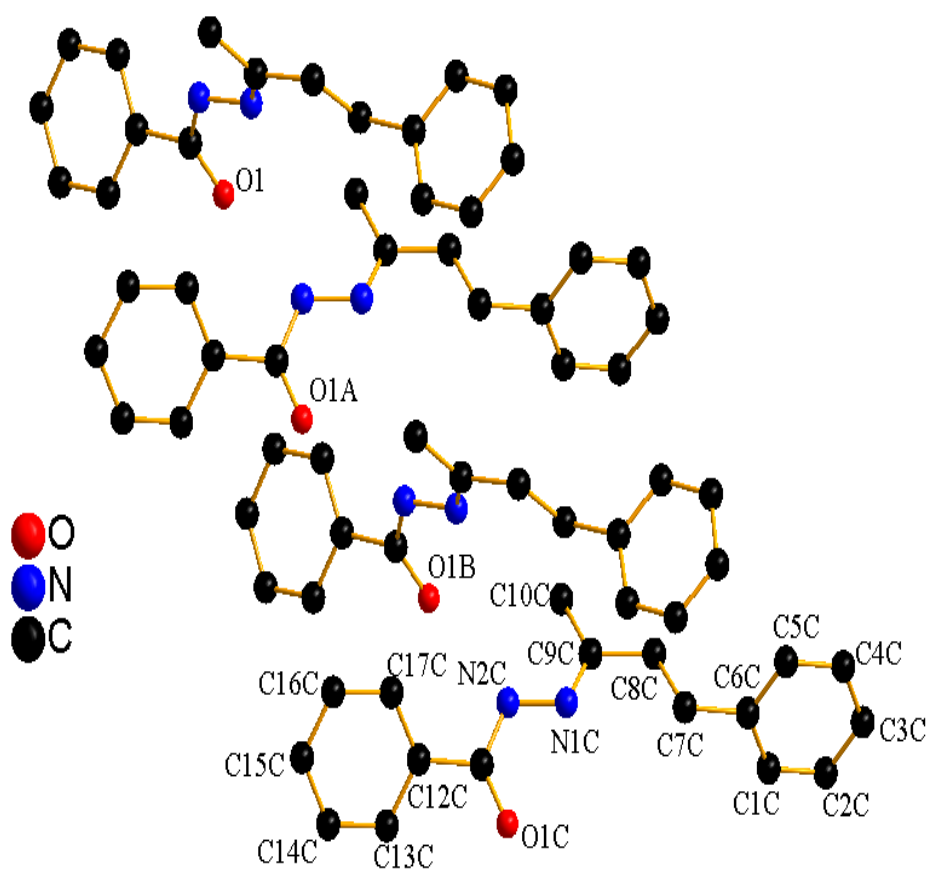


Figure 6.67. Crystal structure of benzylacetone benzoylhydrazone (babh)

Crystal data and structure refinement for babh.

Identification code	babh
Empirical formula	C ₁₇ H ₁₈ N ₂ O
Formula weight	266.34
Temperature/K	296(2)
Crystal system	triclinic
Space group	P-1
a/Å	14.103(2)
b/Å	15.298(2)
c/Å	16.325(2)
α/°	64.063(5)
β/°	77.115(6)
γ/°	76.550(6)
Volume/Å ³	3050.7(7)
Z	39
ρ _{calc} /cm ³	1.162
μ/mm ⁻¹	0.073
F(000)	1138.0
Crystal size/mm ³	0.280 × 0.170 × 0.080
Radiation	MoKα (λ = 0.71073)
2θ range for data collection/°	3.898 to 179.172
Index ranges	-19 ≤ h ≤ 19, -19 ≤ k ≤ 19, -42 ≤ l ≤ 42
Reflections collected	76863
Independent reflections	16992 [R _{int} = 0.0395, R _{sigma} = 0.0403]
Data/restraints/parameters	16992/0/721
Goodness-of-fit on F ²	11.139
Final R indexes [I ≥ 2σ (I)]	R ₁ = 0.7123, wR ₂ = 0.9226
Final R indexes [all data]	R ₁ = 0.7371, wR ₂ = 0.9333
Largest diff. peak/hole / e Å ⁻³	2.77/-2.26

Fractional Atomic Coordinates ($\times 10^4$) and Equivalent Isotropic Displacement Parameters ($\text{\AA}^2 \times 10^3$) for babh. U_{eq} is defined as 1/3 of the trace of the orthogonalised U_{IJ} tensor.

Atom	x	Y	z	U(eq)
O1	8724(15)	9228(18)	-660(10)	105(11)
O1A	7230(20)	6650(20)	1710(9)	70(8)
O1C	7025(19)	1569(16)	6833(12)	67(7)
O1B	8830(30)	4130(30)	4260(20)	112(12)
N2B	7581(19)	5670(20)	3520(20)	87(10)
N2C	7670(40)	3100(50)	6134(16)	130(20)
N1B	7160(11)	5503(13)	4373(7)	20(4)
N2	7740(30)	10380(20)	-1426(12)	132(18)
N1A	7720(20)	8040(30)	1897(12)	79(12)
N2A	7827(18)	7993(18)	879(17)	54(8)
N1C	7850(30)	3066(17)	6856(10)	78(10)
N1	7220(40)	10660(40)	-607(11)	150(20)
C12B	9040(30)	4980(40)	2600(20)	102(18)
C11C	7310(30)	2370(20)	5989(14)	65(8)
C12A	7162(19)	7510(30)	11(9)	101(14)
C9A	8358(18)	8490(19)	1940(20)	89(13)
C6B	5860(20)	5305(16)	7047(19)	85(13)
C11B	8480(50)	4760(60)	3760(50)	140(20)
C6C	7970(40)	3160(80)	9370(70)	320(60)
C12C	7320(30)	2270(30)	5277(13)	74(11)
C9B	6410(30)	5960(40)	4420(30)	96(14)
C6A	7910(30)	7850(20)	4510(11)	68(10)
C12	9060(20)	9970(18)	-2387(15)	49(8)
C17A	6820(30)	8393(18)	-601(14)	46(7)
C17B	9300(30)	5570(40)	1847(14)	80(20)
C9	6160(20)	11010(20)	-617(13)	71(11)
C11	8462(19)	9848(18)	-1473(9)	56(7)

C17C 7050(30)	3320(50)	4409(16)	150(30)
C11A 7450(30)	7250(30)	1089(10)	80(14)
C6 5820(30)	10680(50)	1914(18)	100(20)
C17 9170(30)	10930(30)	-3020(30)	81(13)
C8A 8450(60)	8570(30)	2850(30)	190(30)
C1C 8380(40)	2380(40)	9900(20)	120(20)
C16B 9730(30)	6010(40)	1170(30)	120(20)
C8 5740(40)	10860(50)	440(40)	150(30)
C9C 8360(50)	3730(60)	6890(20)	160(30)
C7C 7520(30)	3050(50)	8730(40)	100(20)
C1 5390(40)	9610(70)	2550(40)	160(30)
C8B 5890(30)	6050(20)	5358(12)	83(12)
C7B 6470(30)	5350(40)	6100(40)	115(19)
C13 9530(40)	9100(50)	-2480(30)	200(30)
C1A 8390(30)	6940(30)	5170(30)	80(14)
C5C 7570(50)	3850(30)	9720(20)	150(20)
C13C 7320(40)	1770(30)	4906(17)	104(18)
C3C 8160(30)	2970(70)	11220(30)	170(40)
C16C 6860(40)	3410(80)	3590(30)	230(50)
C8C 8210(30)	3560(30)	7880(20)	60(10)
C13A 7450(20)	6400(40)	110(30)	93(14)
C10A 8970(40)	9260(40)	1240(30)	130(20)
C2C 8690(30)	2090(50)	10881(16)	130(30)
C7A 7800(40)	7990(20)	3573(12)	111(18)
C16A 6540(80)	8390(30)	-1490(40)	240(60)
C3 4830(70)	10320(130)	3680(70)	370(100)
C10C 8950(30)	4140(30)	6080(20)	82(14)
C10B 5560(50)	6550(40)	3790(40)	120(20)
C13B 9490(30)	3990(60)	2480(30)	160(30)
C16 9860(40)	10810(30)	-3872(10)	110(19)
C15 10110(50)	10220(40)	-3910(20)	100(20)

C15C 6950(60)	2350(40)	3540(20)	110(30)
C10 5780(20)	11667(19)	-1420(20)	140(20)
C1B 5350(50)	4640(30)	7669(15)	160(30)
C7 6380(40)	10720(50)	1055(19)	160(30)
C5A 7500(30)	8220(30)	5050(20)	74(11)
C15B 10140(30)	4820(70)	1060(30)	190(40)
C2A 8870(30)	6990(30)	5740(30)	102(19)
C2B 4740(30)	4510(20)	8430(30)	94(15)
C14B 9830(20)	4138(16)	1648(11)	68(11)
C14C 7270(20)	1660(30)	4167(10)	98(16)
C5B 5690(40)	6110(60)	7250(20)	140(20)
C3A 8530(50)	7720(30)	6080(40)	130(30)
C2 4940(70)	9470(70)	3510(30)	230(50)
C15A 6973(19)	7670(30)	-1573(15)	80(17)
C5 6090(50)	11030(20)	2350(40)	110(20)
C4C 7710(18)	3518(18)	10673(9)	53(7)
C14 9880(40)	9180(70)	-3320(40)	170(30)
C14A 7170(110)	6310(60)	-740(30)	360(80)
C4A 7690(120)	8500(120)	5770(80)	380(100)
C4B 5240(40)	5860(30)	8240(30)	76(14)
C4 5440(30)	11040(50)	3160(10)	140(30)
C3B 4880(40)	5070(30)	8810(30)	150(20)

Anisotropic Displacement Parameter ($\text{\AA}^2 \times 10^3$) for babh. Anisotropic displacement factor exponent take the form: $-2\pi^2[h^2a^*U_{11}+2hka^*b^*U_{12}+\dots]$.

Atom	U_{11}	U_{22}	U_{33}	U_{23}	U_{13}	U_{12}
O1	53(11)	109(15)	25(5)	54(8)	17(6)	36(10)
O1A	120(20)	91(18)	10(4)	-29(8)	-3(7)	-32(16)
O1C	95(16)	54(12)	20(7)	16(7)	10(8)	-32(11)
O1B	100(30)	190(40)	82(19)	-90(20)	1(18)	-30(20)
N2B	35(12)	50(14)	95(19)	34(12)	-14(12)	18(11)
N2C	140(40)	240(60)	8(5)	-34(15)	-18(12)	-40(40)
N1B	18(8)	40(9)	8(3)	-15(4)	13(4)	-22(7)
N2	180(40)	66(17)	19(6)	28(8)	58(12)	50(20)
N1A	86(19)	80(20)	14(6)	-7(10)	9(9)	44(18)
N2A	38(12)	49(12)	41(12)	15(9)	-5(9)	-10(10)
N1C	170(30)	48(12)	9(4)	20(6)	-20(9)	-63(16)
N1	190(40)	170(30)	4(4)	10(9)	-24(11)	50(30)
C12B	130(30)	170(50)	52(16)	-90(30)	6(18)	-10(30)
C11C	150(30)	42(13)	16(7)	-8(8)	-16(11)	-35(15)
C12A	56(15)	140(20)	1(3)	14(7)	12(6)	70(17)
C9A	21(11)	41(13)	95(17)	64(13)	4(11)	0(10)
C6B	82(19)	21(10)	62(14)	21(9)	64(14)	9(11)
C11B	140(50)	230(70)	100(40)	-150(50)	10(40)	0(40)
C6C	120(30)	590(150)	390(120)	-400(120)	-210(60)	250(70)
C12C	80(20)	90(20)	11(6)	1(9)	32(10)	-15(19)
C9B	52(18)	130(30)	70(20)	-40(20)	-29(16)	80(20)
C6A	100(20)	62(17)	10(4)	13(7)	21(8)	-30(16)
C12	53(15)	30(12)	36(9)	23(9)	-13(10)	-21(11)
C17A	80(20)	28(11)	25(7)	-2(7)	-16(10)	-20(12)
C17B	100(40)	110(40)	18(6)	19(13)	-18(12)	-110(40)
C9	66(19)	61(16)	22(6)	37(9)	-9(9)	-1(14)
C11	63(14)	51(13)	7(3)	21(6)	1(6)	6(11)
C17C	100(30)	260(60)	18(8)	-70(20)	-34(13)	160(40)

C11A	90(30)	110(30)	3(3)	-2(8)	18(8)	-10(20)
C6	43(18)	250(60)	24(10)	-70(20)	4(11)	-30(30)
C17	100(30)	70(20)	90(20)	-69(18)	-70(20)	80(20)
C8A	330(70)	80(30)	80(20)	30(20)	70(30)	-130(40)
C1C	200(50)	190(50)	40(12)	-70(20)	90(20)	-180(40)
C16B	30(17)	140(40)	90(30)	-10(30)	49(19)	20(20)
C8	160(40)	210(60)	130(30)	-160(40)	-100(30)	150(40)
C9C	240(60)	270(70)	40(14)	-100(30)	20(20)	-100(60)
C7C	40(19)	170(50)	180(50)	-160(40)	-80(30)	60(30)
C1	40(30)	350(100)	170(50)	-190(60)	0(30)	-20(40)
C8B	130(30)	52(16)	12(5)	18(8)	21(10)	0(17)
C7B	32(18)	170(50)	240(50)	-170(40)	-40(20)	-10(20)
C13	100(30)	220(50)	79(19)	130(30)	-30(20)	-30(30)
C1A	60(20)	45(18)	70(20)	18(15)	-20(18)	38(18)
C5C	300(70)	80(20)	29(11)	39(14)	-80(20)	-50(30)
C13C	90(30)	120(30)	20(8)	24(13)	-27(14)	40(30)
C3C	70(20)	430(110)	60(18)	-150(40)	-21(17)	-10(40)
C16C	50(30)	500(130)	70(20)	-30(40)	-40(20)	-40(50)
C8C	70(20)	80(30)	56(14)	-49(19)	-41(14)	10(20)
C13A	35(15)	170(40)	100(20)	-80(30)	59(17)	-60(20)
C10A	130(40)	100(30)	100(30)	10(20)	-80(30)	70(30)
C2C	70(20)	240(70)	17(7)	-40(20)	-4(10)	70(30)
C7A	220(50)	54(16)	10(5)	-1(7)	48(14)	-10(20)
C16A	460(130)	40(20)	120(40)	-50(20)	150(60)	10(40)
C3	200(90)	800(300)	230(80)	-390(140)	-190(80)	250(130)
C10C	80(30)	150(30)	73(15)	-90(20)	72(17)	-100(30)
C10B	220(70)	120(50)	100(40)	-70(40)	-80(40)	-50(40)
C13B	70(20)	400(80)	130(30)	-220(50)	80(20)	-110(40)
C16	290(60)	46(18)	1(3)	10(6)	-21(11)	-90(30)
C15	170(60)	80(30)	26(11)	16(14)	10(20)	-70(40)
C15C	250(80)	80(30)	29(14)	-40(20)	50(30)	-80(50)

C10	90(20)	32(12)	120(20)	55(13)	99(19)	51(13)
C1B	290(60)	56(18)	11(6)	21(9)	26(16)	70(30)
C7	140(40)	190(60)	38(10)	-10(19)	72(17)	10(40)
C5A	61(18)	90(20)	34(14)	-25(16)	10(12)	42(17)
C15B	34(17)	490(120)	70(20)	-180(50)	-48(17)	110(40)
C2A	100(30)	70(20)	90(30)	60(20)	-80(20)	-60(20)
C2B	110(30)	47(17)	150(30)	-41(19)	-120(30)	52(18)
C14B	90(20)	23(10)	19(5)	17(6)	38(9)	22(11)
C14C	73(16)	140(30)	4(3)	-17(8)	-4(6)	92(19)
C5B	110(30)	250(70)	43(14)	-70(30)	60(20)	-30(40)
C3A	120(50)	46(19)	130(40)	20(20)	50(30)	-20(20)
C2	280(100)	230(100)	60(20)	40(40)	90(40)	-120(90)
C15A	27(12)	100(30)	30(9)	52(15)	-4(8)	-29(15)
C5	210(70)	6(13)	130(40)	-21(17)	-60(50)	-10(20)
C4C	52(13)	57(12)	8(4)	23(6)	1(5)	-7(10)
C14	120(40)	400(110)	100(30)	-170(50)	-20(30)	-70(50)
C14A	800(200)	260(70)	60(30)	60(30)	-60(60)	-400(120)
C4A	600(200)	500(200)	270(130)	-270(150)	120(130)	-400(190)
C4B	120(40)	39(19)	100(30)	-60(20)	-60(30)	30(20)
C4	110(30)	270(70)	0(3)	16(12)	-3(8)	-130(40)
C3B	210(40)	70(20)	120(30)	-50(20)	160(30)	-80(30)

Bond Lengths for babh.**Atom Atom Length/Å**

O1 C11 1.323(19)
O1A C11A 1.07(3)
O1C C11C 1.44(3)
O1B C11B 1.06(7)
N2B N1B 1.33(4)
N2B C11B 1.62(7)
N2C N1C 1.24(3)
N2C C11C 1.45(7)
N1B C9B 1.13(3)
N2 N1 1.55(4)
N2 C11 1.16(4)
N1A N2A 1.67(4)
N1A C9A 1.28(6)
N2A C11A 1.24(5)
N1C C9C 1.40(8)
N1 C9 1.47(6)
C12B C11B 1.79(6)
C12B C17B 1.21(5)
C12B C13B 1.57(8)
C11C C12C 1.23(4)
C12A C17A 1.34(3)
C12A C11A 1.75(4)
C12A C13A 1.59(6)
C9A C8A 1.58(8)
C9A C10A 1.52(7)
C6B C7B 1.58(6)
C6B C1B 1.30(5)
C6B C5B 1.37(8)
C6C C1C 1.22(10)

Atom Atom Length/Å

C17B C16B 1.13(4)
C9 C8 1.62(5)
C9 C10 1.39(4)
C17C C16C 1.36(6)
C6 C1 1.68(10)
C6 C7 1.43(3)
C6 C5 1.22(6)
C17 C16 1.58(5)
C8A C7A 1.41(5)
C1C C2C 1.60(5)
C16B C15B 1.85(10)
C8 C7 1.42(8)
C9C C8C 1.50(3)
C9C C10C 1.36(6)
C7C C8C 1.51(8)
C1 C2 1.49(8)
C8B C7B 1.48(6)
C13 C14 1.32(7)
C1A C2A 1.29(6)
C5C C4C 1.45(3)
C13C C14C 1.30(5)
C3C C2C 1.63(9)
C3C C4C 1.12(6)
C16C C15C 1.63(12)
C13A C14A 1.61(7)
C16A C15A 1.18(6)
C3 C2 1.41(17)
C3 C4 1.41(19)
C13B C14B 1.27(4)

C6C C7C 1.43(7)

C6C C5C 1.37(9)

C12C C17C 1.64(5)

C12C C13C 1.17(6)

C9B C8B 1.60(5)

C9B C10B 1.59(6)

C6A C1A 1.45(4)

C6A C7A 1.49(4)

C6A C5A 1.23(4)

C12 C11 1.50(3)

C12 C17 1.40(5)

C12 C13 1.40(9)

C17A C16A 1.59(10)

C16 C15 0.92(7)

C15 C14 1.52(10)

C15C C14C 1.18(7)

C1B C2B 1.30(6)

C5A C4A 1.50(8)

C15B C14B 1.17(10)

C2A C3A 1.40(8)

C2B C3B 1.33(6)

C5B C4B 1.50(5)

C3A C4A 1.5(2)

C15A C14A 1.92(8)

C5 C4 1.44(8)

C4B C3B 1.29(6)

Bond Angles for babh.**Atom Atom Atom Angle/°**

C11B N2B N1B 97(3)
C11C N2C N1C 129(4)
C9B N1B N2B 113(3)
C11 N2 N1 129(3)
C9A N1A N2A 113(2)
C11AN2A N1A 102(2)
C9C N1C N2C 124(3)
C9 N1 N2 114(4)
C17B C12B C11B 147(6)
C17B C12B C13B 101(4)
C13B C12B C11B 112(5)
O1C C11C N2C 113(2)
O1C C11C C12C 116(3)
N2C C11C C12C 131(3)
C17A C12A C11A 126(3)
C17A C12A C13A 139(3)
C13A C12A C11A 95(2)
N1A C9A C8A 123(3)
N1A C9A C10A 135(4)
C10A C9A C8A 100(4)
C1B C6B C7B 130(4)
C1B C6B C5B 110(3)
C5B C6B C7B 120(3)
O1B C11B N2B 149(5)
O1B C11B C12B 114(5)
N2B C11B C12B 98(5)
C1C C6C C7C 113(8)
C1C C6C C5C 116(6)
C5C C6C C7C 122(4)

Atom Atom Atom Angle/°

N2A C11A C12A 99(2)
C1 C6 C7 113(5)
C5 C6 C1 115(4)
C5 C6 C7 119(6)
C12 C17 C16 104(2)
C9A C8A C7A 108(5)
C6C C1C C2C 131(5)
C15B C16B C17B 86(5)
C9 C8 C7 121(5)
N1C C9C C8C 105(5)
N1C C9C C10C 112(3)
C10C C9C C8C 141(6)
C8C C7C C6C 96(6)
C2 C1 C6 115(6)
C7B C8B C9B 109(3)
C8B C7B C6B 108(3)
C12 C13 C14 116(5)
C2A C1A C6A 119(4)
C6C C5C C4C 113(5)
C14C C13C C12C 150(4)
C2C C3C C4C 107(3)
C15C C16C C17C 113(6)
C9C C8C C7C 135(4)
C14A C13A C12A 110(5)
C3C C2C C1C 107(4)
C6A C7A C8A 115(5)
C15A C16A C17A 108(7)
C2 C3 C4 121(7)
C14B C13B C12B 112(6)

C17C C12C C11C 113(4)
C17C C12C C13C 96(3)
C13C C12C C11C 150(3)
N1B C9B C8B 121(3)
N1B C9B C10B 139(4)
C10B C9B C8B 100(3)
C1A C6A C7A 124(3)
C1A C6A C5A 97(3)
C5A C6A C7A 136(4)
C17 C12 C11 117(3)
C13 C12 C11 115.7(19)
C13 C12 C17 127(3)
C12AC17AC16A 115(3)
C12B C17B C16B 165(7)
N1 C9 C8 104(2)
N1 C9 C10 121.9(19)
C10 C9 C8 129(3)
O1 C11 N2 113(2)
O1 C11 C12 126(2)
N2 C11 C12 120.2(16)
C12C C17C C16C 125(7)
O1A C11AN2A 137(4)
O1A C11AC12A 124(4)

C15 C16 C17 125(3)
C16 C15 C14 132(5)
C16CC15CC14C 115(4)
C6B C1B C2B 139(5)
C6 C7 C8 110(4)
C6A C5A C4A 143(8)
C14B C15B C16B 117(2)
C3A C2A C1A 120(5)
C3B C2B C1B 110(5)
C15B C14B C13B 129(5)
C15C C14C C13C 119(4)
C6B C5B C4B 111(5)
C2A C3A C4A 122(7)
C3 C2 C1 114(8)
C16AC15AC14A 134(5)
C6 C5 C4 116(6)
C3C C4C C5C 144(4)
C15 C14 C13 110(6)
C15AC14AC13A 100(4)
C3A C4A C5A 98(9)
C3B C4B C5B 128(4)
C3 C4 C5 122(6)
C2B C3B C4B 115(4)

Hydrogen Atom Coordinates ($\text{\AA}\times 10^4$) and Isotropic Displacement Parameters ($\text{\AA}^2\times 10^3$) for babh

Atom	<i>x</i>	<i>Y</i>	<i>z</i>	U(eq)
H2B	7475	5989	3045	61
H2C	7954	3495	5547	59
H2	7481	10967	-1955	63
H2AA	7982	8475	543	64
H17A	6723	8883	-447	72
H17B	8988	6416	2027	78
H17C	6778	3883	4524	71
H17	9001	11408	-2945	65
H8AA	8263	9231	2759	79
H8AB	9060	8288	2982	79
H1C	8820	1628	9813	80
H16B	9986	6461	676	92
H8A	5239	10767	498	83
H8B	5656	11722	268	83
H7CA	7731	2350	8645	83
H7CB	7027	3341	8532	83
H1	5379	9157	2377	87
H8BA	5676	6719	5281	78
H8BB	5246	5773	5504	78
H7BA	7005	5799	6001	89
H7BB	6678	4824	6147	89
H13	9279	8490	-2036	87
H1A	8777	6615	4829	82
H5C	7041	4134	9560	95
H13C	7614	980	5441	85
H3C	8511	2659	11717	108
H16C	6541	3924	3150	91
H8CA	8283	4228	7757	77

H8CB 9061	3272	7974	77
H13A 7603	5964	438	86
H10D 8653	9637	661	111
H10E 9488	8722	865	111
H10F 9397	9452	1326	111
H2CA 9178	1480	11173	108
H7AA 7023	8315	3537	80
H7AB 7745	7332	3649	80
H16A 6533	8944	-1846	98
H3 4469	10148	4325	125
H10G 8679	4688	5700	115
H10H 9426	3719	5824	115
H10I 9481	4347	6351	115
H10J 5983	7271	3289	119
H10K 5076	6740	3865	119
H10L 5862	6301	3243	119
H13B 9258	3493	2964	83
H16 9984	11464	-4316	91
H15 10579	10058	-4536	103
H15C 6887	2510	2914	104
H10A 6197	12038	-1885	109
H10B 5226	12063	-1200	109
H10C 5539	11214	-1543	109
H1B 5386	4167	7362	89
H7A 6685	9832	1155	91
H7B 6995	10815	1005	91
H5A 7035	9121	4569	93
H15B 10592	5026	481	106
H2AB 9210	6481	6142	92
H2BA 4485	4029	8739	106
H14B 10230	3554	1608	107

H14C 7435	1040	4043	106
H5B 6158	6632	7035	104
H3A 8518	7633	6722	104
H2A 4479	9044	3752	116
H15A 6909	7542	-2112	106
H5 6170	11625	2041	109
H4C 7427	3977	10920	110
H14 10224	8566	-3408	108
H14A 7422	6067	-978	115
H4A 7445	8972	5932	114
H4B 5261	6475	8455	128
H4 5272	11471	3450	136
H3B 4483	5126	9324	115

Crystal structure determination of **babh**

Crystal Data for $C_{17}H_{18}N_2O$ ($M = 266.34$ g/mol): triclinic, space group P-1 (no. 2), $a = 14.103(2)$ Å, $b = 15.298(2)$ Å, $c = 16.325(2)$ Å, $\alpha = 64.063(5)^\circ$, $\beta = 77.115(6)^\circ$, $\gamma = 76.550(6)^\circ$, $V = 3050.7(7)$ Å³, $Z = 39$, $T = 296(2)$ K, $\mu(\text{MoK}\alpha) = 0.073$ mm⁻¹, $D_{\text{calc}} = 1.162$ g/cm³, 76863 reflections measured ($3.898^\circ \leq 2\Theta \leq 179.172^\circ$), 16992 unique ($R_{\text{int}} = 0.0395$, $R_{\text{sigma}} = 0.0403$) which were used in all calculations. The final R_1 was 0.7123 ($I > 2\sigma(I)$) and wR_2 was 0.9333 (all data).

Refinement model description

Number of restraints - 0, number of constraints - unknown.

Details:

1. Others

Fixed Uiso: H2B(0.061) H2C(0.059) H2(0.063) H2AA(0.064) H17A(0.072)
H17B(0.078) H17C(0.071) H17(0.065) H8AA(0.079) H8AB(0.079) H1C(0.08)
H16B(0.092) H8A(0.083) H8B(0.083) H7CA(0.083) H7CB(0.083) H1(0.087)
H8BA(0.078) H8BB(0.078) H7BA(0.089) H7BB(0.089) H13(0.087) H1A(0.082)
H5C(0.095) H13C(0.085) H3C(0.108) H16C(0.091) H8CA(0.077) H8CB(0.077)
H13A(0.086) H10D(0.111) H10E(0.111) H10F(0.111) H2CA(0.108) H7AA(0.08)
H7AB(0.08) H16A(0.098) H3(0.125) H10G(0.115) H10H(0.115) H10I(0.115)
H10J(0.119) H10K(0.119) H10L(0.119) H13B(0.083) H16(0.091) H15(0.103)
H15C(0.104) H10A(0.109) H10B(0.109) H10C(0.109) H1B(0.089) H7A(0.091)
H7B(0.091) H5A(0.093) H15B(0.106) H2AB(0.092) H2BA(0.106) H14B(0.107)
H14C(0.106) H5B(0.104) H3A(0.104) H2A(0.116) H15A(0.106) H5(0.109)
H4C(0.11)

H14(0.108) H14A(0.115) H4A(0.114) H4B(0.128) H4(0.136) H3B(0.115)

Fixed X: H2B(0.747499) H2C(0.7954) H2(0.7481) H2AA(0.798201) H17A(0.6723)
H17B(0.898801) H17C(0.6778) H17(0.9001) H8AA(0.826301) H8AB(0.905999)
H1C(0.882) H16B(0.9986) H8A(0.523901) H8B(0.5656) H7CA(0.7731)
H7CB(0.7027)

H1(0.5379) H8BA(0.5676) H8BB(0.5246) H7BA(0.7005) H7BB(0.667801)
H13(0.9279)

H1A(0.8777) H5C(0.7041) H13C(0.7614) H3C(0.851101) H16C(0.6541)
H8CA(0.828301)

H8CB(0.906099) H13A(0.760301) H10D(0.865301) H10E(0.9488) H10F(0.939699)
H2CA(0.9178) H7AA(0.7023) H7AB(0.774499) H16A(0.653301) H3(0.446899)
H10G(0.867901) H10H(0.942599) H10I(0.9481) H10J(0.598301) H10K(0.5076)
H10L(0.5862) H13B(0.9258) H16(0.9984) H15(1.0579) H15C(0.688701)
H10A(0.6197)
H10B(0.5226) H10C(0.553901) H1B(0.5386) H7A(0.668501) H7B(0.6995)
H5A(0.7035)
H15B(1.0592) H2AB(0.921) H2BA(0.4485) H14B(1.023001) H14C(0.7435)
H5B(0.615801) H3A(0.851801) H2A(0.4479) H15A(0.690901) H5(0.617001)
H4C(0.7427) H14(1.0224) H14A(0.7422) H4A(0.744499) H4B(0.5261) H4(0.527201)
H3B(0.4483)
Fixed Y: H2B(0.598901) H2C(0.3495) H2(1.0967) H2AA(0.8475) H17A(0.888301)
H17B(0.641601) H17C(0.388301) H17(1.1408) H8AA(0.9231) H8AB(0.828801)
H1C(0.162801) H16B(0.6461) H8A(1.076699) H8B(1.1722) H7CA(0.235)
H7CB(0.3341)
H1(0.9157) H8BA(0.671901) H8BB(0.5773) H7BA(0.5799) H7BB(0.482399)
H13(0.849)
H1A(0.661501) H5C(0.4134) H13C(0.098001) H3C(0.265901) H16C(0.3924)
H8CA(0.4228) H8CB(0.327201) H13A(0.596399) H10D(0.9637) H10E(0.8722)
H10F(0.9452) H2CA(0.148001) H7AA(0.8315) H7AB(0.7332) H16A(0.8944)
H3(1.0148)
H10G(0.468801) H10H(0.371901) H10I(0.434699) H10J(0.7271) H10K(0.674)
H10L(0.6301) H13B(0.3493) H16(1.146399) H15(1.0058) H15C(0.251)
H10A(1.2038)
H10B(1.2063) H10C(1.121401) H1B(0.416699) H7A(0.9832) H7B(1.0815)
H5A(0.9121)
H15B(0.5026) H2AB(0.648101) H2BA(0.4029) H14B(0.3554) H14C(0.104)
H5B(0.663201) H3A(0.763301) H2A(0.904399) H15A(0.7542) H5(1.1625)
H4C(0.3977) H14(0.8566) H14A(0.6067) H4A(0.897201) H4B(0.6475) H4(1.1471)
H3B(0.5126)
Fixed Z: H2B(0.3045) H2C(0.5547) H2(-0.1955) H2AA(0.0543) H17A(-0.0447)
H17B(0.2027) H17C(0.452399) H17(-0.2945) H8AA(0.2759) H8AB(0.298201)
H1C(0.9813) H16B(0.0676) H8A(0.0498) H8B(0.0268) H7CA(0.8645)

H7CB(0.853201)

H1(0.2377) H8BA(0.528101) H8BB(0.5504) H7BA(0.600101) H7BB(0.6147) H13(-
0.203601) H1A(0.4829) H5C(0.955999) H13C(0.5441) H3C(1.1717)
H16C(0.315001)

H8CA(0.7757) H8CB(0.7974) H13A(0.0438) H10D(0.0661) H10E(0.086499)
H10F(0.1326) H2CA(1.117301) H7AA(0.353701) H7AB(0.364901) H16A(-0.1846)
H3(0.432499) H10G(0.57) H10H(0.582399) H10I(0.6351) H10J(0.328901)
H10K(0.386499) H10L(0.324301) H13B(0.296399) H16(-0.4316) H15(-0.453601)
H15C(0.2914) H10A(-0.188499) H10B(-0.12) H10C(-0.1543) H1B(0.736199)
H7A(0.1155) H7B(0.1005) H5A(0.4569) H15B(0.0481) H2AB(0.614201)
H2BA(0.8739)

H14B(0.160801) H14C(0.4043) H5B(0.7035) H3A(0.6722) H2A(0.3752) H15A(-
0.2112)

H5(0.2041) H4C(1.092) H14(-0.340799) H14A(-0.0978) H4A(0.593201)
H4B(0.8455)

H4(0.345) H3B(0.932399)

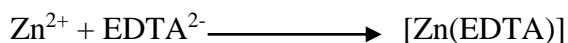
Appendix 5. Determination of Percentage Metals by Complexometric Titration,

Table 6.1 Titration of 0.01 M zinc sulphate solution against EDTA solution

Burette Readings	1	2	3
Final reading (ml)	20.80	25.80	27.80
Initial reading (ml)	0.00	5.00	7.00
Volume used(ml)	20.80	20.80	20.80

$$\text{Average titre volume (ml)} = \left\{ \frac{20.80 + 20.80 + 20.80}{3} \right\} \text{ml} = 20.80 \text{ ml}$$

Equation for the reaction,



Molarity of Zn^{2+} ($M_{\text{Zn}^{2+}}$) = 0.005M

Molarity of EDTA = ?

Volume of Zn^{2+} ($V_{\text{Zn}^{2+}}$) = 20.00 ml

Volume of EDTA (V_{EDTA}) = 20.80 ml

$$\left\{ \frac{M_{\text{Zn}^{2+}} \times V_{\text{Zn}^{2+}}}{M_{\text{EDTA}} \times V_{\text{EDTA}}} \right\} = \frac{1}{1}$$

$$M_{\text{EDTA}} = \left\{ \frac{M_{\text{Zn}^{2+}} \times V_{\text{Zn}^{2+}}}{V_{\text{EDTA}}} \right\}$$

$$M_{\text{EDTA}} = \frac{(0.005 \times 20.00)}{20.80} = 0.0048 \text{ M}$$

Molarity of EDTA = 0.0048 M

Percentage metal determination

The percentage nickel(II) in $\text{Ni}(\text{p-NO}_2\text{ babb})_2(\text{OAc})_2$ was determined as follows:

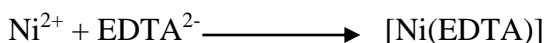
$$\text{Weight of sample} = 0.0228\text{g}$$

Table 6.2 Titration of digested metal complex solution of using EDTA solution

Burette reading	1	2	3
Final reading (ml)	16.20	17.40	18.60
Initial reading (ml)	15.00	16.20	17.40
Volume used	1.20	1.20	1.20

Average volume of EDTA used = 1.20ml

Equation for reaction



Mole ratio of reactants is:



Molarity of EDTA solution (M_{EDTA}) = 0.0048 M

Volume of EDTA solution (V_{EDTA}) = 1.20 ml

Since number of moles of Ni^{2+} = number of moles of EDTA^{2-}

$$\text{Number of moles} = \frac{(M_{\text{EDTA}} \times V_{\text{EDTA}})}{1000}$$

$$\text{Therefore, number of moles of Ni}^{2+} \text{ in 20 ml solution titrated} = \frac{(0.0048 \times 1.20)}{1000}$$

$$= 5.76 \times 10^{-6} \text{mol}$$

Then, number of moles of Ni^{2+} in 100ml standard solution of digest

$$= \frac{5.76 \times 10^{-6} \times 100\text{ml}}{20\text{ml}}$$

$$= 2.88 \times 10^{-5} \text{mole}$$

Weight of Ni²⁺ in 100ml digested solution = Moles in 100 ml solution x Atomic mass of Ni

$$= 2.88 \times 10^{-5} \text{ mol} \times 58.69 \text{ g mol}^{-1}$$

$$= 1.69 \times 10^{-3} \text{ g}$$

$$\% \text{ Ni in complex} = \frac{\text{Weight of Ni}^{2+} \text{ in solution}}{\text{Weight of Ni complex digested}} \times 100$$

$$= \frac{1.69 \times 10^{-3} \text{ g} \times 100 \%}{0.0228 \text{ g}}$$

$$= 7.41\%$$

The same steps were taken to determine the percentage metal content of other complexes. The values obtained were then compared with the values calculated for 1:3, 1:2 and 1:1 metal to ligand complexes.

REFERENCES

- Adekunle, F. A., Woods, J. A. O., Onawumi, O. O. E and Odunola, A. 2010. Synthesis, Characterization and Structural Studies of Nickel(II) complexes of some New Substituted Acid hydrazides. *Synthesis and Reactivity in Inorganic, Metal-organic and Nano-metal Chemistry* 40.6: 430 - 437.
- Agarwal, R. K., Sharma, D., Singh, L and Agarwal, H. 2006. Synthesis, Biological Spectral, and Thermal Investigations of Cobalt(II) and Nickel(II) Complexes of N-Isonicotinamido-2', 4' - Dichlorobenzalaldimine. *Bioinorganic Chemistry and Applications* Article ID 29234: 1 – 9.
- Ainscough, E. W., Brodie, A. M., Dobbs, A. J., Ranford, J. D., Water, J. M. 1998. Antitumor Copper(II) Salicyladehyde benzoylhydrazone (H₂Sb) complexes. *Inorganica Chimica Acta* 267: 27 - 38.
- Ajani, O. A., Iyaye, King. T., Audu, O. Y., Olorunshola, S. J., Alice, O., and Olanrewaju, I. O. 2018. Microwave Assisted Synthesis and Antimicrobial potential of 2-quinoline-based 4hydrazide-hydrazone derivatives. *Journal of Heterocyclic Chemistry* 55: 302-312.
- Alhadi, A. A., Shaker, S. A., Yehye, W. A., Ali, H. M and Abdullah, A. M. 2012. Synthesis, Magnetic and Spectroscopic studies of Ni(II), Cu(II), Zn(II) and Cd(II) complexes of a newly Schiff base derived from 5-bromo-2-hydroxyl Benzylidene-3,4,5-trihydroxybenzohydrazone. *Bulletin of the Chemical Society of Ethiopia* 26.1: 95 - 101.
- Al-Shaalan. N. H. 2011. Synthesis, Characterization and Biological Activities of Cu(II), Co(II), and Mn(II), Fe(II), UO₂(VI) Complexes with a New Schiff Base Hydrazone: *O*-Hydroxyacetophenone-7-chloro-4-quinolineHydrazone *Molecules* 16: 8629 - 8645.
- Anacona, J. R and Maria, R. 2015. Tridentate hydrazone metal complexes derived from cephalixin and 2-hydrazinopyridine: Synthesis, characterization and antibacterial activity. *Spectrochimica Acta Part A: Molecular and Biomolecular Spectroscopy* 141: 169 – 175.

- Ang, M. T. C., Gumbau-Brisa, R., Allan, D. S., McDonald, R., Ferguson, M. J., Holben, B. E and Bierenstiel, M. 2018. DIBI, a 3-hydroxypyridin-4-one chelator iron-binding polymer with enhanced antimicrobial activity. *Medicinal Chemistry Communication* 9: 1206-1212.
- Baliga, R. S and Revankar, V. K. 2006. Coordination diversity of new mononucleating hydrazone in 3d metal complexes. Synthesis, Characterization and Structural Studies. *Journal of Serbia Chemical Society* 71.12: 1301 - 1310.
- Bertrand, J. A., Kelley, J. A. and Breece, J. L. 1970. Sub-normal magnetic moments in copper(II) complexes: Five-coordinate copper in an oxygen-bridged dimer. *Inorganica Chimica Acta* 4: 247 - 250.
- Brune, K. 1997. The early history of non-opioid analgesics. *Acute Pain* 1.1: 33 - 40.
- Buu-Hoi, N. P., Xuong, N. D., Nam, N. H., Binon, F and Royer, R. 1953. Tuberculostatic hydrazides and their derivatives. *Journal of Chemical Society* 0: 1358 - 1364.
- Cao, W., Liu Y., Zhang, T., Jia, J. 2018. Synthesis, characterisation, theoretical and antimicrobial studies of tridentate hydrazone metal complexes of Zn(II), Cd(II), Cu(II) and Co(III). *Polyhedron* 147: 62 - 68.
- Chen, L., Hou, J., Sun, W. 2003. Ethylene oligomerisation by hydrazone Ni(II) complexes/MAO. *Applied Catalysis A: General* 246: 11 - 16
- Chen, Z., Wua, Y., He, C., Wang, B., Gu, D., Gan, F. 2010. Insights into the physical basis of metal(II) hydrazone complexes with isoxazole and barbituric acid moieties for recordable Blu-ray media. *Synthetic Metals* 160: 2581 - 2586.
- Chitrapriya, N., Mahalingam, V., Zeller, M., Natarajan, K. 2008. Synthesis, characterization and crystal structures of cyclometallated Ru(II) carbonyl complexes formed by hydrazones. *Polyhedron* 27: 1573 - 1580
- Christie, R. J., Anderson, D. J and Grainger, D. W. 2010. Comparison of Hydrazone Heterobifunctional Crosslinking Agents for Reversible Conjugation of Thiol Containing Chemistry. *Bioconjugation Chemistry* 21.10: 1779 - 1787.

- Cotton, F. A., Wilkinson, G., Murillo, C. A., Bochmann, M. 2003. *Advanced Inorganic Chemistry*, 6th Ed. New York. John Wiley and Sons Inc. 814 – 824.
- Debnath, D., Roy, S., Li, B-H., Lin, C-H., Misra, T. K. 2015. Synthesis, structure and study of azo-hydrazone tautomeric equilibrium of 1, 3-dimethyl-5-(arylo)-6-amino-uracil derivatives. *Spectrochimica Acta Part A: Molecular and Biomolecular Spectroscopy* 140: 185–197
- Deepa, K. P and Aravindakshan, K. K. 2005. Synthesis, Characterization and Antifungal Studies of Metal Complexes of Benzoyl- and Salicylhydrazones of ω -Bromoacetanilide. *Synthesis and Reactivity in Inorganic, Metal- Organic and Nano-Metal Chemistry* 35.5: 409 - 416.
- Dell'erba, C., Novi, M., Petrillo, G., Tavani, C. 1996. Electrophilic α -p-tolylhydrazonylation of tert-butyl-p-tolylazosulphide. *Tetrahedron* 52: 5889 - 5898
- Devi, O. S and Singh A. M. 2011. Synthesis and Characterisation of Cobalt(II) Complexes with Benzil Isonicotinoyl Hydrazone. *Journal of Chemical and Pharmaceutical Research* 3.6: 1055 - 1060.
- Diouf, O., Gaye, M., Sall, D. G., Sall, A. S., Pontillon, Y and Caneschi, A. 2006. Copper(II) complexes of o-Vanillin acetylhydrazone (H₂L) and the single-crystal X-ray structure of [(Cu(HL)(H₂O)(HPZ)]NO₃. *Bulletin of the chemical Society of Ethiopia* 20.1: 35 - 43.
- Domiano, P., Musatti, A., Nardelli, M and Pelizzi, C. 1975. Crystal structure and chemical properties of bis(N-picolinylidene-N' salicyloylhydrazinato)nickel (II). *Journal of Chemical Society Dalton Trans* 4: 295 - 298.
- Dutta, R. L and Syamal. 1993. *Elements of Magnetochemistry*. 2nd Edition. New Delhi Affiliated East-West Press. 206 – 253.
- Earnshaw, A and Greenwood, N. N. 1984. *Chemistry of the elements* 1st Edition. Oxford. Pergamon. 1321 - 1386.

- Eflhymiou, C. G., Kito, A. A., Raptopoular, C. P., Perlepes, S. P., Escuer, A and Papatriantafyllopoulos, C. 2009. Employment of the sulphate ligand in 3d metal cluster chemistry: A novel hexanuclear nickel(II) complex with a chair metal topology. *Polyhedron* 28: 3177 - 3184.
- El-Sherif, A. A. 2009. Synthesis, spectroscopic characterisation and biological activity on newly synthesised copper(II) and nickel(II) complexes incorporating bidentate oxygen-nitrogen hydrazine Ligands. *Inorganica Chimica Acta* 362.14: 4991 – 5000.
- European Committee for Antimicrobial Susceptibility Testing (EUCAST) 2000. Determination of minimum inhibitory concentrations (MIC's) of antibacterial agents by agar dilution. *Clinical Microbiology and Infection* 6.9: 509 - 515.
- Fischer, E. 1875. Ueber Aromatische Hydrazinverbindungen. (On aromatic hydrazine compounds). *Berichte der deutschen chemischen Gesellschaft* 8: 589 – 594.
- Geary, 1971. The use of conductivity measurements in organic solvents for the Characterization of coordination compounds, *Coordination Chemistry Review* 7: 81 - 90.
- Gup, R., Gokce, C., Akturk, S. 2015. Copper(II) complexes with 4-hydroxyacetophenone-derived acylhydrazones: Synthesis, characterization, DNA binding and cleavage properties. *Spectrochimica Acta Part A: Molecular and Biomolecular Spectroscopy* 134: 484–492
- Gupta, L. K., Bansal, U and Chandra, S. 2007. Spectroscopic and physicochemical studies on nickel(II) complexes of isatin-3, 2-quinolyl-hydrazones and their adducts. *Spectrochimica Acta Part A: Molecular and Biomolecular Spectroscopy* 66: 972–975
- Halli, M. B and Malipatil, R. S. 2011. Synthesis, characterisation and spectral studies of metal(II) complexes derived from benzofuran-2-carbohydrazide and 2-acetylthiophene Schiff's base. *Scholar Research Library. Der Pharma Chemica* 3.4: 146 - 157

- Hosny, M. M., Mahmoud, M. A and Aly, R. E. M. 2010. 2-hydroxybenzaldehyde-(4, 6-dimethylquinolin-2-yl)-hydrazone (HBDH). Synthesis, characterization and ligational behaviour towards some metals. *Synthesis and Reactivity in Inorganic, Metal-Organic and Nano-Metal Chemistry* 40: 439 – 446.
- Howlader, M. B. H., Tarafder, M. T. H and Islam, M. A. A. A. 2009. Palladium(II) Complexes of hydrazones derived from 4-dodecyloxybenzoylhydrazine with some aliphatic and aromatic aldehydes and their mesogenic behaviour *Indian Journal of chemistry* 48A: 1078-1084.
- Housecroft, C. E. and Sharpe, A. G. 2008. *Inorganic Chemistry*. 3rd edition, England, Pearson prentice Hall. 637 – 640.
- Huang, L., Cheng, J., Xie, K., Xi, P., Hou, F., Li, Z., Xie, G., Shi, Y., Liu, H., Bai, D and Zeng, Z. 2011. Cu²⁺ selective fluorescent chemosensor based on coumarin and its application in bioimaging. *Dalton Transactions* 40: 10815 - 10817
- Hueso-Urena, F., Illan-Cabeza, N. A., Moreno-Carretero, M. N., Penas-Chamorro, A. L and Faure, F. 2000. Ni(II) and Co(II) complexes with the dianionic N, N,O-tridentate Schiff base 6-amino-5-formyl-1,3-dimethyluracil-benzoylhydrazone. Crystal structure of the monodimensionally hydrogen-bonded aqua-(6-amino-1, 3-dimethyl-uracilato-benzoylhydrazone (2-)-N-6,N-51,O-52)-copper(II)hydrate *Polyhedron* 19: 689 - 693.
- Jing-lin, W., Ya-qin, Z., Bin-sheng, Y. 2014. Transition metal complexes of asymmetrical aroyl-hydrazone ligand: Syntheses, structures, DNA binding and cleavage studies. *Inorganica Chimica Acta* 409: 484 – 496
- Jorgensen, C. K. 1954. Studies of absorption spectra III: Absorption Bands as Gaussian Error Curves. *Acta Chemica Scandinavica* 8.9: 1495-1501.
- Kim, S., Yoon, J-Y. 2004. Hydrazones in Science and Synthesis. *Science of Synthesis* 27: 671 - 722.

- Knittl, E. T., Abou-Hussein, A. A., Linert, W. 2018. Syntheses, characterisation and biological activity of novel mono and binuclear transition metal complexes with a hydrazone Schiff base derived from a coumarin derivative and oxalyldihydrazine. *Monatshefte fur Chemie* 149: 431 – 443.
- Lakshmi, B., Avaji, P. G., Shivananda, K. N., Nagella, P., Manohar, S. H., Mahendra, K. N. 2011. Synthesis, spectral characterization and *in vitro* microbiological evaluation of novel glyoxal, biacetyl and benzil bis-hydrazone macrocyclic Schiff bases and their Co(II), Ni(II) and Cu(II) complexes. *Polyhedron* 30: 1507 – 1515.
- Mohanan, K and Murakan, B. 2005. Complexes of Manganese(II), Iron(II), Cobalt(II), Nickel(II), Copper(II), Zinc(II) with a bishydrazone. *Synthesis and Reactivity in Inorganic, Metal-Organic and Nano-Metal Chemistry* 35: 837–844.
- Mostafa, M. 2011. Metal chelates of hydrazone ligand chelating tendencies of 2-carboxyphenyl hydrazoacetanilide (2-(phaa)) ligand. *Research Journal of Chemical Sciences* 1.7: 1 – 14.
- Mustafa, A., Asker, W., Harhash, A., Nessina, N., Elnagdi, M. H. 1965. Reactions with 1, 2, 3-trione-2-arylhydrazones. *Tetrahedron* 21: 217 - 225.
- Nakamoto, K 1997. *Infrared and Raman Spectra of Inorganic and Coordination Compounds*. 5th Edition, New York. John Wiley and Sons Incorporated. 140 – 167.
- Nawar, N., and Hosny, N. M. 1999. Transition Metal Complexes of 2-Acetylpyridine *o*-Hydroxybenzoylhydrazone (APo-OHBH): Their Preparation, Characterisation and Antimicrobial Activity. *Chemical and Pharmaceutical Bulletin*. 47.7: 944 - 949.
- Odola, A. J and Woods, J. A. O. 2011. New Nickel(II) mixed ligand complexes of dithiocarbamates with Schiff base. *Journal of Chemical and Pharmaceutical Research* 3.6: 865 - 871.

- Odunola, O. A, Adeoye, I. O, Woods, J. A. O and Gelede, A. C. 2003. Synthesis and characterization of nickel(II) complexes of benzoic acid and methyl substituted benzoic acids hydrazides and X-ray structure of $\text{Ni}[\text{C}_6\text{H}_5\text{CONHNH}_2]_2\text{Cl}_2 \cdot 3\text{CH}_3\text{OH}$. *Synthesis and Reactivity in Inorganic and Metal-Organic Chemistry* 33.2: 205 - 221
- Omoregie, H. O. and Woods, J. A. O. 2011. Synthesis and Physicochemical Studies of Nickel(II) Complexes of Various 2-Alkyl-1-phenyl-1, 3-butanediones and Their 2, 2'-Bipyridine and 1,10-Phenanthroline Adducts. *International Journal of Chemistry* 3.1: 23-35
- Osowole, A. A and Balogun, S. A. 2012. Spectral, Magnetic, Thermal and Antibacterial properties of some Metal(II) complexes of Aminoindanyl Schiff base. *European Journal of Applied Sciences* 4.1: 6-13.
- Osowole, A. A., Malumi, E. O and Odutemu, A. E. 2015. Synthesis, magnetic spectra and antioxidant properties of some metal(II) mixed-drug complexes of Aspirin and Vitamin B₃. *Research and Reviews: Journal of Chemistry* 4.1: 60 - 65
- Owolabi, B. J and Olarinoye, N. O. 2008. *Organic Chemistry. The Fundamentals*. 1st Impression. Bohan Press Nigeria. Ltd, Akure, Nigeria. 442 – 446.
- Ozmen, U. O and Olgun, G. 2008. Synthesis, characterisation and antibacterial activity of new sulfonyl hydrazone derivatives and their nickel(II) complexes. *Spectrochimica Acta Part A* 70: 641 - 645
- Parmeter, S. M. 1959. *Inorganic Reactions*. New York. John Wiley & Sons Incorporated. 103 - 135.
- Patel, K. S and Woods, J. A. O. 1990. Synthesis and physicochemical properties of Bis(3-alkyl-2, 4-pentanedionato). Copper (II) complexes and their adducts with 2, 2 - bipyridine and 1,10-phenanthroline. *Synthesis and Reactivity of Inorganic and Metal-Organic Chemistry* 20.7: 909 - 922.

- Patel, R. N., Patel, D. K., Shodhiya, V. P., Shukla, K. K., Singh, Y., and Kumar, A. 2013. Synthesis, crystal structure and superoxide dismutase activity of two new bis(μ -acetato/ μ -nitrate) bridged copper(II) complexes with N¹-[phenyl(pyridine-2-yl)methylidene]benzohydrazone. *Inorganica Chimica Acta* 405: 209 - 217
- Rodriguez-Arguelles, M. C., Cao, R., Garcia-Deibe, A. M., Pelizzi, C., Matalobos, J. S., Zani, F. 2009. Antibacterial and antifungal activity of metal(II) complexes of acylhydrazones of 3-isatin and 3-(N-methyl)isatin. *Polyhedron* 28: 2187 – 2195
- Rollas, S., and Kucukguzel S. G. 2007. Biological Activities of Hydrazone Derivatives. *Molecules* 12: 1910 - 1939.
- Saeed, A., Arshad, M. I., Bolte, M., Fantoni A. C., Espinoza, and Z.Y.D., Erben, and M. F. 2016. On the roles of close shell interactions in the structure of acyl-substituted hydrazones: An experimental and theoretical approach. *Spectrochimica Acta Part A: Molecular and Biomolecular Spectroscopy* 157: 138 – 145.
- Sangcharoen, N and Wilaipun, P. 2017. Antimicrobial activity optimisation of nisin, ascorbic acid and ethylenediamine tetraacetic acid disodium salt (EDTA) against *Salmonella Enteritidis* ATCC 13076 using response surface methodology. *Agriculture and Natural Resources* 51(3): 355-364
- Salem, N. M. H., El Sayed, L., Haase W, Iskander, M. F. 2015. Metal complexes derived from hydrazoneoxime ligands: V. Spectral and structural studies on diacetylmonoxime n-alkanoylhydrazones and their nickel(II) and copper(II) complexes. *Spectrochimica Acta Part A: Molecular and Biomolecular Spectroscopy* 134: 257 – 266.
- Seleem, H. S. 2011. Transition metal complexes of an Isatinic quinolyhydrazone. *Chemistry Central Journal* 5: 35: 1 – 8.
- Shaw, E. 1950. A new synthesis of the Purines, Hypoxanthine, Xanthine and Isoguanine. *Journal of Biological Chemistry* 185: 439 - 448.

- Shebl, M., El-ghamry, M. A., Khalil, S. M. E., Kishk, M. A. A. 2014. Mono- and binuclear copper(II) complexes of new hydrazone ligands derived from 4, 6-diacetylresorcinol: Synthesis, spectra studies and antimicrobial activity. *Spectrochimica Acta Part A: Molecular and Biomolecular Spectroscopy* 126: 232 - 241
- Shen, X Y.Y., Jiang, H. L 1995. Lanthanide(III) complexes with hydrazone derived from a novel amino acid and isonicotinic acid hydrazide. Synthesis, characterization and antibacterial activity. *Synthesis and Reactivity in Inorganic and Metal-Organic Chemistry* 25.4: 511 – 519.
- Shen, S., Chen, H., Zhu, Taofeng., Ma, X., Xu,J., Zhu, W., Chen, R., Xie, J., Ma, T., Jia, L., Wang, Y and Peng, C. 2017. Synthesis, characterisation and anticancer activities of transition metal complexes with a nicotinohydrazone ligand. *Oncology Letters*. 13.5: 3169 – 3176.
- Singh, V. P and Gupta, P. 2008. Synthesis, Structural and bio-activity of some metal(II) complexes with glyoxal salicylaldehyde acyldihydrazones. *Journal of Coordination Chemistry* 61.10: 1532 - 1544.
- Singh, V. P and Singh, A. 2008. Synthesis, Spectral studies of copper(II) tetrathiocyanato dithallate(I) complexes with some acylhydrazones and their antimalarial activity. *Journal of Coordination Chemistry* 61.17: 2767 - 2780.
- Singh, V. P., Katiyar, A and Singh, S. 2009. Synthesis, Physicochemical investigations and Biological Studies on Mn(II), Co(II), Ni(II), Cu(II), and Zn(II) complexes with p-amino-acetophenone-isonicotinoylhydrazone. *Journal of Coordination Chemistry* 62: 1339 - 1346.
- Sousa-Pedrares, A., Camina, N., Romero, J., Duran, M. L., Garcia-Vazquez, J. A., Sousa, A. 2008. Electrochemical synthesis and crystal structure of cobalt(II), nickel(II), copper(II), zinc(II) and cadmium(II) complexes with 2-pyridinecarbaldehyde-(2¹-aminosulfonylbenzoyl)hydrazone. *Polyhedron* 27: 3391 - 3397.

- Stork, G., and Benaim, J. 1977. Monoalkylation of α , β -unsaturated ketones via metalloenamines: 1-butyl-10-methyl- Δ -octalone. *Organic Synthesis* 57: 69; 6: 42.
- Toro, C., Thibert, A., De Boni, L., Masunov, A. E and Hernandez, F. E. 2008. ‘‘Fluorescence emission of disperse red 1 in solution at room temperature’’ *Journal of Physical Chemistry B* 112.3: 929 - 937.
- Uma, V and Mittal, P. 2010. Synthesis, Spectroscopic and Cytotoxic Studies of biologically active new Co(II), Ni(II), Cu(II) and Mn(II) complexes of Schiff base hydrazones. *Pelagia Research Library* 3: 124-137.
- Urnikaite, S., Daskeviciene, M., Send, R., Wonneberger, H., Sackus, A., Bruder, I., Getautis, V. 2015. Organic dyes containing a hydrazone moiety as auxiliary donor for solid-state DSSC applications. *Dyes and Pigments* 114: 175-183
- Walcourt, A., Loyeysky, M., Lovejoy, D. B., Gordeuk, V. R., Ricardson, D. R. 2004. Novel aroylhydrazone and thiosemicarbazone Iron chelators with anti-malaria activity against Chloroquine-Resistant and sensitive parasites. *International Journal of Biochemistry and Cell Biology* 36: 401-407.
- Woods, J. A. O., Omoregie, H. O., Retta, N., Chebude, Y., and Capitelli, F., and Ivan, D. S. 2009a. Synthesis and characterisation of some Nickel(II) and copper(II) complexes of 2-substituted-4,4,4-trifluoro-1-(2-thienyl)butane-1,3-dione (TTAH), their (2,2'-bipyridine) and 1, 10-phenanthroline Adducts and X-ray structure of (2,2'-bipyridine)Bis(4,4,4-trifluoro-1-(2-thienyl)butane-1,3-dionato)Nickel(II). *Synthesis and Reactivity in Inorganic, Metal-Organic and Nano-Metal Chemistry* 39.10: pp. 704 – 717.
- Woods, J. A. O., Omoregie, H. O., Retta, N., Chebude, Y., and Capitelli, F. 2009b. Synthesis and physicochemical studies of Nickel(II) complexes of 2-substituted-1,3-diphenyl-1,3-propanedione, their 2,2'-bipyridine and 1, 10-phenanthroline adducts and X-ray structure of (2,2'-bipyridine)Bis(1,3-diphenyl-1,3-propanedionato)Nickel(II). *Synthesis and reactivity in Inorganic, Metal-Organic and Nano-Metal Chemistry* 39.10: 694 – 703.

Zhang, Y., Zhang, L., Liu, L., Guo, J., Wu, D., Xu, G., Wang, X., and Jia, D. 2010. Anticancer activity, structure, and theoretical calculation of N-(1-phenyl-3methyl-4-propyl-pyrazolone-5)-salicylidene hydrazone and its copper(II) complex. *Inorganica Chimica Acta* 363.2: 289 – 293.